Syntheses and Structural Characterisations of Amidinates, Diaminates and Phenolates Antimony (I and III) and Aluminium (III) Complexes

A thesis submitted to the

James Cook University, in partial achievement of the requirements of the degree of

DOCTOR OF PHILOSOPHY

By

Areej Kamal Aldabbagh

M.Sc. (Chemistry) College of Sciences for Women, Baghdad University, Iraq

Supervisors:

Professor. Peter C. Junk

D. Murray Davies

College of Science and Engineering

James Cook University

Townsville, Australia

August 2018

"O my Lord! Increase me in knowledge"

Al-Quran, Ta-Ha, 114

Dedicated to …

My homeland Iraq, the warmest womb…

My greatest parents, Mr. Kamal A. Aldabbagh and Mrs. Feryal A. Alssafar, who never stop giving of themselves in countless ways…

My dearest husband, Mr. Ahmed Alalili, who leads me through the valley of darkness with light of hope and support…

My beloved children: Fahad, Faidh and Fatimah, whom I can't force myself to stop loving, you have made me stronger, better and more fulfilled than I could have ever imagined, I love you to the moon and back.…

All the people in my life who touch my heart, I dedicate this simple work.

TABLE OF CONTENTS

CHAPTER THREE

Syntheses and molecular structures of heteroleptic and homoleptic antimony (III) tetrafluorophenylethylenediamidate complexes

CHAPTER FOUR

Syntheses and structural characterisation of heteroleptic aluminium (III) formamidinates and bimetalic antimony/aluminium (III) compounds

APPENDICES

APPENDIX 1

The Synthesis and X-ray Structure Determination of

[Sb(OC$_6$H$_2$-2,6-*t*Bu$_2$-4-Me)$_3$]

APPENDIX 2

The Synthesis and X-ray Structure Determination of

[Al(OC$_6$H$_2$-2,6-*t*Bu$_2$-4-Me)(OH)Cl(thf)]

ABSTRACT

This thesis focuses on the synthesis and characterisation of antimony(III) and aluminium(III) amidates with an emphasis on structural characterisation, presenting the isolation of 22 new complexes. In addition, some chemistry of (2,6-di–*tert*-butyl-4-methyl) antimony and aluminium (III) complexes is added in the appendix of this thesis. Below is a general outline for each chapter of original research (2-4), showing the diverse range of compounds obtained from the following formamidinate and polyfluorophenylamidate ligands.

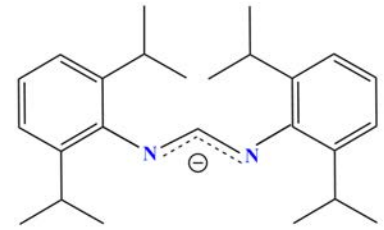

N,N′-bis (2,6-diisopropylphenyl)formamidinate
DippForm
Chapters: Two, Four

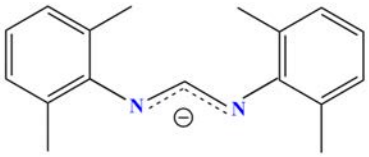

N,N′-bis (2,6-dimethylphenyl)formamidinate
XylForm
Chapter: Four

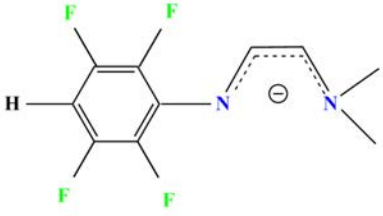

N,N-dimethyl-N`-2,3,5,6-tetrafluorophenylethane-1,2-diaminate
L^{Me}
Chapter: Three

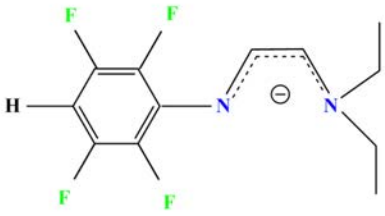

N,N-diethyl-N`-2,3,5,6-tetrafluorophenylethane-1,2-diaminate
L^{Et}
Chapter: Three

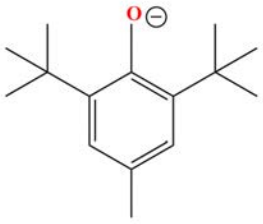

2,6-di-*tert*-butyl-*p*-cresolate
OAr
Appendix

Ligands used throughout Chapters Two-Four

ABSTRACT

Chapter 1 gives an overall introduction to antimony and aluminium (III) chemistry. This chapter describes the general aspects and overview of the relevant literature highlighting the most common synthetic methods used to synthesis antimony and aluminium compounds, particularly formamidinates, amidates, phenolates and their applications.

Chapter 2 describes the metathesis reactions employed for the preparation of a range of *mono*- and *bis*-substituted formamidinato antimony (III) complexes. The *bis*-substituted complexes include [Sb(DippForm)$_2$Cl] (**2.2**), [Sb(DippForm)$_2$Br] (**2.3**) and [Sb(DippForm)$_2$I] (**2.4**) and *mono*-substituted products include [Sb(DippForm)Br$_2$] (**2.5**) and [Sb(DippForm)I$_2$] (**2.6**). Other complexes have been prepared as dimers [Sb(DippForm)(NSiMe$_3$)]$_2$ (**2.8**) and [Sb(DippForm)Cl(C$_6$F$_5$)]$_2$.(THF)$_2$ (**2.12**), also the formamidinato-bridged distibane [Sb$_2${μ-(DippForm}$_2$].(THF)$_8$ (**2.1**) that represents an example of monovalent antimony. Fundamentally, the synthesis of antimony (I) and (III) formamidinate complexes was accomplished through deprotonation of N,N′-2,6-diisopropylphenylformamidine (DippFormH) by a metal alkyl/amide reagent (*n*-BuLi, LiN(SiMe$_3$)$_2$, NaN(SiMe$_3$)$_2$) in a donor solvent THF or in PhMe and then combined with SbX$_3$ in THF and/or PhMe. The unexpected [(DippForm)ClSb(μ-O)SbCl$_2$(Me$_2$NC$_2$H$_4$NMe$_2$)]$_2$.(C$_6$D$_6$) (**2.11**) was the only type of halogenated hetero dinuclear complex isolated in this study.

Chapter 3 details the synthesis and characterisation of a series of heteroleptic and homoleptic N,N-dimethyl-N'-2,3,5,6-tetrafluorophenylethane-1,2-diaminate antimony (III) complexes. [Sb(*p*-HC$_6$F$_4$NC$_2$H$_4$NMe$_2$)$_2$Cl] (**3.2**) and [Sb(*p*-HC$_6$F$_4$NC$_2$H$_4$NMe$_2$)$_3$] (**3.3**) complexes were isolated by metathesis reactions between SbCl$_3$ and Li(*p*-HC$_6$F$_4$N(CH$_2$)$_2$NMe$_2$), a common synthetic route to antimony complexes; while the direct reaction between SbCl$_3$ and *p*-HC$_6$F$_4$NH(CH$_2$)$_2$NMe$_2$ was used to synthesise [Sb(*p*-HC$_6$F$_4$NC$_2$H$_4$NMe$_2$)Cl$_2$] (**3.1**). Halo- and nonhalo-polyfluorophenylamido antimony (III) complexes were gained as monomers in the solid state.

ABSTRACT

Chapter 4 Extending this chemistry to formamidinate aluminium resulted in the isolation of a group of new and interesting formamidinato aluminium (III) complexes ranging from *mono*- to *bis*-substituted, involving different bonding modes. Metathesis reactions between AlX_3 (X = Cl, Br, I) and two different deprotonated N,N'-chelating ligands (XylForm) and (DippForm) of varying steric bulk and functionality were used to increase the range of the haloorgano(formamidinato) aluminium (III) system. These complexes are [Al(XylForm)$_2$Cl] (**4.1**), [Al(XylForm)$_2$I].PhMe (**4.2**), [Al(XylFormH)Br$_3$] (**4.3**), [Al(DippFormH)Br$_3$] (**4.5**) and [Al(DippForm)$_2$Cl] (**4.8**). Using the bulkier formamidinate ligand (DippForm) allowed the isolation of [Al(DippForm)Cl$_2$(thf)] (**4.6**) and [Al(DippForm)ClBr(thf)] (**4.7**). The heteroleptic [Al$_3$(XylForm)$_2$(μ_3-O)(OH)Cl$_4$]$_2$.PhMe (**4.4**) was isolated as a monomer and represents a compound contained three aluminium atoms bridged by an oxygen atom. In a different approach, a chlorine/methyl exchange reaction was used for forming bimetallic Al/Sb (III) ionic complexes [Me$_3$Sb-SbMe$_2$][AlCl$_4$] (**4.9**) and [Br$_3$Sb-μBr-SbBr$_3$][AlCl$_2$(thf)$_4$] (**4.10**), showing relatively rare coordination modes.

Overall, the knowledge regarding amidato antimony and aluminium (III) complexes has been enhanced and more information has been obtained regarding their structural motifs and bonding modes. The N,N′-*bis*(aryl)formamidinate ligands can form stable and structurally interesting mono/trivalent antimony and trivalent aluminium species using metathesis route, due to their ease of steric variability. In addition, this thesis demonstrates the ability of N,N-dimethyl-N'-2,3,5,6-tetrafluorophenylethane-1,2-diaminate ligand to stabilise antimony in its most common and stable oxidation state (III). Many of these compounds, particularly the compounds with M-X bonds, are now well set for potential reduction to low valent species. Reaction with KC_8 should form isolable low valent Sb or Al complexes and this work could be performed in future work. There are also many other formamidinate, guanidinate and amidinate ligands that could be used to extend this work.

STATMENT

To the best of the author's knowledge and belief, this thesis contains no material which has been accepted for the award of any other degree or diploma at any university or other institution, and contains no material previously published or written by another person except where due reference is made in the text.

Areej Kamal Assim Aldabbagh
Discipline of Chemistry
College of Science and Engineering
James Cook University, Queensland, Australia
August 2018

ACKNOWLEDGEMENTS

First and foremost, I would like to thank God to help me, without whose blessings I could not have achieved this milestone.

I wish to express deep thanks to my supervisors, Professor Peter C. Junk and Dr. Murray Davies, for their assistance anytime, support and encouragement, without whom the completion of this research and this thesis would not have been possible.

I owe a deep debt of gratitude to Dr. Jun Wang for enlightening me the first glance of research, collecting X-ray data, mainly from the Australian Synchrotron, assistance with my many crystallography-related questions and for always finding that piece of equipment/chemical whenever I need.

I am appreciative of the assistance and advice given by many people. These include Dr. Mark Robertson, for his assistance in NMR spectroscopy; Dr. Dana Roberts for assistance with Nicolet-Nexus FTIR spectrophotometer; Stephen Boyer for his help with C,H,N analyses at London Metropolitan University. Thanks to Dr. Liz Tynan and Kellie Johns for the linguistic support and editorial feedback on my writing.

A huge thank you goes to my fellow laboratory members, past and present: Md Elius Hossain, Nazli Rad, Mehdi Salehisaki, Safaa Hussein Ali, Aymeric Delon, Dr. Ioana Bowden and Dr. Guillaume Bousrez for all the fun times, the interesting discussions, the advice and the support. Also I thank my Iraqi friends in the James Cook University.

I would also like to thank James Cook University for giving me an opportunity to complete this work. I am grateful to all JCU staff for their support and help, particularly the Graduate Research School (GRS) and the administrative staff. Thanks also to Melissa Norton, the academic services officer, and for Katherine Elliott, the international student support officer for the warm welcome to JCU and all the answered subsequent requests throughout my duration at the University.

It is with gratitude that I admit the support and help of Iraqi families who are living in Townsville, Mr Al Shakarji's family; Dr. Mudaher's family and special thanks to Safaa's family to host me with my family during the first days in Townsville.

ACKNOWLEDGEMENTS

A very special thanks goes to my honest friend Nawres, for her motivation, beautiful friendship and appreciated support that made me overcome the homeless feeling throughout my experience in Australia.

To my dear husband (Ahmed), you are always with me and continually supporting me in all aspects of my life, you always listen to me in my bad and good time giving me the strength to complete my study, I can't find a word of thanks expresses everything that you have done for me. It is your passion that has always encouraged me to achieve my very best, with my sincere thanks.

I owe a huge thanks to my neighbour, the kindest couple in the world Sue and Jeff, for being like mum and dad to me and to my children throughout all my stay in Australia.

I recognise that this study would not have been possible without the financial assistance and scholarship fund from the Iraqi Ministry of Higher Education and Scientific Research, and I would express my gratitude to The Embassy of the Republic of Iraq/Cultural Attaché-Canberra (Representative of the (MOHESR) in Australia).

Finally, I would like to acknowledge my parents, Kamal and Feryal, who have supported me throughout my education and life, I would like to express sincere gratitude from the bottom of my heart to all what you have done for me.

ABBREVIATIONS

Ar = Aryl

n-Bu = *n*-butyl = Normal butyl group

CN = Coordination Number

Et_2O = Diethyl Ether

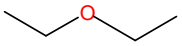

h = Hour

IR = Infrared

Me = Methyl

M.P = Melting Point

NMR = Nuclear Magnetic Resonance

ArO = Aryloxide

Ph = Phenyl

ppm = Parts Per Million

RTP = Redox Transmetallation/Protolysis

RT = Redox Transmetallation

r.t. = Room Temperature

EtOH = Ethanol

MeOH = Methanol

THF = Tetrahydrofuran (Solvent)

thf = Tetrahydrofuran (Coordinated)

L = Ligand

M = Central (Usually metal) atom in compound

TMEDA, tmeda = N,N,N',N'-tetramethylethylenediamine(tmen)

X = Halogen

Å = Ångström, 10^{-10} m

CVD = Chemical Vapor Deposition

LUMO = Lowest Unoccupied Molecular Orbital

Hz = Hertz, s^{-1}

υ = Frequency (cm^{-1})

br = Broad

ABBREVIATIONS

dec. = Decomposition

m = Multiplet

s = Singlet

t = Triplet

δ = Chemical shift in n.m.r. (ppm)

Pro-ligands:

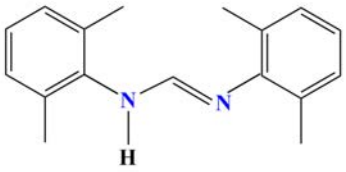

N,N′-*bis*(2,6-dimethylphenyl)formamidine
XylFormH

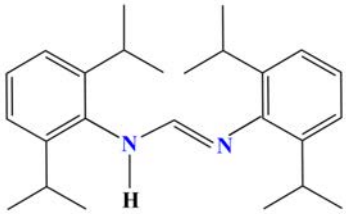

N,N′-*bis*(2,6-diisopropylphenyl)formamidine
DippFormH

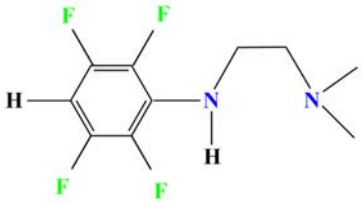

N,N-dimethyl-N`-2,3,5,6-tetrafluorophenylethane-1,2-diamine
HL^{Me}

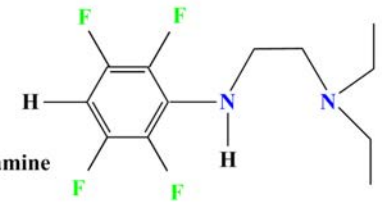

N,N-diethyl-N`-2,3,5,6-tetrafluorophenylethane-1,2-diamine
HL^{Et}

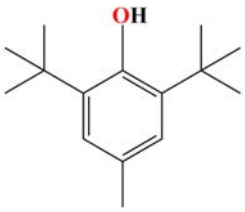

2,6-di-*tert*-butyl-p-cresol
(HOAr)

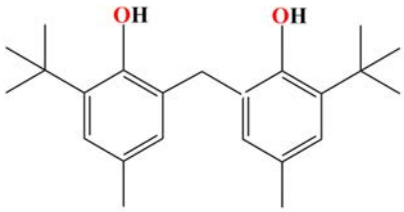

2,2'-methylenebis(6-*tert*-butyl-4-methylphenol)
$BP(OH)_2$

CHAPTER ONE

INTRODUCTION TO ANTIMONY (III) AND ALUMINIUM (III) AMIDINATE, DIAMINATE AND PHENOLATE COMPLEXES

CHAPTER ONE: INTRODUCTION

Outline

Each chapter in this thesis presents a diverse compilation of antimony and/or aluminium N,N′-bis(aryl)formamidinate, N,N-dialkyl-N′-(2,3,5,6-tetrafluorophenyl) ethane-1,2-di-aminate or phenolate chemistry, and begins with an introduction. This preliminary chapter provides an overview of the properties of antimony and aluminium chemistry, a brief summary of cyclopentadienyl (Cp) antimony and aluminium chemistry as a basis for nitrogen based Cp replacement ligands, and a review of the current literature regarding antimony and aluminium amides and phenolate complexes.

1.1 *Introduction*

1.1.1 Antimony: General Aspects

Antimony is a metal located between arsenic and bismuth in group 15 of the periodic table, and is well-known for its relatively high toxicity. There are some health concerns, but elemental antimony metal has rather low toxicity. It is the 63rd most abundant element in the earth's crust and is mainly found as a sulfide ore (Sb_2S_3) or combined with other metal ores such as copper, silver as dicrasite (Ag_2Sb) or pyrargyrite (Ag_3SbS_3), nickel as breithauptite (NiSb) or ullmanite (NiSbS) and lead ores.[1]
Elemental antimony adopts five allotropes but the α allotropic form is the most stable.[2] Antimony has two stable isotopes: ^{121}Sb and ^{123}Sb, in addition to 35 radioisotopes, including the longest-lived ^{125}Sb with a half-life of 2.75 years.[3] Sb being a metalloid and therefore a semiconductor has low electrical and thermal conductivities compared with those of metallic elements.[1] To date, atomic absorption spectrometry is the most commonly used method for detecting antimony with atomisation in a graphite tube and with generation of hydrides.[4,5] However, the most recent used technique is hydride generation inductively coupled plasma optical emission spectrometry (HG-ICP-OES).[6]

Not much attention has been given to antimony chemistry compared to its lighter congeners. Over the past two decades, various interesting studies and novel inorganic and organometallic chemistry of antimony have been performed. This consideration can mainly be attributed to the following myriad of applications: (a) biological importance i.e.: treatment against leishmaniasis,[7] anti-tumour,[8] and anti-bacterial activity [9,10,11,12,13]; (b) industrial uses as precursors for the chemical vapour deposition (CVD) techniques for generating antimony oxide thin films, [14] which have potential applications in electronic ceramics components and catalysis; [15,16,17,18,19,20,21,22,23,24,25 26] (c) superconductors; and (d) ferroelectrics.

Compounds of antimony normally contain the element in either the (+III) or (+V) oxidation states, with the latter being the most common, and can occur in oxidation states ($^{-}$III), (+IV) and the very rare form (+I).[27] According to Pearson's hard soft acid base theory, Sb(III) can be classified as a borderline metal ion,[28] and has a high capacity to bind with nitrogen and sulfohydryl-containing ligands. Many compounds of Sb(III) are analogous to those of P, As and Bi compounds. The majority of SbX_3 molecules such as $SbPh_3$ and $SbCl_3$ in the valence state three show three pyramidally directed single bonds, with a lone pair occupying the fourth tetrahedral position (Figure 1.1).

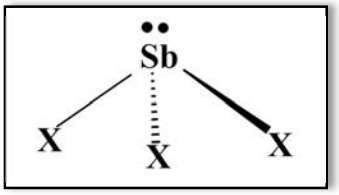

Figure 1.1

The general coordination number of Sb ranges between 3 and 6.[29] The antimony atom has empty *d* orbitals of fairly low energy. Compounds of Sb in oxidation states (III) or (V) are strong Lewis acids (Lewis acceptors) that accept electron pairs from donors. There are uncommon compounds in which antimony in the (I) oxidation state forms trigonal planar geometry at the Sb center (Figure 1.2), and this may be attributed to $d\pi$-$p\pi$ interactions.[29]

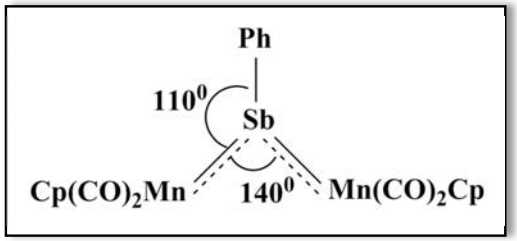

Figure 1.2

Although the chloride ion affinity of $SbCl_5$ has been shown by the Gutmann group to be stronger than BCl_3,[30] utilising antimony penta-halide derivatives is problematic because they have extreme reactivity and an inconvenient corrosive nature; specifically, both SbF_5 and $SbCl_5$ react severely with water, releasing the corresponding hydrohalic acid. This property has discouraged many from investigating the synthesis of such derivatives.

1.1.2 Aluminium: General Aspects

Aluminium is a silvery-white metal of main Group 13 of the periodic table. Aluminium is the third most abundant element in the earth's crust (7.4 %) behind oxygen and silicon, and all the earth's aluminium has combined with other elements to form compounds such as alumina Al_2O_3 and cryolite Na_3AlF_6.[1] It is an excellent electrical and thermal conductor. The only stable isotope of aluminium is ^{27}Al. Al metal is stabilised by almost instantaneously formation of an oxide coating allowing the metal to be used in construction…etc. The vast majority of aluminium compounds are found in the oxidation state (III) for the aluminium atom with varied coordination numbers ranging between 3-6 that can be attributed to the high stability of (III) oxidation state;[31] however, a substantial increase in the synthesis of low valent aluminium compounds like AlH, Al_2O, Al_2S, Al_2Se and AlX (X = F, Cl, Br, and I) has been noticed in the past two decades.[32,33,34] Aaluminium (I) complexes have found wide applications in materials and agrochemicals. The efficacy of aluminium as Lewis acid lay in its ability to attract and coordinate the electrons of neighbouring atoms and molecules. Aluminium reacts strongly with hydrochloric acid and caustic soda. The reaction with sulfuric acid is weaker, whereas it is inactive towards cold nitric acid.

1.2 *Applications of antimony and its compounds and aluminium and its compounds*

1.2.1 Commercial applications of antimony and its compounds

Antimony and its complexes have had many uses dating back centuries; in fact, certain products were initially used for cosmetic purposes in ancient Egypt thousands of years ago. That usage was to darken the eyelashes and as an eyeliner that it is still used for this purpose in many countries. In the past two decades, antimony has been used in industry in the form of fire-retardant chemicals added to textiles, rubber, paper, etc. (e.g. bromine-based flame retardants are often used with an antimony synergist Sb_2O_3).[35,36,37,38]

Today the most common use of antimony is as an alloy with lead to harden the material,[39] which can be used then for electrical storage batteries, sheathing for electrical and TV cables, semiconductor and infrared devices, matches, glassware, ceramics, enamels, paints, pottery, fireworks and lacquers.[40] Along with many other metals, such as barium-cadmium, tin, lead, calcium-zinc, antimony is used as a heat stabiliser in the plastics industry; a disadvantages being its presence in plastic containers, which could lead to increased oral exposure in humans, as Sb has a strong affinity towards the materials.[40] Recently, addition of antimony oxide to polyvinyl chloride (PVC pipe) to act as a flame retardant was a valuable innovation.[41]

1.2.2 Commercial applications of aluminium and its compounds

Aluminium has very versatile properties with wide industrial uses, the most common of which are in construction (including sheets, tubes, castings, windows, doors, sidings, building wire, sheathing and roofing), as well used in the aviation-space and automobile industries.[42,43] Alloying the natural soft aluminium with small amounts of copper or magnesium prominently increase its strength.[44] In addition, the strength of the aluminium Lewis acid can be controlled by halides having different electronegativities.

While an aluminium is a very reactive metal, it is strong and light and can be used as a building material that is protected from corrosion by the incorporation of a thin protective oxide layer. Aluminium features by its fundamental role in a large scope of chemical transformations. It is now the most commonly used material in the home food and drinks cans and beverage containers,[45] also for other home cooking utensils and in common household aluminium foils in its elemental form, as well in large power transmission lines (not in household wiring). Another popular use of aluminium represented in its ability to transfer hydrides to electron deficient atoms. It can be used also in pyrotechnics, to manufacture die casting auto engine blocks and parts, for incendiary bombs, and for all types of alloys with other metals.

Recycling an aluminium scrap is less expensive than extracting the metal from its bauxite ore. Corundum, a pure oxide crystals of aluminium, is used as an abrasive for sandpaper and grinding wheels. As this material resists heat, therefore it is used for lining high-temperature ovens, and to form a protective coating on many electronic devices such a transistors. Synthetic rubies and sapphires that used for lasers beams are made from aluminium oxide.

For more than 70 years, aluminium compounds have been used extensively as adjuvants in both human and veterinary practical inoculations, such as boehmite and aluminium hydroxyphosphate.[46] Aluminium compounds have also various pharmaceutical uses, for example in ointments, toothpaste, deodorants and shaving creams.

1.2.3 Biological application of antimony compounds

Despite their heavy metal nature, antimony compounds are considered to be less mutagenic, teratogenic and carcinogenic than many other heavy metals, such as arsenic, chromium, or nickel, among others, although they are more toxic than bismuth and its compounds.[40] Antimony's therapeutic activity has been known for centuries. Thus, its compounds have found applications in metabolic and biochemical studies. The major clinical use of organoantimonials during the twentieth century was to treat leishmaniasis.[7] Leishmaniasis is a human infective parasitic disease that is widespread in the world but mainly localised to the tropics and subtropics.

Some studies have cited that Old World cutaneous disease was recognised by the second millennium B.C. in Iraq,[47] and this is why the disease was formerly known as Baghdad boil. The Leishmaniasis parasites have been detected in Australia, which could lead to growth of the disease in Australia's tropical regions.[48] The parasite is transmitted to humans via the bite of sand flies, and the illness manifests as cutaneous, muco-cutaneous and visceral lesions that may be fatal if untreated.[47] Gaspar Vianna, in 1912, reported the first use of the internal administration of antimony(III) potassium tartrate (tartar emetic), $K_2[Sb(d\text{-}C_4O_6H_2)]_2.3H_2O$, in the treatment of muco-cutaneous leishmaniasis.[49]

Later, tartar emetic was found to be a valuable anthelmintic agent for the control of Schistosomal blood flukes.[50,51] In the late nineteenth century, tartar emetic was used for fever and pneumonia, but its clinical use slowly diminished because of severe side-effects.

Since 1940, the less toxic Sb(V) complexes have continued as the frontline drugs in the treatment of leishmaniasis.[52] However, their uses have several limitations, such as high cost and toxicity, difficult route of administration and lack of efficacy in endemic areas.[53,54] Typically, local pain has accompanied antimony therapy through intramuscular injections and also systemic side effects, necessitating superfluous medical control. Furthermore, drug resistance is the second key problem for treating this disease.[55] Whether Sb(III) or Sb(V) is the active form remains an interesting question.

Recently pentavalent antimonials such as *N*-methyl-D-glucamine (meglumine antimoniate/commercialised as Glucantime) (Fig. 1.3 a) and sodium gluconate (sodium stibogluconate/Pentostam)[56] (Fig. 1.3 b) have proven highly effective in cancer, hepatitis C virus (HCV) and AIDS experimental models,[57] emphasising revived interest in the chemistry and biochemistry of these old drugs, as well as in developing more effective pharmaceutical formulations.

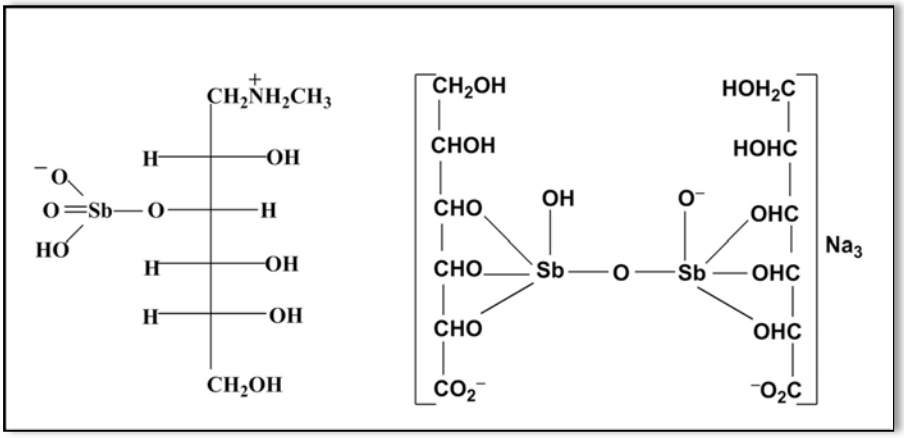

Figure 1.3 **a**: Meglumine Antimoniate [56] **b**: Sodium Stibogluconate [56]

Pro-drug Sb^{5+} compounds are non-covalent chelates and are bioreduced or activated to the active form Sb^{3+} intracellularly,[58] to have antileishmanial activity against extracellular promastigotes.[59] Antimony binds to biomolecules such as glutathione, trypanothione, and nucleotides, and forms binary and ternary complexes that may allow it to be trafficked in cells.

In 2006, Wyllie and Fairlamb showed that trivalent antimonial compounds (Sb^{III}) are extremely effective in treating acute promyelocytic leukemia (APL) when examined on glutathione homeostasis, oxidative stress and apoptosis in the human leukemia monocyte cell line, THP-1 macrophages.[60] They also showed that antimony might induce apoptosis and kill through DNA fragmentation and externalisation of phosphatidylserine.[61]

Guéguéniat *et al.* introduced the role of the radioisotope ^{125}Sb as an excellent tracer material for identifying pathways and transit times for the waste derived from the nuclear fuel reprocessing plant. The importance of the ^{125}Sb tool can be attributed to its conventional behaviour in the environment within the water mass, which is characteristic of releases from La Hague, France.[62]

1.2.4 Aluminium compounds in organic synthesis

Aluminium is employed in a wide arrange of applications. Jordan, Teuben and their co-workers have achieved an extensive set of *mono*-amidinate, *bis*-amidinate, and dinuclear cationic aluminium complexes that have significant function as catalysts. These catalysts can be utilised in olefin polymerisation, polymerisation of ethylene as new transition-metal-free homogeneous Al catalysts [63] and C–H bond activation.[64]

Since 1964, alkylaluminium and alkylaluminium hydride compounds have gained considerable attention as reagents in organic synthesis. Diisobutylaluminium hydride and triisobutylaluminium have been presented as excellent options for reducing agents.[65] An amide moiety of acyclic and macrocyclic amidoketals was best selectively reduced in the presence of lithium aluminium hydride $LiAlH_4$ with drops of triethylamine.[66]

The use of methylaluminoxane (MAO) as co-catalyst was the latest discovery of the tailored synthesis in polyolefins industry, which was performed at the chemical department of the University of Hamburg and is probably the biggest use in organic synthesis.[67,68] Consequently, Metallocences or other transition metal complexes in combination with the conventional aluminum alkyl co-catalysts used in Ziegler–Natta systems have expanded the possibility to design the microstructure of polyolefins in a manner wasn't reachable in years before, playing a crucial part in the olefin polymerisation.[69]

A series of organic aluminium compounds were introduced as new polycondensation catalysts in poly(ethylene terephthalate) (PET) synthesis. These compounds including aluminium alkoxide, β-diketones, β-ketoesters and ethylene glycol.[70]

1.3 *Antimony and Aluminium amidinate complexes*

In 1858, Gerhardt prepared amidines ($R^2N{=}C(R^1){-}NHR^3$) (Fig. 1.4) for the first time through the reaction of aniline with *N*-phenylbenzimidyl chloride.[71] More specifically, when R^1= H in an amidine, the ligand is classified as formamidine (Fig. 1.5).[72]

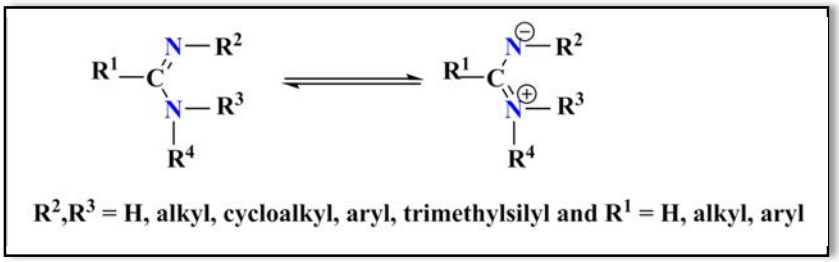

Figure 1.4 The overall configuration of an amidine.

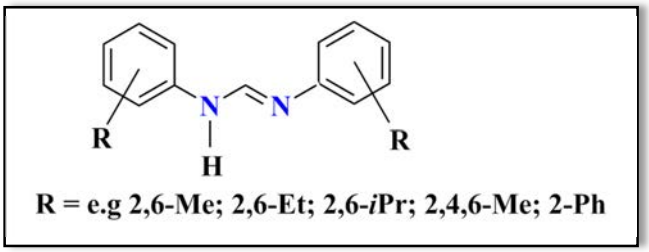

Figure 1.5 N,N′-bis(aryl)formamidine.

These ligands are valuable principally because they can be prepared in high yields, crystallise without difficulty and offer different coordination modes. The steric requirements of these ligands can help to realise low valent metal complexes. Furthermore, it can be simple to modify their steric and electronic properties by variation of the organic substituent R^1, R^2 and R^3 groups attached to the carbon and nitrogen atoms of the ligand backbone.[73,74] In particular, amidinate (N-H deprotonated amidines) products have proven to be useful precursors for chemical vapour deposition (CVD)[75,76,77,78,79,80,81,82,83] and atomic layer deposition (ALD),[84,85,86,87] as well as organic-inorganic hybrids. In addition, the proficiency of such ligands to flexibly coordinate the metal centre has enabled them to be very valuable materials in catalysis [88,89,90,91] and material sciences.[92,93,94,95]

Notably, amidines are important organic compounds for use as starting materials and fundamental intermediates in synthetic chemistry.[96,97,98,99,100,101,102] Due to their biochemical activities, they have been employed in some valuable drugs.[102] In 2012, some therapeutically effective natural products containing amidine components, such as noformycin were isolated as a metabolite from actinobacteria, and pentamidine was found to have two amidine units which are used to treat protozoan infections.[103] In addition, beside their assistive roles in asymmetric synthesis,[104] amidines have extensive capacity to actively form complexes with metals.[105,106]

For over ten years, a number of small amidine and guanidine molecules containing basic functional groups have been revealed as effective nucleophilic catalysts in organic synthesis, despite the likely problems associated with their high basicity. Moreover, their derived catalysts have proven to be efficient in catalysing aldol reactions, Morita–Baylis–Hillman reactions, conjugate additions, carbonylations, methylations, silylations and brominations.[107]

Amidines and amidinates can bind to metals, forming a diversity of possible binding modes, such as monodentate (Fig. 1.6, i), bidentate chelating (Fig. 1.6, ii) and bimetallic bridging monodentate (Fig. 1.6, iii) modes. As well, the monodentate (i) has two potential types of four-electron donation (Fig. 1.6, iv and v). There are also the types of bridging–chelating mode (Fig. 1.6, vi, vii, viii and ix).[71, 108]

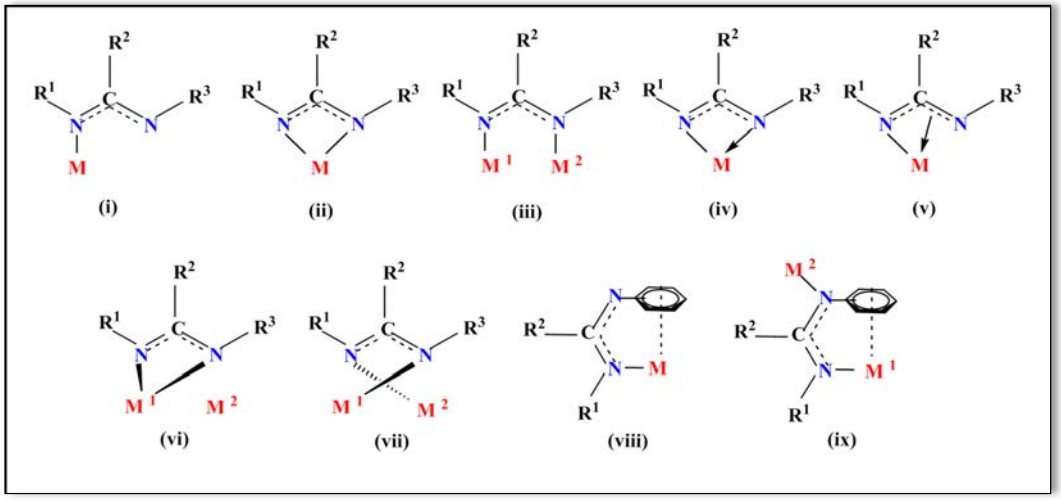

Figure 1.6 Distinctive binding modes of amidinate metal complexes.[71, 108]

Jordan, *et al.* assert that the diverse structural products of the amidinate ligand are dependent on steric influences, such as the ideally amidinate structure (Fig. 1.6 ii) with 120° angles at the C and N centers that enables nitrogen sp^2 orbitals to project in parallel directions.[63,64] These types of ligands have π-bonds allowing the negative charge to be located across the N–C–N backbone.[109] Amidines are classified based on the number and distribution of the substituents into five general structures (Fig. 1.7).[110]

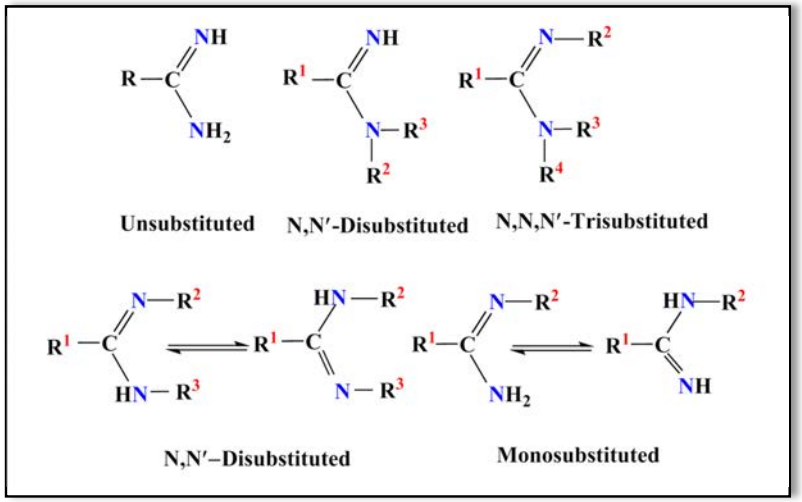

Figure 1.7 General categories of the amidine.

According to Cole, *et al.* [108,111,112,113] amidinates coordinated to metal centres can have different binding modes, with their classification based on the stereoisomer form of the amidine ($R^2N{=}C(R^1){-}NHR^3$), such as E-syn, E-anti, Z-syn and Z-anti. These binding dissimilarities depend on the position of the substituents relative to each other with respect to the single bond (C–N) and double bond (C=N) (Fig. 1.8).

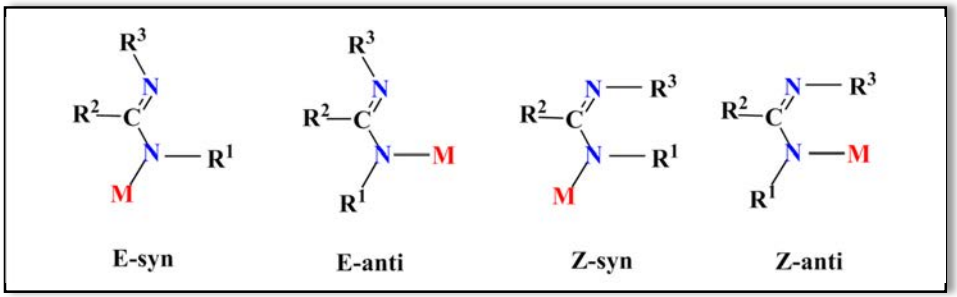

Figure 1.8 Possible isomeric classes of amidinate employed in metal amidinate complexes.

N,N'-chelating organic ligands have attracted growing attention in organometallic chemistry over the past decade due to their ability to flexibly coordinate a large variety of main-group *f*-block and transition metal centres. More specifically, β-diketiminate **I**,[114] guanidinate **II**[115] and amidinate anions **III** [71,108,116,111] (Fig. 1.9) are becoming increasingly common because their steric and electronic properties can easily be tuned by varying the organic substituents R and R′. Amidinates act as four-electron nitrogen *σ*-donors via the more basic and less sterically crowded imino lone pair to form simple adducts.

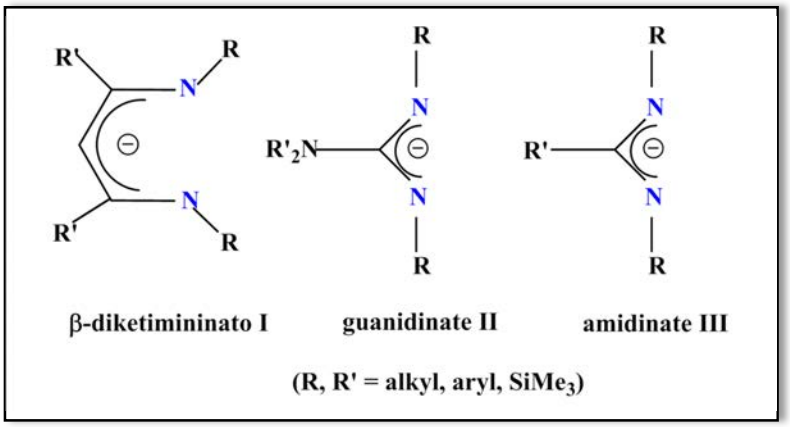

Figure 1.9 The more increasingly common types of N,N'-chelating ligands.

Over the past 40 years, the amidinate $(R^2N{=}C(R^1){-}NR^3)^-$ family of ligands has motivated different investigations into the synthesis of main-group metal amidinate complexes, such as Group 1,[109,117] Group 2,[118] Group 13,[119] Group 14,[120] and Group 15 element complexes.[121] These stimulating syntheses generate rather unusual oxidation states and a significant number of structurally-characterised metal complexes. For example, mono-substituted complexes of the general type LMX_2 (M = Al, Ga, In; X = halide, alkyl) function as suitable starting components in olefin polymerisation reactions and synthesis of low-valent (oxidation state $^+1$) group 13 metal complexes LM.[122,123,124,125] A series of very bulky guanidinate ligands, $[(ArN)_2CNR_2]^-$ [Ar = $C_6H_3iPr_2$-2,6; R = cyclohexyl (Giso$^-$), R = *i*Pr (Priso$^-$)], have been developed for use in stabilising low oxidation-state group 13 complexes such as $[:M^I(\kappa^2\text{-N,N}'\text{-Giso})]$ (M = Ga or In).[126] The trisubstituted guanidine ligand has a chelating angle at the metal (N–Sb–N), which typically is required to be 90 °.[127]

Various forms of ArFormH pro-ligands N,N′-bis(aryl)formamidines (ArN=CH-NHAr (Ar = aryl)) (Fig. 1.5) can be readily synthesised in high yields by heating to reflux one equivalent of triethylorthoformate with two equivalents of the appropriately substituted aniline in the presence of acetic acid (eqn. 1.1).[128] This method can readily provide formamidines with differing electronic effects and varying steric bulk.

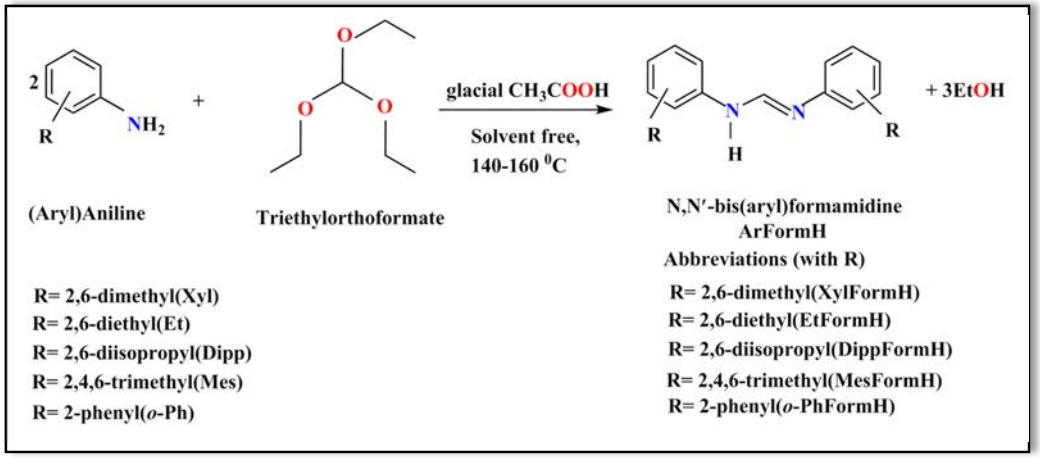

Equation 1.1 Synthesis of various N,N′-diphenylformamidines catalysed by glacial acetic acid (FormH abbreviations shown).

Syntheses of compounds introducing group 15 elements have attracted many researchers for a range of reasons. First, examples of low valent antimony complexes are very rare compared with the corresponding phosphorus analogues.[129] Second, the prospective applications of group 15 heterocyclic compounds can lead to valuable studies in various industrial and medical fields.[130] Third, researchers can further explore the chemistry in this field through investigating the potential role of these compounds as precursors in organometallic syntheses.

Despite the ability of ArForm ligands to adopt a variety of coordination modes, ArForm coordination to the heavier group 15 elements is comparatively new, and to the best of our knowledge prefers this type of chelation (Fig. 1.6, ii). Regarding the work presented in this thesis, there have not been many reported examples.[131,132,133] The field of antimony N,N'-chelating chemistry is still largely unexplored, opening the possibility for further exciting discoveries.

Chemistry of the Lewis base coordinated dipnictenes is still limited and only a few types have been synthesised and structurally characterised such as α-(*t*BuN)$_4$P$_4$ (Fig. 1.10).[134] Further, Green and his team prepared [As$_2${μ-(ArN)$_2$CR}$_2$] (Ar = C$_6$H$_3$*i*Pr$_2$-2,6; R = N(C$_6$H$_{11}$)$_2$, N*i*Pr$_2$, or *t*Bu) as a dimeric complexes (Fig. 1.11).[121]

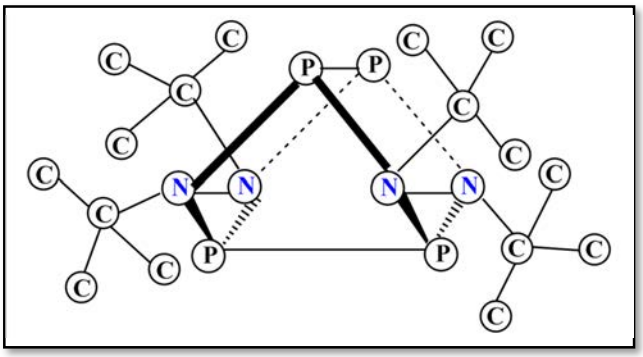

Figure 1.10 Structure of α-(*t*BuN)$_4$P$_4$.

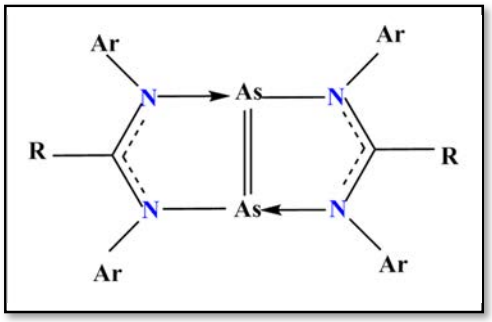

Figure 1.11 Structures of [As$_2${μ-(ArN)$_2$CR}$_2$] (Ar = C$_6$H$_3$*i*Pr$_2$-2,6; R = N(C$_6$H$_{11}$)$_2$, N*i*Pr$_2$, *t*Bu).

Recently, Hinz and co-workers reported different complexes of the Lewis base–stabilised dipnictenes such as [Sb$_2$-{μ-(TerN)$_2$P}$_2$] ((TerN)$_2$P = bis(terphenylimino)phosphide), which were obtained in high yield by a simple metathesis reaction (Fig. 1.12).[135] These types of complexes and publications are relevant to work described in this thesis and are introduced in more detail in ***Chapter2***.

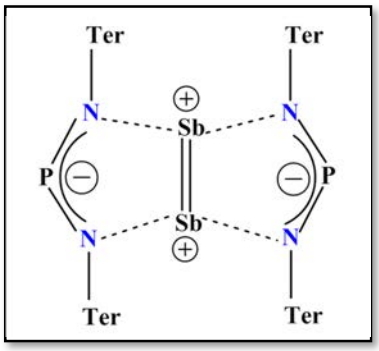

Figure 1.12 Structure of $[Sb_2\text{-}\{\mu\text{-}(TerN)_2P\}_2]$ ($(TerN)_2P$ = bis(terphenylimino)phosphide).

1.4 *Polyfluorophenyletheylenediamidate complexes*

In 1988, Buxton first reported the in situ composition of polyfluorophenyletheylenediamidato ligands, N-dialkyl-N'-2,3,5,6-tetrafluorophenylethane-1,2-di-aminate $L^{Me/Et}$, through synthesis of polyfluorophenylaminatoplatinum (II) complexes $[Pt(L^{Me/Et})X(py)]$ (X=Cl, Br, I) (eqn. 1.2, i and ii). The procedure combined decarboxylation reactions between (N,N-dialkylethane-1,2-diamine)(dihalogeno)platinum(II) or dichloro(ethane-1,2-diamine)platinum(II) complexes and thallium(I) polyfluorobenzoates with added polyfluorobenzene in pyridine (nucleophilic substitutions).[136,137,138,139]

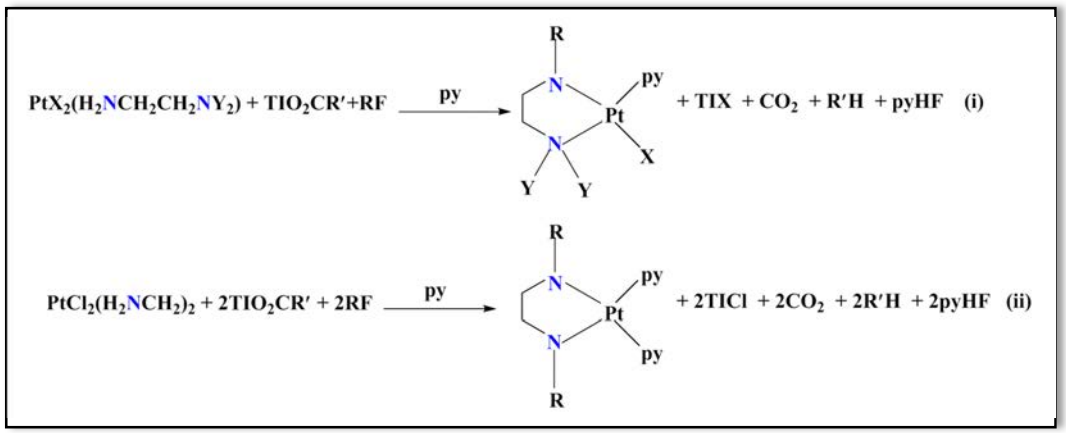

Equation 1.2 Initial synthesis of polyfluorophenyletheylenediaminato ligands $L^{Me/Et}$.

Overall, reaction of the appropriate N,N-dialkylethane-1,2-diamine with C_6F_5H by heating to reflux in EtOH (eqn. 1.3) can readily produce the two types of substituted ligands $L^{Me/Et}H$.[140]

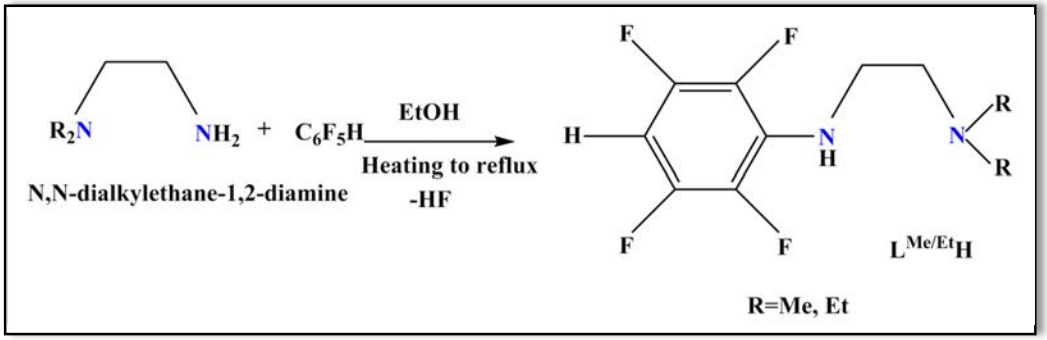

Equation 1.3 Synthesis of N,N-dialkyl-N'-2,3,5,6-tetrafluorophenylethane-1,2-di amine ligands $HL^{Me/Et}$.

The coordination mode of polyfluorophenylethylenediamidate to a metal can vary either by fluorine and nitrogen or most commonly N,N'-chelating as in the tetrafluorophenylethylenediamidate complexes.[141,142,143]

Tetrafluorophenylethylenediamidato metal complexes are accessible via a wide array of synthetic strategies. For example, $[Yb(L^{Me/Et})_2(thf)_2]$ complexes were prepared by metathesis, by protolysis of $[Yb\{N(SiMe_3)_2\}_2(thf)_2]$ with $L^{Me/Et}H$, and by redox transmetallation/protolysis (RTP) between Yb metal, $Hg(C_6F_5)_2$ and $L^{Me,Et}H$.[144]

By using the former route in tetrahydrofuran, a new class of homoleptic organoaminato rare earth complexes $[Ln(L^{Me}$ or $L^{Et})_3]$ (Ln = La, Ce, Nd; $L^{Me/Et} = p$-$HC_6F_4N(CH_2)_2NMe_2/Et_2$) has been isolated, demonstrating (Ar)CF–Ln interactions.[145] The structures of these complexes feature eight-coordinate Ln metals with two tridentate (N,N′,F) aminate ligands including (Ar)CF–Ln bonds, and either a bidentate (N,F) ligand (Ln = La, Ce, Nd; L^{Et}) or a bidentate (N,N′) ligand (Ln = Nd; L^{Me}) showing a rare case of connection variation. Recently, divalent europium complexes, $[Eu(L^{Me/Et})_2(thf)_2]$ and $[Eu(L^{Et})_2(dme)]$ have been achieved using the same method; they are thermally robust but experience C–F activation upon exposure to light.[146] Synthesis of metal tetrafluorophenylethylenediaminate complexes are detailed in ***Chapter 3*** of this thesis.

1.5 *Antimony aryloxidate/alkoxidate complexes*

Aromatic rings with a hydroxyl functional group are known as phenols and are shown in (Fig. 1.13). These are also called carbolic acids and are naturally derived from coal tar. Aryloxidates are the anionic forms of the hydroxyl groups upon deprotonation.[147] Figure 1.13 displays some widely used aryloxide ligands that have attracted much attention.

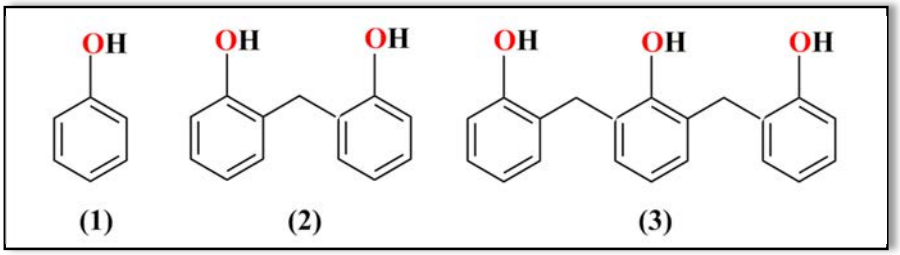

Figure 1.13 some common aryloxide ligands.

Phenols are weak acids; however, they are more acidic compared with aliphatic alcohols, which can be attributed to aryloxide ion stability by resonance, along with the delocalisation of the negative charge at the *ortho* and *para* positions (Fig. 1.14).[148] Notably, phenol proton acidity can be positively or negatively affected by adding substituents. For example, a fluorine substituent might be able to increase the acidity of the phenolic residue by enhancing the resonance that has been brought from the electron withdrawing group. In contrast, alkyl substituents, which exist as an electron donating group, can decrease acidity by obstructing resonance.[149]

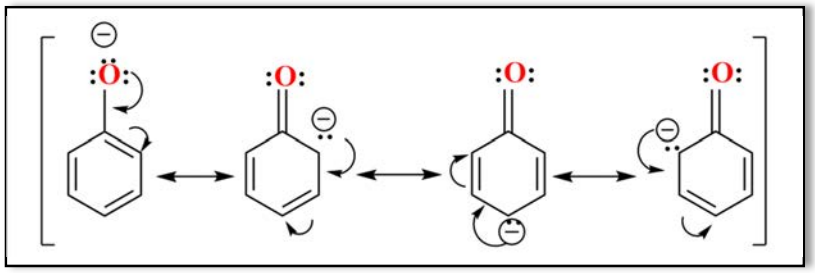

Figure 1.14 Charge delocalisation in the phenoxide ion

Moreover, despite the fact that alkyl substituents in the *para* position of the aryloxides might increase solubility and change the spectroscopic properties, they usually have little steric effect in coordination with the metal ion. However, alkyl *ortho*-phenyl substituents can have a distinct influence on the structural properties and metal reactivity in the complex. *Meta* substituents greatly affect the steric aspects of the ligands through hampering the confirmed flexibility of nearby substituents employed in the *ortho* position.[150,151]

The pro-ligand 2,6-di-*tert*-butyl-*p*-cresol, commercialised as butylated hydroxy toluene (BHT), is widely used in the production of phenolic resins as antioxidants[152] and polymerisation inhibitors.[153] The alkoxide/aryloxide chemistry of antimony complexes has been known for over half a century and remains the subject of much interest,[154] due to the myriad of applications in organic and oxidation catalysis, medicine and biochemistry, superconductors, ferroelectrics, and many other oxide based materials.

The two structures of Sb(V) and Sb(III) alkoxide, $[Sb(OCH_3)_5]$[155] and $[Sb\{OCH(CH_3)_2\}_3]$,[156] respectively, have been crystallographically authenticated, adopting a dinuclear motif including alkoxide bridges and forming distinct centrosymmetric dimers in the solid state by Sb–O–Sb interactions (Fig. 1.15).

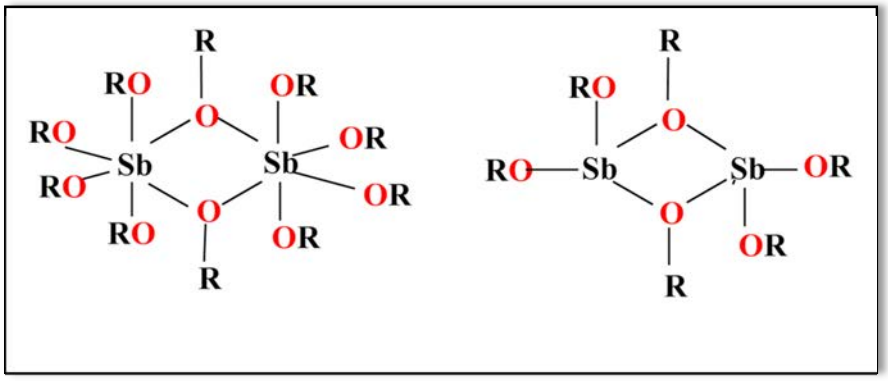

Figure 1.15 Two types of Sb(V) and Sb(III) alkoxides.

Antimony phenolate complexes are reachable by common synthetic methods. For example, the two diantimony calix-4-arene complexes, $Bu^tC4(SbCl)_2$, have been synthesised by the direct reaction at room temperature between $SbCl_3$ with the monosodium salt of *p*-tert-butylcalix-4-arene (Bu^tC4), Bu^tC4Na, and the tetralithium salt of *p*-tert-butylcalix-4-arene, Bu^tC4Li_4. Another reaction of $SbCl_3$ with $RC4{\cdot}Li_4$ (R = Bu^t, H, or allyl) in a 2:1 molar ratio in THF led to producing a range of diantimony chlorides of calix-4-arene and *p*-allylcalix-4-arene such as $(HC4(SbCl)_2$, $AC4(SbCl)_2$. These complexes feature on central planar $Sb_2(\mu\text{-}O)_2$ four-membered rings (eqn. 1.4).[24]

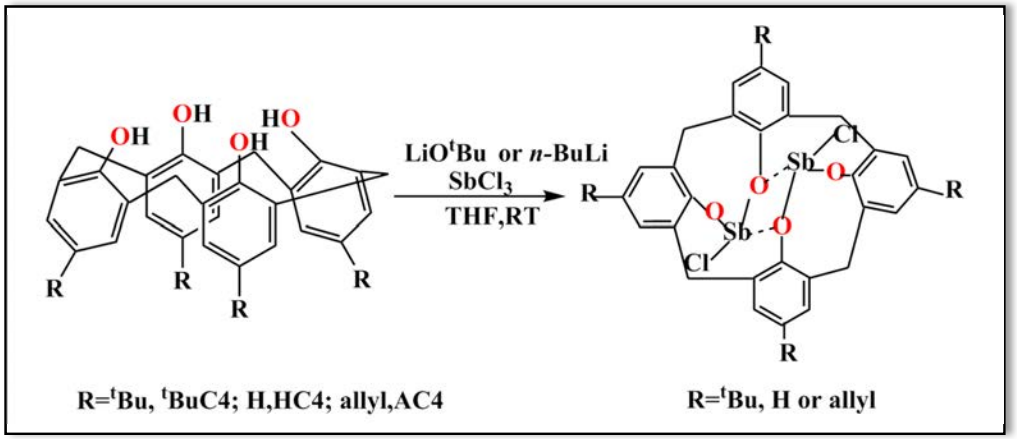

Equation 1.4

Later, Espinosa and Hanna reported a chain of calix[5]arene Sb^{+3} mono complexes $[Sb\{Bu^tC5(H)_2\}]$ from either the reaction of *p-tert*-butylcalix[5]arene ($Bu^tC5(H)_5$) trianionic salts $M'_3{\cdot}Bu^tC5(H)_2$ (M' = Li, Na, K) with $SbCl_3$ or by reacting $Bu^tC5(H)_5$ in a 1:1 ratio with $M(OBu^t)_3$ in lower yield. $[Bu^tC5(Bn)(H)_4]$ reacts with $Sb(NMe_2)_3$ or $Sb(OBu^t)_3$ in a 1:2 ratio to produce the bimetallic complex $[Sb_2O\{Bu^tC5(Bn)\}]$. Treatment of calix[5]arene $[HC5(H)_5]$ with ¾ equivalents of $Sb(NMe_2)_3$ yielded the bimetallic complex $[Sb_2O\{HC5(H)\}]$. The reaction of $[Sb\{Bu^tC5(H)_2\}]$ with $Sb(OBu^t)_3$ in a 1:1 ratio yields $[Sb_2O\{Bu^tC5(H)\}]$.[154]

In 1998, a room temperature metathesis reaction of $SbCl_3$ with a solution of $Li[OC_6H_2Bu^t_3\text{-}2,4,6]$ in THF led to the production of colourless block crystals of $SbCl_2(OC_6H_2Bu^t{}_3\text{-}2,4,6)$.[157]

The first monomeric Sb^{+3} aryloxide $Sb(OC_6H_3Me_2)_3$ that adopts a trigonal pyramidal geometry, has been synthesised by a direct reaction between 2,6-$Me_2C_6H_3OH$ with $Sb(NMe_2)_3$ in hexane, which was redissolved in toluene from which colourless crystals were obtained.[23] This complex is important as a precursor for the chemical vapour deposition (CVD) of Sb_2O_3 and Sb_6O_{13} thin films,[14] which have many potential applications, including parts of electronic ceramics and catalysis.[158,159] Phenol has an affinity with electropositive metals, forming a protective surface oxide layer.

Homoleptic $[Sb(Odpp)_3]\cdot C_6H_{12}$; HOdpp = 2,6-diphenylphenol) has been synthesised by direct reaction of anhydrous $SbCl_3$ with LiOdpp in THF having a mononuclear distorted trigonal pyramidal geometry in the solid state (eqn. 1.5).[22]

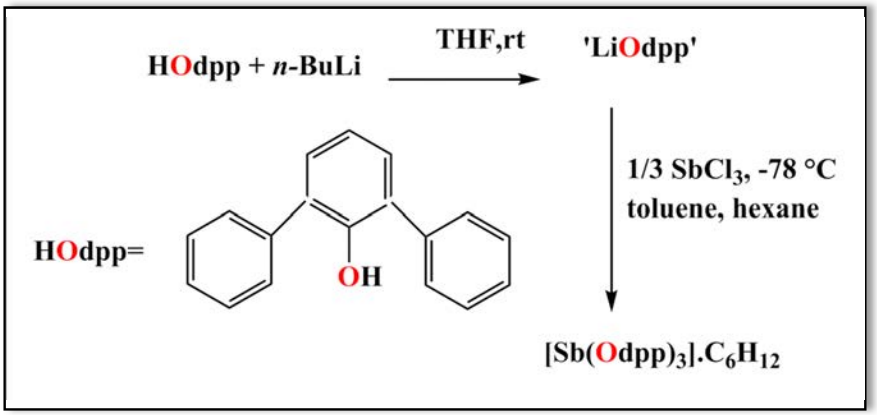

Equation 1.5

A few years ago, Tanski *et al.* prepared a mixture of antimony compounds involving multidentate aryloxide ligands, $N(o\text{-}C_6H_4OH)_3$ and $PhN(o\text{-}C_6H_4OH)_2$. These complexes are $[\eta^4\text{–}N(o\text{-}C_6H_4O)_3]Sb(OSMe_2)$, $\{\{[\eta^3\text{-}N(o\text{-}C_6H_4OH)(o\text{-}C_6H_4O)_2]Sb\}_2(\mu_2\text{-}O)\}_2$ and $\{[\eta^3\text{-}PhN(o\text{-}C_6H_4O)_2]Sb\}_4$ $(\mu_3\text{-}O)_2$, in addition to $[\eta^4\text{-}N(o\text{-}C_6H_4O)_3]Sb(OSMe_2)$, which present as a discrete mononuclear species and multinuclear oxo complexes $\{\{[\eta^3\text{-}N(o\text{-}C_6H_4OH)(o\text{-}C_6H_4O)_2]Sb\}_2(\mu_2\text{-}O)\}_2$ and $\{[\eta^3\text{-}PhN(o\text{-}C_6H_4O)_2]Sb\}_4(\mu_3\text{-}O)_2$.[160] Syntheses of antimony and aluminium phenolate complexes is presented in detail in ***Appendix 1 and Appendix 2*** of this thesis.

1.6 *The Current Study*

This thesis presents work done, including the formation and characterisation of a range of varied ArForm antimony and aluminium complexes using two ArForm ligands with different functionalities (Figure 1.16). In addition, the chemistry of antimony N,N-dialkyl-N'-2,3,5,6-tetrafluorophenylethane-1,2-di-aminate complexes is discussed, and the thesis further explores the phenolate complexes. The ligands shown in (Fig. 1.16) were selected, firstly, to study the possible coordination modes of the amidates and phenolate functional group. Secondly, these ligands contain electron donating substituents (NH, OH) in different positions, which can have an impact on the properties and final composition of the antimony complex.

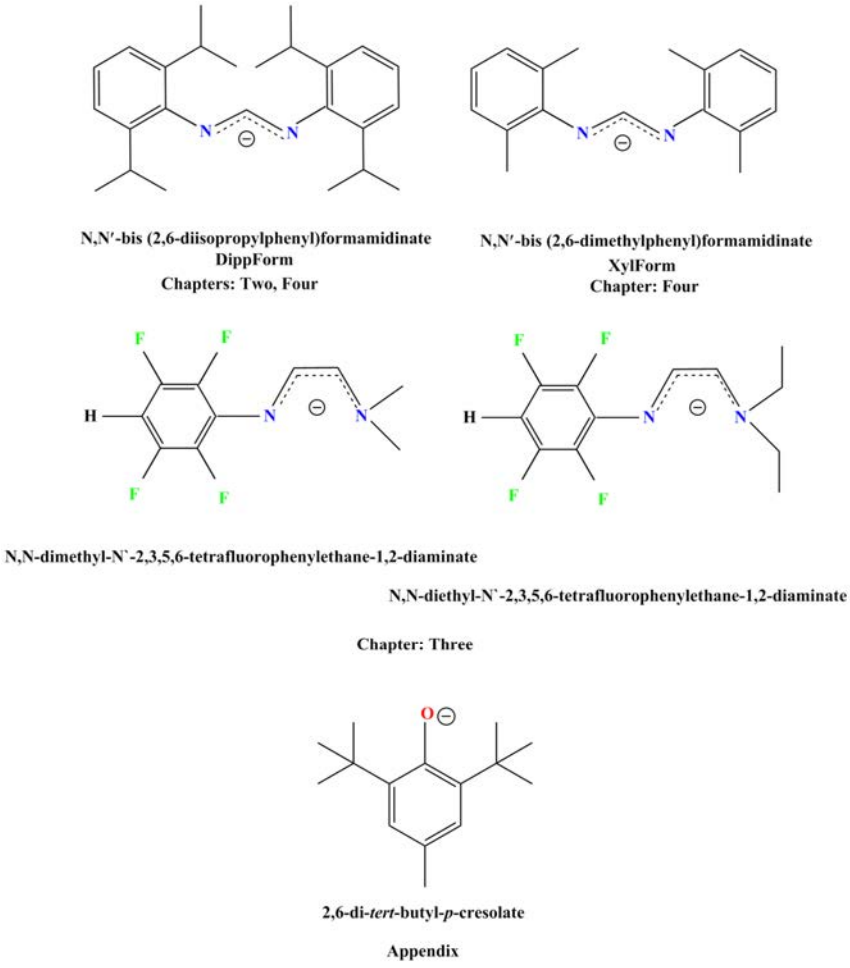

Figure 1.16 Substituted formamidinate, polyfluorophenylethylenediaminate and phenolate ligand used in this work.

Salt metathesis in THF/PhMe was the method used to synthesise the majority of trivalent antimony and aluminium ArForm complexes. ***Chapter 2*** describes the successful use of the N,N′-bis(2,6-diisopropylphenyl)formamidinate DippForm ligand for stabilisation of both Sb(III) and Sb(I) compounds presenting the synthesis, characterisation and structural features of these complexes with the general formula $[Sb(DippForm)_{3-n}X_n]$ (n = 2,1) {X = Cl, Br, I}. Initially, complexes were generated by the reaction of M(DippForm) with SbX_3 through the metathesis method utilising three different solvent media (THF, PhMe, and hexane) and four different reagents (M = *n*-BuLi, $LiN(SiMe_3)_2$, $NaN(SiMe_3)_2$, $KN(SiMe_3)_2$), where the oxidation state of one resulting complex was reliant on the reagent used. Indeed, this technique proved to be an effective synthetic route to trivalent antimony DippForm complexes. Additionally, treatment of haloformamidinatoantimony with tetramethylethylendiamine (TMEDA), has been investigated to increase the scope of the haloorganoantimony system that unpredictably led to the creation of μ-oxygen bridged dinuclear antimony **$[(Dipp)ClSb\text{-}\mu\text{-}OSbCl_2(Me_2NC_2H_4NMe_2)]_2.C_6D_6$**. This result can open exciting novel investigations into the coordination manner that occurs in this reaction. However, when $Hg(C_6F_5)_2$, the material usually used as a reagent in the redox transmetallation/ protolysis (RTP) protocol, was employed in a reaction of the bulky DippForm ligand system with SbX_3, the result was unforeseen. Formation of the dimeric compound, **$[Sb(DippForm)(NSiMe_3)]_2$**, is also discussed in this chapter.

Chapter 3 discusses the use of N,N-dimethyl-N'-2,3,5,6-tetrafluorophenylethane-1,2-di-aminate in metathesis reactions. A series of mononuclear heteroleptic and homoleptic $[Sb(p\text{-}HC_6F_4NC_2H_4NMe_2)_{3-n}Cl_n]$ (n = 2, 1, 0) complexes has been obtained by this method, and showed interesting structures. More specifically, an antimony (III) in $[Sb(p\text{-}HC_6F_4NC_2H_4NMe_2)_{3-n}Cl_n]$ (n = 2) was successfully generated by an alternative synthetic method, namely direct reaction between $p\text{-}HC_6F_4NHC_2H_4NMe_2$ and $SbCl_3$ in THF.

Chapter 4 ventures away from the chemistry of antimony formamidinate and further explores the extensive coordination chemistry of aluminium formamidinate complexes $[Al(ArForm)_{3-n}X_n]$ {(Form (ArNCHNAr) = XylForm (Ar = 2,6-$Me_2C_6H_3$), DippForm (Ar = 2,6-*i*$Pr_2C_6H_3$); X = Cl, Br, I} in terms of structures and synthesis, where it appears that these complexes preferentially produce monomeric units. Diversity of heteroleptic aluminium formamidinates complexes has been demonstrated, with new binding modes to aluminium identified, new synthetic methods determined using different metal alkyls/amides as reagents, for example, $AlMe_3$, *n*-BuLi, $LiN(SiMe_3)_2$, $NaN(SiMe_3)_2$ and $KN(SiMe_3)_2$ in THF/PhMe. An ionic **$[Me_3Sb\text{-}SbMe_2][AlCl_4]$** and **$[Br_4Sb\text{-}SbBr_3][AlCl_2(thf)_4]$** structures consequential from these reactions are also discussed.

The appendix section contains the use of (2,6-di–tert-butyl-4-Me) (HOAr) in metathesis reactions. A mononuclear **$[Sb(OAr)_3]$** complex has been prepared by this method, and **$[Al(OAr)(OH_2)Cl(thf)]$**, and structural features are discussed.

By navigating between chapters of this thesis, a wide range of antimony and aluminium amidates and phenolate complexes has been demonstrated, showing somewhat new binding modes to antimony and aluminium, new synthetic manipulations identified along with the known former technic methods, and the outcomes have offered many more prospects for further interesting chemistry.

1.7 *References*

1. R. E. Krebs, *The history and use of our earth's chemical elements: a reference guide*, Greenwood Publishing Group, 2006.
2. C. N. Singman, *J. Chem. Educ.*, 1984, **61**, 137-142.
3. G. Audi, O. Bersillon, J. Blachot and A. H. Wapstra, *Nucl. Phys. A.*, 2003, **729**, 3-128.
4. M. O. Andreae, J. F. Asmode, P. Foster and L. Van 't dack, *Anal. Chem.*, 1981, **53**, 1766-1771.
5. M. S. P. Niedzielski, J. Przybyłek and J. Siepak, *Pol. J. Environ. Stud.*, 2002, **11**, 457-466.
6. A. Ilander and A. Väisänen, *Anal. Chim. Acta.*, 2011, **689**, 178-183.
7. E. R. T. Tiekink, *Crit. Rev. Oncol. Hematol.*, 2002, **42**, 217-224.
8. J.-S. Li, M. Yong-Qiang, J.-R. Cui and R.-Q. Wang, *Appl. Organomet. Chem.*, 2001, **15**, 639-645.
9. C. Demicheli and F. Frezard, *Drug Design Rev.*, 2005, **2**, 243-249.
10. P. Shaked-Mishan, N. Ulrich, M. Ephros and D. Zilberstein, *J. Biol. Chem.*, 2001, **276**, 3971-3976.
11. Y. Zhou, N. Messier, M. Ouellette, B. P. Rosen and R. Mukhopadhyay, *J. Biol. Chem.*, 2004, **279**, 37445-37451.
12. R. Ge and H. Sun, *Acc. Chem. Res.*, 2007, **40**, 267-274.
13. C. Demicheli, F. Frezard, J. B. Mangrum and N. P. Farrell, *Chem. Commun.*, 2008, **39**, 4828-4830.
14. P. W. Haycock, G. A. Horley, K. C. Molloy, C. P. Myers, S. A. Rushworth and L. M. Smith, *Chem. Vap. Deposition.*, 2001, **7**, 191-193.
15. D. C. Bradley, *Chem. Rev.*, 1989, **89**, 1317-1322.
16. D. C. Bradley, *Polyhedron.*, 1994, **13**, 1111-1121.
17. K. G. Caulton and L. G. Hubert-Pfalzgraf, *Chem. Rev.*, 1990, **90**, 969-995.
18. W. G. Van der Sluys and A. P. Sattelberger, *Chem. Rev.*, 1990, **90**, 1027-1040.
19. R. C. Mehrotra, A. Singh and S. Sogani, *Chem. Rev.*, 1994, **94**, 1643-1660.
20. R. K. Grasselli and J. D. Burrington, *in Advances in Catalysis, eds.* D. D. Eley, H. Pines and P. B. Weisz, Academic Press, 1981, **30**, 133-163.

21. G. Centi and S. Perathoner, *Appl. Catal: A.*, 1995, **124**, 317-337.
22. M. Brym, C. Jones and P. C. Junk, *Main Group Chem.*, 2006, **5**, 13-19.
23. G. A. Horley, M. F. Mahon, K. C. Molloy, M. M. Venter, P. W. Haycock and C. P. Myers, *Inorg. Chem.*, 2002, **41**, 1652-1657.
24. L. Liu, L. N. Zakharov, J. A. Golen, A. L. Rheingold and T. A. Hanna, *Inorg. Chem.*, 2008, **47**, 11143-11153.
25. S. M. Biros, B. M. Bridgewater, A. Villeges-Estrada, J. M. Tanski and G. Parkin, *Inorg. Chem.*, 2002, **41**, 4051-4057.
26. S. C. Wilson, P. V. Lockwood, P. M. Ashley and M. Tighe, *Environ. Pollut.*, 2010, **158**, 1169-1181.
27. H. G. Seiler, H. Sigel and A. Sigel, *Handbook on Toxicity of Inorganic Compounds*., New York, 1988, 67-76.
28. J. R. R. F. s. d. Silva, *The biological chemistry of the elements : the inorganic chemistry of life / J.J.R. Frausto da Silva and R.J.P. Williams*, Clarendon Press; Oxford University Press, Oxford [England] : New York, 1991.
29. D. Rabinovich, *Advanced Inorganic Chemistry, 6th Edition (Cotton, F. A.; Wilkinson, G.; Murillo, C. A.; Bochmann, M.)*, 2000.
30. V. Gutmann, H. Hubacek and A. Steininger, *Monatsh. Chem.*, 1964, **95**, 678-686.
31. R. Benn, A. Rufińska, H. Lehmkuhl, E. Janssen and C. Krüger, *Angew. Chem. Int. Ed.*, 1983, **22**, 779-780.
32. P. P. Power, *J. Chem. Soc., Dalton Trans.*, 1998, 2939-2951.
33. P. P. Power, *Chem. Rev.*, 1999, **99**, 3463-3504.
34. H. Roesky and S. Kumar, *Chem. Commun.*, 2005, **32**, 4027-4038.
35. M. Zanetti, G. Camino, D. Canavese, A. B. Morgan, F. J. Lamelas and C. A. Wilkie, *Chem. Mater.*, 2002, **14**, 189-193.
36. S. Zhang and A. R. Horrocks, *Prog. Polym. Sci.*, 2003, **28**, 1517-1538.
37. N. M. Stark, R. H. White, S. A. Mueller and T. A. Osswald, *Polym. Degrad. Stab.*, 2010, **95**, 1903-1910.
38. E. D. Weil, *Fire retardancy of polymeric materials*, 2000, 115-145.
39. K. L. Stemmer, *Pharmacology & Therapeutics. Part A: Chemotherapy, Toxicology and Metabolic Inhibitors.*, 1976, **1**, 157-160.

40. A. Léonard and G. B. Gerber, *Mutat. Res-Rev. Gen. Tox.*, 1996, **366**, 1-8.
41. H. SQu, W. Wu, Y. Zheng, J. Xie and J. Xu, *Fire Safety J.*, 2011, **46**, 462-467.
42. E. A. Starke and J. T. Staley, *Prog. Aerosp. Sci.*, 1996, **32**, 131-172.
43. W. S. Miller, L. Zhuang, J. Bottema, A. J. Wittebrood, P. De Smet, A. Haszler and A. Vieregge, *Mater. Sci. Eng: A.*, 2000, **280**, 37-49.
44. M. J. Starink, *Mater. Sci. Technol.*, 2013, **17**, 1324-1328.
45. J. P. Lyle, D. A. Granger and R. E. Sanders, in *Ullmann's Encyclopedia of Industrial Chemistry*, Wiley-VCH Verlag GmbH & Co. KGaA, 2000.
46. E. B. Lindblad, *Vaccine.*, 2004, **22**, 3658-3668.
47. J. D. Berman, *Rev. Infect. Dis.*, 1988, **10**, 560-586.
48. A. Dougall, C. Shilton, J. Low Choy, B. Alexander and S. Walton, *Epidemiol. Infect.*, 2009, **137**, 1516-1520.
49. K. C. Kato, E. Morais-Teixeira, P. G. Reis, N. M. Silva-Barcellos, P. Salaün, P. P. Campos, J. Dias Corrêa-Junior, A. Rabello, C. Demicheli and F. Frézard, *Antimicrob. Agents Chemother.*, 2014, **58**, 481-488.
50. D. Marcovich and R. E. Tapscott, *J. Am. Chem. Soc.*, 1980, **102**, 5712-5717.
51. J. Duffin and P. RenÉ, *J. Hist. Med. Allied Sci.*, 1991, **46**, 440-456.
52. S. L. Croft and G. H. Coombs, *Trends. Parasitol.*, 2003, **19**, 502-508.
53. P. D. Marsden, *Revista da Sociedade Brasileira de Medicina Tropical*, 1985, **18**, 187-198.
54. J. D. Berman, *Clin. Infect. Dis.*, 1997, **24**, 684-703.
55. P. J. Guerin, P. Olliaro, S. Sundar, M. Boelaert, S. L. Croft, P. Desjeux, M. K. Wasunna and A. D. M. Bryceson, *Lancet. Infect. Dis.*, 2002, **2**, 494-501.
56. F. Frézard, P. S. Martins, M. C. M. Barbosa, A. M. C. Pimenta, W. A. Ferreira, J. E. de Melo, J. B. Mangrum and C. Demicheli, *J. Inorg. Biochem.*, 2008, **102**, 656-665.
57. S. Yan, L. Jin and H. Sun, *in Metallotherapeutic Drugs and Metal-Based Diagnostic Agents.*, John Wiley & Sons, Ltd, 2005, 441-461.
58. C. d. S. Ferreira, P. S. Martins, C. Demicheli, C. Brochu, M. Ouellette and F. Frézard, *Biometals.*, 2003, **16**, 441-446.
59. W. L. Roberts, J. D. Berman and P. M. Rainey, *Antimicrob. Agents Chemother.*, 1995, **39**, 1234-1239.

60. S. Wyllie and A. H. Fairlamb, *Biochem. Pharmacol.*, 2006, **71**, 257-267.
61. G. Sudhandiran and C. Shaha, *J. Biol. Chem.*, 2003, **278**, 25120-25132.
62. P. Guéguéniat, P. B. Du Bois, R. Gandon, J. C. Salomon, Y. Baron and R. Leon, *Estuar. Coast. Shelf Sci.*, 1994, **39**, 59-74.
63. M. P. Coles and R. F. Jordan, *J. Am. Chem. Soc.*, 1997, **119**, 8125-8126.
64. M. P. Coles, D. C. Swenson, R. F. Jordan and V. G. Young, *Organometallics.*, 1997, **16**, 5183-5194.
65. E. Winterfeldt, *Synthesis.*, 1975, **1975**, 617-630.
66. R. Affani and D. Dugat, *Synth. Commun.*, 2007, **37**, 3729-3740.
67. H. Sinn and W. Kaminsky, *in Adv. Organomet. Chem., eds.* F. G. A. Stone and R. West, Academic Press, 1980, **18**, 99-149.
68. H. Sinn, W. Kaminsky, H. J. Vollmer and R. Woldt, *Angew. Chem. Int. Ed.*, 1980, **19**, 390-392.
69. W. Kaminsky, *Macromolecules.*, 2012, **45**, 3289-3297.
70. B. Xiao, L. P. Wang, R. H. Mei and G. Y. Wang, *Asian J. Chem.*, 2012, **24**, 42-46.
71. J. Barker and M. Kilner, *Coord. Chem. Rev.*, 1994, **133**, 219-300.
72. R. M. Roberts, *J. Organ. Chem.*, 1949, **14**, 277-284.
73. J. A. R. Schmidt, *J. Chem. Soc., Dalton Trans.*, 2002, 3454-3461.
74. C. A. Nijhuis, Jellema E., Sciarone T. J. J., Meetsma A., Budzelaar P. H. M., Hessen B, *Eur. J. Inorg. Chem.*, 2005, 2089-2099.
75. V. Volkis, E. Nelkenbaum, A. Lisovskii, G. Hasson, R. Semiat, M. Kapon, M. Botoshansky, Y. Eishen and M. S. Eisen, *J. Am. Chem. Soc.*, 2003, **125**, 2179-2194.
76. V. C. Gibson and S. K. Spitzmesser, *Chem. Rev.*, 2003, **103**, 283-316.
77. R. J. Keaton, L. A. Koterwas, J. C. Fettinger and L. R. Sita, *J. Am. Chem. Soc.*, 2002, **124**, 5932-5933.
78. J. M. Decker, S. J. Geib and T. Y. Meyer, *Organometallics.*, 1999, **18**, 4417-4420.
79. G. Talarico and P. H. M. Budzelaar, *Organometallics.*, 2000, **19**, 5691-5695.

80. M. P. Coles, D. C. Swenson and R. F. Jordan, *Organometallics*., 1998, **17**, 4042-4048.
81. M. P. Coles, D. C. Swenson, R. F. Jordan and V. G. Young, *Organometallics*., 1997, **16**, 5183-5194.
82. M. P. Coles and R. F. Jordan, *J. Am. Chem. Soc*., 1997, **119**, 8125-8126.
83. A. L. Brazeau, Z. Wang, C. N. Rowley and S. T. Barry, *Inorg. Chem*., 2006, **45**, 2276-2281.
84. B. S. Lim, A. Rahtu, J. Park and R. G. Gordon, *Inorg. Chem*., 2003, **42**, 7951-7958.
85. B. S. Lim, A. Rahtu and R. G. Gordon, *Nat. Mater.*, 2003, **2**, 749-754.
86. Z. Li, S. T. Barry and R. G. Gordon, *Inorg. Chem.*, 2005, **44**, 1728-1735.
87. Z. Li, A. Rahtu and R. G. Gordon, *J. Electrochem. Soc.*, 2006, **153**, C787-C794.
88. C. E. Radzewich, M. P. Coles and R. F. Jordan, *J. Am. Chem. Soc.*, 1998, **120**, 9384-9385.
89. S. Dagorne, I. A. Guzei, M. P. Coles and R. F. Jordan, *J. Am. Chem. Soc.*, 2000, **122**, 274-289.
90. S. Bambirra, M. W. Bouwkamp, A. Meetsma and B. Hessen, *J. Am. Chem. Soc.*, 2004, **126**, 9182-9183.
91. S. Dagorne and D. A. Atwood, *Chem. Rev.*, 2008, **108**, 4037-4071.
92. A. Baunemann, D. Bekermann, T. B. Thiede, H. Parala, M. Winter, C. Gemel and R. A. Fischer, *Dalton Trans.*, 2008, 3715-3722.
93. J. P. Coyle, W. H. Monillas, G. P. A. Yap and S. T. Barry, *Inorg. Chem.*, 2008, **47**, 683-689.
94. A. L. Brazeau, Z. Wang, C. N. Rowley and S. T. Barry, *Chem. Mater.*, 2008, **20**, 7287-7291.
95. J. P. Coyle, P. A. Johnson, G. A. DiLabio, S. T. Barry and J. Müller, *Inorg. Chem.*, 2010, **49**, 2844-2850.
96. S. Enthaler, K. Schröder, S. Inoue, B. Eckhardt, K. Junge, M. Beller and M. Drieß, *Eur. J. Org. Chem.*, 2010, 4893-4901.

97. H.-R. Tsou, N. Mamuya, B. D. Johnson, M. F. Reich, B. C. Gruber, F. Ye, R. Nilakantan, R. Shen, C. Discafani, R. DeBlanc, R. Davis, F. E. Koehn, L. M. Greenberger, Y.-F. Wang and A. Wissner, *J. Med. Chem.,* 2001, **44**, 2719-2734.

98. Y. D. Wang, D. H. Boschelli, S. Johnson and E. Honores, *Tetrahedron.*, 2004, **60**, 2937-2942.

99. D. S. Yoon, Y. Han, T. M. Stark, J. C. Haber, B. T. Gregg and S. B. Stankovich, *Org. lett.*, 2004, **6**, 4775-4778.

100. C. Willemann, R. Grünert, P. J. Bednarski and R. Troschütz, *Bioorg. Med. Chem.*, 2009, **17**, 4406-4419.

101. A. Foucourt, C. Dubouilh-Benard, E. Chosson, C. Corbière, C. Buquet, M. Iannelli, B. Leblond, F. Marsais and T. Besson, *Tetrahedron.*, 2010, **66**, 4495-4502.

102. O. Kim, Y. Jeong, H. Lee, S. S. Hong and S. Hong, *J. Med. Chem.*, 2011, **54**, 2455-2466.

103. J. E. Taylor, S. D. Bulla and J. M. J. Williamsa, *Chem. Soc. Rev.*, 2012, **41**, 2109-2121.

104. M. A. Matulenko and A. I. Meyers, *J. Org. Chem.*, 1996, **61**, 573-580.

105. D. I. Arnold, F. A. Cotton, J. H. Matonic and C. A. Murillo, *Polyhedron.*, 1997, **16**, 1837-1841.

106. D. B. Mitzi and K. Liang, *J. Solid State. Chem.*, 1997, **134**, 376-381.

107. J. E. Taylor, S. D. Bull and J. M. Williams, *Chem. Soc. Rev.*, 2012, **41**, 2109-2121.

108. P. C. Junk and M. L. Cole, *Chem. Commun.*, 2007, **16**, 1579-1590.

109. M. L. Cole and P. C. Junk, *J. Organomet. Chem.*, 2003, **666**, 55-62.

110. J.-A. Gautier, M. Miocque and C. C. Farnoux, in *The chemistry of amidines and imidates*, ed. S. Patai, Wiley, London, 1975, **1**, ch. 7, 283–348.

111. M. P. Coles, *Dalton Trans.*, 2006, 985-1001.

112. Boer, eacute, Ren, eacute and T, *J. Chem. Soc., Dalton trans.*, 1998, 4147-4154.

113. S. H. Oakley, D. B. Soria, M. P. Coles and P. B. Hitchcock, *Dalton Trans.*, 2004, 537-546.

114. L. Bourget-Merle, M. F. Lappert and J. R. Severn, *Chem. Rev.*, 2002, **102**, 3031-3066.

115. P. J. Bailey and S. Pace, *Coord. Chem. Rev.*, 2001, **214**, 91-141.

116. F. T. Edelmann, *in Adv. Organomet. Chem., eds.* A. F. Hill and M. J. Fink, Academic Press, 2008, **57**, 183-352.

117. M. L. Cole, P. C. Junk and L. M. Louis, *J. Chem. Soc., Dalton Trans.*, 2002, 3906-3914.

118. S. P. Green, C. Jones and A. Stasch, *Science.*, 2007, **318**, 1754-1757.

119. M. N. Sudheendra Rao, H. W. Roesky and G. Anantharaman, *J. Organomet. Chem.*, 2002, **646**, 4-14.

120. S. P. Green, C. Jones, P. C. Junk, K.-A. Lippert and A. Stasch, *Chem. Commun.*, 2006, 3978-3980.

121. S. P. Green, C. Jones, G. Jin and A. Stasch, *Inorg. Chem.*, 2007, **46**, 8-10.

122. C. Cui, H. W. Roesky, H.-G. Schmidt, M. Noltemeyer, H. Hao and F. Cimpoesu, *Angew. Chem. Int. Ed.*, 2000, **39**, 4274-4276.

123. N. J. Hardman, B. E. Eichler and P. P. Power, *Chem. Commun.*, 2000, 1991-1992.

124. C. Jones, P. C. Junk, J. A. Platts and A. Stasch, *J. Am. Chem. Soc.*, 2006, **128**, 2206-2207.

125. G. Jin, C. Jones, P. C. Junk, A. Staschab and W. D. Woodula, *New J. Chem.*, 2008, **32**, 835-842.

126. C. Jones, P. C. Junk, J. A. Platts and A. Stasch, *J. Am. Chem. Soc.*, 2006, **128**, 2206-2207.

127. P. J. Bailey, R. O. Gould, C. N. Harmer, S. Pace, A. Steiner and D. S. Wright, *Chem. Commun.*, 1997, 1161-1162.

128. R. M. Roberts, *J. Org. Chem.*, 1949, **14**, 277-284.

129. L. M. Opris, A. Silvestru, C. Silvestru, H. J. Breunig and E. Lork, *Dalton Trans.*, 2004, 3575-3585.

130. L. Weber, *Angew. Chem. Int. Ed.*, 2002, **41**, 563-572.

131. M. Brym, C. M. Forsyth, C. Jones, P. C. Junk, R. P. Rose, A. Stasch and D. R. Turner, *Dalton Trans.*, 2007, 3282-3288.

132. L. A. Lesikar and A. F. Richards, *J. Organomet. Chem.*, 2006, **691**, 4250-4256.

133. B. Lyhs, S. Schulz, U. Westphal, D. Bläser, R. Boese and M. Bolte, *Eur. J. Inorg. Chem.*, 2009, 2247-2253.
134. D. DuBois, E. N. Duesler and R. T. Paine, *J. Chem. Soc., Chem. Commun.*, 1984, 488-489.
135. A. Hinz, J. Rothe, A. Schulz and A. Villinger, *Dalton Trans.*, 2016, **45**, 6044-6052.
136. D. P. Buxton, G. B. Deacon, B. M. Gatehouse, I. L. Grayson and D. S. Black, *Aust. J. Chem.*, 1988, **41**, 943-956.
137. G. B. Deacon, B. M. Gatehouse and J. Ireland, *Aust. J. Chem.*, 1991, **44**, 1669-1681.
138. D. P. Buxton, G. B. Deacon, B. M. Gatehouse, I. L. Grayson, R. J. Thomson and D. S. Black, *Aust. J. Chem.*, 1986, **39**, 2013-2036.
139. D. P. Buxton and G. B. Deacon, *Polyhedron.*, 1991, **10**, 747-751.
140. D. P. Buxton, G. B. Deacon, A. M. James, S. J. Knowles and T. L. Williams, *Polyhedron.*, 1989, **8**, 2943-2945.
141. D. R. Click, B. L. Scott and J. G. Watkin, *Chem. Commun.*, 1999, 633-634.
142. H. Memmler, K. Walsh, L. H. Gade and J. W. Lauher, *Inorg. Chem.*, 1995, **34**, 4062-4068.
143. A. n. Lara-Sanchez, A. Rodriguez, D. L. Hughes, M. Schormann and M. Bochmann, *J. Organomet. Chem.*, 2002, **663**, 63-69.
144. G. B. Deacon, C. M. Forsyth, P. C. Junk and J. Wang, *Chemistry.*, 2009, **15**, 3082-3092.
145. G. B. Deacon, C. M. Forsyth, P. C. Junk, R. P. Kelly, A. Urbatsch and J. Wang, *Dalton Trans.*, 2012, **41**, 8624-8634.
146. G. B. Deacon, P. C. Junk, R. P. Kelly and J. Wang, *Dalton trans.*, 2016, **45**, 1422-1435.
147. R. Anwander, *Angew. Chem. Int. Ed.*, 2002, **41**, 1801-1803.
148. T. Kremer and P. V. Schleyer, *Organometallics.*, 1997, **16**, 737-746.
149. B. G. Tehan, E. J. Lloyd, M. G. Wong, W. R. Pitt, J. G. Montana, D. T. Manallack and E. Gancia, *Quantitative structure-activity relationships*, 2002, **21**, 457-472.

150. D. Bradley, R. C. Mehrotra, I. Rothwell and A. Singh, *Alkoxo and aryloxo derivatives of metals*, Academic press, 2001.
151. J. S. Vilardo, M. A. Lockwood, L. G. Hanson, J. R. Clark, B. C. Parkin, P. E. Fanwick and I. P. Rothwell, *J. Chem. Soc., Dalton Trans.*, 1997, 3353-3362.
152. J. Pospíšil, *Polym. Degrad. Stab.*, 1988, **20**, 181-202.
153. S. del Teso, aacute and K. nchez, *J. vinyl Add. Tech.*, 2016, **22**, 117-127.
154. D. Mendoza-Espinosa and T. A. Hanna, *Dalton Trans.*, 2009, 5211-5225.
155. N. Tempel, W. Schwarz and J. Weidlein, *Z. Anorg. Allg. Chem.*, 1981, **474**, 157-170.
156. H. Fleischer, H. Bayram, S. Elzner and N. W. Mitzel, *J. Chem. Soc., Dalton Trans.*, 2001, 373-377.
157. P. Hodge, S. C. James, N. C. Norman and A. Guy Orpen, *J. Chem. Soc., Dalton trans*, 1998, 4049-4054.
158. Z. Tianshu and P. Hing, *J. Mater. Sci.- Mater. Electron.*, 1999, **10**, 509-518.
159. R. J. Cava, R. J. Cava, J. J. Krajewski, Y. L. Qin and H. W. Zandbergen, *J. Mater. Res.*, 2000, **15**, 2672-2676.
160. J. M. Tanski, B. V. Kelly and G. Parkin, *Dalton Trans.*, 2005, 2442-2447.

CHAPTER TWO

SYNTHESIS AND STRUCTURAL CHARACTERISATION OF HETEROLEPTIC ANTIMONY (I) AND (III) COMPLEXES INVOLVING FORMAMIDINATE LIGANDS

Outline

This chapter presents the synthesis and structural characterisation of a range of mono- and tri-valent antimony N,N′-*bis*(2,6-diisopropylphenyl)formamidinate complexes. Conventionally, the syntheses were by treatment of the deprotonated formamidine ligand with anhydrous SbX_3 (X = Cl, Br, I) in THF and/or PhMe under varying conditions. Halo- and nonhalo-formamidinatoantimony complexes have been successfully gained as monomers or dimers in the solid state featuring a variety of coordination geometries and have been comprehensively characterised. Mono- and bis-substituted formamidinato antimony (III) complexes are expected to have stereochemically active lone pairs of electrons, except where the coordination number is high. To the best of our knowledge, there have been no formamidinato antimony (III) structures reported to date, which have prompted us to further study this field.

2.1 *Introduction*

Study on the potentially bioactive organometallic compounds revealed that the activity of these types of compounds vastly relies on: the nature and number of organic groups, nature of ligands, existence of fluoro substituents for hydrophilic and lipophilic components and the hydrolytic stability of the metal-carbon bond.[1] Nitrogen-based systems, such as amides, amidinates and guanidinates are of major importance, however the literature cites only a very few examples of mono- and tri-valent group 15 element complexes that have been isolated and crystallographically authenticated. The majority of the produced complexes however, are present in the trivalent oxidation state. Therefore, it is of interest to further explore the chemistry of amidinato antimony (III) complexes. The first structurally characterised mononuclear amidinato antimony (III) dichloride was $[Sb\{(Me_3SiN)_2CPh\}Cl_2]$ (Scheme 2.1), which was obtained by the reaction of N,N,N'-*tris*(trimethylsilyl)benzamidine, $[C_6H_5\text{-}C(NSiMe_3)N(SiMe_3)_2]$, with $SbCl_3$ in CH_2C1_2.[2] A guanidinato antimony (III), $[Sb\{(i\text{PrN})_2CN\text{-}(H)i\text{Pr}\}\{(i\text{PrN})_2CNi\text{Pr}\}]$, was obtained by the reaction between 1,2,3-triisopropylguanidine $[(i\text{PrNH})_2C{=}Ni\text{Pr}]$ with antimony *tris*(dimethylamide) $[Sb(NMe_2)_3]$ in PhMe, which featured the formation of helices through N–H···N hydrogen bonding of the single proton in the solid state of the complex.[3]

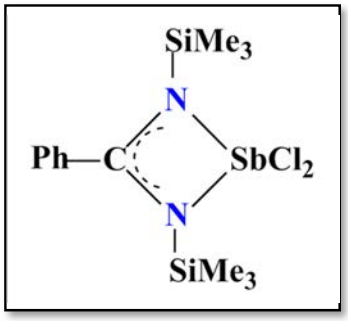

Scheme 2.1: $[Sb\{(Me_3SiN)_2CPh\}Cl_2]$.

A much more practicable route, namely salt metathesis, was adopted by the reaction of lithium amidate, [2-(6-methyl)pyridyl]trimethylsilylamido-lithium, with $SbCl_3$ in diethyl ether under a nitrogen atmosphere that led to acquisition of colourless prisms of the monomeric $Sb[\{2\text{-}(6\text{-}Me)C_5H_3N\}NSiMe_3]_2Cl$.[4] In 2006, Lesikar and Richards reported the novel β-diketiminato antimony crystalline complexes were also achieved by salt metathesis reactions between the appropriate lithium β-diketiminate with large steric demands, either (DippnacnacLi) (Dippnacnac = $[\{N(C_6H_3iPr_2 2,6)C(Me)\}_2CH]^-$) or (MesnacnacLi) (Mesnacnac = $[\{N(Mes)C(Me)\}_2CH]^-$, Mes = 2,4,6, trimethyl benzene) and antimony (III) halide SbX_3 (X = Br, Cl) in THF/PhMe (Scheme 2.2) that are dependent on the reaction stoichiometry, the R substituent on the nacnac and manipulation of the halide precursor.[5]

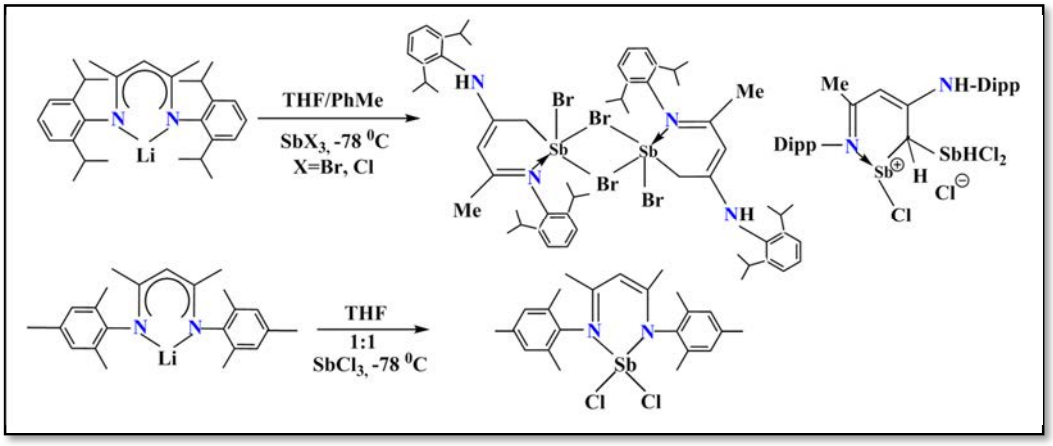

Scheme 2.2: Synthesis of the novel β-diketiminato antimony complexes.

The reactions of $SbCl_3$ with (Li_2bam) (bam = [PhB(N*t*Bu)$_2$]) (Scheme 2.3) in 1:1, 1:1.5 and 1:2 molar ratios in diethyl ether led to producing the *mono*-boraamidinate ClSb[PhB(N*t*Bu)$_2$], the novel 2:3 bam complex [PhB(N*t*Bu)$_2$]Sb-μ-N(*t*Bu)B(Ph)N(*t*Bu)-Sb[PhB(N*t*Bu)$_2$] and the *bis*-boraamidinate LiSb[PhB(N*t*Bu)$_2$]$_2$ respectively. In the structurally distinctive 2:3 bam complex, each metal center is chelated by the N,N'-bam ligand, and the two $[Sb(bam)]^+$ units are bridged by the third $[bam]^{2-}$ ligand.[6]

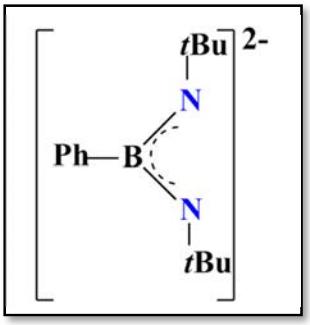

Scheme 2.3: bam = $[PhB(NtBu)_2]^{2-}$.

X-ray structural studies are reported for complexes $[Sb(L)X_2]\cdot(½\ thf)\cdot(½\ Et_2O)$, (X = Cl, Br) and $[\{SbI(L)(\mu\text{-}I)\}_2]\cdot(½\ Et_2O)$, which are generated in a good yield from reactions between $SbCl_3$, $SbBr_3$ or SbI_3 with an equivalent portion of β-dialdiminatopotassium, K[{N(C_6H_3*i*Pr$_2$-2,6)C(H)}$_2$CPh] (KL), as described by (Scheme 2.4). A feature that differentiates β-dialdiminato from the former β-diketiminato ligands is that substitution at any of the endocyclic carbon atoms is energetically prohibitive.[7]

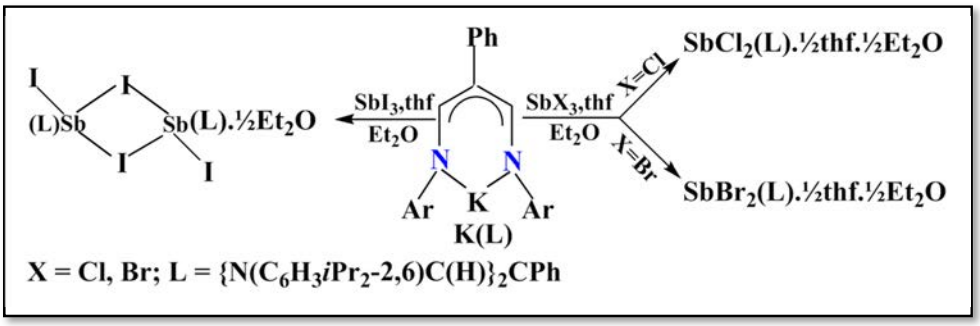

Scheme 2.4: Synthesis of $[Sb(L)X_2]\cdot(½\ thf)\cdot(½\ Et_2O)$ and $[\{SbI(L)(\mu\text{-}I)\}_2]\cdot(½\ Et_2O)$.

A set of *mono*-substituted antimony (III) amidinate complexes [Sb{*t*BuC(N*i*Pr)$_2$}Cl$_2$], [Sb{*t*BuC(NCy)$_2$}Cl$_2$], [Sb{*t*BuC(NDipp)$_2$}Cl$_2$] and [Sb{*n*BuC(N*i*Pr)$_2$}Cl$_2$] were gained in high yields by salt elimination reactions between $SbCl_3$ and Li-amidinates.[8]

N,N′-*bis*(aryl)amidinate (RNC(R')NR), more specifically the sterically demanding N,N′-*bis*(aryl)formamidinate (RNC(H)NR) ligands are a very distinct class of nitrogen based ligand. That distinction belongs to the ability of their phenyl substituents to be readily adjusted in order to achieve synthetic requirements, such as increasing steric bulk at the *ortho* position (H→*i*Pr) or modification of the electronic effects. Utilising amidinate ligands of high steric demand could result in complexes with uncommon coordination numbers, and also kinetically stabilising unusual oxidation states. For example, Brym, *et al*. have achieved a variety of bismuth (III) formamidinate complexes of the form Bi(Form)X_2, Bi(Form)$_2$X and Bi(Form)$_3$ through metathesis reactions of the alkali metal formamidinates M(RNC(H)NR), M = Li or K; R = C_6H_3-2,6-*i*Pr$_2$ (DippForm), C_6H_3-2,6-Et$_2$ (EtForm), C_6H_2-2,4,6-Me$_3$ (MesForm), C_6H_3-2,6-Me$_2$ (XylForm) or C_6H_4-2-Ph (*o*-PhForm), with BiX_3 (X= Cl, Br or *n*Bu).[9] The bulky substitutes affect the ligand's flexibility, and as a consequence, different coordination modes for all of the range of formamidinates can be adopted. Moreover, all the reported structures containing trivalent bismuth ions and formamidinate ligands have preferring displayed N,N′-chelation mode.[9] Bismuth (III) and antimony (III) are in the same group (group 15 of the periodic table) and therefore formamidinate ligands will potentially provide great opportunities for the appropriate expansion of organoamidoantimony (III) complexes. Stepping away from N,N' bidentate structures (Scheme 2.5), the monodentate *tris*(trimethylsilyl)amine N(SiMe$_3$)$_3$ reacted with $SbCl_3$ and produced an unusual nitridoantimony complex with a heterocubane framework [SbN(SbCl)$_3$(NSbCl$_2$)(NSiMe$_3$)$_2$.SbCl$_3$] in quantitative yield.[10] Also, (Me$_3$Si)$_2$N–SbCl$_2$ reacted with $GaCl_3$ at low temperature to produce a novel amino(chloro)stibenium cation, the recommended intermediate in methyl exchange reactions.

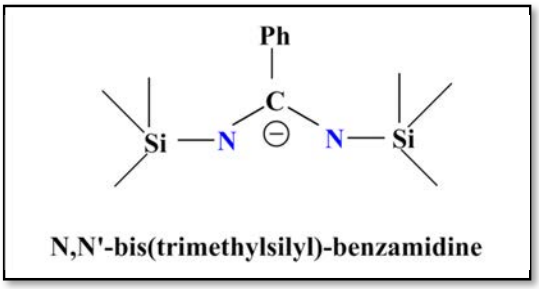

Scheme 2.5: A nitrogen-based ligand used to stabilise trivalent Sb ion.

In addition, a new type of silylated aminostibane compound of the type $Ter(Me_3Si)N{-}SbCl_2$ (Ter = terphenyl = 2,6-*bis*(2,4,6-trimethyl-phenyl)phenyl) can be treated with AgOTf, AgN_3, KO*t*Bu, $GaCl_3$, and $Me_3SiN_3/GaCl_3$ leading to triflate/methyl, azide/methyl, and chlorine/methyl exchange reactions at ambient temperature (Scheme 2.6).[11]

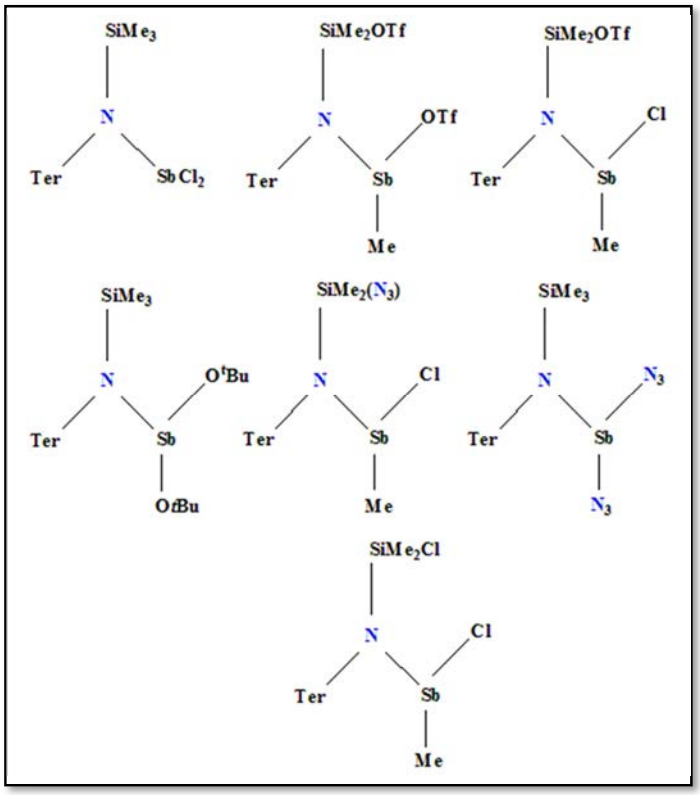

Scheme 2.6: Different products gained by triflate/methyl, azide/methyl, and chlorine/methyl exchange reactions with a silylated aminostibane.

Most of the antimony species discussed above were synthesised by salt metathesis protocols between the relevant antimony halide and the group one salt of the respective ligands. However, salt metathesis can have some weaknesses such as the requirement of two air-sensitive starting materials, as well, this method is practically dependent on the solubility of the anticipated product. The potential formation of group one "ate" components as side products is another synthetic obstacle, as was observed in some cases of the DippForm ligand system.[9] The reaction was 1:2 $BiBr_3$ and K(DippForm), which gave $[Bi(DippForm)Br(\mu\text{-}Br)(thf)]_2$ and K(DippForm).

Treatment of primary amine *tris*(trimethylsilyl)hydrazine, $R{-}N(SiMe_3)H$ (R = $Si(SiMe_3)_3$ = Hyp), with PCl_3 and base such as *n*-BuLi is the typical method to prepare *cyclo*-diphosphadiazanes, through formation of $R{-}N(SiMe_3)PCl_2$. A new synthetic technique leading to *cyclo*-diphosph (III)-azanes, $[R_fOP(\mu\text{-}NSiMe_3)]_2$, from a one pot reaction was simply by adding a mixture of R_fOH/base (R_fOH = hexafluoroisopropanol) to trimethylsilyl-substituted amino(dichloro)phosphanes $R{-}N(SiMe_3)PCl_2$ (Scheme 2.7). The difficulties arising from preparation of *cyclo*-diphosphadiazanes depend on the preliminary materials, solvents, and bases due to the rivalry of different potential reactions.[12]

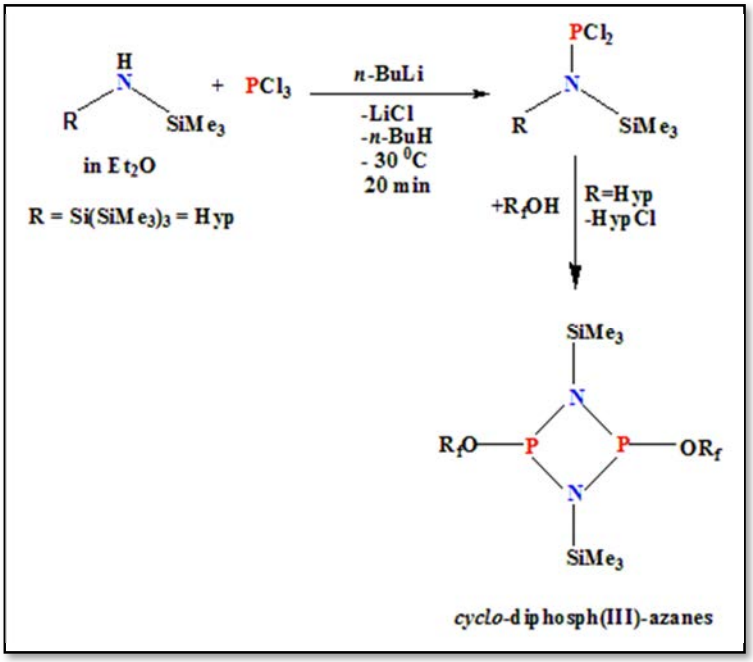

Scheme 2.7: Synthesis of hexafluoroisopropoxy-substituted *cyclo*-diphosphazanes utilising silylated amines.

The chemistry of heavier pnictogen (As, Sb, Bi) analogues of this classic inorganic ring system (cyclodipnict (III) azanes) has been slower to develop. Initial interest for the kinetically stabilised low-coordination Group 15 chemistry occurred in 1981 when Yoshifuji reported the synthesis and isolation of the first stable *bis*($C_6H_2tBu_3$-2,4,6)diphosphene compound,[13] with a formal Mes*P=PMes* double bond in which steric hindrance marks a significant involvement to the stabilisation. This compound prepared from the addition of phosphorus trichloride to the solution of Li(2,4,6-$tBu_3C_6H_2$) in THE at − 78 °C and then refluxed for 1 h. This achievement was followed by products of base coordinated heavier dipnictenes, RE=ER (E = P, As, Sb, or Bi).[14,15]

It has been agreed that the lowest unoccupied molecular orbitals (LUMOs) of dipnictenes, including antimony, have the ability to be given electrons from reducing agents.[16] This was evidenced by achievement of ArSb=SbAr (Ar = Tbt = 2,4,6-$[CH(SiMe_3)_2]_3C_6H_2$), establishing the doubly bonded system of the heavier Group 15 elements (dipnictenes).[17] These species show reversible one-electron reduction couples and that the distibene system has the lowest reduction potential among the corresponding dipnictenes.

Reduction of As (III) precursors, (e.g. [Cl_2-As{κ^2-N,N′-$(ArN)_2CR$}]) by KC_8 in PhMe led to bulky guanidinato- or amidinato-bridged diarsenes [As_2{μ-$(ArN)_2$-CR}$_2$] (Ar = $C_6H_3iPr_2$-2,6; R = $N(C_6H_{11})_2$, N*i*Pr, or *t*Bu), having the coordination mode μ-N,N′ bridging instead of κ^2-N,N′ chelating mode.[18] According to theoretical studies, the As–As bonds forming the dimers have significant double-bond character, the σ and π components of which are resultant mainly from As *p*-orbital overlap.

A very recent study reported on a different synthetic approach, showing that initial treatment of $SbCl_3$ with K[$(TerN)_2P$] (Ter = 2,6-dimesityl-phenyl) led to a diazadipnictane, [Ter_2N_2P(III)Sb(III)Cl_2], which was transformed to a cyclic diazastibaphosphenium cation [P(μ-$NTer)_2SbCl]^+$ by the halide abstraction step using $GaCl_3$. A donor-stabilised $[Sb_2]^{2+}$ ion of a dimerised biradical [Sb_2-{μ-$(TerN)_2P$}$_2$] was obtained from a subsequent reduction process of [$Ter_2N_2PSbCl_2$] with KC_8 in non-polar solvent.[19]

Salts of both the $[PhSbCl_3]^-$ and $[PhSbCl_4]^{2-}$ anions were obtained from reactions between phenylantimony dichloride with ionic chlorides such as Me_4NCl or HpyCl, while reactions of the latter with the associated diphenylantimony chloride afforded $[Ph_2SbCl_2]^-$ salts.[20] Since 1970, a number of methods employed in the preparation of species analogous to phenyl antimony (III) halides, were not easy, and the reactions were low yielding.[21] Particularly, those compounds comprising pentafluorophenyl groups are very rare and are limited to *tris*(pentafluorophenyl)antimony (V) compounds such as $(C_6F_5)_3SbX_2$ (X = Cl, Br, NO_3, ClO_4, OCH_3)[22,23] and $(C_6F_5)_3SbIY$ (Y = Cl, Br, N_3, NCO).[24] In 1989, the first combining of pentafluorophenyl and antimony (III) chloride was successfully achieved by redistribution reactions between $(C_6F_5)_3Sb$ (prepared as described previously),[25] and $SbCl_3$ in 2:1 and 1:2 molar ratios giving $(C_6F_5)_2SbCl$ and $(C_6F_5)SbCl_2$ respectively in good yield. Oxidative chlorination of ice cold solutions of these resultant complexes led to formation of Sb (V) species, *bis*(pentafluorophenyl)antimony (V) trichloride $(C_6F_5)_2SbCl_3$ and (pentafluorophenyl)antimony (V) tetrachloride $(C_6F_5)SbCl_4$. While bromination of Sb (III) products at –178 °C generated mixed halide forms, $(C_6F_5)_nSbCl_{3-n}Br_2$ (n = 1, 2) (eqn. 2.1).[26] A fluoro based organoantimony compound has recently been patented for its biological effectiveness.[27]

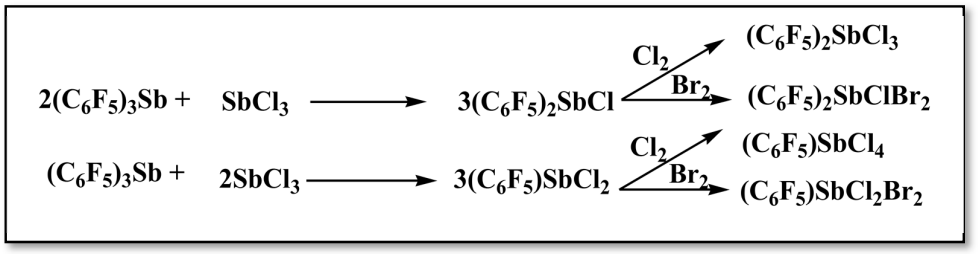

Equation 2.1

2.2 *The current study*

The current study is a prelude to other chapters within this thesis, representing the synthetic protocols that have been employed for the other systems discussed in all consequent chapters, in addition to the different binding modes that can be obtained using formamidinate ligands. Beside one monovalent formamidinatoantimony complex, uncharted trivalent haloformamidinatoantimony complexes have been synthesised in this chapter. The reaction between antimony (III) halides SbX_3 (X = Cl, Br, I) and the deprotonated formamidine $(DippForm)^-$ has been examined to increase the scope of the haloorgano(amido)antimony system. Fundamentally, the synthesis of antimony (I) and (III) formamidinate complexes was accomplished through deprotonation of N,N′-2,6-diisopropylphenylformamidine (DippFormH) by a group of metal alkyl/amide reagents (*n*-BuLi, $LiN(SiMe_3)_2$, $NaN(SiMe_3)_2$) in a donor solvent THF or in PhMe and then combined with SbX_3 in THF and/or PhMe. The major products obtained were *bis*-substituted complexes; for example, **[Sb(DippForm)$_2$Cl]** (**2.2**), **[Sb(DippForm)$_2$Br]** (**2.3**), **[Sb(DippForm)$_2$I]** (**2.4**), and *mono*-substituted complexes of **[Sb(DippForm)Br$_2$]** (**2.5**), **[Sb(DippForm)I$_2$]** (**2.6**). Whereas unpredictable products with differing binding modes are described, such as **[Li$_2$I(DippForm)(μ-thf)(thf)$_2$]** (**2.7**), **[Sb(DippForm)(NSiMe$_3$)]$_2$** (**2.8**), **[SiMe$_3$(DippForm)]** (**2.9**) and **[SbCl$_3$(Me$_2$NC$_2$H$_4$NMe$_2$)]** (**2.10**). Work-up for synthesis of a *tri*-substituted complex of the type [Sb(DippForm)$_3$] was unsuccessful, due to steric complications. The reduction reaction of Sb^{+3} to Sb^{+1} occurred through treatment of DippFormH with $NaN(SiMe_3)_2$ in THF, then added to $SbCl_3$ producing the formamidinato-bridged distibane **[Sb$_2${μ-(DippForm}$_2$].(THF)$_8$** (**2.1**), which is discussed along with the difficulties associated with the synthesis of a monovalent antimony complex as a further comparison. After retreatment of **[SbCl$_3$(Me$_2$NC$_2$H$_4$NMe$_2$)]** (**2.10**) with DippFormH in THF, an attempt to recrystallise the product from C_6D_6 is described, unexpectedly affording an antimony complex **[(DippForm)ClSb(μ-O)SbCl$_2$(Me$_2$NC$_2$H$_4$NMe$_2$)]$_2$.(C$_6$D$_6$)** (**2.11**), and it was the only type of halogenated hetero dinuclear complex isolated in this study. Reaction of DippFormH in THF with $Hg(C_6F_5)_2$, as a source of the pentafluorophenyl group, followed by its combination with $SbCl_3$ gave the unexpected product **[Sb(DippForm)Cl(C$_6$F$_5$)]$_2$.(THF)$_2$** (**2.12**) in low yield.

Different studies have been implemented to explore the nature of the formamidinatoantimony derivatives in the solid state and in solution. Structures of all the complexes were obtained using single crystal X–ray structure determination/analysis and further characterised by ^{1}H-, ^{7}Li-(**2.7**) and ^{13}C-NMR spectroscopy, IR spectra, elemental analysis as well as melting points (to complete characterisation providing thermal stability information). Structural elucidation revealed that some of the isolated complexes showed somewhat infrequent Dippform coordination modes with the antimony.

GLOSSARY OF COMPOUNDS AND CODES

The following structures are a summary of the antimony complexes discussed throughout this chapter, together with respective codes. These structures show antimony atoms in different colours representing the colours of the compounds observed in the solid state.

$[Sb_2\{\mu\text{-(DippForm}\}_2].(THF)_8$ (2.1)

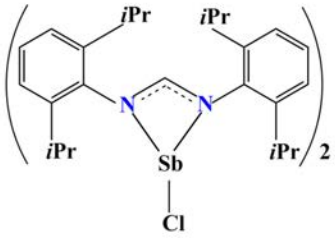

$[Sb(DippForm)_2Cl]$ (2.2)

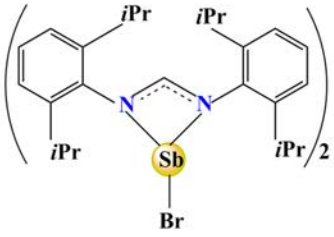

$[Sb(DippForm)_2Br]$ (2.3)

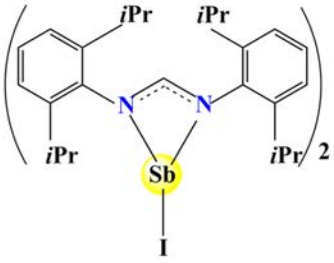

$[Sb(DippForm)_2I]$ (2.4)

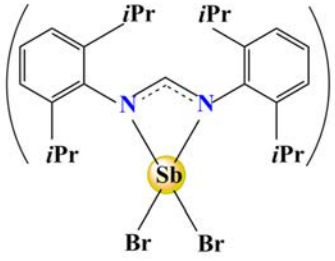

$[Sb(DippForm)Br_2]$ (2.5)

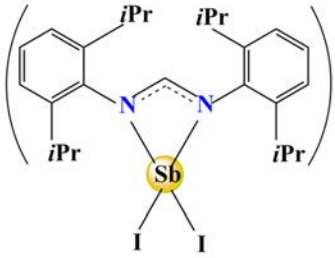

$[Sb(DippForm)I_2]$ (2.6)

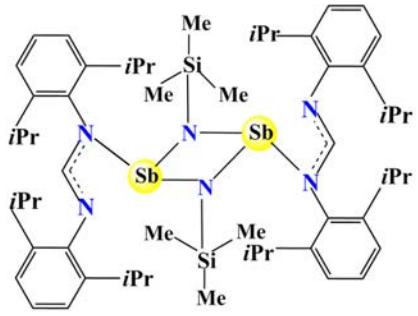

$[Sb(DippForm)NSiMe_3]_2$ (2.8)

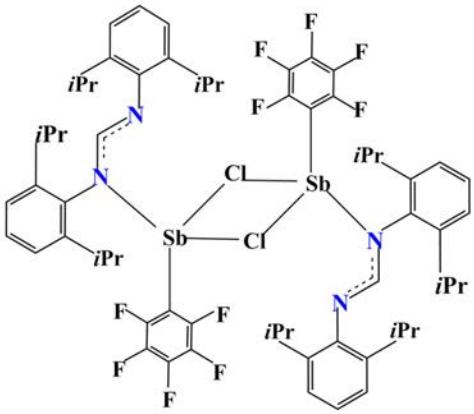

$[Sb(DippForm)(C_6F_5)Cl]_2.(THF)_2$ (2.12)

2.3 *Results and discussion*

2.3.1 Synthesis by metathesis reactions in THF/PhMe

In this chapter, we started to investigate the synthesis of a variety of antimony (III) formamidinate complexes by means of metathesis reactions in THF/PhMe. The reaction yields were relatively dependent on stoichiometric and synthetic techniques used for preparing the complexes, although some unpredicted results were gained. Scheme 2.13 (outlined below) shows the reagents and conditions used within this study.

A range of synthetic routes seeking the formation of haloformamidinatoantimony (I)/(III) complexes have been investigated as outlined in (Scheme 2.8).

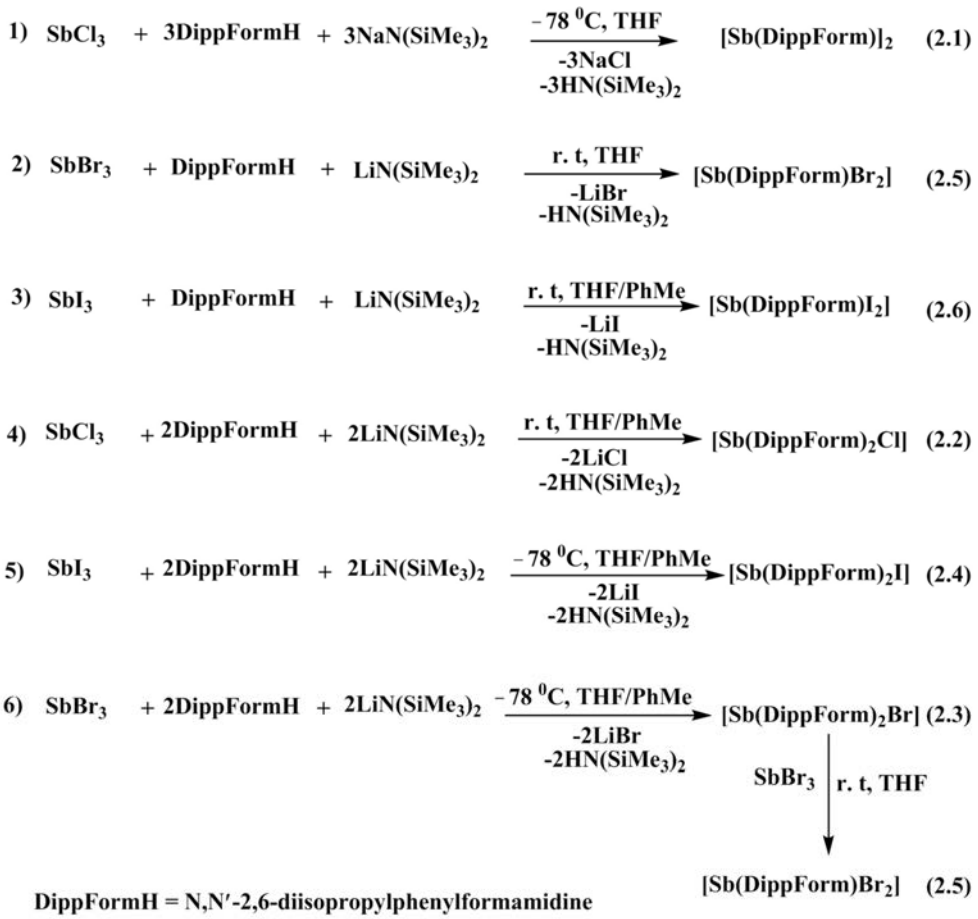

Scheme 2.8: Synthetic routes to formamidinato antimony (I)/(III) complexes.

The methods described above have been used to prepare antimony formamidinates as moisture sensitive compounds, and all of the procedures required utilising the common organic solvents, either THF or PhMe, under varying conditions. The standard metathetical reaction (Scheme 2.8) can produce more complicated products by contamination from salt formation. The reaction of SbX_3 with alkali metal formamidinate M(DippForm) can yield Sb(DippForm)X_2, Sb(DippForm)$_2$X and Sb(DippForm)$_3$ (due to the steric demands of DippForm, it is improbable) (see later), depending on the molar ratio of the SbX_3 vs. (DippFormH) used. It was noticed that the reaction of the deprotonated N,N′-2,6-diisopropylphenylformamidinate with SbX_3 in THF at any ratio (1:1, 2:1, 3:1) can provide both the *mono*- and *bis*-substituted complex (Scheme 2.9).

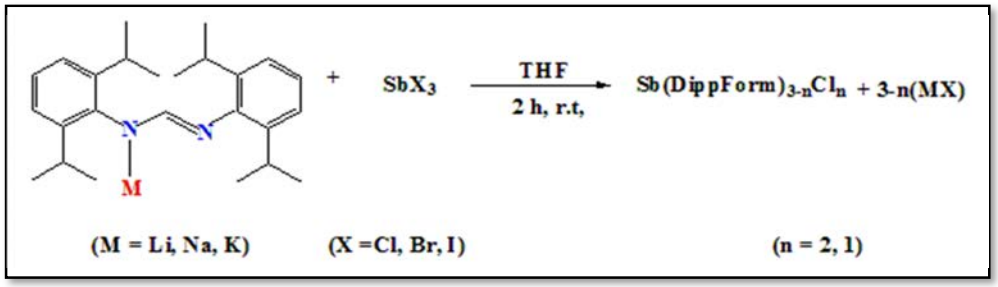

Scheme 2.9: Synthesis of *mono*- and *bis*-substituted complexes.

Sb(DippForm)$_2$Br (**2.3**) reacted as starting material instead of using DippFormH ligand in one of the reactions, which represents other synthetic technique proving successfully synthesis of Sb(DippForm)Br_2 through it (Scheme 2.8, eqn. 6). Several coordination modes have been gained, including the three most common ones as shown in (Scheme 2.10).

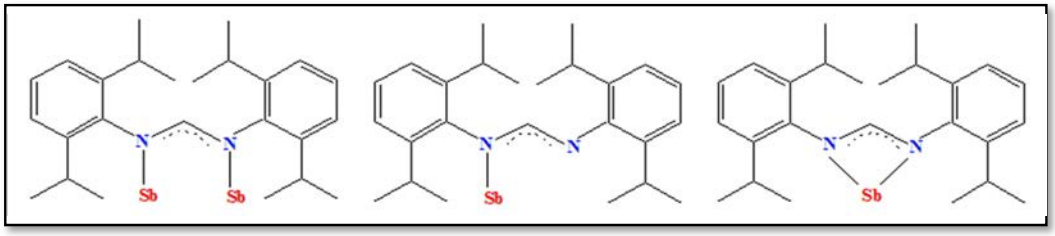

Scheme 2.10: Three common coordination modes for substituted formamidinate with antimony.

An adequate amount of very shiny orange block-shaped crystals of $[Sb_2\{\mu\text{-}(DippForm\}].(THF)_8$ (**2.1**) (Fig. 2.1) were gained. The processed reaction was between $NaN(SiMe_3)_2$ and DippFormH, and then combination with the anhydrous $SbCl_3$ in THF in 3:1 molar ratio. The reaction pathway is proposed in (Scheme 2.11). The dimeric crystalline complex (**2.1**) was isolated instead of an expected Sb^{+3} complex $[SbL_{3-n}Cl_n]$ (n = 2, 1, 0) due to an unanticipated reduction reaction, reducing Sb^{+3} to Sb^{+1}. NaCl was displaced and Sb (I) sat in the C–N pocket forming a bridged Sb^{+1} compound. In this chapter, we attempted reduction reactions of SbX_3 (X = Cl, Br, I) combined with DippFormH and several reducing agents (Na, K, Mg), as well as reactions with hydride transfer reagents (NaH, KH, $LiAlH_4$) in different solvents (THF, PhMe, hexane), with the aim of forming low valent Sb species. However, the reduction reaction results were generally unsuccessful and only gave dark, insoluble precipitates.

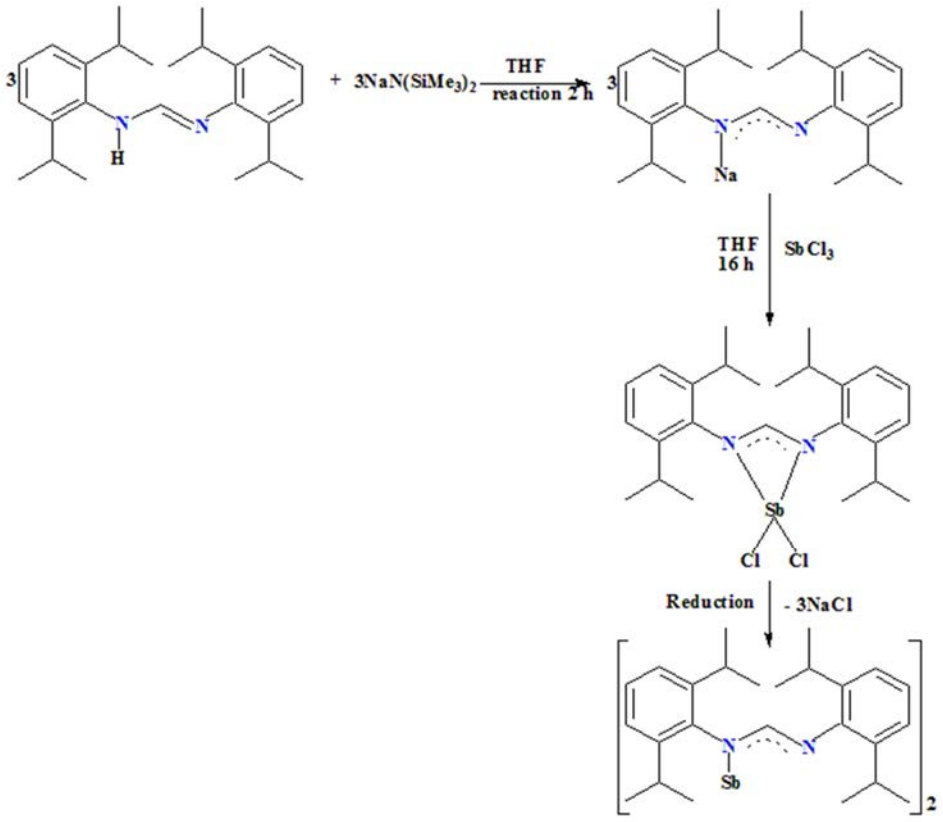

Scheme 2.11: A proposed route to the synthesis of complex (**2.1**).

2.3.1.1 *Mono*-formamidinato antimony (III) complexes

DippFormH was stirred at room temperature in THF/PhMe and deprotonated by dropwise addition of $LiN(SiMe_3)_2$. This was followed by the addition of Li(Dippform) to anhydrous SbX_3 (X = Br, I) pre-dissolved in THF/PhMe in 1:1 molar ratios to produce the new antimony formamidinate species. A colour change was observed in the solution (after ~10 minutes). Consequently, crystalline complexes containing examples of the corresponding *mono*-substituted formamidinate complexes of the general type $[Sb(DippForm)X_2]$, (X = Br (**2.5**), I (**2.6**)) have been generated. Both of the complexes were obtained in almost quantitative yields (Scheme 2.12).

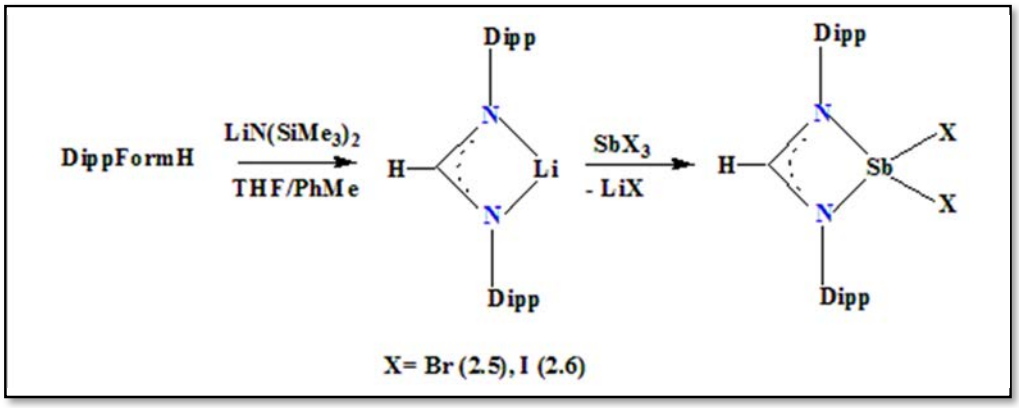

Scheme 2.12: Synthesis of *mono*-substituted formamidinate complexes (**2.5** and **2.6**).

2.3.1.2 *Bis*-formamidinato antimony (III) complexes

[Sb(DippForm)$_2$Cl] (**2.2**), [Sb(DippForm)$_2$Br] (**2.3**) and [Sb(DippForm)$_2$I] (**2.4**) were synthesised by treating SbX_3 with Li(Dippform) in a 1:3 molar ratio (Scheme 2.13). However, reactions of different metal alkyls/amides such as (*n*-BuLi, $LiN(SiMe_3)_2$ and $NaN(SiMe_3)_2$) with DippFormH, followed by combination with the corresponding SbX_3 in 3:1 molar ratio in different solvents failed to give the *tri*-substituted stibines Sb(DippForm)$_3$, in spite of comparable findings having previously been described for organobismuth complexes.[9] This implies that the Dippform ligand is too sterically demanding to form the *tris*-substituted product with the antimony (ionic radius 0.76 Å), which is smaller than bismuth (ionic radius 0.96 Å). A ratio of 1:2 was therefore used to synthesise the *bis*-substituted antimony (III) complexes in THF or PhMe under variant conditions in good yield. The general equation of the reaction is given below (eqn. 2.2):

$$SbX_3 + 2DippFormH + 2LiN(SiMe_3)_2 \xrightarrow[\text{reaction 10-12 h}]{\text{THF or PhMe}} Sb(DippForm)_2X + 2LiX + HN(SiMe_3)_2$$

X = Cl (2.2), Br (2.3), I (2.4)

Equation 2.2: Overall synthesis of *bis*-substituted Sb^{+3} complexes in THF/PhMe.

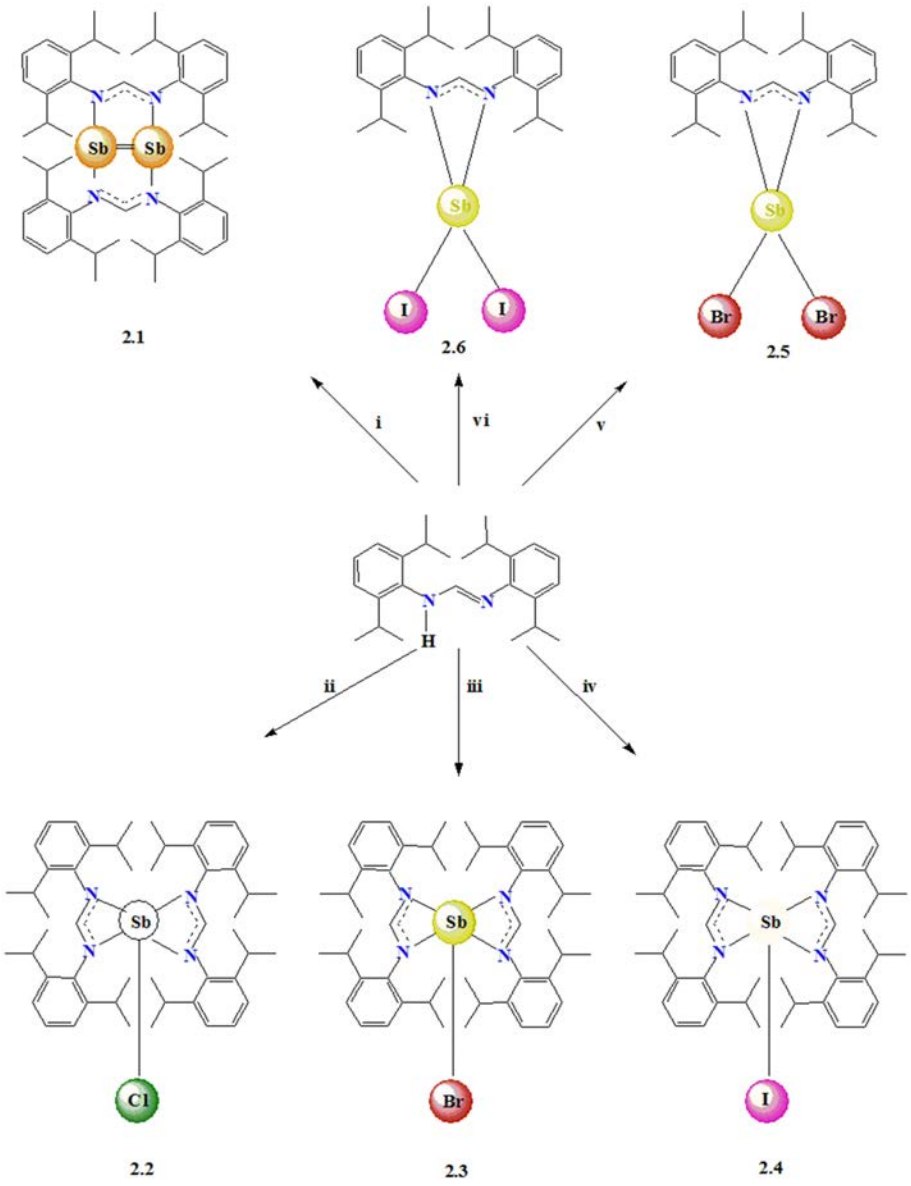

Scheme 2.13. Synthesis of halo- and nonhalo-formamidinatoantimony complexes, reagents and under different conditions: (i) $NaN(SiMe_3)_2$, $SbCl_3$, –78 ^{0}C, 3:1 molar ratio in THF. Note: compound (**2.1**) crystallised as a dimer with eight THF molecules in the crystallographic asymmetric unit. (ii) $LiN(SiMe_3)_2$, $SbCl_3$, r.t, 1:2 molar ratio in THF/PhMe. (iii) $LiN(SiMe_3)_2$, $SbBr_3$, – 78 ^{0}C, 1:2 molar ratio in THF/PhMe and hexane. (iv) $LiN(SiMe_3)_2$, SbI_3, – 78 ^{0}C, 1:2 molar ratio in THF/PhMe. (v) (**2.3**) + $SbBr_3$ in 1:1 molar ratio, r.t, THF. (vi) $LiN(SiMe_3)_2$, SbI_3, r.t, 1:1 molar ratio in THF/PhMe. The metathesis reactions described in (Scheme 2.13) generally produce Sb in (III) valence complexes (except for **2.1** with monovalent Sb).

[Li_2I(DippForm)(μ-thf)$(thf)_2$] was obtained unexpectedly as a primary product in very reasonable yield from the reaction of Li(DippForm) (prepared *in situ*) with SbI_3 in 3:1 molar ratio (Scheme 2.14). Storage of the reaction mixture in PhMe at room temperature gave off white-yellow crystals of (**2.7**) suitable for single-crystal X-ray diffraction studies.

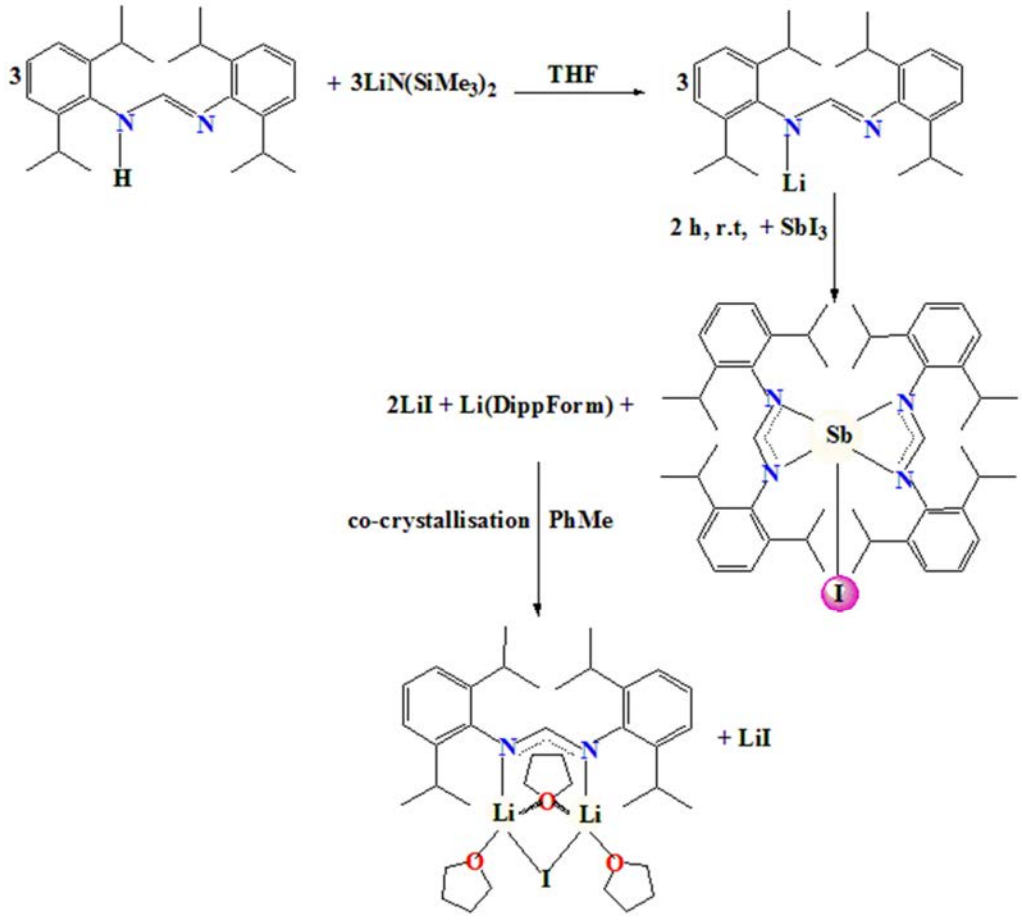

Scheme 2.14 The proposed mechanism for the formation of complex (**2.7**).

A reaction between Li(DippForm) and $SbBr_3$ in the presence of THF and PhMe at room temperature produced an unanticipated components **[Sb(DippForm)(NSiMe$_3$)]$_2$** (**2.8**) and **[SiMe$_3$(DippForm)]** (**2.9**), suggesting an interaction activation process occurred according to the proposed route (eqn. 2.3):

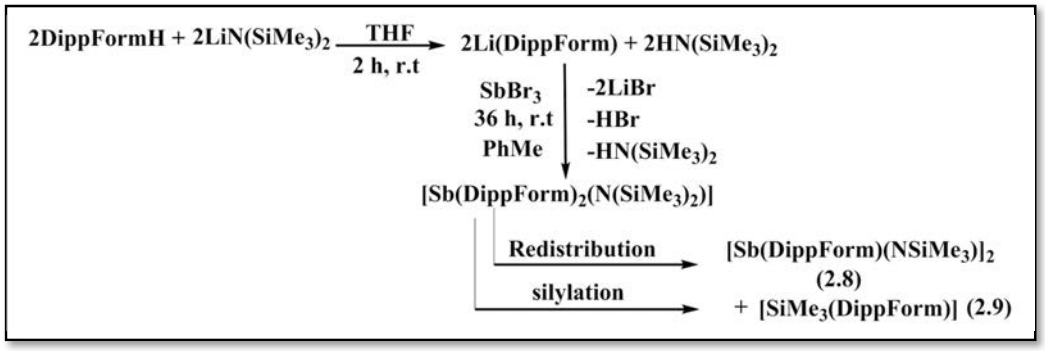

Equation 2.3

Addition of N,N,N′,N′-tetramethyl-1,2-ethanediamine (TMEDA) to $SbCl_3$ pre-dissolved in THF and pre-treated with Li(DippForm) gave the crystallisable complex **[SbCl$_3$(Me$_2$NC$_2$H$_4$NMe$_2$)]** (**2.10**). An attempt to deliberately synthesise this complex was achieved by the reaction of $SbCl_3$ with an equivalent of (TMEDA) in THF (eqn. 2.4).

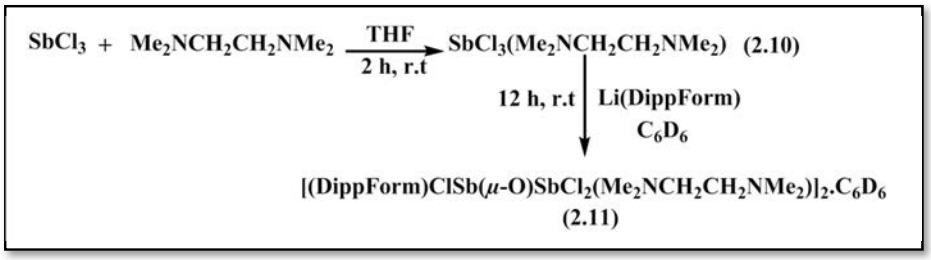

Equation 2.4

On the basis of an NMR-spectroscopic-scale recrystallisation experiment in C_6D_6 at ambient temperature, an attempted synthesis of (**2.10**) was performed by treating (DippFormH) with $LiN(SiMe_3)_2$ in THF and (TMEDA), followed by unintentional exposure to small amounts of H_2O, resulted in the formation of an unexpected new heterocyclic cage **[(DippForm)ClSb(μ-O)SbCl$_2$(Me$_2$NC$_2$H$_4$NMe$_2$)]$_2$.C$_6$D$_6$** (**2.11**) (Scheme 2.15).

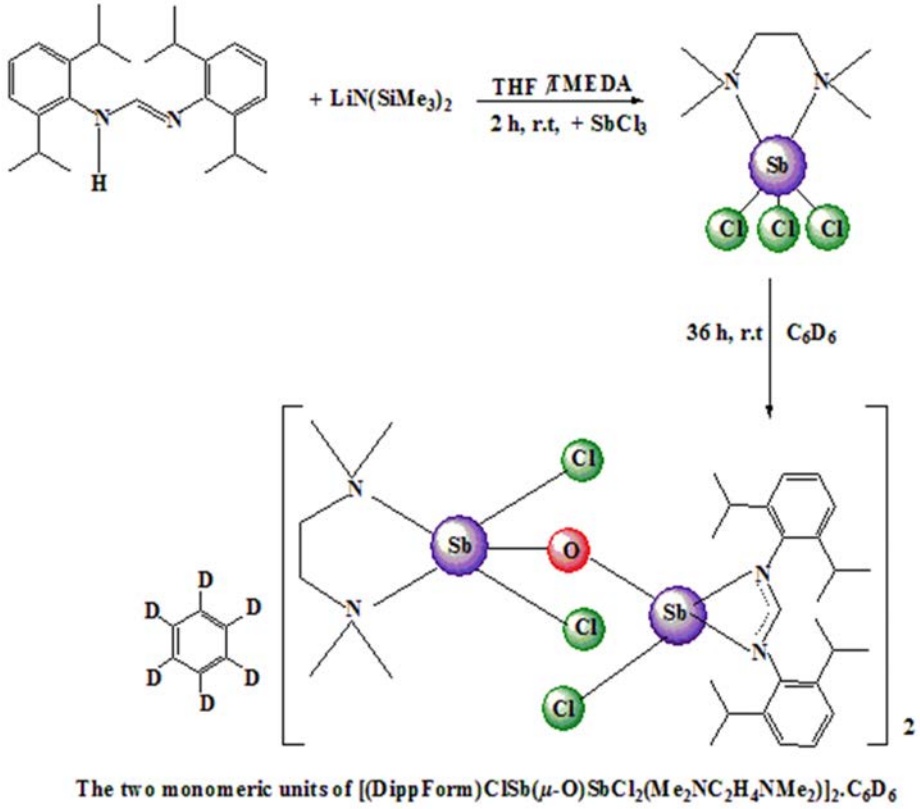

The two monomeric units of $[(DippForm)ClSb(\mu\text{-}O)SbCl_2(Me_2NC_2H_4NMe_2)]_2.C_6D_6$

Scheme 2.15. Synthesis of complex (**2.10**) and (**2.11**).

Complex **[Sb(DippForm)Cl(C_6F_5)]$_2$.(THF)$_2$** (**2.12**) was obtained in low yield from one pot reaction of DippFormH with $Hg(C_6F_5)_2$ and $SbCl_3$ in THF (eqn. 2.5).

$$2SbCl_3 + 2Hg(C_6F_5)_2 + 2DippFormH \xrightarrow[2\ h,\ r.t]{THF} [Sb(DippForm)Cl(C_6F_5)]_2.(THF)_2 + 2HgCl_2 + 2H(C_6F_5)$$

Equation 2.5

In an attempt to co-crystallise M(DippForm), an intractable combination formed when the alkali metal formamidinate combined with SbX_3, which can be attributed to the extremely air sensitivity of the starting materials. To illustrate that, the 2:1 reaction of Li(DippForm) with SbI_3 gave [Sb(DippForm)$_2$I] (**2.4**) and Li(DippForm). It is not unexpected, where no pure material was observed.[9] Therefore, it was recommended to perform the reaction *in situ* to minimise the potential mixed materials. Overall, Sb-including product could be entirely distinguishable.

Some of the products presented within this chapter were isolated from the reaction mixture by filtration from the unwanted precipitate MX (M = Li, Na, Hg; X = Cl, Br) as shown in (eqn. 2.6), followed by fractional crystallisation from THF (**2.1**, **2.5**, **2.9**, **2.10**, **2.12**). Whereas the others were evaporated to the point of dryness under vacuum, due to the high solubility of the precipitate in THF, and recrystallisation from PhMe after filtration from MX (M = Li; X = Cl, I) (**2.2**, **2.4**, **2.6**, **2.7**, **2.8**) (eqn. 2.6). Experiment (**2.3**) was performed in a mixture of THF/PhMe and for further purification were required hexane. Only [(DippForm)ClSb(μ-O)$SbCl_2(Me_2NC_2H_4NMe_2)]_2.(C_6D_6)$ (**2.11**) was isolated from the reaction mixture in THF/TMEDA by filtration from LiCl and recrystallised from C_6D_6. Complex $[Sb(DippForm)_2Br]$ (**2.3**) was gained with the highest yield of (80 %).

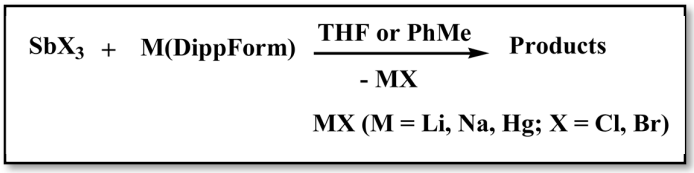

Equation 2.6

2.3.2 Characterisation

Characterisation was primarily authenticated through single crystal X-ray structure identification of the isolated crystalline samples [Sb(DippForm)$_{3-n}$X$_n$] (n = 1, 2; X = Cl, Br, I) displayed in (scheme 2.13) using the MX1 beamline at the Australian Synchrotron. To develop an understanding of the bonding and structural diversity, the experimental observations were interpreted with additional characterisation by IR spectroscopic techniques (Table 2.1), ^{1}H-NMR (Table 2.2), ^{13}C-NMR (Table 2.3), ^{7}Li-NMR (**2.7**) spectroscopy, elemental analyses and melting point determination (with the exception of (**2.12**), which was obtained only in very poor yield).

The ^{1}H-NMR spectra for some of the complexes such as (**2.1**, **2.7**) revealed that the ratios of solvent to ligand are not consistent with the composition identified in the solid state X-ray crystal structure. Loss of some THF of solvation occurred during drying the product under vacuum. To illustrate this, the ^{1}H-NMR spectrum of [Sb$_2${μ-(DippForm}$_2$].(THF)$_8$ (**2.1**) revealed the loss of 2 THF molecules, shown by the integration of two resonances at δ = 3.64 and 1.34, where a DippForm methyl (48 ^{1}H, CH(C*H*$_3$)$_2$):THF (24 ^{1}H, OC*H*$_2$-thf) ratio was found to be 2 to 1.

In the ^{1}H-NMR spectra of the DippFormH proligand, the methine proton NCHN resonance on the backbone typically occurred at δ = 7.05 ppm, while upon deprotonation of the NH group on the formamidine and coordination with antimony, the methine proton resonances occurred at δ = 10.60, 10.93, 8.04, 8.31 and 8.29 ppm for the corresponding (**2.1**), (**2.2**), (**2.3**), (**2.6**) and (**2.8**) compounds respectively, representing one NCHN enviroment shifted to higher frequencies when compared with the neutral ligand. The ^{13}C-NMR spectrum of the compounds displayed the predictable resonances and were identifiable, however the only resonances were amassed together in (**2.10**) restricting full resolution of the signals.

The IR spectra of all antimony compounds (except **2.10**) revealed comprehensive deprotonation of the N–H group of the formamidine ligand upon formation of the antimony complex. This was evident by absence of the *v* (N–H) absorption band typically observed at 3300-3100 cm^{-1}. This indication was combined with the absence of a N–H resonance in the ^{1}H-NMR spectra of the bulk vacuum dried materials. The only one case was observed in (**2.8**) when N–H band showed very weak resonance at the region of 5.31 ppm in the ^{1}H-NMR spectrum. This was coupled with the presence of a very weak band analogous to the formamidine in the IR spectrum of (**2.8**), suggesting high intensity of the *v* (N=C) band for the NCHN vibrational mode, which could be attributed to the extreme sensitivity of the DippForm complex to air. More specifically, the potential slight decomposition on movement from the glovebox to the infrared spectrometer could have occurred even when the sample was protected in a Nujol mull (dried over sodium) between NaCl plates. Complexes (**2.1 - 2.9** and **2.11**) had absorptions at 1644-1698 cm^{-1} through N–C stretching (Table 2.1), which belonged to a metal (Sb, Li, Si)-coordinated formamidinate ligand.

Analysis of the bulk material provided a satisfactory elemental analysis (C, H, N), which is consistent with the formation of the compounds (**2.2**, **2.3**, **2.5**, **2.8**, **2.9**, **2.10**). The acceptable range of error in C, H, and N is ± 0.50 % from the calculated value. Attempts to gain satisfactory carbon and nitrogen analysis data for compound (**2.1**) were unsuccessful, most likely because of the product contamination or possibly from the high air and/or moisture sensitivity and extreme ease of solvent loss or even potential decomposition in transit.

The existence of TMEDA in **[$SbCl_3(Me_2NC_2H_4NMe_2)$]** and **[(DippForm)ClSb-μ-O-$SbCl_2(Me_2NC_2H_4NMe_2)]_2.(C_6D_6)$** complexes was confirmed by the ^{1}H-NMR spectra with resonances at ppm = 2.15 (CH_3-(TMEDA)), 2.31 (CH_2-(TMEDA)) and 2.05 (CH_3-(TMEDA)), 2.10 (CH_2-(TMEDA)), respectively, although the elemental analyses were repeatedly showing slightly low in the C percentage for (**2.11**). This could be attributed to loss of C_6D_6 solvation upon standing.

Table 2.1 N–C Stretching in IR spectra for antimony formamidinate complexes 2.1 - 2.9 and 2.11 (υ 4000 - 400 cm^{-1})

Compound		N–C stretching vibration (cm^{-1})
$[Sb_2\{\mu\text{-}(DippForm\}_2].(THF)_8$	(**2.1**)	1668
$[Sb(DippForm)_2Cl]$	(**2.2**)	1666
$[Sb(DippForm)_2Br]$	(**2.3**)	1662
$[Sb(DippForm)_2I]$	(**2.4**)	1651
$[Sb(DippForm)Br_2]$	(**2.5**)	1644
$[Sb(DippForm)I_2]$	(**2.6**)	1667
$[Li_2I(DippForm)(\mu\text{-}thf)(thf)_2]$	(**2.7**)	1698
$[Sb(DippForm)(NSiMe_3)]_2$	(**2.8**)	1670
$[SiMe_3(DippForm)]$	(**2.9**)	1661
$[(DippForm)ClSb(\mu\text{-}O)SbCl_2(Me_2NC_2H_4NMe_2)]_2.(C_6D_6)$	(**2.11**)	1662
DippFormH		1600

Table 2.2 ^{1}H-NMR chemical shift data in ppm for antimony formamidinate complexes 2.1 - 2.9 and 2.11 in C_6D_6

^{1}H-NMR	2.1	2.2	2.3	2.4	2.5	2.6	2.7	2.8	2.9	2.11
NC*H*N	10.60	10.93	8.04	7.86	7.56	8.31	7.86	8.29	7.21	7.77
Aromatic *H*	6.98-7.06	6.91-7.03	6.99-7.03	6.98-7.06	6.88-7.08	6.76-6.99	6.99-7.06	6.95-7.08	6.96-7.04	6.92-7.09
C*H*$(CH_3)_2$	3.42	3.44	3.45	3.42	3.33	3.22	3.43	3.46	3.43	3.41
OCH_2, thf	3.64	–	–	–	–	–	3.55	–	–	–
CH_2, thf	1.34	–	–	–	–	–	2.10	–	–	–
CH(CH_3)$_2$	1.12	1.13	1.15	1.15	1.21	1.11	1.16	1.16	1.10	1.22
CH_2-(TMEDA)	–	–	–	–	–	–	–	–	–	2.10
CH_3-(TMEDA)	–	–	–	–	–	–	–	–	–	2.05

Table 2.3 ^{13}C-NMR chemical shift data in ppm for antimony formamidinate complexes 2.1 - 2.9 and 2.11 in C_6D_6

^{13}C-NMR	2.1	2.2	2.3	2.4	2.5	2.6	2.7	2.8	2.9	2.11
NCN	157.39	155.62	161.27	155.54	159.80	158.89	146.47	152.60	147.00	163.22
Aromatic *C*	123.3-143.1	123.4-143.6	123.9-145.6	123.4-145.8	123.5-145.5	123.9-145.5	123.6-144.1	123.3-145.9	123.0-127.1	122.9-146.0
***C*H(CH$_3$)$_2$**	28.51	28.17	29.60	28.39	29.13	29.21	28.40	28.25	28.43	28.41
OCH$_2$, thf	66.50	–	–	–	–	–	68.63	–	–	–
***C*H$_2$, thf**	25.12	–	–	–	–	–	25.35	–	–	–
CH(*C*H$_3$)$_2$	23.84	23.47	25.58	23.71	24.60	25.43	24.16	23.86	24.09	23.91
***C*H$_2$-(TMEDA)**	–	–	–	–	–	–	–	–	–	54.62
***C*H$_3$-(TMEDA)**	–	–	–	–	–	–	–	–	–	41.62

2.3.3 Crystal structure determinations

[Sb_2{μ-(DippForm}$_2$].$(THF)_8$ (2.1)

By means of metathesis in THF, the monovalent antimony complex **[Sb_2{μ-(DippForm}$_2$].$(THF)_8$** (**2.1**) was synthesised (Scheme 2.11). The Lewis base–stabilised diantimony (**2.1**) complex was achieved in low to moderate yield as light orange block-shaped crystals, while the X-ray data was established only in moderate quality but the connectivity has been established and is unambiguous. Compound (**2.1**) crystallised in the monoclinic space group $P2_1/c$ (Table 2.5), with one dinuclear molecule within the asymmetric unit. As it can be seen from the crystal structure depicted in (Figure 2.1), antimony is tri-coordinate with the coordination sphere involving two bridging DippForm ligands that symmetrically link between Sb–Sb. Eight uncoordinated THF molecules per dimer are present in the lattice. The overall geometry of the Sb (I) complex displays a planar structure of the central structural motif. [Sb_2{μ-(DippForm}$_2$].$(THF)_8$ dimerises via Sb=Sb double bond formation, and this double bond has two contributions, a σ bond and a substantial degree of π bonding, both of them are predominantly formed by interactions of *p* atomic orbitals located at each Sb centre. The molecular structure shows there is no stereochemically active lone pair of electrons at the antimony centres (Scheme 2.16).

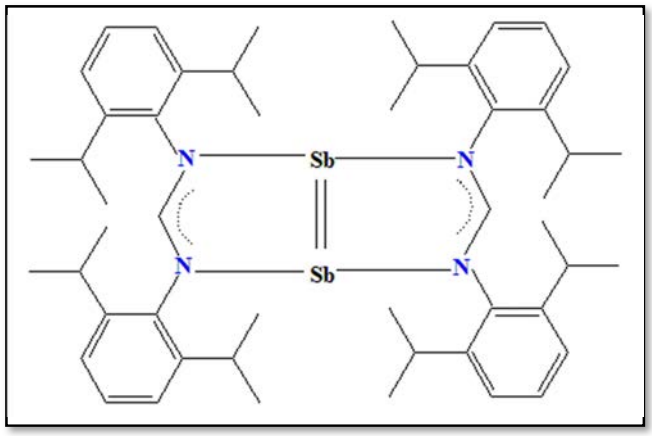

Scheme 2.16. Diagram of dinuclear antimony (I) compound (**2.1**).

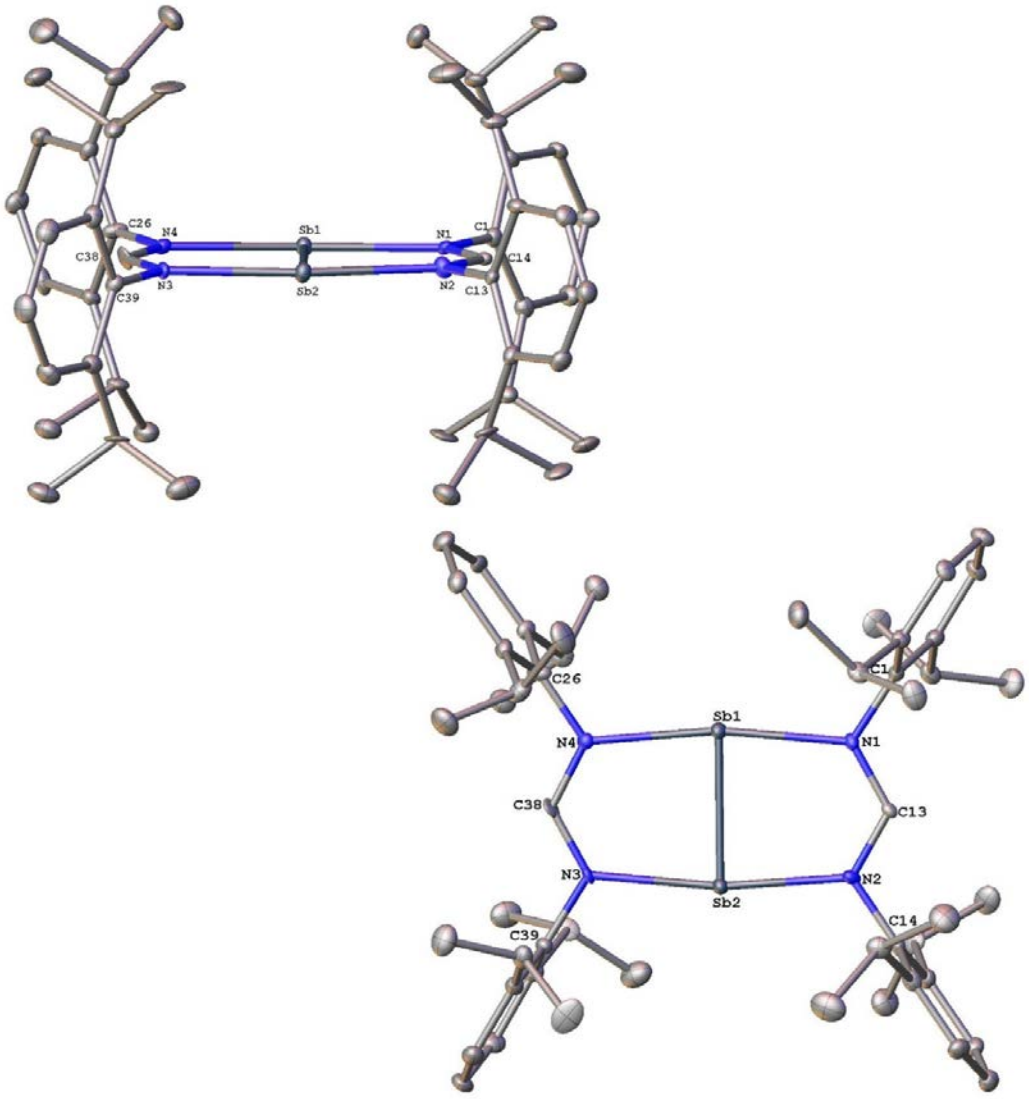

Figure 2.1. Molecular structure of dimeric **[Sb$_2${*μ*-(DippForm}$_2$].(THF)$_8$** (**2.1**) (*left* view: along the Sb–Sb bond, *right*: top view) with the atom numbering system; thermal ellipsoids are drawn at the 50 % probability level, and hydrogen atoms and lattice THF have been omitted for clarity. Selected bond lengths (Å) and angles (°): Sb(1)–Sb(2): 2.6806(11), Sb(1)–N(1): 2.302(9), Sb(1)–N(4): 2.307(9), Sb(2)–N(3): 2.290(8), Sb(2)–N(2): 2.288(10), N(3)–C(38): 1.311(14), N(1)–C(1): 1.421(14), N(1)–C(13): 1.344(13), N(4)–C(38): 1.307(14), N(4)–C(26): 1.412(14), N(2)–C(14): 1.434(13), N(2)–C(13): 1.330(13), N(1)–Sb(1)–Sb(2): 85.5(2), N(4)–Sb(1)–Sb(2): 85.4(2), N(3)–Sb(2)–Sb(1): 85.3(2), N(2)–Sb(2)–Sb(1): 85.9(2), C(39)–N(3)–Sb(2): 117.7(7), C(38)–N(3)–Sb(2): 123.2(7), C(1)–N(1)–Sb(1): 119.1(6), C(13)–N(1)–Sb(1): 123.3(7), C(38)–N(4)–Sb(1): 122.2(7), C(13)–N(2)–Sb(2): 123.8(7).

The most prominent structural feature is the highly symmetric, a novel planar eight-membered $N_4C_2Sb_2$ heterocycle, also described as two condensed five-membered rings, highlighting a relatively short Sb(1)–Sb(2) bond length of 2.6806(11) Å, ($\sum r_{cov}$ (Sb–Sb) = 2.8 vs. $\sum r_{cov}$ (Sb=Sb) = 2.66 Å).[28] A Sb=Sb bond length in (**2.1**) is slightly longer than the bond lengths measured for the formerly established of 2.6438(4) Å for [Sb_2-{μ-$(TerN)_2P$}$_2$],[19] 2.642(1) for Tbt_2Sb_2, 2.6558(5) for Ter_2Sb_2, but shorter than the bond length of 2.7104(5) for [Ar*N(Si*i*Pr_3)]$_2Sb_2$ (Ar* = 2,6-*bis*(diphenylmethyl)-4-isopropyl-phenyl), where these compounds also had a Sb=Sb double bond with Sb in the +1 oxidation state.[16, 29,30,31,32,28,33]

Complex (**2.1**) is the first structurally characterised formamidinate/amidinate-substituted distibine, and is also considered as one of the series of Lewis base-coordinated dipnictenes, with a Sb–N bond length range of 2.288(10)–2.307(9) Å, which is slightly shorter than the Sb–N bond length range of 2.372(2) Å reported for [Sb_2–{μ–$(TerN)_2P$}$_2$],[19] and significantly longer than the sum of covalent radii ($\sum r_{cov}$ (Sb–N) = 2.11 Å).[28] In addition, the short C–N distances of N1/3–C13/38 1.344(13)/1.311(14), N2/4–C13/38 1.330(13)/1.307(14) Å are in the midway between the typical range of CN double bonds ((C=N) =1.25 Å) and the CN single bonds ((C–N) =1.47 Å), establishing the delocalisation of the anionic charge across the N-C-N moiety. Thus, the symmetrically bridging NCN ligand retains its anionic nature within the bridging mode, as assigned by the carbon–nitrogen bond lengths above. In contrast, an example of related structures having μ-N,N′ bridging mode that have been recently reported by Jones and co-workers, each Sb centre is being coordinated by an amide centre of one ligand, and the imine arm from the other ligand constructing a dative interaction (by view of the ligand geometry). In these structures, an average C–N distances 1.340 Å in the planar [As_2{μ–$(ArN)_2CR$}$_2$] bicyclic fragment (Ar = C_6H_3*i*Pr_2–2,6; R = N(C_6H_{11})$_2$, N(*i*Pr)$_2$, *t*Bu).[18] This geometry is also comparable to the planar amidinato-bridged copper (I) dimers.[34] By obtaining complex (**2.1**), the sterically bulky formamidinate ligand (DippForm), synthesised and developed in our laboratory, further highlights its ability to stabilise low oxidation state *p*-block compounds with unusual coordination mode.

[Sb(DippForm)$_2$X] (X = Cl (2.2), Br (2.3) and I (2.4))

The trivalent antimony complexes [Sb(DippForm)$_2$X] (X= Cl (**2.2**), Br (**2.3**) and I (**2.4**)) were synthesised (Scheme 2.10). These complexes crystallised in the monoclinic space group *P2$_1$/c* (Table 2.5), with one mononuclear molecule within the asymmetric unit. The three complexes (**2.2**, **2.3** and **2.4**) are the first reported five coordinate antimony formamidinate/amidinate compounds, with an Sb-N bond length range: 2.112(4) – 2.646(3) Å showing asymmetric formamidinate chelation. Complexes (**2.2**, **2.3** and **2.4**) are isostructural, including the very similar coordination environment observed for the Sb atoms in the three structures, where the iodide or bromide ligand was placed instead of chloride ligand. The Sb^{+3} metal centre in each of the three structures is five coordinate, bounded by two of η^2(N,N') DippForm ligands through the nitrogen donor atoms, and one terminal halide ligand (Figures 2.2, 2.3 and 2.4). The antimony atom shares a plane with a halide atom and two nitrogen from both of the two ligands in equatorial position, while the other two nitrogen atoms from both of the ligands above and below the plane (axial or apical position).

The coordination geometry of (**2.2**, **2.3** and **2.4**) was very symmetrical and most probably distorted as a consequence of the steric effect of the ligand–ligand dislikes compressed by the bulky aryl substituents and the acute bite angle of the Dippform ligand N(3)–Sb(1)–N(4) 55.54(5), 54.96(11) and 54.833(11)° respectively. The ligands are asymmetrically bound to Sb, with the four N atoms forming an estimated trapezium, such as in (**2.2**) (N(2)–Sb(1)–N(3) 86.56(5)°, N(1)–Sb(1)–N(4) 154.63(5)°) (Figure 2.2). In the three complexes, the two DippForm ligands attached to Sb atom were positioned by the NCN planes approximately perpendicular to each other (interplanar angles average between 86.56(5)–88.194(11)°), these positions were generally blocked by the bulky pendant aryl groups of the formamidinate ligand inhibiting additional coordination of potential donor groups. On the other hand, the steric bulk of the DippForm ligand does not allow for a dinuclear arrangement formed by bridging halides.

The crystallographic analysis for (**2.2**) revealed normal Sb–Cl of 2.3980(6) Å, Sb–N1/N2/N3/N4 of 2.5634(15)/2.1131(14)/2.6044(13)/2.1624(15) Å distances, average NCN bond angle of 117.29(13)° and other bond angles.[5,35,36,37,38] The bond angles in (**2.2**): N(3)–Sb(1)–Cl(1) 139.43(3), N(1)–Sb(1)–Cl(1) 78.84(3) and N(3)–Sb(1)–N(1) 132.04(4)° indicate the formation of a rather distorted trigonal bipyramid geometry, which is the same as for (**2.3** and **2.4**) (Scheme 2.17).

The N(4)–Sb(1)–N(1) bond angles of 154.63(5)/156.24(11)/156.06(15)°, show a high distortion from the expected 180° that may due to the rather acute bite angles of 56.80(5)/55.54(5), 56.31(11)/54.96(5) and 55.85(15)/54.83(5)° for N1–Sb1–N2/N3–Sb1–N4, respectively. The unsymmetrical C–N bond lengths (Figure 2.2) of NCN (N1/N2–C13 of 1.282(2)/1.363(2) Å, N3/N4–C38 of 1.291(19)/1.349(19) Å; DippFormH:1.311(17) and 1.310(16) Å), suggest limited delocalisation of the anionic charge across the backbone.[39,40]

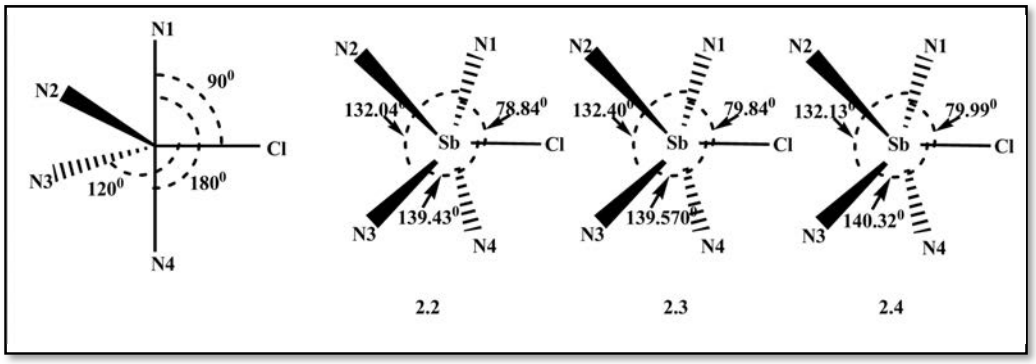

Scheme 2.17. Diagram of a typical trigonal bipyramid with bond angles shown for a rather disordered trigonal bipyramid geometry formed by (**2.2**, **2.3** and **2.4**).

The Sb–Cl bond length in (**2.2**) 2.3980(6) Å is approximately in agreement with the Sb–Cl 2.366(8) and 2.398(6) Å of [Sb{*t*BuC(NR)$_2$}Cl$_2$] (R = Cy and Dipp)[8], and is much shorter than the sum of the van der Waals radii of ($\sum_{vdw}$ (Sb–Cl)= 3.81 Å.[28]

In the formamidinate compounds, the sum of the three bond angles around the backbone C is normally 360°, resulting in a trigonal planar geometry consistent with the expected sp^2 geometry. However, the 120° N(1)-C(13)-N(2) and N(3)-C(38)-N(4) angle in the formamidine is reduced to a slightly tight 117.37(14)/117.29(13)° in the formamidinate of (**2.2**) due to the existence of the four-membered rings (Scheme 2.18), which is the same observation in the other two structures (**2.3** and **2.4**). Unsurprisingly, the C(13)-N(1)-C(1), C(13)-N(2)-C(14), H-C(13)-N(1) and H-C(13)-N(2) angles are increased in comparison to the angles of the free formamidine.

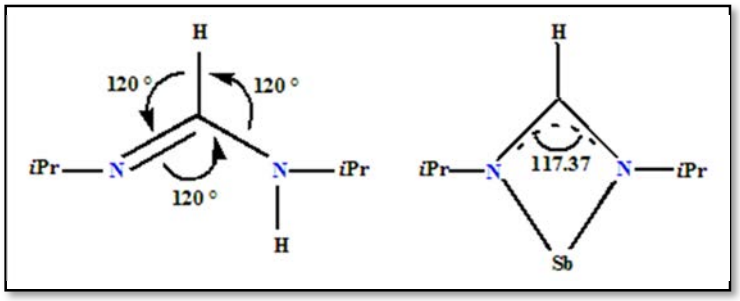

Scheme 2.18. Diagram of a trigonal planar geometry around NCHN in complex (**2.2**).

As expected, it can be noticed the decrease in the values of the bond angles of (**2.2**), C(13)–N(1)–Sb(1), C(13)–N(2)–Sb(1), C(38)–N(3)–Sb(1) and C(38)–N(4)–Sb(1) that found to be 83.88(10), 101.94(10), 82.79(8) and 100.94(10)° respectively; whereas in the free formamidine ligand such C–N–H bond angles are typically calculated 120°.

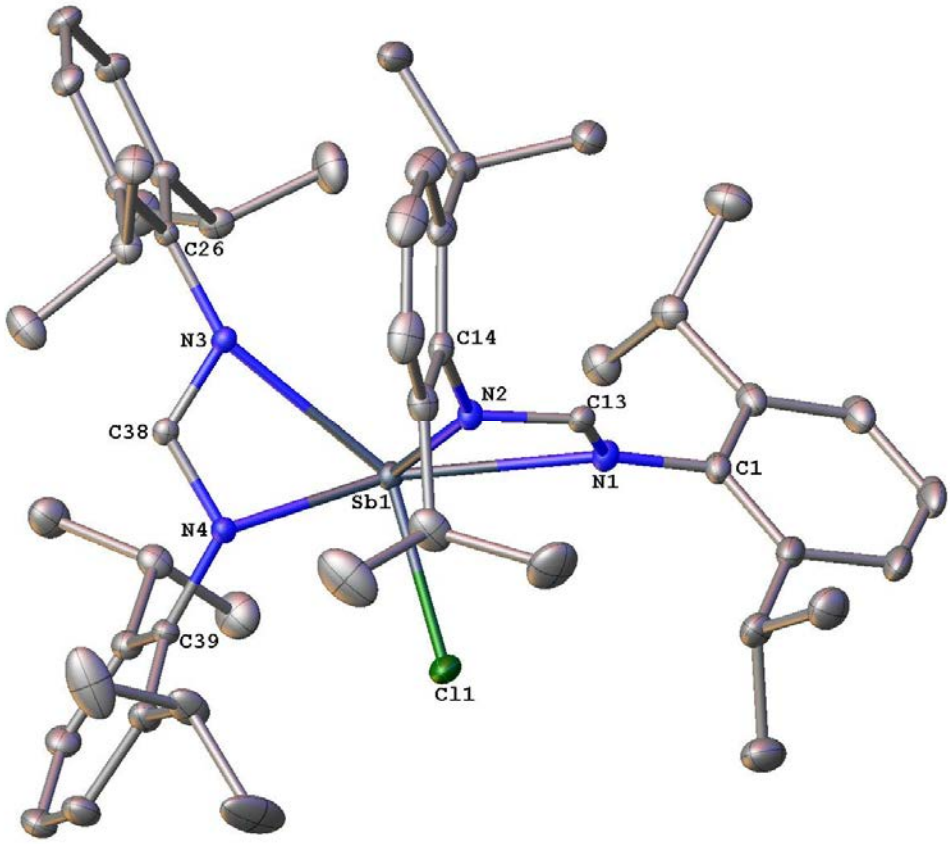

Figure 2.2. Molecular structure of monomeric **[Sb(DippForm)$_2$Cl] (2.2)** with the atom numbering system; thermal ellipsoids are drawn at the 50 % probability level, and hydrogen atoms have been omitted for clarity. Selected bond lengths (Å) and angles (°): Sb(1)–N(1): 2.5634(15), Sb(1)–N(2): 2.1131(14), Sb(1)–N(3): 2.6044(13), Sb(1)–N(4): 2.1624(15), Sb(1)–Cl(1): 2.3980(6), N(3)–C(38): 1.2911(19), N(3)–C(26): 1.4260(18), N(2)–C(13): 1.363(2), N(2)–C(14): 1.434(2), N(4)–C(38): 1.3497(19), N(4)–C(39): 1.438(2), N(1)–C(13): 1.282(2), N(1)–C(1): 1.413(2), N(1)–Sb(1)–Cl(1): 78.84(3), N(2)–Sb(1)–Cl(1): 94.67(4), N(3)–Sb(1)–Cl(1): 139.43(3), N(4)–Sb(1)–Cl(1): 85.44(4), N(2)–Sb(1)–N(3): 86.56(5), N(2)–Sb(1)–N(4): 105.46(6), N(1)–Sb(1)–N(3): 132.04(4), N(1)–Sb(1)–N(2): 56.80(5), N(3)–Sb(1)–N(4): 55.54(5), N(1)–Sb(1)–N(4): 154.63(5), C(38)–N(3)–Sb(1): 82.79(8), C(26)–N(3)–Sb(1): 152.72(9), C(38)–N(3)–C(26): 119.24(12), C(13)–N(2)–Sb(1): 101.94(10), C(14)–N(2)–Sb(1): 138.00(11), C(14)–N(2)–C(13): 116.98(14), C(13)–N(1)–Sb(1): 83.88(10), C(1)–N(1)–Sb(1): 152.95(11), C(1)–N(1)–C(13): 123.11(14), C(39)–N(4)–Sb(1): 126.88(11), C(38)–N(4)–Sb(1): 100.94(10), C(38)–N(4)–C(39): 117.81(13), N(4)–C(38)–N(3): 117.29(13), N(1)–C(13)–N(2): 117.37(14).

An Sb-N bond length range in (**2.3**) was found to be 2.576(3)-2.113(3) Å **(**Figure 2.3), which has as expected slightly shorter than the Bi-N bond length range: 2.643(7)–2.323(6) Å for the bulky formamidinate coordinated to Group 15 (analogous angles and bond lengths for [Bi(DippForm)$_2$(Bu^n)]) (Table 2.4),[9] due to the metal size differences. The variance in the Sb–N bond lengths in (**2.3**) (0.463, 0.488 Å) is slightly different to those (0.320, 0.243 Å) reported for the [Bi(DippForm)$_2$Br] complex.[9] The position of Sb–Cl bond is almost vertical with the SbN4 plane and 2,6-diisopropyl groups involved above and below the plane. The Sb–Br bond length 2.5576(6) Å is between those of 2.446 Å for Sb(1)–Br(1) and 2.98 Å for Sb(2)–Br(2) noted in [({N(C$_6$H$_3$*i*Pr$_2$2,6)C(Me)}$_2$CH)$_2$Sb$_2$(μ-Br)$_2$Br$_2$].[5] These values are not unusual for Sb–Br bonds,[41] and this dissimilarity appears to be a common characteristic in the 32 stated Sb–Br bridged structures.[42]

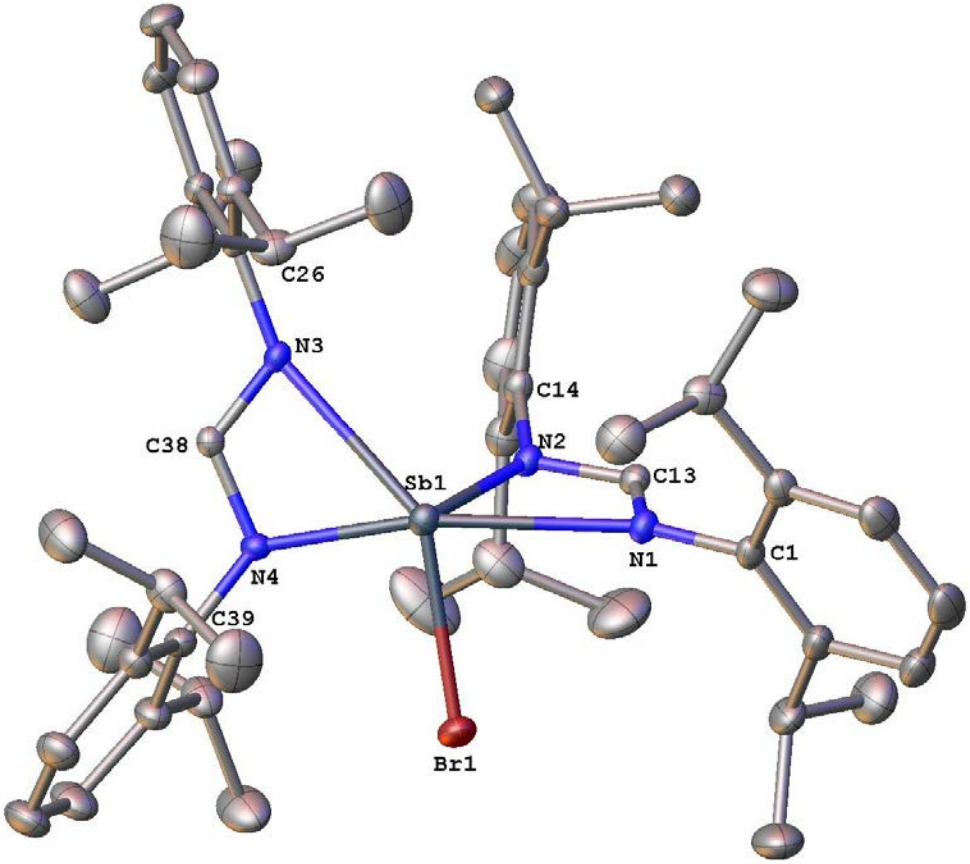

Figure 2.3. Molecular structure of monomeric **[Sb(DippForm)$_2$Br] (2.3)** with the atom numbering system; thermal ellipsoids are drawn at the 50 % probability level, and hydrogen atoms have been omitted for clarity. Selected bond lengths (Å) and angles (°): Sb(1)–N(1): 2.576(3), Sb(1)–N(2): 2.113(3), Sb(1)–N(3): 2.646(3), Sb(1)–N(4): 2.158(3), Sb(1)–Br(1): 2.5576(6), N(3)–C(38): 1.280(4), N(3)–C(26): 1.414(4), N(2)–C(13): 1.362(5), N(2)–C(14): 1.450(5), N(4)–C(38): 1.343(4), N(4)–C(39): 1.452(5), N(1)–C(13): 1.262(5), N(1)–C(1): 1.429(5), N(2)–Sb(1)–Br(1): 95.39(8), N(3)–Sb(1)–Br(1): 139.570(8), N(4)–Sb(1)–Br(1): 85.80(8), N(2)–Sb(1)–N(3): 88.142(11), N(2)–Sb(1)–N(4): 106.91(11), N(1)–Sb(1)–N(2): 56.31(11), N(3)–Sb(1)–N(4): 54.963(11), N(4)–Sb(1)–N(1): 156.24(11), C(38)–N(3)–Sb(1): 81.487(2), C(26)–N(3)–Sb(1): 153.080(2), C(38)–N(3)–C(26): 121.7(3), C(13)–N(2)–Sb(1): 102.0(2), C(13)–N(1)–Sb(1): 83.7(2), C(14)–N(2)–Sb(1): 138.4(2), C(14)–N(2)–C(13): 117.0(3), C(1)–N(1)–C(13): 123.6(3), C(39)–N(4)–Sb(1): 127.6(2), C(38)–N(4)–Sb(1): 101.7(2), C(38)–N(4)–C(39): 117.1(3), N(4)–C(38)–N(3): 118.8(3), N(1)–C(13)–N(2): 118.0(4).

An average Sb-N bond length of (**2.4**) was found to be 2.291 Å, range: 2.112(4) -2.634(3) Å (Figure 2.4). Despite the same coordination number in (**2.4**), the Sb–I bond distance was found to be 2.7725(6) Å, which is longer, as expected, than the Sb–Cl distance in (**2.2**) of 2.3972(7) Å and the Sb–Br distance in (**2.3**) of 2.5576(6) Å, due to the differing halide at sizes in the three compounds. The coordination environment for the Sb atom in (**2.2**, **2.3** and **2.4**) is similar with the Bi literature complexes [Bi(XylForm)$_2$Br] and [Bi(2-PhForm)$_2$Br], where XylForm and 2-PhForm ligands were involved instead of the bulky DippForm ligand.[9]

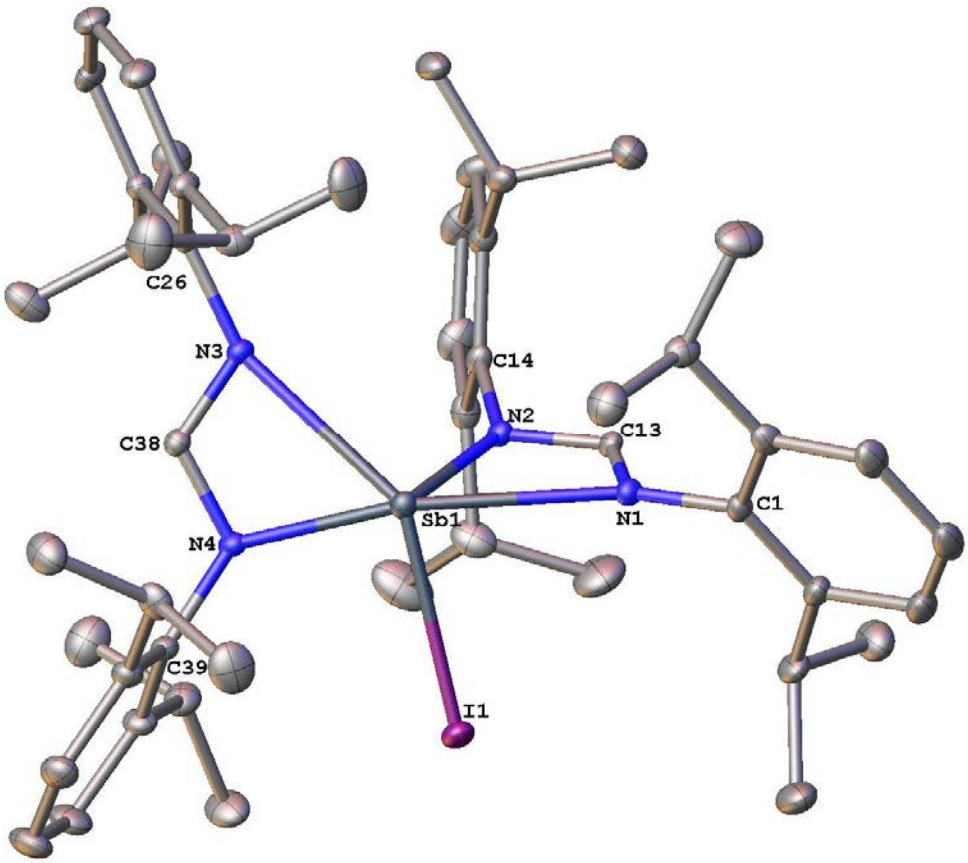

Figure 2.4. Molecular structure of monomeric **[Sb(DippForm)$_2$I] (2.4)** with the atom numbering system; thermal ellipsoids are drawn at the 50 % probability level, and hydrogen atoms and lattice PhMe have been omitted for clarity. Selected bond lengths (Å) and angles (°): Sb(1)–N(1): 2.597(4), Sb(1)–N(2): 2.112(4), Sb(1)–N(3): 2.634(3), Sb(1)–N(4): 2.165(4), Sb(1)–I(1): 2.7725(6), N(3)–C(38): 1.283(6), N(3)–C(26): 1.433(6), N(2)–C(13): 1.350(6), N(2)–C(14): 1.454(6), N(4)–C(38): 1.346(6), N(4)–C(39): 1.449(7), N(1)–C(13): 1.264(6), N(1)–C(1): 1.410(7), N(2)–Sb(1)–I(1): 96.58(11), N(3)–Sb(1)–I(1): 140.329(8), N(4)–Sb(1)–I(1): 86.40(10), N(2)–Sb(1)–N(3): 88.194(11), N(2)–Sb(1)–N(4): 106.94(16), N(4)–Sb(1)–N(1): 156.06(15), N(3)–Sb(1)–N(4): 54.833(11), N(1)–Sb(1)–N(2): 55.85(15), C(38)–N(3)–Sb(1): 82.556(2), C(26)–N(3)–Sb(1): 154.133(2), C(38)–N(3)–C(26): 119.6(4), C(13)–N(2)–Sb(1): 102.6(3), C(13)–N(1)–Sb(1): 83.9(3), C(14)–N(2)–Sb(1): 137.9(3), C(14)–N(2)–C(13): 117.4(4), C(1)–N(1)–C(13): 124.4(5), C(39)–N(4)–Sb(1): 127.0(3), C(38)–N(4)–Sb(1): 102.0(3), C(38)–N(4)–C(39): 116.9(4), N(4)–C(38)–N(3): 117.6(5), N(1)–C(13)–N(2): 118.6(5).

	2.2	**2.3**	**2.4**	**[Bi(DippForm)$_2$(Bu^n)]**	
Sb-N1	2.563(15)	2.576(3)	2.597(4)	**Bi-N1**	2.323(6)
Sb-N2	2.113(14)	2.113(3)	2.112(4)	**Bi-N2**	2.643(7)
Sb-N3	2.604(13)	2.646(3)	2.634(3)	**Bi-N3**	2.333(7)
Sb-N4	2.162(15)	2.158(3)	2.165(4)	**Bi-N4**	2.576(7)

Table 2.4 Selected Sb-N bond lengths (Å) for complexes: [Sb(DippForm)$_2$Cl] (**2.2**), [Sb(DippForm)$_2$Br] (**2.3**), [Sb(DippForm)$_2$I] (**2.4**) and [Bi(DippForm)$_2$(Bu^n)].[9]

Table 2.5 Crystallographic data for compounds 2.1 - 2.4

Compound	**2.1**	**2.2**	**2.3**	**2.4**
Formula	$C_{82}H_{134}N_4O_8Sb_2$	$C_{50}H_{70}ClN_4Sb$	$C_{50}H_{70}BrN_4Sb$	$C_{50}H_{70}IN_4Sb$
Fw	1547.51	884.32	928.80	975.79
crystal system	monoclinic	monoclinic	monoclinic	monoclinic
space group	$P2_1/c$	$P2_1/c$	$P2_1/c$	$P2_1/c$
a, Å	21.243(4)	18.443(4)	18.7239(14)	18.616(2)
b, Å	18.997(4)	20.455(4)	20.5497(17)	20.713(2)
c, Å	21.743(4)	12.817(3)	12.9785(10)	12.9942(13)
α, deg	90	90	90	90
β, deg	118.60(3)	97.46(3)	96.886(4)	96.750(5)
γ, deg	90	90	90	90
V, Å^3	7704(3)	4794.3(17)	4957.7(7)	4975.8(9)
Z	2	4	4	4
T, K	173.15	100.15	296(2)	296.15
no. of rflns collected	71852	87850	63608	63063
no. of indep rflns	21388	12579	8732	8728
Rint	0.0697	0.0406	0.1091	0.0889
Final *R1* values ($I > 2\sigma(I)$)	0.1352	0.0359	0.0402	0.0468
Final *wR*(F^2) values ($I > 2\sigma(I)$)	0.3964	0.1280	0.0876	0.1220
Final *R1* values (all data)	0.1556	0.0381	0.0825	0.0923
Final *wR*(F^2) values (all data)	0.4021	0.1321	0.1061	0.1580
GooF (on F^2)	1.198	1.194	1.009	0.869

[Sb(DippForm)X_2] (X= Br in 2.5, I in 2.6)

The crystalline monomeric complexes **[Sb(DippForm)Br_2]** (**2.5**) and **[Sb(DippForm)I_2]** (**2.6**) are isostructural and crystallised in the triclinic space group *P-1* (Table 2.8), with one molecule within the asymmetric unit. Single crystals were obtained from solution in THF (**2.5**) after storage at 15 ^{0}C for 1 day or in PhMe (**2.6**) after storage at – 30 ^{0}C for 12 hours. The formamidinate moiety in (**2.5**) and (**2.6**) again adopted the N,N′-chelating coordination mode, with four–electron donor ligands as observed for the literature corresponding *mono*-substituted amidinate dichloride complexes [Sb{RC(NR')$_2$}Cl_2] (R = *t*Bu, R' = *i*Pr, Cy, 2,6-*i*Pr$_2$C$_6$H$_3$; R = *n*Bu, R' = *i*Pr).[8] The antimony atom is coordinated by a bidentate (N,N') DippForm ligand and two bromide ligands in (**2.5**) or two iodide ligands in (**2.6**), giving a coordination number of four for the antimony atom. The molecular structure of the crystalline compound (**2.5**) is depicted in (Fig. 2.5). Both of (**2.5**) and (**2.6**) complexes have average Sb-N bond lengths 2.27 Å, which is significantly longer than the very short average of the Sb-N bond lengths (1.17 Å) reported for [Sb(ArNRNAr)I_2] (Ar = 2,6-*i*PrC$_6$H$_3$; R = NCy$_2$) due to the ligand size differences.[18] The structures of (**2.5**) and (**2.6**) were comparable somewhat with that of [Sb({N(2,4,6-Me$_3$C$_6$H$_2$)C(Me)}$_2$CH)Cl_2] (Scheme 2.16), in which π-delocalisation was much more noticeable, with Sb-N and N-C endocyclic bond lengths of 2.088/2.083 and 1.334/1.334 Å, respectively.[5]

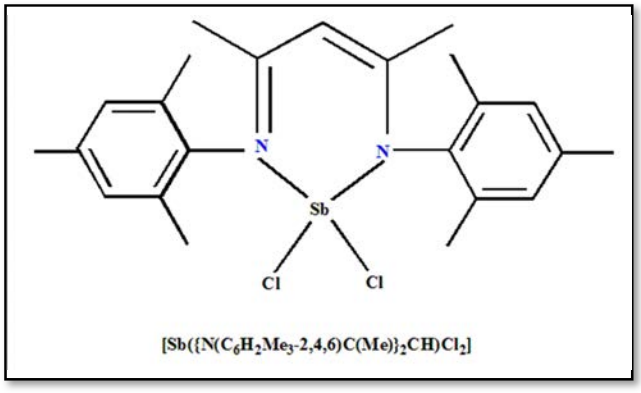

Scheme 2.16. Structure of [Sb({N(2,4,6-Me$_3$C$_6$H$_2$)C(Me)}$_2$CH)Cl_2].[5]

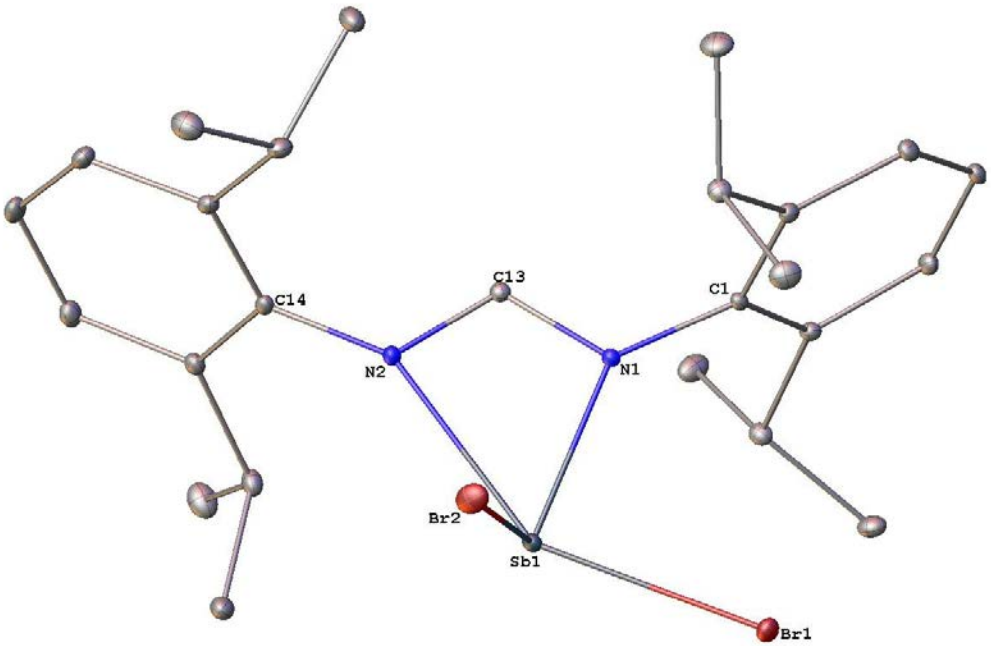

Figure 2.5. Molecular structure of monomeric **[Sb(DippForm)Br_2] (2.5)** with the atom numbering system; thermal ellipsoids are drawn at the 50 % probability level, and hydrogen atoms have been omitted for clarity. Selected bond lengths (Å) and angles (°):Sb(1)–N(1): 2.091(2), Sb(1)–N(2): 2.435(2), Sb(1)–Br(1): 2.5989(13), Sb(1)–Br(2): 2.5172(7), N(2)–C(13): 1.295(3), N(1)–C(13): 1.348(3), Br(2)–Sb(1)–Br(1): 94.98(3), Br(1)–Sb(1)–N(1): 90.13(6), N(1)–Sb(1)–Br(2): 98.92(5), N(2)–Sb(1)–Br(1): 148.10(5), N(2)–Sb(1)–Br(2): 87.08(5), N(2)–Sb(1)–N(1): 58.20(7), C(1)–N(1)–Sb(1): 137.39(15), C(13)–N(1)–Sb(1): 100.51(14), C(13)–N(2)–Sb(1): 86.43(14), C(14)–N(2)–Sb(1): 149.66(15), N(1)–C(13)–N(2): 114.4(2).

The N1–Sb1–N2 bond angles of 58.20(7)° (**2.5**) and 57.6(3)° (**2.6**) were normal as for metal amidinate complexes. The N1–C13–N2 bond angles of 114.5(11)° (**2.5**) and 114.4(2)° (**2.6**) were virtually identical. Even though the endocyclic bond lengths show that there is substantial π-delocalisation over the N1C13N2 moiety, the pairs of Sb–N1/Sb–N2 bond lengths vary by *ca.* 0.34, 2.091(2)–2.435(2) Å in (**2.5**), which is exactly the same difference for 2.457(9)–2.111(11) Å in (**2.6**). On the other hand, the dissimilar N1/N2–C13 bond lengths of 1.348(3)/1.295(3) Å (**2.5**) and 1.360(14)/1.281(15) Å (**2.6**) confirmed the limited delocalisation of the π-electrons in the amidinate backbone.

The overall coordination environment observed for the central Sb atoms in (**2.5** and **2.6**) was similar, where iodide ligands replace bromide ligands, and could possibly be described as a heavily distorted tetrahedral geometry. In contrast, the solid state structures of Group 15 *tetra*-coordinated bismuth (III) formamidinate complexes of the general formula [Bi(Form)X_2] have previously observed, forming symmetrical dimers, bridged by two bromides and a coordinated thf molecule on each Bi atom, namely [Bi(Form)Br(μ-Br)(thf)]$_2$ (Form = 2,6-*i*Pr$_2$C$_6$H$_3$, 2,6-Me$_2$C$_6$H$_3$). Whereas a thf deficient species have a weakly associated trinuclear array with two coordinated thf molecules per three Bi atoms [{Bi(2,6-*i*Pr$_2$C$_6$H$_3$)Cl$_2$(thf)}$_2$Bi(2,6-*i*Pr$_2$C$_6$H$_3$)Cl$_2$].[9] Complexes (**2.5**) and (**2.6**) are also similar to the structures of [Sb(Form)X_2] (X = F, N_3; Form = *t*BuC(N*i*Pr)$_2$, *t*BuC{N(2,6-*i*Pr$_2$C$_6$H$_3$)}$_2$), forming four membered ring NSbNC rhomboid.[43] The most prominent structural consistency between (**2.5**) and (**2.6**) is shown by the exocyclic X1–Sb–X2 bond angles (X = Br or I), 94.98(3)° in complex (**2.5**), which is almost identical with that in complex (**2.6**) 95.80(5)°.

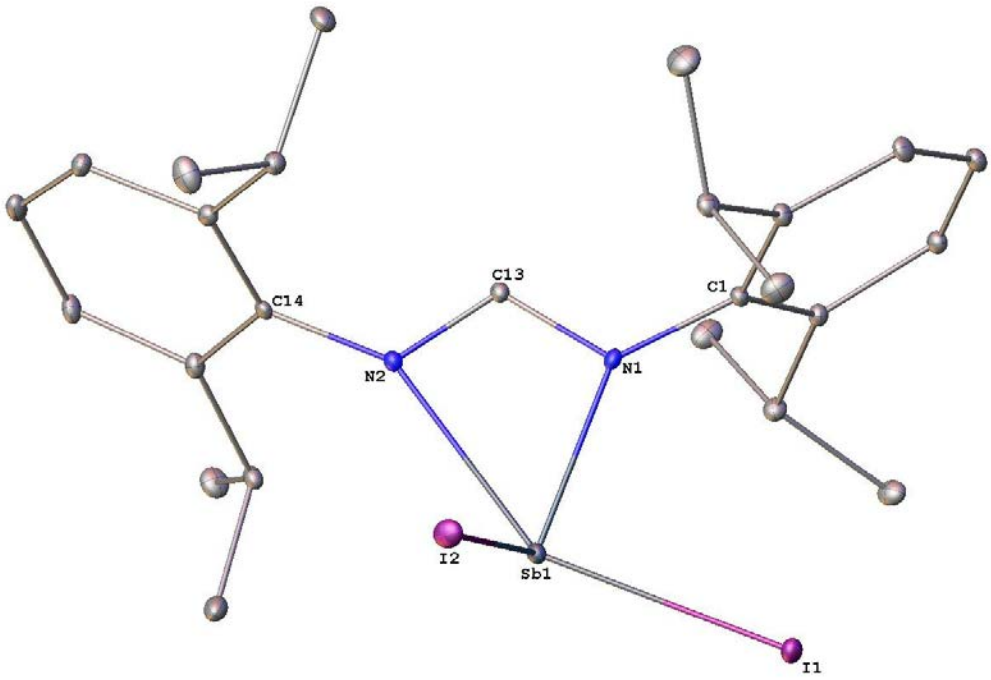

Figure 2.6. Molecular structure of monomeric **[Sb(DippForm)I_2] (2.6)** with the atom numbering system; thermal ellipsoids are drawn at the 50 % probability level, hydrogen atoms have been omitted for clarity. Selected bond lengths (Å) and angles (°): Sb(1)–N(2): 2.457(9), Sb(1)–N(1): 2.111(11), Sb(1)–I(1): 2.8215(13), Sb(1)–I(2): 2.7287(13), N(2)–C(13): 1.281(15), N(1)–C(13): 1.360(14), I(2)–Sb(1)–I(1): 95.80(5), N(2)–Sb(1)–I(1): 148.5(2), N(1)–Sb(1)–I(1): 91.1(2), N(1)–Sb(1)–I(2): 99.6(3), N(2)–Sb(1)–I(2): 86.9(2), N(1)–Sb(1)–N(2): 57.6(3), C(13)–N(2)–Sb(1): 87.1(7), C(13)–N(1)–Sb(1): 100.5(7), C(14)–N(2)–Sb(1): 149.2(8), C(1)–N(1)–Sb(1): 137.9(7), N(1)–C(13)–N(2): 114.5(11).

A feature of complexes of the form Sb(DippForm)$_2$X and Sb(DippForm)X_2 (X = Cl, Br, I) (**2.2 – 2.6)** is that the formation of the monomeric structures was favoured rather than a dimeric structures and showed noticeable asymmetry of the formamidinate binding, suggesting that they have reached coordination saturation.

	2.5	**2.6**	**[Sb{*t*BuC(N*i*Pr)$_2$}Cl$_2$]**	**[Sb{*t*BuC(NCy)$_2$}Cl$_2$]**	**[Sb{*t*BuC(NDipp)$_2$}Cl$_2$]**	**[Sb{*n*BuC(NiPr)$_2$}Cl$_2$]**	**[Sb(ArNRNAr)I$_2$] Ar = C$_6$H$_3$*i*Pr-2,6; R = NCy$_2$**
Sb-N1	2.091(2)	2.111(11)	2.101(16)	2.220(17)	2.104(2)	2.205(3)	2.230(2)
Sb-N2	2.435(2)	2.457(9)	2.190(17)	2.102(16)	2.305(19)	2.116(2)	2.123(2)
N1–C13	1.348(3)	1.360(14)	1.352(2)	1.320(3)	1.361(3)	1.319(4)	1.349(3)
N2–C13	1.295(3)	1.281(15)	1.320(2)	1.366(3)	1.323(3)	1.346(4)	1.374(3)
Sb-X1	2.598(13)	2.821(13)	2.403(6)	2.611(6)	2.366(8)	2.673(9)	2.907(6)
Sb-X2	2.517(7)	2.728(13)	2.643(6)	2.398(6)	2.473(7)	2.412(9)	2.743(6)
N1–Sb–N2	58.20(7)	57.60(3)	60.69(6)	60.41(6)	59.21(8)	60.99(10)	60.85(8)
N1–C13–N2	114.4(2)	114.5(11)	108.5(16)	108.2(18)	109.0(2)	110.8(3)	108.2(2)
X1–Sb–X2	94.98(3)	95.80(5)	88.02(2)	87.65(2)	90.27(3)	95.49(7)	87.43(13)

Table 2.6 Selected bond lengths (Å) and angles (°) for complexes: [Sb(DippForm)Br$_2$] (**2.5**), [Sb(DippForm)I$_2$] (**2.6**), [Sb{*t*BuC(NR)$_2$}Cl$_2$] (R = *i*Pr, Cy, Dipp),[8] [Sb{*n*BuC(N*i*Pr)$_2$}Cl$_2$][8] and [Sb{NCy$_2$(C$_6$H$_3$*i*Pr-2,6)$_2$}I$_2$].[18]

[Li_2I(DippForm)(μ-thf)$(thf)_2$] (2.7)

The lithium iodide adduct **[Li_2I(DippForm)(μ-thf)$(thf)_2$]** crystallised in the monoclinic space group $P2_1/n$ (Table 2.8), with one molecule within the asymmetric unit. Examination of the crystal structure in the solid state revealed that the monomeric structure of (**2.7**) featured a six-membered ring made up of one N,N′-formamidinato ligand, bridging two lithium centres by bimetallic bridging coordination mode (μ-[κ^1-N: κ^1-N']), and to maintain charge balance both lithium atoms pincer a single μ bridged iodide anion located between the two adjacent Li ions. The coordination sphere of the two lithium centres is accompanied by coordination of a μ bridging thf donor between the two lithium centres and a single donating thf molecule is coordinated to each lithium cation as shown in (Figure 2.**7**). An analogous structures were achieved with *p*-TolForm[44] and MesForm[45] ligands, even though with the less steric bulk of the ligand. The N,N′–chelating mode is usually observed with Li formamidinate, amidinate, guanidinate and β-diketiminate compounds.

Most of Li(*bis*(aryl)formamidinate) compounds are synthesised and used in *situ* during salt elimination reactions, and they have widespread synthetic applications.[46,47,48] [Li(DippForm)$(THF)_2$] is an example of these compounds.[49] The exact mechanism for the formation of (**2.7**) is illustrated in (Scheme 2.14), and as a result it appears that the compound is primary product formed, and it was stable enough to be isolated and characterised. There are two relatively short Li-I bond lengths 2.820(8) and 2.783(9) Å in [Li_2I(DippForm)(μ-thf)$(thf)_2$] comparing with the Li-I bond lengths 2.912(8) and 2.960(12) Å observed in [$(thf)_3Li_3(\mu_3$-I){$(NtBu)_3S$}].[50] The delocalisation of the anionic charge across the formamidinate backbone NCN in (**2.7**) is indicated by virtually identical C–N bonds 1.315(5) and 1.313(5) Å (Figure 2.7). The N–C–N bond angle of 124.2(4)° was bigger than what is usually stated for Li amidinate complexes displaying η^2-chelating mode such as the N–C–N bond angle of 122.01(15)° reported for [Li(DippForm)(PMDETA)] and 120.0(2)° for [Li(DippForm)$(THF)_2$].[49] The Li–N distances are found to be 1.971(8) and 2.003(8) Å, which are in the typical range of Li–N bond lengths.[49]

The Li–I–Li bond angle in (**2.7**) is 59.2(2)°, which is significantly smaller than the Li–I–Li bond angle (83.0(5)°) reported for [2,6-$Pmp_2C_6H_3Cd(\mu_3\text{-}I)_2\{Li(THF)\}]_2$,[51] while it is slightly smaller than the average Li–I–Li bond angle (57.7(1)°) reported for $[(ad)(SiMe_3)N]_2Li_3(\mu_3\text{-}I)(thf)_2$ (ad = adamantyl).[52] The formation of formamidinate bridged monomers have been commonly observed for lithium complexes involving formamidinate ligands (Scheme 2.17).[49]

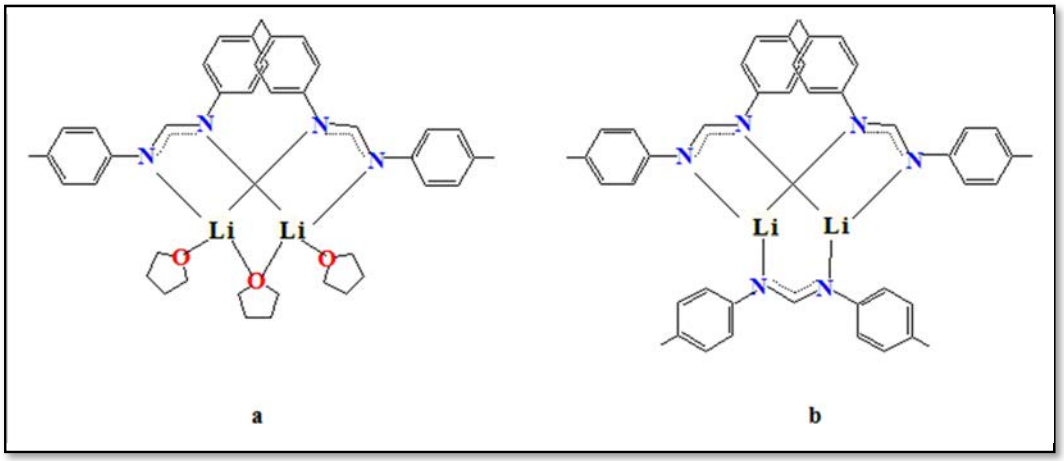

Scheme 2.17. Molecular structure of a: $[Li_2(p\text{-TolForm})_2(\mu\text{-THF})(THF)_2]$ and b: $[Li_2(p\text{-TolForm})_3]^-$.[49]

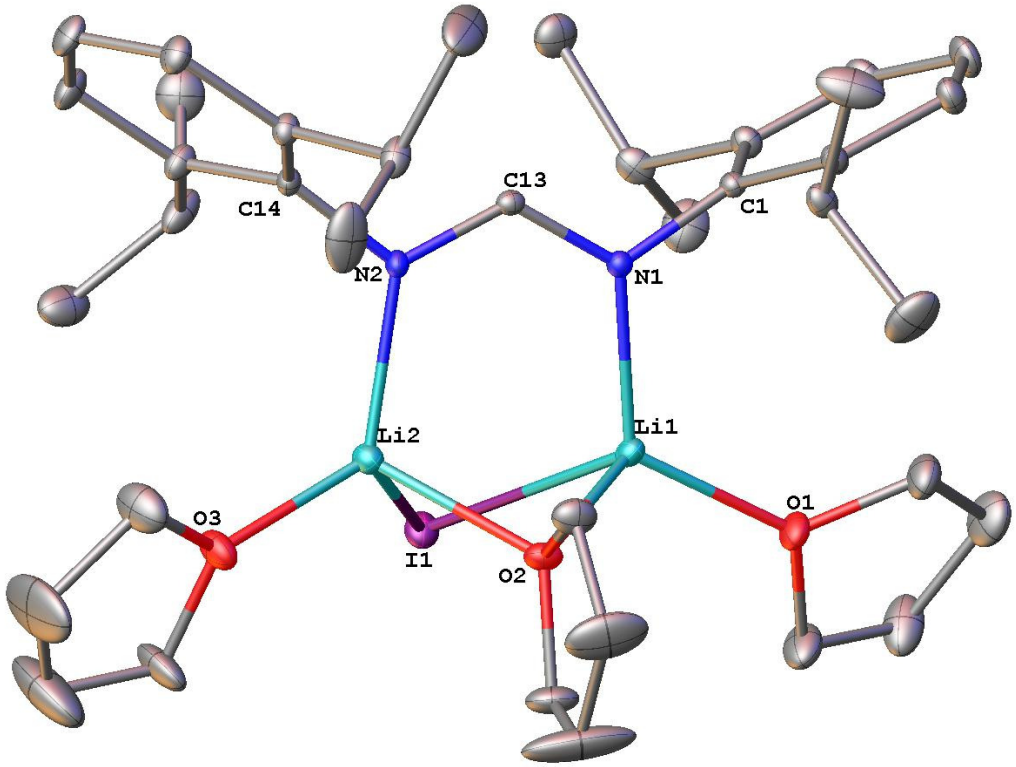

Figure 2.7. Molecular structure of monomeric **[Li_2I(DippForm)(μ-thf)(thf)$_2$] (2.7)** with the atom numbering system; thermal ellipsoids are drawn at the 50 % probability level, and hydrogen atoms have been omitted for clarity. Selected bond lengths (Å) and angles (°): Li(1)–N(1): 1.971(8), Li(2)–N(2): 2.003(8), Li(1)–I(1): 2.820(8), Li(2)–I(1): 2.783(9), N(2)–C(13): 1.315(5), N(2)–C(14): 1.432(5), N(1)–C(13): 1.313(5), N(1)–C(1): 1.427(5), O(2)–Li(2): 2.128(9), O(2)–Li(1): 2.105(8), O(1)–Li(1): 1.940(8), O(3)–Li(2): 1.901(9), I(1)–Li(1)–N(1): 113.6(3), I(1)–Li(2)–N(2): 112.7(4), N(1)–C(13)–N(2): 124.2(4), Li(2)–I(1)–Li(1): 59.2(2), Li(1)–O(2)–Li(2): 81.6(3), C(14)–N(2)–Li(2): 120.3(3), C(13)–N(2)–Li(2): 122.7(3), C(1)–N(1)–Li(1): 114.4(3), C(13)–N(1)–Li(1): 125.4(3), O(2)–Li(2)–I(1): 92.5(3), O(3)–Li(2)–I(1): 113.6(4), O(3)–Li(2)–O(2): 107.2(4), O(3)–Li(2)–N(2): 120.8(4), N(2)–Li(1)–I(1): 92.0(3), O(1)–Li(1)–I(1): 107.4(4), O(1)–Li(1)–O(2): 114.5(4), O(1)–Li(1)–N(1): 122.1(4), N(1)–Li(1) –O(2): 103.2(4).

[Sb(DippForm)(NSiMe$_3$)]$_2$ (2.8)

The Sb^{+3} complex **[Sb(DippForm)(NSiMe$_3$)]$_2$** (**2.8**) crystallised as a solvent free product in the triclinic space group *P-1* (Table 2.8), with one molecule within the asymmetric unit. No significant intermolecular contacts were observed. X-ray determination for the structure in the solid state revealed that the complex is dimer resides on an inversion centre at centre of the Sb_2N_2 ring, more specifically the inversion centre located at the midpoint of the Sb(1)···Sb(1)# vector. The whole molecule generated by the symmetry operation ^{1}1-X,1-Y,1-Z as depicted in (Figure 2.8).

The two **[Sb(DippForm)(NSiMe$_3$)]** units are joined through N atoms from symmetrical bridging silyl amide moieties and one nitrogen bridging terminal DippForm ligand, giving the antimony atom a coordination number of three and a stereochemistry best described as distorted trigonal pyramidal with a stereochemically active lone pair residing in a fourth coordination site (Scheme. 2.18). Generally, the cationic charge of +3, from each Sb^{3+} ion in the dimer is balanced by a (–1) charge detected for terminal formamidinate ligand, and a (–2) charge for bridged silyl amide moiety $[N(SiMe_3)]^{2-}$.Thus, the Sb_2N_2 ring in (**2.8**) is planar with a slight difference between bond lengths of Sb1-N3 2.057(12) and Sb1-N3# 2.071(12) Å, adopting the *trans* configuration with respect to the capped monodentate DippForm ligand. The N3−Sb1−N3# bond angle of 81.7(5)° was significantly smaller compared with the Sb1−N3#−Sb1# angle of 98.3(5)° (Figure 2.8). The N1−Sb1−N3 and N1#−Sb1#−N3# angles were found between 98.2(4) and 103.0(5)°, which is similar to the angles N−P−O (97.6 and 103.7°) reported in the structure of $[R_fOP(\mu\text{-}NSiMe_3)]_2$.[12]

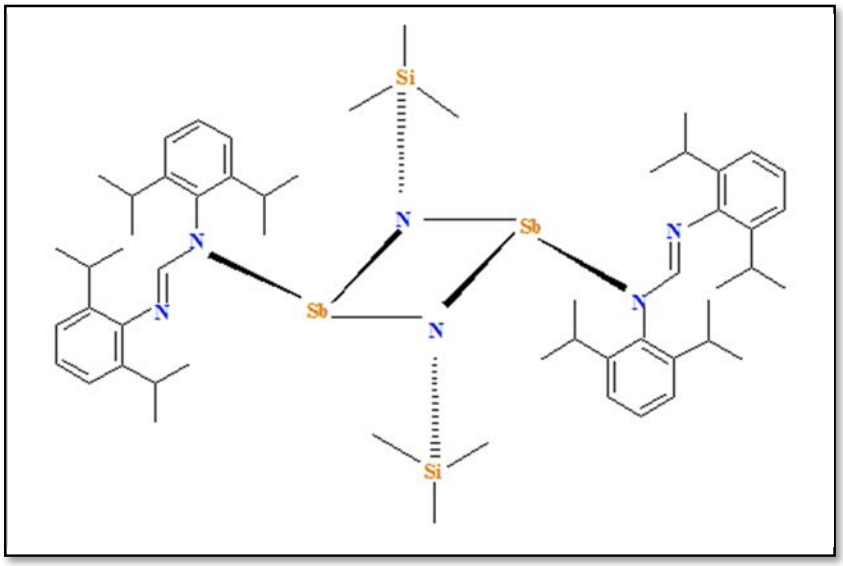

Scheme 2.18 Diagram of the dinuclear antimony (III) complex (**2.8**).

The Sb-N bond length associated with the DippForm of (**2.8**) was found to be 2.150(12) Å, while Sb-N bond length that belongs to the $SiMe_3$ moiety was 2.057(12) Å, which is slightly longer than the Sb–N bond length (2.033 Å) reported for [Ter(Me_3Si)N-$SbCl_2$] (Ter = terphenyl = 2,6-bis(2,4,6-trimethyl-phenyl)phenyl),[11] presumably due to steric demand differences. Whereas, it is not surprisingly almost the same as the Sb–N bond length (2.059(2) Å) reported for [Mes*{Me_2(Cl)Si}N-Sb(Cl)Me] (Mes* = supermesityl = 2,4,6-tri-*tert*-butylphenyl).[11] The Sb–N bond distance 2.057(12) Å in respect to the $SiMe_3$ moiety of (**2.8**) was in close proximity into the Ga–N bond distance 1.989(5) Å in a known four-coordinate Ga of [($Me_3Si)_2$NSbCl][($Me_3Si)_2$N($GaCl_3)_2$],[11] in spite of metals size differences.

The Sb–N($SiMe_3$) bond length is found to be 2.057(12) Å, which is in the typical range found for Sb–N single bonds. For example, (Sb–N) = 2.056(3) in Mes*N($SiMe_3$)–$SbCl_2$,[53] 2.092(2) in [*t*BuC(*i*PrN)$_2$]Sb($N_3)_2$,[54] ($\sum r_{cov}$ (Sb–N) = 2.11 Å).[28] However, the N($SiMe_3$) group in (**2.8**) is covalently bound to the antimony centre. The Si–N bond length found to be 1.715(13) Å ($\sum r_{cov}$ (Si–N) = 1.87 Å).[28]

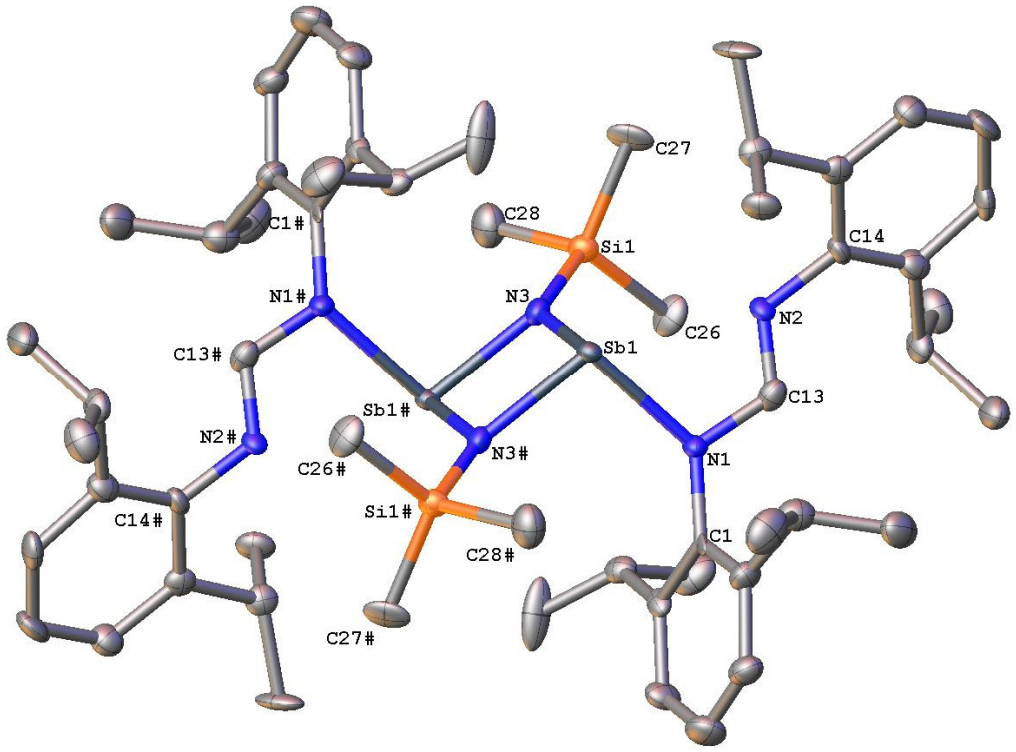

Figure 2.8. Molecular structure of dimeric **[Sb(DippForm)(NSiMe$_3$)]$_2$ (2.8)** with the atom numbering system; thermal ellipsoids are drawn at the 50 % probability level, and hydrogen atoms have been omitted for clarity. Selected bond lengths (Å) and angles (°): Sb(1)–N(3): 2.057(12), Sb(1)–N(3)#: 2.070(12), Sb(1)–N(1): 2.150(12), N(3)–Si(1): 1.715(13), Si(1)–C(26): 1.842(17), Si(1)–C(27): 1.838(15), Si(1)–C(28): 1.866(18), N(2)–C(13): 1.285(18), N(2)–C(14): 1.412(16), N(1)–C(13): 1.359(18), N(1)–C(1): 1.420(17), N(1)–Sb(1)–N(3): 103.0(5), N(3)–Sb(1)–N(3)#: 81.705(5), N(1)–Sb(1)–N(3)#: 98.2(5), Sb(1)–N(3)–Sb(1)#: 98.295(7), N(3)–Si(1)–C(26): 110.8(7), N(3)–Si(1)–C(27): 113.7(7), N(3)–Si(1)–C(28): 107.0(7), Si(1)–N(3)–Sb(1): 132.5(7), C(13)–N(1)–Sb(1): 105.5(9), C(1)–N(1)–Sb(1): 129.1(9), N(2)–C(13)–N(1): 117.6(13).

= Atoms generated by symmetry: [1]1-X,1-Y,1-Z.

	2.8	**[Ter(Me$_3$Si)N-SbCl$_2$]**	**Ter(Me$_3$Si)N–Sb(O*t*Bu)$_2$**	**Ter(Me$_3$Si)N–Sb(N$_3$)$_2$**	**(Me$_3$Si)$_2$N–SbCl$_2$**	**[(Me$_3$Si)$_2$NSbCl][(Me$_3$Si)$_2$N(GaCl$_3$)$_2$]**
Sb-N(SiMe$_3$)	2.057	2.033(3)	2.033(1)	2.013(2)	2.002(2)	1.953(5)
N-Si	1.715(13)	1.783(4)	1.770(1)	1.782(2)	1.767(3) –1.776(3)	1.868(7) –1.715(7)
Sb–N–Si	132.5(7)	126.1(2)	121.7(6)	125.1(1)	113.5(13) –124.9(14)	109.7(3) –132.3(4),

Table 2.7 Selected bond lengths (Å) and bond angles (°) for [Sb(DippForm)N(SiMe$_3$)]$_2$ (**2.8**) and literature aminostibane complexes [Ter(Me$_3$Si)N-SbCl$_2$], Ter(Me$_3$Si)N–Sb(O*t*Bu)$_2$, Ter(Me$_3$Si)N–Sb(N$_3$)$_2$, (Me$_3$Si)$_2$N–SbCl$_2$, [(Me$_3$Si)$_2$NSbCl][(Me$_3$Si)$_2$N(GaCl$_3$)$_2$].[11]

Table 2.8 Crystallographic data for compounds (2.5 - 2.8).

Compound	**2.5**	**2.6**	**2.7**	**2.8**
Formula	$C_{25}H_{35}Br_2N_2Sb$	$C_{25}H_{35}I_2N_2Sb$	$C_{37}H_{59}ILi_2N_2O_3$	$C_{56}H_{88}N_6Sb_2Si_2$
Fw	645.12	739.12	720.67	1145.05
crystal system	triclinic	triclinic	monoclinic	triclinic
space group	*P-1*	*P-1*	$P2_1/n$	*P-1*
a, Å	10.105(2)	10.4137(4)	9.7157(7)	9.7000(19)
b, Å	10.332(2)	10.5559(4)	18.4703(13)	11.793(2)
c, Å	14.240(3)	14.6097(5)	22.9728(15)	14.246(3)
α, deg	96.69(3)	95.876(2)	90	74.24(3)
β, deg	103.93(3)	104.946(2)	94.165(4)	70.22(3)
γ, deg	111.72(3)	111.754(2)	90	73.62(3)
V, Å^3	1305.2(5)	1405.64(9)	4111.6(5)	1443.0(6)
Z	2	2	4	2
T, K	293(2)	296(2)	296.15	100.15
no. of rflns collected	23525	35754	75506	12213
no. of indep rflns	6299	6393	12018	4429
Rint	0.0324	0.0773	0.1342	0.0234
Final *R1* values ($I > 2\sigma(I)$)	0.0283	0.0710	0.0698	0.0950
Final *wR*(F^2) values ($I > 2\sigma(I)$)	0.0755	0.2050	0.1614	0.2892
Final *R1* values (all data)	0.0291	0.0884	0.2143	0.0954
Final *wR*(F^2) values (all data)	0.0760	0.2263	0.2284	0.2892
GooF (on F^2)	1.077	1.039	0.910	1.255

[SiMe$_3$(DippForm)] (2.9)

Si^{+4} complex **[SiMe$_3$(DippForm)]** (**2.9**) was isolated by fractional crystallisation from the mother liquor of (**2.8**) as another component of the Schlenk equilibrium involving Dippform ligand. Compound (**2.9**) crystallised in the monoclinic space group *P2$_1$/c* (Table 2.9), with one molecule within the asymmetric unit. The monomeric unit of the four-coordinate Si metal centre displays tetrahedral geometry and is coordinated by one monodentate Dippform ligands through the nitrogen donor atom and the other three sites are occupied by three methyl groups. Selected bond lengths and angles of (**2.9**) are showed in (Figure 2.9).

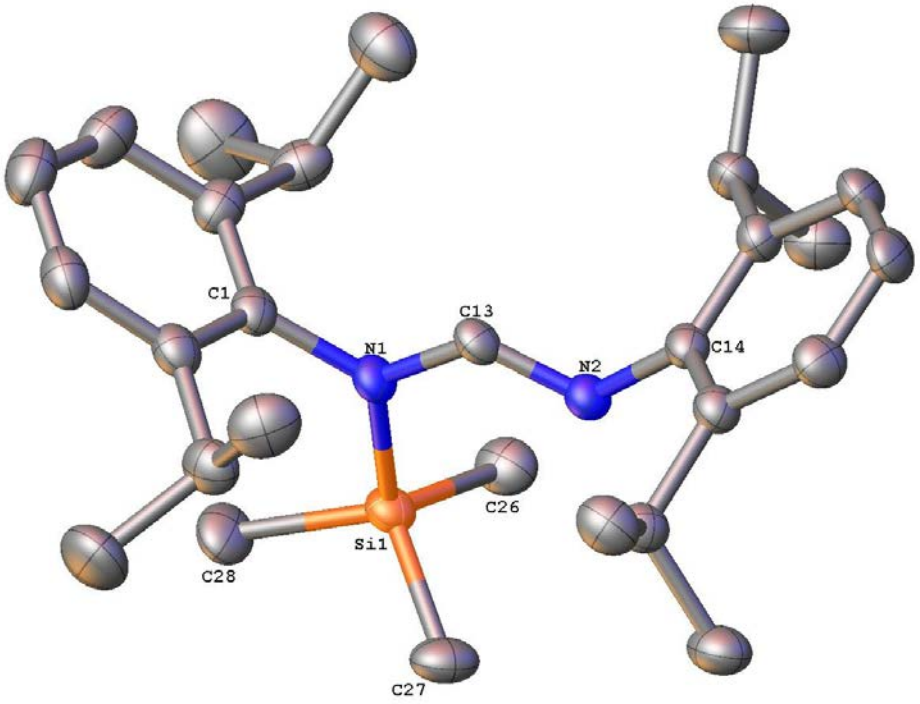

Figure 2.9. Molecular structure of a monomeric unit of **[SiMe$_3$(DippForm)] (2.9)** with the atom numbering system; thermal ellipsoids are drawn at the 50 % probability level, and hydrogen atoms have been omitted for clarity. Selected bond lengths (Å) and angles (°):Si(1)–N(1): 1.783(2), Si(1)–C(26): 1.856(3), Si(1)–C(27): 1.860(3), Si(1)–C(28): 1.860(3), N(2)–C(13): 1.275(3), N(2)–C(14): 1.426(3), N(1)–C(13): 1.373(3), N(1)–C(1): 1.451(3), N(1)–Si(1)–C(26): 110.30(12), N(1)–Si(1)–C(27): 111.35(12), N(1)–Si(1)–C(28): 104.90(12), C(13)–N(1)–Si(1): 120.48(17), C(1)–N(1)–Si(1): 124.15(16), N(2)–C(13)–N(1): 122.9(2).

[$SbCl_3(Me_2NC_2H_4NMe_2)$] (2.10)

The incorporation of N,N,N',N'-tetramethylethylenediamine (TMEDA) into antinmony chemistry provided typical N-donor binding modes. In the solid state, **[$SbCl_3(Me_2NC_2H_4NMe_2)$]** a mononuclear monomeric complex is formed using the usually chelating TMEDA ligand. Complex (**2.10**) crystallised in the monoclinic space group $P2_1/c$ (Table 2.9), with one molecule within the asymmetric unit. The central antimony atom is surrounded by the two nitrogens of a chelating (TMEDA) ligand and three chloride ligands. The overall geometry of the pentacoordinated Sb metal centre can be assigned as distorted square-pyramidal arrangement. An average Sb-N bond length: 2.45 Å, range: 2.436(3) – 2.471(4) Å. The Sb atom in (**2.10**) is bonded to a bidentate TMEDA ligand Sb–N 2.436(3) and 2.471(4) Å and three chloride ligands Sb–Cl 2.5349(11), 2.5859(10) and 2.3956(11) Å with N1–Sb1–N2 bond angle found to be 74.42(15)°. Slightly longer Sb–N bond distances 2.490(3) and 2.595(3)° with somewhat smaller N1–Sb1–N2 71.96(9) bond angle were observed in [$Sb(CO_2Ph$-*o*-$CO_2Me)_2(OMe)(tmeda)$] complex.[55]

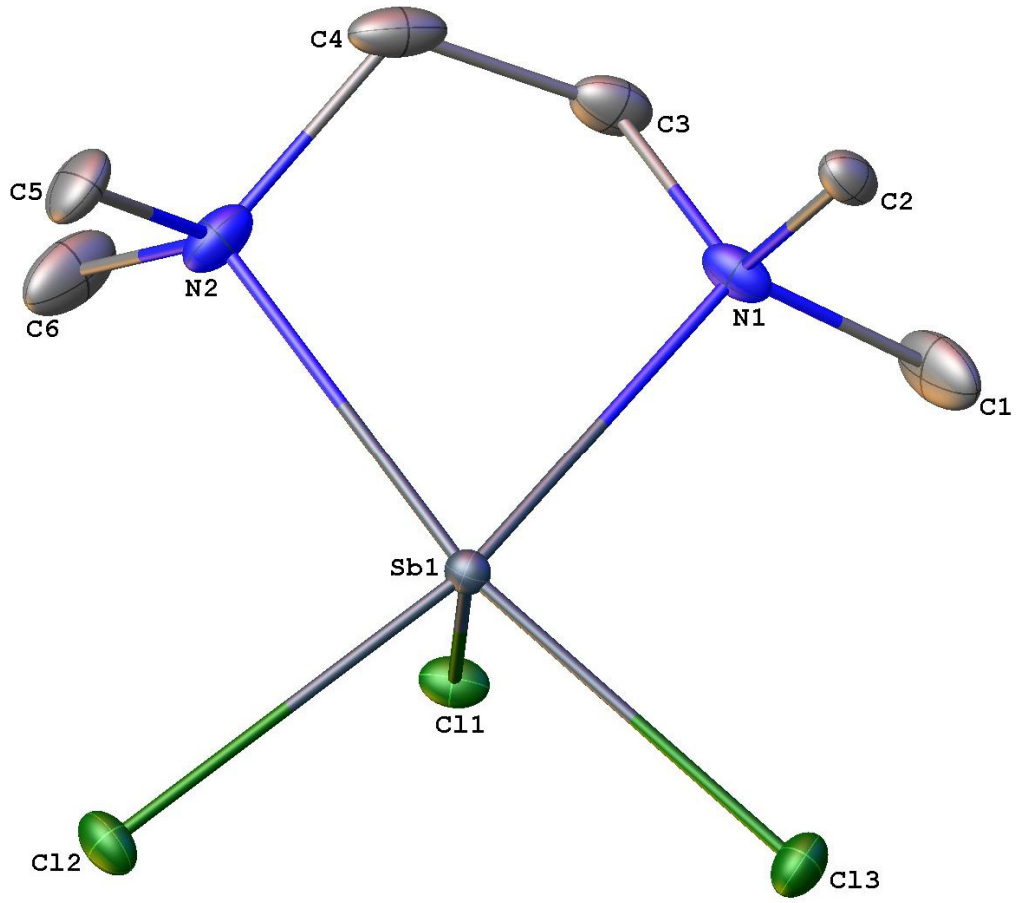

Figure 2.10. Molecular structure of monomeric **[$SbCl_3(Me_2NC_2H_4NMe_2)$] (2.10)** with the atom numbering system; thermal ellipsoids are drawn at the 50 % probability level, and hydrogen atoms have been omitted for clarity. Selected bond lengths (Å) and angles (°): Sb(1)–N(1): 2.436(3), Sb(1)–N(2): 2.471(4), Sb(1)–Cl(3): 2.5349(11), Sb(1) – Cl(2): 2.5859(10), Sb(1)–Cl(1): 2.3956(11), N(1)–C(1): 1.516(7), N(1)–C(2): 1.477(5), N(1)–C(3): 1.414(6), N(2)–C(4): 1.572(8), N(2)–C(5): 1.457(6), N(2)–C(6): 1.451(7), N(1)–Sb(1)–N(2): 74.42(15), Cl(2)–Sb(1)–Cl(1): 86.55(4), Cl(2)–Sb(1)–Cl(3): 100.72(4), Cl(1)–Sb(1)–Cl(3): 87.77(4), N(1)–Sb(1)–Cl(1): 83.13(9), N(1)–Sb(1)–Cl(2): 163.62(10), N(1)–Sb(1)–Cl(3): 91.58(10), N(2)–Sb(1)–Cl(1): 85.27(10), N(2)–Sb(1)–Cl(2): 92.11(12), N(2)–Sb(1)–Cl(3): 165.00(11), C(1)–N(1)–Sb(1): 113.8(3), C(2)–N(1)–Sb(1): 104.5(2), C(3)–N(1)–Sb(1): 109.3(3), C(4)–N(2)–Sb(1): 103.7(3), C(5)–N(2)–Sb(1): 104.3(3), C(6)–N(2)–Sb(1): 116.9(3).

[(DippForm)ClSb(μ-O)SbCl$_2$(Me$_2$NC$_2$H$_4$NMe$_2$)]$_2$.C$_6$D$_6$ (2.11)

The obtained small offwhite single crystals grown in C_6D_6 were suitable for identification by X-ray diffraction studies, illuminating the establishment of a dinuclear oxide complex **[(DippForm)ClSb-μ-OSbCl$_2$(Me$_2$NC$_2$H$_4$NMe$_2$)]$_2$.(C$_6$D$_6$)**. The Sb^{+3} complex crystallised in the monoclinic space group *P2$_1$/c* (Table 2.9). Two crystallographically independent molecules with similar core coordination geometries were present within the asymmetric unit.

Overall, the molecular structure of the dineclear (**2.11**) complex was undoubtedly asymmetrical, showing an oxygen associated as a bridge between the two antimony atom centres. One of the Sb metal centre chelated by terminal η^2 (N,N') DippForm ligand through the nitrogen donor atoms Sb–N (2.153(11) and 2.570(10) Å), with one apical chlorine atom Sb–Cl (2.346(5) Å) and a ***μ*** oxygen atom with Sb–O distance of 1.979(9) Å giving the Sb a coordination number of four and geometry best described as a distorted tetrahedron (considering DippForm to occupy a single coordination site at the mid-point of the N–N vector). While the other Sb atom in (**2.11**) is bonded to a bidentate TMEDA ligand Sb–N (2.259(13) and 2.535(15) Å), two chloride ligands Sb–Cl (2.795(4) and 2.484(5) Å) and a ***μ*** oxygen atom with Sb–O distance of 1.923(9) Å (Fig. 2.11), giving the Sb a coordination number of five, and stereochemistry best described as a distorted trigonal bipyramid. Complex (**2.11**) had one C_6D_6 molecule filling the space in the X-ray crystal structure lattice. Furthermore, the structure had two *transoid* angles of Cl(2)–Sb(2)–Cl(3) 96.24(18)◦ and Cl(1)–Sb(1)–N(2) 95.47(3)◦. Slightly longer Sb–N bond distances of 2.490(3) and 2.595(3), with a smaller N–Sb–N 71.96(9) bond angle and a similar Sb–O bond distance of 1.951(2) were observed in [Sb(CO$_2$Ph-*o*-CO$_2$Me)$_2$(OMe)(tmeda)] complex,[55] In fact, attempt to deliberate synthesise (**2.11**) was impossible, as only starting materials isolated and could be identified by ^{1}H-NMR spectra. However, the obtained complex showed how the steric protection offered by DippForm ligand governs the nuclearity of the product and affords monomers. The average Sb–N bond lengths in (**2.10**) and (**2.11**) were found to be 2.45 Å, 2.37 Å respectively. The average N–Sb–N bond angles of (Me$_2$NC$_2$H$_4$NMe$_2$) in (**2.10**) and (**2.11**) were found to be 74.4 °, 75.8(6)° respectively.

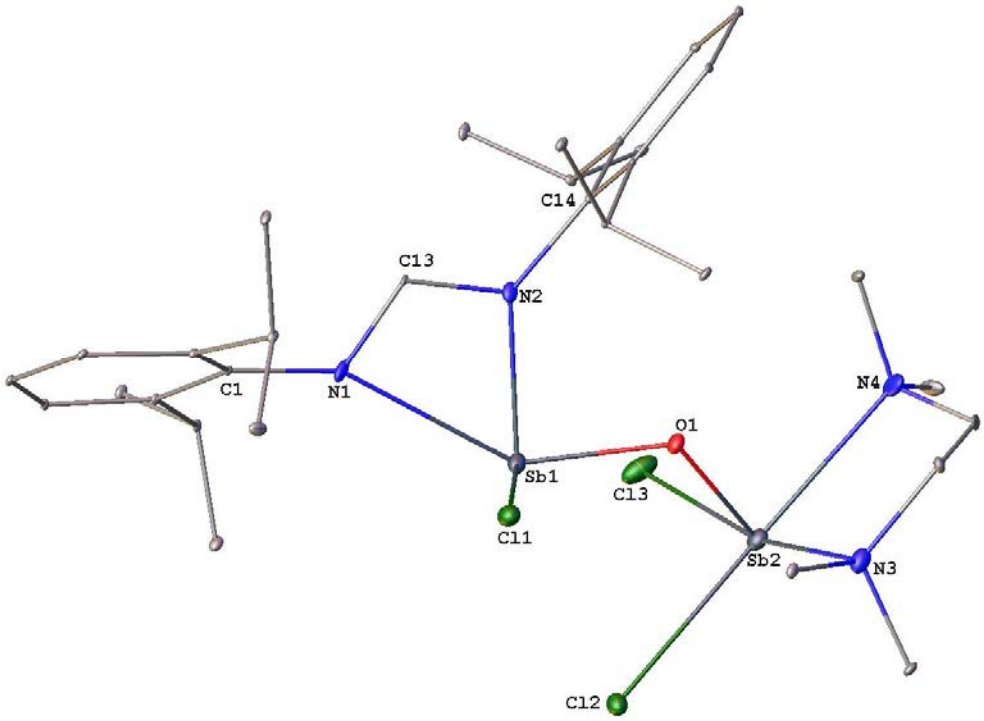

Figure 2.11. Molecular structure of monomeric **[(DippForm)ClSb(*μ*-O)SbCl$_2$(Me$_2$NC$_2$H$_4$NMe$_2$)]$_2$.(C$_6$D$_6$) (2.11)** with the atom numbering system; thermal ellipsoids are drawn at the 50 % probability level, and hydrogen atoms and lattice C$_6$D$_6$ have been omitted for clarity. This is one of the two molecules in the asymmetric unit and the other molecule is essentially the same. Selected bond lengths (Å) and angles (°): Sb(1)–N(2): 2.153(11), Sb(1)–N(1): 2.570(10), Sb(2)–N(3): 2.259(13), Sb(2)–N(4): 2.535(15), Sb(1)–Cl(1): 2.346(5), Sb(2)–Cl(2): 2.795(4), Sb(2)–Cl(3): 2.484(5), Sb(2)–O(1): 1.923(9), Sb(1)–O(1): 1.979(9), N(2)–C(13): 1.363(18), N(1)–C(13): 1.371(16), N(1)–C(1): 1.451(16), N(2)–C(14): 1.516(17), N(1)–Sb(1)–N(2): 58.29(4), N(3)–Sb(2)–N(4): 75.84(6), N(2)–C(13)–N(1): 116.79(11), Sb(2)–O(1)–Sb(1): 119.35(5), Cl(1)–Sb(1)–N(1): 77.80(3), O(1)–Sb(1)–Cl(1): 98.97(3), N(2)–Sb(1)–Cl(1): 95.47(3), Cl(3)–Sb(2)–Cl(2): 96.24(18), Cl(3)–Sb(2)–N(4): 95.18(5), O(1)–Sb(2)–Cl(3): 85.06(3), N(3)–Sb(2)–Cl(3): 165.66(4), O(1)–Sb(2)–Cl(2): 86.94(3), N(4)–Sb(2)–Cl(2): 165.42(5), N(3)–Sb(2)–Cl(2): 91.11(4), O(1)–Sb(2)–N(4): 85.05(4), O(1)–Sb(2)–N(3): 83.05(4), C(13)–N(1)–Sb(1): 83.54(7), C(13)–N(2)–Sb(1): 101.35(8), C(1)–N(1)–Sb(1): 153.65(9), C(14)–N(2)–Sb(1): 136.23(8), O(1)–Sb(1)–N(1): 143.4(4), O(1)–Sb(1)–N(2): 86.17(4).

[Sb(DippForm)Cl(C_6F_5)]$_2$.(THF)$_2$ (2.12)

In a simple one–pot synthesis, antimony trichloride, Hg(C_6F_5)$_2$ and one equivalent of DippFormH were stirred in THF for several days. During this, the reaction mixture became cloudy as elemental mercury is liberated. A small number of single crystals of **[Sb(DippForm)Cl(C_6F_5)]$_2$.(THF)$_2$** were isolated from the filtered reaction mixture; thus, the very poor yield disallowed additional characterisation. The antimony complex (**2.12**) crystallised in the triclinic space group *P-1* (Table 2.9), with two molecules within the asymmetric unit. Compound (**2.12**) is a centrosymmetric dimer species (Scheme 2.19), composed of two [Sb(DippForm)Cl(C_6F_5)] units. The X-ray crystal structure of (**2.12**) showed a pair of chloro ligands are symmetrically bridging between the two antimony centres with the complex coordination sphere consisting of one κ^1-bound DippForm ligand and one pentafluorophenyl ligand coordinated to each Sb metal centre, in addition to two uncoordinated THF molecules per dimer. The stereochemistry around each four-coordinate Sb metal centre in the dimer can be best described as distorted tetrahedral. Half of the structure was generated by symmetry through an inversion centre located at the midpoint of the Sb(1)···Sb(1)# vector.

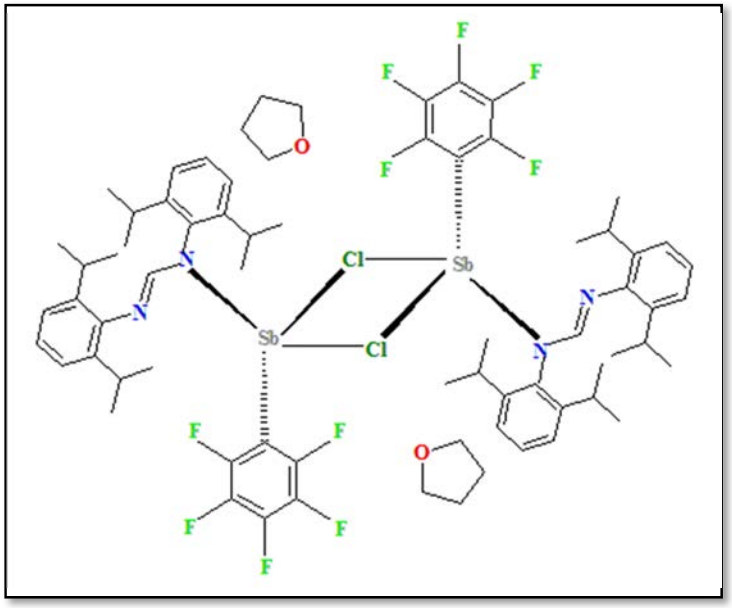

Scheme 2.19 Diagram of dinuclear antimony complex (**2.12**).

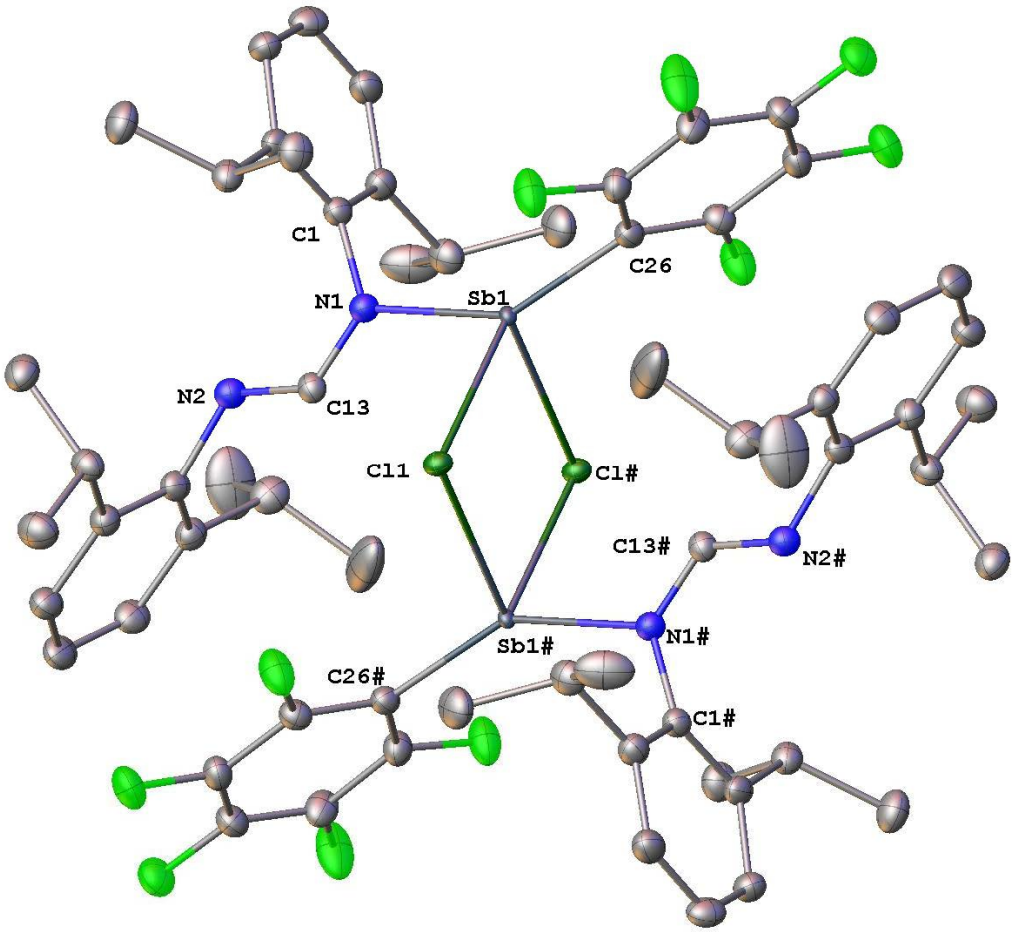

Figure 2.12. Molecular structure of dimeric **[Sb(DippForm)Cl(C_6F_5)]$_2$.(THF)$_2$** (**2.12**) with the atom numbering system; thermal ellipsoids are drawn at the 50 % probability level, and hydrogen atoms have been omitted for clarity. Selected bond lengths (Å) and angles (°): Sb(1)–N(1): 2.189(6), Sb(1)–Cl(1): 2.705(16), Sb(1)–Cl(1)#: 2.757(17), Sb(1)–C(26): 2.097(7), N(1)–C(13): 1.281(8), N(2)–C(13): 1.314(8), N(1)–Sb(1)–Cl(1): 91.93(16), N(1)–Sb(1)–Cl(1)#: 91.83(15), N(1)–Sb(1)–C(26): 146.3(2), C(26)–Sb(1)–Cl(1): 113.6(2), C(26)–Sb(1)–Cl(1)#: 111.0(2), N(1)–C(13)–N(2): 126.3(6).
= Atoms generated by symmetry: [1]2-X,1-Y,-Z; [2]1-X,1-Y,1-Z

Complex (**2.12**) was the first reported pentafluorophenyl antimony formamidinate/amidinate complex, with the Sb–N bond length found to be 2.189(6) Å. Antimony (III) complexes containing an aryl ligand such as (**2.12**) are uncommon, and only three structures have been described previously in the literature; $(C_6F_5)_3Sb$,[25] $(C_6F_5)SbCl_2$,[26] and a carboxylato complex $[CH_3CO_2SbPh_4]$.[56]

Replacement of one or more of the chlorine atoms by phenyl groups will give $[Sb(DippForm)Cl(C_6F_5)]_2.(THF)_2$, with potential change in antimony Lewis acidity. This subject has been little examined, and compounds previously described were very hard making sensitive samples of the related antimony (III) species. Because of the lack of data in this area, we have systematically examined reaction of $SbCl_3$ with the formamidine ligand and *bis*-pentafluorophenyl mercury, the latter as the source of pentafluorophenyl ions, in order to assess the ability of antimony to coordinate variety of an inions. The Sb–C distance in (**2.12**) is value of 2.097 Å, which is shorter than the Sb–C bond lengths (2.196 Å) reported for $[CH_3CO_2SbPh_4]$,[56] and was also shorter than the average value of Sb–C bond lengths (2.170 Å) reported for the well compared *tris*(pentafluorophenyl)stibine $Sb(C_6F_5)_3$.[57]

The Sb–Cl bond lengths of **$[Sb(DippForm)Cl(C_6F_5)]_2.(THF)_2$** were found to be 2.705(16), 2.757(17) Å for Sb1–Cl1 and Sb1–Cl1# respectively, which are shorter than the Sb–Cl bond lengths 2.817(3) and 2.859(3) Å reported for an asymmetric chloride bridged dimer $[H_2L]_2[Sb_2OCI_6]Cl_2$.[58]

The formation of halide bridged dimers (Figure 2.13) have been more commonly detected for haloorganoantimony complexes. Figure 2.13 shows some known halide-bridged dimeric and non-dimeric haloorgano Sb^{+3} and Sb^{+5} complexes. [5,7,20]

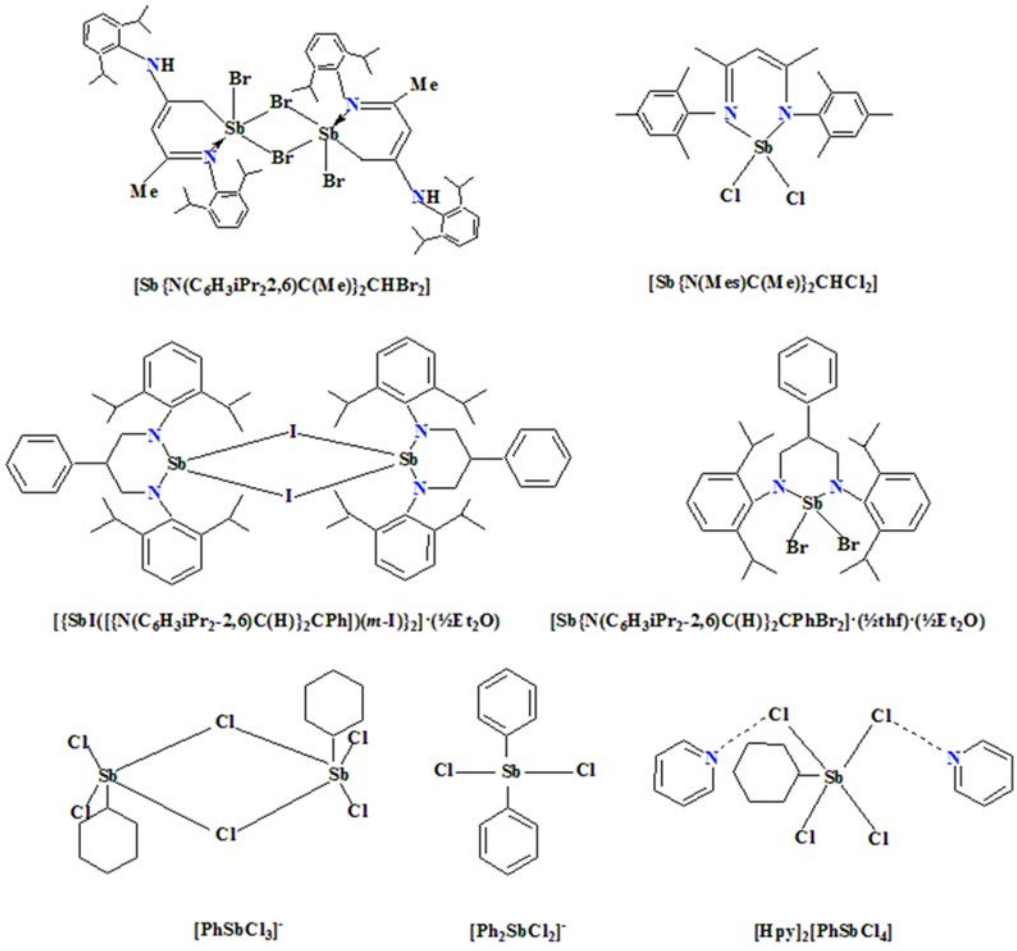

Figure 2.13 Some halide-bridged dimeric and non-dimeric haloorgano Sb^{+3} and Sb^{+5} complexes.[5,7,20]

Table 2.9 Crystallographic data for compounds 2.9 - 2.12

Compound	**2.9**	**2.10**	**2.11**	**2.12**
Formula	$C_{28}H_{44}N_2Si$	$C_6H_{16}Cl_3N_2Sb$	$C_{34}H_{54}Cl_3N_4OSb_2$	$C_{70}H_{88}Cl_2F_{10}N_4O_2Sb_2$
Fw	436.74	344.31	884.70	1520.90
crystal system	monoclinic	monoclinic	monoclinic	triclinic
space group	$P2_1/c$	$P2_1/c$	$P2_1/c$	$P\text{-}1$
a, Å	13.873(3)	11.140(2)	12.741(3)	12.043(2)
b, Å	10.859(2)	7.1720(14)	20.780(4)	16.684(3)
c, Å	18.874(4)	16.159(3)	29.811(6)	19.801(4)
α, deg	90	90	90	103.49(3)
β, deg	105.06(3)	106.70(3)	93.53(3)	105.17(3)
γ, deg	90	90	90	103.72(3)
V, Å^3	2745.6(10)	1236.6(5)	7878(3)	3540.5(15)
Z	4	4	8	2
T, K	293(2)	173.15	173.15	293(2)
no. of rflns collected	29911	14797	96844	58194
no. of indep rflns	7723	3118	13206	15192
Rint	0.0936	0.0465	0.2557	0.0243
Final *R1* values ($I > 2\sigma(I)$)	0.0779	0.0388	0.0920	0.0712
Final $wR(F^2)$ values ($I > 2\sigma(I)$)	0.1951	0.0952	0.2311	0.2768
Final *R1* values (all data)	0.1329	0.0395	0.1676	0.0829
Final $wR(F^2)$ values (all data)	0.2280	0.0956	0.2837	0.2834
GooF (on F^2)	1.083	1.050	1.021	2.452

Table (2.10) is a summary of all the selected bond lengths for each of the obtained *mono*- and *tri*-valent antimony compounds. These Sb-N bond lengths are very asymmetric. The shortest Sb-N bond length for the trivalent species is observed in the four-coordinate [Sb(DippForm)Br_2] (**2.5**) (2.091 Å), while the longest Sb-N bond length was observed for the five-coordinate [Sb(DippForm)$_2$Br] (**2.3**) (2.646 Å).

In addition to the monomeric forms of the DippForm antimony (III) complexes described in this chapter, the bulky steric demand on the *ortho*-positions of the DippForm ligand has showed its ability to adopt a bridging coordination mode forming dimers and thus, low and high coordination numbers were achieved.

	2.1	**2.2**	**2.3**	**2.4**	**2.5**	**2.6**	**2.8**	**2.11**	**2.12**
Sb-N1	2.301(9)	2.563(15)	2.576(3)	2.597(4)	2.091(2)	2.111(11)	2.150(12)	2.153(11)	2.168(5)
Sb-N2	-	2.113(14)	2.113(3)	2.112(4)	2.435(2)	2.457(9)	-	2.570(10)	-
Sb-N3	-	2.604(13)	2.646(3)	2.634(3)	-	-	2.057(12)	-	-
Sb-N4	-	2.162(15)	2.158(3)	2.165(4)	-	-	-	-	-

Table 2.10 Selected bond lengths (Å) for complexes: [Sb_2{μ-(DippForm}].$(THF)_8$ (**2.1**), [Sb(DippForm)$_2$Cl] (**2.2**), [Sb(DippForm)$_2$Br] (**2.3**), [Sb(DippForm)$_2$I] (**2.4**), [Sb(DippForm)Br_2] (**2.5**), [Sb(DippForm)I_2] (**2.6**), [Sb(DippForm)$(NSiMe_3)]_2$ (**2.8**), [(DippForm)ClSb(μ-O)$SbCl_2(Me_2NC_2H_4NMe_2)]_2.(C_6D_6)$ (**2.11**) and [Sb(DippForm)$Cl(C_6F_5)]_2.(THF)_2$ (**2.12**).

2.4 *Conclusion*

This work is the first contribution to formamidinato-based mono and trivalent antimony chemistry. This chapter reported the results of metathesis reactions, which produced monomeric structures with the generic formula $[Sb(DippForm)_{3-n}X_n]$ (n = 1, X = Cl **2.2**, Br **2.3**, I **2.4**; n = 2, X = Br **2.5**, I **2.6**). Initially, these complexes were synthesised by the addition of N,N′-*bis*(2,6-diisopropylphenyl)formamidine (DippFormH), pre-treated with various metal alkyl/halide reagents (*n*-BuLi, $LiN(SiMe_3)_2$, $NaN(SiMe_3)_2$), to the appropriate SbX_3 (X = Cl, Br, I) compounds. Reactions using Li(DippForm), in particular with $SbCl_3$, $SbBr_3$ and SbI_3 proceeded rapidly. In several instances, despite the use of a 3:1 ratio of (DippFormH) to SbX_3, only *mono*- and *bis*-substituted complexes were obtained, which prompted us to deliberately synthesise the *mono*- and *bis*-substituted complexes. Isolation of an Sb^{+1} dimeric structure of **$[Sb_2\{\mu$-(DippForm$\}_2]$.$(THF)_8$** was the alternative to an expected Sb^{+3} monomeric structure and a deliberate synthesis remains elusive; nevertheless, could be corroborated by treatment of DippFormH with $NaN(SiMe_3)_2$ followed by the addition of the result from this step to the solution of $SbCl_3$ in THF. The dimeric compound **$[Sb(DippForm)(NSiMe_3)]_2$** (**2.8**) was prepared in an attempt to achieve **$[Sb(DippForm)Br_2]$** (**2.5**) deliberately using $LiN(SiMe_3)_2$ for (DippFormH) deprotonation and then combined with $SbBr_3$ and leaving the mixture stirring for 36 h at room temperature. The TMEDA solvated monomeric compound **$[SbCl_3(Me_2NC_2H_4NMe_2)]$** (**2.10**) was prepared by performing the reaction in TMEDA and isolated as a main product instead of isolation of the anticipated product **[Sb (DippForm)Cl_2]** owing to a shift in the Schlenk equilibrium. A shifts in the Schlenk equilibrium for most complexes could certainly contribute to isolate low yields. Consequently, existent yields in solution are hard determinable since we depended on the isolated crystal yields. The dinuclear **$[(DippForm)ClSb(\mu$-O$)SbCl_2(Me_2NC_2H_4NMe_2)]_2.(C_6D_6)$** (**2.11**) was isolated by fractional crystallisation of **$[SbCl_3(Me_2NC_2H_4NMe_2)]$** (**2.10**) from C_6D_6, after retreatment with DippFormH in THF.

The (μ-Cl)$_2$-bridged dimeric four-coordinate antimony complex **[Sb(DippForm)Cl(C_6F_5)]$_2$.(THF)$_2$** (**2.12**) was gained in an attempt to examine the ability of antimony to coordinate variety of an anions by using $Hg(C_6F_5)_2$ as the source of pentafluorophenyl group. Overall, the described results add to the large field of main group metal N,N'-chelated compounds by introducing new ligands to antimony chemistry. Compounds (**2.1** – **2.12**), (except **2.7**, **2.9** and **2.10**) are novel formamidinato antimony complexes and show that through manipulation of the halide precursor, reaction stoichiometry and reaction conditions diverse reaction products have been achieved and much more information has been obtained regarding their structures and bonding modes.

2.5 *Experimental*

General Considerations/Air Sensitive Techniques

Antimony complexes described herein are extremely air and/or moisture sensitive, thus all manipulations, including synthesis, were performed under oxygen- and moisture-free conditions requiring Schlenk-type glassware (flask), using both conventional standard Schlenk techniques interfaced to a high vacuum (10^{-2} Torr) line, under an inert atmosphere of dry nitrogen in a glovebox. All glassware were dried at 120 ^{0}C for no less than of 12 h before use, then used immediately from the oven to avoid exposure to moisture.

Hexane and PhMe were dried and deoxygenated by an LC solvent purification system, whereas tetrahydrofuran was purified and deoxygenated by refluxing over and fresh distilled from sodium wire/benzophenone *ketyl* under nitrogen. After distillation solvents were stored in vacuum Schlenk flasks and degassed prior to use. The syntheses of the formamidine proligand, DippFormH = N,N′-2,6-diisopropylphenylformamidine,[59,60] and $Hg(C_6F_5)_2$[61] were according to published procedures. Anhydrous $SbCl_3$ and other starting materials such as *n*-BuLi, $LiN(SiMe_3)_2$, and $NaN(SiMe_3)_2$ were commercially available from Aldrich and were freshly used as supplied and unless stated otherwise, without further purification.

Multinuclear ^{1}H- and ^{13}C-NMR spectra of air and moisture sensitive compounds were recorded by J.Young valve inert atmosphere NMR tubes protecting the sample from air at 25 ^{0}C on a Bruker AVANCE III HD 400 MHz spectrometer instrument. The chemical shifts were expressed in parts per million (ppm). ^{1}H-NMR resonances were referenced against residual H in C_6D_6 (δ = 7.15), while ^{13}C-NMR resonances were referenced to the deuterated C_6D_6 solvent (δ = 128.39). *Perdeutero*-benzene (C_6D_6) (all ≥ 99 atom % D) as solvent for NMR spectroscopy was obtained from Sigma-Aldrich, and was degassed, pre-dried over sodium metal for 24 h, then distilled under an atmosphere of nitrogen before being stored in a resealable greaseless Schlenk flask prior to use.

Infrared spectra were obtained from samples in Nujol mulls between NaCl plates, with a Nicolet-Nexus FTIR spectrophotometer within the range (ύ = 4000 - 400 cm^{-1}). Samples were sent in sealed glass pipettes under nitrogen to the Microanalytical Laboratory service, Science Centre, London Metropolitan University, England, for elemental analyses (C,H,N) on the bulk material. Melting points were determined in sealed glass capillaries under nitrogen and were uncalibrated.

Synthesis by metalation reactions in THF/PhMe or hexane

$[Sb_2\{\mu\text{-(DippForm}\}_2].(THF)_8$ (2.1)

A solution of Na(DippForm), prepared from DippFormH (1.08 g, 3.0 mmol) and $NaN(SiMe_3)_2$ (0.6 M solution in PhMe, 1.8 ml, 3.0 mmol) in THF (5 ml), was added dropwise through a cannula to a solution of $SbCl_3$ (0.22 g, 1.0 mmol) in THF (10 ml) at – 78 ^{0}C while stirring. The solution adopted a dark green colour after 5 minutes. To ensure completion of the reaction, the suspension was stirred for 5 h and allowed to warm to ambient temperature, and continued to be stirred for 18 h. The solution was filtrated and concentrated under vacuum to the point of crystallisation *ca*.5 ml, then slow cooling to – 30 ^{0}C overnight gave light orange block - shaped crystals of (**2.1**). The crystals were dried in vacuo after separation from the mother solution via syringe. Yield = 0.66 g (62 %).

2.1: M.P. 210-212 ^{0}C. ^{1}H-NMR (400 MHz, C_6D_6, 25 ^{0}C) for $[Sb_2\{\mu$-(DippForm}].$(THF)_8$ losing 2(THF): δ (ppm) = 1.12 (d, J = 6.7 Hz, 48H, CH(C*H*$_3$)$_2$), 1.34 (m, 24H, C*H*$_2$-thf), 3.42 (sept, 8H, C*H*(CH$_3$)$_2$), 3.64 (m, 24H, OC*H*$_2$-thf), 6.98 (m, 4H, *p*-Ar*H*), 7.06 (m, 8H, *m*-Ar*H*), 10.60 (s, 2H, NC(*H*)N); ^{13}C-NMR (101 MHz, C_6D_6, 25 ^{0}C): δ (ppm) = 23.84 (*C*H$_3$-*i*Pr), 25.12 (*C*H$_2$-thf) 28.51 (*C*H-*i*Pr), 66.50 (O*C*H$_2$-thf), 123.37 (*p-C*), 126.20 (*m-C*), 127.70 (*o-C)*, 143.16 (N-*C*), 157.39 (N*C*N); Elemental analysis calcd. (%) for $C_{82}H_{134}N_4O_8Sb_2$ (M = 1547.51 g/mol): C 63.64, H 8.72, N 3.62. Calcd (%) for $C_{50}H_{70}N_4Sb_2$ (970.65 g/mol after loss of all THF solvation): C 61.87, H 7.26, N 5.77; found: C 58.61, H 7.22, N 3.57, showing low carbon and nitrogen percentage. IR (υ/cm^{-1}, Nujol mull): 2923 (s), 2728 (w), 2364 (m), 2183 (m), 1926 (s), 1861 (s), 1792 (s), 1668 (m), 1581 (m), 1462 (s), 1377 (s), 1257 (m), 1182 (m), 1093 (m), 930 (s), 823 (w), 721 (s), 672 (m).

[Sb(DippForm)$_2$Cl] (2.2)

A solution of Li(DippForm), prepared from DippFormH (0.72 g, 2.0 mmol) and LiN(SiMe$_3$)$_2$ (1 M solution in thf, 2.0 ml, 2.0 mmol) in THF (20 ml), was added dropwise through a cannula to a solution of SbCl$_3$ (0.22 g, 1.0 mmol) in THF (10 ml) at room temperature with stirring. The reaction progressed smoothly, changing the colour of the solution to a pale yellow within seconds of combination between Li(DippForm) and SbCl$_3$ in THF. The reaction mixture continued to be stirred for two days at ambient temperature. The solvent was evaporated under vacuum to the point of dryness and PhMe (20 ml) added. The mixture was then filtered to remove LiCl. The solvent was then concentrated under reduced pressure, then slowly cooled at – 30 ^{0}C, whereupon light colourless block crystals deposited. The composition was determined as [Sb(DippForm)$_2$Cl] (**2.2**) by X-ray crystallography. Yield = 0.43 g (60 %).

2.2: M.P. 198-200 ^{0}C. ^{1}H-NMR (400 MHz, C$_6$D$_6$, 25 ^{0}C): δ (ppm) = 1.13 (d, J = 6.8, 48H, CH(C*H*$_3$)$_2$), 3.44 (sept, 8H, C*H*(CH$_3$)$_2$), 6.91 (m, 4H, *p*-Ar*H*), 7.03 (m, 8H, *m*-Ar*H*), 10.93 (s, 2H, NC(*H*)N); ^{13}C-NMR (101 MHz, C$_6$D$_6$, 25 ^{0}C): δ (ppm) = 23.47 (*C*H$_3$-*i*Pr), 28.17 (*C*H-*i*Pr), 123.47 (*p*-*C*), 126.12 (*m*-*C*), 139.29 (*o*-*C)*, 143.65 (N-*C*), 155.62 (NCN); Elemental analysis calcd. (%) for C$_{50}$H$_{70}$ClN$_4$Sb (M = 884.32 g/mol): C 67.91, H 7.98, N 6.34; found: C 67.49, H 7.83, N 6.20. IR (υ/cm^{-1}, Nujol mull): 2922 (m), 2727 (w), 2166 (w), 2097 (m), 2060 (m), 2008 (vs), 1926 (s), 1862 (s), 1796 (s), 1734 (vs), 1666 (s), 1640 (w), 1586 (s), 1464 (vs), 1454 (vs), 1377 (s), 1294 (w), 1232 (m), 1184 (m), 1156 (m), 1097 (s), 1057 (s), 1011 (s), 956 (s), 934 (s), 881 (m), 821 (s), 798 (s), 721 (s), 672 (s), 474 (w).

[Sb(DippForm)$_2$Br] (2.3)

Following the same method to that employed for synthesis (**2.2**), LiN(SiMe$_3$)$_2$ (1 M solution in thf, 6.0 ml, 6.0 mmol) was added to DippFormH (2.16 g, 6.0 mmol) in THF (20 ml) and the solution stirred at room temperature for 2 h, then added dropwise to SbBr$_3$ (1.8 g, 3.0 mmol) in PhMe (10 ml) at – 78 ^{0}C. After warming to room temperature, the mixture was stirred for 36 h to yield a yellow-brown solution with a white precipitate. Volatiles were removed under reduced pressure, and the residue extracted with hexane (30 ml). Filtration and concentration followed by slowly cooling to – 30 ^{0}C overnight led to isolation of Sb^{+3} mononuclear structure [Sb(DippForm)$_2$Br]. Large yellow crystals of (**2.3**) were grown upon standing for one week. Yield = 1.73 g (80 %). **2.3**: M.P. 168-170 ^{0}C. ^{1}H-NMR (400 MHz, C$_6$D$_6$, 25 ^{0}C): δ (ppm) = 1.15 (d, J = 6.8 Hz, 48H, CH(C*H*$_3$)$_2$), 3.45 (sept, 8H, C*H*(CH$_3$)$_2$), 6.99 (m, 4H, *p*-Ar*H*), 7.03 (m, 8H, *m*-Ar*H*), 8.04 (s, 2H, NC(*H*)N); ^{13}C-NMR (101 MHz, C$_6$D$_6$, 25 ^{0}C): δ (ppm) = 25.58 (*C*H$_3$-*i*Pr), 29.60 (*C*H-*i*Pr), 123.98 (*p*-*C*), 124.37 (*m*-*C*), 141.16 (*o*-*C*), 145.66 (N-*C*), 161.27 (N*C*N); Elemental analysis calcd. (%) for C$_{50}$H$_{70}$BrN$_4$Sb (M = 928.80 g/mol): C 64.60, H 7.64, N 6.02; found: C 64.85, H 7.79, N 5.97. IR (υ/cm^{-1}, Nujol mull): 2922 (m), 2722 (vs), 2665 (m), 2599 (vs), 2482 (vs), 2359 (s), 2290 (s), 2193 (s), 2122 (vs), 2060 (vs), 2001 (s), 1976 (s), 1929 (s), 1864 (s), 1793 (s), 1776 (vs), 1699 (vs), 1587 (w), 1454 (m), 1380 (m), 1259 (m), 1097 (m), 1056 (s), 987 (s), 797 (s), 694 (s), 608 (s), 590 (s), 537 (s). A reaction stoichiometry of 2:1 (Li-DippForm:Sb) gave (**2.3**) as the sole identifiable Sb-containing product.

[Sb(DippForm)$_2$I] (2.4)

LiN(SiMe$_3$)$_2$ (1 M solution in thf, 2.0 ml, 2.0 mmol) was added to DippFormH (0.72 g, 2.0 mmol) in THF (20 ml) and the solution stirred at room temperature for 2 h, then added dropwise to SbI$_3$ (0.50 g, 1.0 mmol) in THF (10 ml) at – 78 ^{0}C. After warming to room temperature, the mixture was stirred for 36 h to yield a yellow solution. The solvent was removed under reduced pressure and PhMe (20 ml) added until a white precipitate composed. The mixture was then filtered to remove LiCl.

The solvent was then concentrated, and storage at – 30 ^{0}C for 12 hour, whereupon small yellow-white crystals of (**2.4**) separated from the brown solution and grew upon standing after two days. Yield = 0.54 g (75 %).

2.4: M.P. 188-190 ^{0}C. ^{1}H-NMR (400 MHz, C_6D_6, 25 ^{0}C): δ (ppm) = 1.15 (d, J = 6.6 Hz, 48H, CH(CH_3)$_2$), 3.42 (sept, 8H, CH(CH$_3$)$_2$), 6.98 (m, 4H, *p*-ArH), 7.06 (m, 8H, *m*-ArH), 7.86 (s, 2H, NC(H)N); ^{13}C-NMR (101 MHz, C_6D_6, 25 ^{0}C): δ (ppm) = 23.71 (*C*H$_3$-*i*Pr), 28.39 (*C*H-*i*Pr), 123.47 (*p*-*C*), 123.55 (*m*-*C*), 144.20 (*o*-*C)*, 145.84 (N-*C*), 155.54 (N*C*N); Elemental analysis calcd. (%) for $C_{50}H_{70}IN_4Sb$ (M = 975.79 g/mol): C 61.56, H 7.18, N 5.74; found: C 53.03, H 6.32, N 4.94 (significantly low in the C percentage). IR (υ/cm^{-1}, Nujol mull): 2915 (w), 2722 (vs), 2665 (m), 2594 (vs), 2544 (m), 2487 (m), 2460 (vs), 2398 (m), 2287 (m), 2187 (s), 2127 (w), 2082 (vs), 2001 (s), 1971 (s), 1928 (s), 1865 (s), 1793 (s), 1736 (w), 1704 (s), 1583 (w), 1462 (m), 1378 (m), 1043 (m), 987 (m), 820 (m), 723 (s), 694 (s), 607 (s), 590 (s), 537 (s), 411 (w). A reaction stoichiometry of 2:1 (Li(DippForm):Sb) gave (**2.4**) and Li(DippForm).

[Sb(DippForm)Br$_2$] (2.5)

[Sb(Dipp)$_2$Br] (**2.3**) prepared previously (0.92 g, 1.0 mmol) was reacted with SbBr$_3$ (0.36 g, 1.0 mmol) in THF (20 ml) at room temperature with stirring. The reaction was continued for 8 h at room temperature; volatiles were removed under vacuum. The orange solution was concentrated to *ca.* 10 ml and set aside for 1 day at 15 ^{0}C, yielding cubic shiny yellow crystals of (**2.5**). Yield = 0.30 g (32 %).

2.5: M.P. 170-172 ^{0}C. ^{1} H-NMR (400 MHz, C_6D_6, 25 ^{0}C): δ (ppm) = 1.21 (d, J = 6.9 Hz, 24H, CH(CH_3)$_2$), 3.33 (sept, 4H, CH(CH$_3$)$_2$), 6.88 (m, 2H, *p*-ArH), 7.08 (m, 4H, *m*-ArH), 7.56 (s, 1H, NC(H)N); ^{13}C-NMR (101 MHz, C_6D_6, 25 ^{0}C): δ (ppm) = 24.60 (*C*H$_3$-*i*Pr), 29.13 (*C*H-*i*Pr), 123.52 (*p*-*C*), 127.49 (*m*-*C*), 137.96 (*o*-*C)*, 145.53 (N-*C*), 159.80 (N*C*N); Elemental analysis calcd. (%) for $C_{25}H_{35}Br_2N_2Sb$ (M = 645.12 g/mol): C 46.54, H 5.43, N 4.34; found: C 43.13, H 5.19, N 4.22 (low in the C percentage only). IR (υ/cm^{-1}, Nujol mull): 2962 (s), 2923 (vs), 2732 (m), 2581 (w), 2393 (s), 2253 (m), 2166 (w), 2020 (m), 1978 (s), 1949 (s), 1877 (s), 1800 (s), 1731 (m), 1644 (vs), 1593 (s), 1511 (s), 1462 (s), 1376 (s), 1311 (m), 1257 (s), 1121 (m), 1042 (s), 969 (m), 802 (m), 763 (s), 676 (w), 627 (w), 426 (w). A reaction stoichiometry of 2:1 (DippForm:Sb) gave (**2.5**) as the sole identifiable Sb-containing product.

[Sb(DippForm)I_2] (2.6)

$LiN(SiMe_3)_2$ (1 M solution in thf, 1.0 ml, 1.0 mmol) was added to DippFormH (0.36 g, 1.0 mmol) in THF (20 ml) and the solution stirred at room temperature for 2 h, then added dropwise to SbI_3 (0.5 g, 1.0 mmol) in THF (10 ml) at room temperature. The mixture was stirred for 36 h to yield a yellow brown solution. The solution evaporated to the point of dryness under vacuum and PhMe (10 ml) added until a white precipitate appeared. Volatiles were removed under reduced pressure. Filtration and concentration following slow cooling to – 30 ^{0}C overnight yielded shiny brown-orange crystals of the expected (**2.6**). Yield = 0.21 g (58 %).

2.6: M.P. 156-158 ^{0}C. ^{1}H-NMR (400 MHz, C_6D_6, 25 ^{0}C): δ (ppm) = 1.11 (d, J = 6.9 Hz, 24H, CH(C*H*$_3$)$_2$), 3.22 (sept, 4H, C*H*(CH$_3$)$_2$), 6.76 (m, 2H, *p*-Ar*H*), 6.99 (m, 4H, *m*-Ar*H*), 8.31 (s, 1H, NC(*H*)N); ^{13}C-NMR (101 MHz, C_6D_6, 25 ^{0}C): δ (ppm) = 25.43 (*C*H$_3$-*i*Pr), 29.21 (*C*H-*i*Pr), 123.95 (*p*-*C*), 124.38 (*m*-*C*), 137.98 (*o*-*C)*, 145.50 (N-*C*), 158.89 (N*C*N); Elemental analysis calcd. (%) for $C_{25}H_{35}I_2N_2Sb$ (M = 739.12 g/mol): C 40.61, H 4.73, N 3.79; found: C 27.47, H 4.92, N 2.91 (low in C and N percentage). IR (υ/cm^{-1}, Nujol mull): 2923 (s), 2853 (vs), 2727 (m), 2663 (w), 2411 (m), 2356 (s), 2290 (m), 1936 (s), 1870 (vs), 1632 (m), 1588 (vs), 1462 (vs), 1376 (s), 1260 (vs), 1168 (vs), 1074 (m), 911 (s), 885 (m), 849 (s), 722 (s), 666 (s). A reaction stoichiometry of 1:1 (L^H: Sb) gave (**2.6**) as the sole identifiable Sb-containing product.

[Li_2I(DippForm)(μ-thf)(thf)$_2$] (2.7)

Complex (**2.7**) was prepared through attempting to gain [Sb(DippForm)$_3$] by recrystalisation from PhMe. $LiN(SiMe_3)_2$ (1 M solution in thf, 3.0 ml, 3.0 mmol) was added to DippFormH (1.08 g, 3.0 mmol) in THF (20 ml) and the solution stirred at room temperature for 2 h, then added dropwise to SbI_3 (0.50 g, 1.0 mmol) in THF (10 ml) at room temperature. The mixture was stirred for 16 h to yield a yellow-brown solution. The solution evaporated to the point of dryness under vacuum and PhMe (10 ml) added, whereupon a white precipitate formed. Filtration and the solvent was then concentrated under vacuum to *ca*.5 ml and left overnight at room temperature.

Big white yellow crystals of [Li_2I(DippForm)$(thf)_3$] were grown upon standing for 1 day. Yield = 0.85 g (78 %).

2.7: M.P. 220-222 ^{0}C. ^{1}H-NMR (400 MHz, C_6D_6, 25 ^{0}C): δ (ppm) = 1.16 (d, J = 6.7 Hz, 24H, CH(CH_3)$_2$), 2.10 (m, 4H, CH_2-thf), 3.43 (sept, 4H, CH(CH_3)$_2$), 3.55 (m, 4H, OCH_2-thf), 6.99 (m, 2H, *p*-Ar*H*), 7.6 (m, 4H, *m*-Ar*H*), 7.86 (s, 1H, NC(*H*)N); ^{13}C-NMR (101 MHz, C_6D_6, 25 ^{0}C): δ (ppm) = 24.16 (*C*H$_3$-*i*Pr), 25.35 (*C*H$_2$-thf), 28.40 (*C*H-*i*Pr), 68.63 (O*C*H$_2$-thf), 123.61 (*p*-*C*), 124.06 (*m*-*C*), 140.18 (*o*-*C)*, 144.19 (N-*C*), 146.47 (N*C*N); ^{7}Li-NMR (156 MHz, C_6D_6): δ 1.15; Elemental analysis calcd. (%) for $C_{37}H_{59}ILi_2N_2O_3$ (M = 720.67 g/mol): C 61.71, H 8.20, N 3.89; found: C 16.52, H 3.35, N 0.1 (significantly low in C,H,N percentage). IR (υ/cm^{-1}, Nujol mull): 2790 (w), 2722 (m), 2601 (m), 2497 (s), 2415 (s), 2360 (s), 2312 (s), 2270 (s), 2178 (vs), 2109 (w), 2055 (s),1998 (s), 1973 (s),1921 (vs), 1860 (vs), 1751 (m), 1724 (m),1701 (vs), 1038 (vs), 988 (s), 673 (m), 506 (s), 405 (m).

[Sb(DippForm)(NSiMe$_3$)]$_2$ (2.8)

LiN(SiMe$_3$)$_2$ (1 M solution in thf, 2.0 ml, 2.0 mmol) was added to DippFormH (0.72 g, 2.0 mmol) in THF (20 ml) and the solution stirred at room temperature for 2 h, then added dropwise to $SbBr_3$ (0.36 g, 1.0 mmol) in THF (10 ml) at room temperature. The mixture was stirred for 36 h to yield a yellow brown solution with a white precipitate. Volatiles were removed under reduced pressure. Filtration and concentration following slow cooling to – 30 ^{0}C overnight yielded slightly unexpected off white crystals of (**2.8**). Yield = 0.32 g (44 %).

2.8: M.P. 180-182 ^{0}C (dec). ^{1}H-NMR (400 MHz, C_6D_6, 25 ^{0}C): δ (ppm) = 0.32 (s, 18H, Si(CH_3)$_3$), 1.16 (d, J = 6.5 Hz, 48H, CH(CH_3)$_2$), 3.46 (sept, 8H, CH(CH$_3$)$_2$), 6.95 (m, 4H, *p*-Ar*H*), 7.08 (m, 8H, *m*-Ar*H*), 8.29 (s, 2H, NC(*H*)N); ^{13}C-NMR (101 MHz, C_6D_6, 25 ^{0}C): δ (ppm) = – 0.018 (Si(*C*H$_3$)$_3$), 23.86 (*C*H$_3$-*i*Pr), 28.25 (*C*H-*i*Pr), 123.31 (*p*-*C*), 123.47 (*m*-*C*), 143.53 (*o*-*C*), 145.95 (N-*C*), 152.60 (N*C*N); Elemental analysis calcd. (%) for $C_{56}H_{88}N_6Sb_2Si_2$ (M = 1145.05 g/mol): C 58.77, H 7.69, N 7.34; found: C 59.36, H 7.63, N 7.04. IR (υ/cm^{-1}, Nujol mull): 2922 (m), 2729 (vs), 2426 (m), 2290 (m), 2092 (m), 2010 (m), 1929 (s), 1875 (vs), 1808 (vs), 1731 (s), 1670 (m), 1628 (vs), 1586 (s), 1462 (vs),1377 (s), 1259 (m), 1179 (s), 1097 (vs), 1043 (vs), 958 (m), 934 (s),842 (s), 799 (s), 753 (s), 722 (s), 672 (s) 622 (m).

[$SiMe_3$(DippForm)] (2.9)

$LiN(SiMe_3)_2$ (1 M solution in thf, 1.0 ml, 1.0 mmol) was added to DippFormH (0.36 g, 1.0 mmol) in THF (20 ml) and the solution stirred at room temperature for 2 h, then added dropwise to $SbBr_3$ (0.36 g, 1.0 mmol) in PhMe (10 ml) at room temperature. The mixture was stirred for 36 h to yield a colourless solution with a white precipitate. Volatiles were removed under reduced pressure, and the residue extracted with hexane (30 ml). Filtration and concentration following slow cooling to – 30 ^{0}C overnight yielded an unexpected white crystals of (**2.9**). Yield = 0.10 g (27 %).

2.9: M.P. 138-140 ^{0}C. ^{1}H-NMR (400 MHz, C_6D_6, 25 ^{0}C): δ (ppm) = 0.41 (s, 9H, $Si(CH_3)_3$), 1.10 (d, J = 6.9 Hz, 24H, $CH(CH_3)_2$), 3.43 (sept, 4H, $CH(CH_3)_2$), 6.96 (m, 2H, *p*-Ar*H*), 7.04 (m, 4H, *m*-Ar*H*), 7.21 (s, 1H, NC(*H*)N); ^{13}C-NMR (101 MHz, C_6D_6, 25 ^{0}C): δ (ppm) = 0.14 ($Si(CH_3)_3$), 24.09 (CH_3-*i*Pr), 28.43 (*C*H-*i*Pr), 123.02, 124.12, 127.11 (Ar*C*), 147.00 (N*C*N); Elemental analysis calcd. (%) for $C_{28}H_{44}N_2Si$ (M = 436.74 g/mol): C 77.06, H 10.09, N 6.42; found: C 77.17, H 9.91, N 6.43. IR (υ/cm^{-1}, Nujol mull): 2923 (s), 2799 (w), 2658 (w), 2547 (s), 2497 (s), 2384 (s), 2282 (s), 2104 (m), 2010 (vs), 1971 (vs), 1877 (vs), 1754 (s), 1661 (w), 1590 (m), 1457 (s), 1377 (s), 1185 (m), 1044 (s), 976 (s), 802 (m), 753 (s), 654 (s), 542 (m), 424 (w).

[$SbCl_3(Me_2NC_2H_4NMe_2)$] (2.10)

n-BuLi (2 M solution in cyclohexane, 1.0 mmol) was added to DippFormH (0.36 g, 1.0 mmol) in THF (20 ml) and the solution stirred at room temperature for 2 h, then added dropwise to a solution of $SbCl_3$ (0.22 g, 1.0 mmol) dissolved in mixture of THF (10 ml) and TMEDA (10 ml) at room temperature. The mixture was stirred for 36 h to yield a purple solution with a white precipitate. Volatiles were removed under reduced pressure. Filtration and concentration following slow cooling to – 30 ^{0}C overnight yielded purple crystals of (**2.10**) suitable for X-ray diffraction. Yield = 0.70 g (60 %).

2.10: M.P. 208-210 ^{0}C. ^{1}H-NMR (400 MHz, C_6D_6, 25 ^{0}C): δ (ppm) = 2.15 (m, 12H, C*H*$_3$-(TMEDA)), 2.31 (m, 4H, C*H*$_2$-(TMEDA)); ^{13}C-NMR (101 MHz, C_6D_6, 25 ^{0}C): δ (ppm) = 45.47 (N*C*H$_3$-(TMEDA)), 57.55 (N*C*H$_2$-(TMEDA)); Elemental analysis calcd. (%) for $C_6H_{16}Cl_3N_2Sb$ (M = 344.31 g/mol): C 20.93, H 4.65, N 8.14; found: C 20.91, H 4.69, N 8.03. IR (υ/cm^{-1}, Nujol mull): 2727 (s), 2667 (w), 2453 (w), 2359 (w), 2025 (w), 1933 (s), 1851 (m), 1772 (m), 1650 (s), 1591 (s), 1466 (m),1398 (m), 1262 (s), 1185 (s), 1091 (s), 1039 (C–N) (s), 990 (m), 942 (s),843 (m), 773 (s), 664 (s) 518 (w), 446 (m), 400 (w).

[(DippForm)ClSb(μ-O)SbCl$_2$(Me$_2$NC$_2$H$_4$NMe$_2$)]$_2$.C$_6$D$_6$ (2.11)

LiN(SiMe$_3$)$_2$ (1 M solution in thf, 1.0 ml, 1.0 mmol) was added to DippFormH (0.36 g, 1.0 mmol) in THF (20 ml) and the solution stirred at room temperature for 2 h, then added dropwise to $SbCl_3$ (0.22 g, 1.0 mmol) dissolved in mixture of THF (10 ml) and TMEDA (10 ml) at room temperature. The mixture was stirred for 24 h to yield an off-white solution with a white precipitate. Volatiles were removed under reduced pressure. Filtration and concentration followed slow cooling to – 30 ^{0}C overnight. On the basis of NMR spectroscopy scale, experiment in dry C_6D_6 resulted in growing unexpected off-white brown crystals of (**2.11**). Yield = 0.07 g (20 %).

2.11: M.P. 232-234 ^{0}C (dec). ^{1}H-NMR (400 MHz, C_6D_6, 25 ^{0}C): δ (ppm) = 1.22 (d, J = 6.9 Hz, 24H, CH(C*H*$_3$)), 2.05 (m, 12H, C*H*$_3$-(TMEDA)), 2.10 (m, 4H, C*H*$_2$-(TMEDA)), 3.41 (sept, 4H, C*H*(CH$_3$)), 6.92 (m, 2H, *p*-Ar*H*), 7.09 (m, 4H, *m*-Ar*H*), 7.77 (s, 1H, NC(*H*)N); ^{13}C-NMR (101 MHz, C_6D_6, 25 ^{0}C): δ (ppm) = 23.91 (*C*H$_3$-*i*Pr), 28.41 (*C*H-*i*Pr), 41.62 (N*C*H$_3$-(TMEDA)), 54.62 (N*C*H$_2$-(TMEDA)), 122.99 (*p*-*C*), 123.64 (*m*-*C*), 140.38 (*o*-*C*), 146.03 (N-*C*), 163.22 (N*C*N); Elemental analysis calcd. (%) for $C_{34}H_{54}Cl_3N_4OSb_2$ (M = 884.70 g/mol): C 46.15, H 6.15, N 6.33. Calcd (%) for $C_{31}H_{51}Cl_3N_4OSb_2$ (845.64 g/mol after loss of ½ C_6D_6 solvation upon standing): C 44.03, H 6.07, N 6.62; found: C 39.75, H 5.96, N 5.85 (low in C percentage). IR (υ/cm^{-1}, Nujol mull): 2923 (s), 2853 (s), 2722 (m), 2678 (m), 2445 (m), 2361 (w), 1936 (vs), 1872 (s), 1800 (vs), 1736 (m), 1662 (s), 1586 (s), 1456 (s), 1376 (s), 1309 (w), 1284 (s), 1257 (w), 1235 (s), 1178 (s), 1158 (s), 1099 (vs), 1062 (vs), 1002 (s), 933 (vs), 842 (s), 822 (s),798 (s), 755 (s), 721 (s), 674 (w).

Synthesis using $Hg(C_6F_5)_2$ in THF

$[Sb(DippForm)Cl(C_6F_5)]_2.(THF)_2$ (2.12)

DippFormH (0.36 g, 1.0 mmol), $Hg(C_6F_5)_2$ (0.25 g, 0.5 mmol) and $SbCl_3$ (0.22 g, 1.0 mmol) were stirred in THF (20 ml) at room temperature through one pot reaction. An immediate colour change to off-white yellow was observed. Stirring was continued for 2 days; volatiles were removed under vacuum through reducing pressure. The mixture was filtered and the volume of the solution was concentrated under vacuum to *ca*.3 ml and set aside for 2 days at -15 ^{0}C, yielding the light white crystals suitable for analysis by X-ray crystallography, leaving the composition $[Sb(DippForm)Cl(C_6F_5)].(THF)_2$ (**2.12**). Unfortunately, the titled complex $C_{70}H_{88}Cl_2F_{10}N_4O_2Sb_2$ (M = 1520.90 g/mol) achieved in a very low yield (5 %), which was characterised by only X-ray structure determination and no other analytical data was obtained.

2.6 Single crystal *X-ray structure determination/analysis and Refinement model description*

Crystals were initially isolated as suitable single crystals immersed in viscous hydrocarbon oil (Paratone-N) and mounted on a glass fibre that was placed on the diffractometer under a stream of liquid nitrogen. Crystalline samples were measured providing intensity data on either a Bruker APEX II CCD diffractometer for complexes (**2.2**, **2.3**, **2.4**, **2.6**, **2.7**), or the Australian Synchrotron diffractometer using the MX1 or MX2 macromolecular beam lines for complexes (**2.1**, **2.5**, **2.8, 2.9, 2.10, 2.11, 2.12**) at 173 K by a single wavelength (λ = 0.71073 Å). Structure solutions and refinements package were performed using SHELXS-97 and SHELXL-97,[62,63] program using Direct Methods via the graphical interface X-Seed [64] and OLEX2,[65] both of which were also used for figures' generating. Absorption improvements using MULTISCAN were applied. All CIF files were checked at www.iucr.org. A summary of crystallographic data and collection parameters can be found for each compound below.

[Sb_2{*μ*-(DippForm}$_2$].(THF)$_8$ (2.1)

1: $C_{82}H_{134}N_4O_8Sb_2$ (*M* = 1547.514 g/mol): monoclinic, space group *P2₁/c*, *a* = 21.243(4) Å, *b* = 18.997(4) Å, *c* = 21.743(4) Å, *α* = 90°, *β* = 118.60(3)°, *γ* = 90°, Volume = 7704(3) Å^3, *Z* = 2(dimer), *T* = 173.15 K, D_{calc} = 1.280 g/cm^3, *μ* = 0.755 mm^{-1}, F (000) = 3124.0, $2\Theta_{max}$ = 2.184 – 63.66°, 71852 reflections collected, 21388 unique (R_{int} = 0.0697, R_{sigma} = 0.0578), 21388/0/845 parameters, GooF on F^2 1.198, The final R_1 was 0.1352 (I>2σ (I)) and wR_2 was 0.4021 (all data), Largest diff. peak/hole / e = 9.23 to - 4.48 Å^{-3}.

[Sb(DippForm)$_2$Cl] (2.2)

2: $C_{50}H_{70}ClN_4Sb$ (*M* = 884.322 g/mol): monoclinic, space group *P2₁/c*, *a* = 18.443(4) Å, *b* = 20.455(4) Å, *c* = 12.817(3) Å, *α* = 90°, *β* = 97.47(3)°, *γ* = 90°, *Volume* = 4794.3(17) Å^3, *Z* = 4, *T* = 100.15 K, *μ* = 0.663 mm^{-1}, D_{calc} = 1.128 g/cm^3, $F_{(000)}$ = 1585.0, $2\Theta_{max}$ = 2.226 – 63.82, 87850 reflections measured, 12579 unique (R_{int} = 0.0406, R_{sigma} = 0.0229), 12579/0/521 parameters, GooF on F^2 1.194, The final R_1 was 0.0359 (I >2σ (I)) and wR_2 was 0.1321 (all data), Largest diff. peak/hole / e = 1.17 to - 3.21 Å^{-3}.

[Sb(DippForm)$_2$Br] (2.3)

3: $C_{50}H_{70}BrN_4Sb$ (M = 928.802 g/mol): monoclinic, space group $P2_1/c$, a = 18.7239(14) Å, b = 20.5497(17) Å, c = 12.9785(10) Å, α = 90°, β = 96.886(4)°, γ = 90°, *Volume* = 4957.7(7) Å^3, Z = 4, T = 296(2) K, μ = 1.397 mm^{-1}, D_{calc} = 1.246 g/cm^3, F $_{(000)}$ = 1940.0, $2\Theta_{max}$ = 2.19 - 50, 63608 reflections measured, 8732 unique (R_{int} = 0.1091, R_{sigma} = 0.0691), 8732/0/522 parameters, GooF on F^2 1.009, The final R_1 was 0.0402 (I >2σ (I)) and wR_2 was 0.1061 (all data), Largest diff. peak/hole / e = 0.63 to - 0.72 Å^{-3}.

[Sb(DippForm)$_2$I] (2.4)

4: $C_{50}H_{70}IN_4Sb$ (M = 975.798 g/mol): monoclinic, space group $P2_1/c$, a = 18.616(2) Å, b = 20.713(2) Å, c = 12.9942(13) Å, α = 90°, β = 96.750(5)°, γ = 90°, *Volume* = 4975.8(9) Å^3, Z = 4, T = 296.15 K, μ = 1.210 mm^{-1}, D_{calc} = 1.303 g/cm^3, F $_{(000)}$ = 2008.0, $2\Theta_{max}$ = 2.952 - 50, 63063 reflections measured, 8728 unique (R_{int} = 0.0889, R_{sigma} = 0.0688), 8728/0/521 parameters, GooF on F^2 0.869, The final R_1 was 0.0468 (I >2σ (I)) and wR_2 was 0.1580 (all data), Largest diff. peak/hole / e = 0.86 to - 1.23 Å^{-3}.

[Sb(DippForm)Br$_2$] (2.5)

5: $C_{25}H_{35}Br_2N_2Sb$ (M = 645.12 g/mol): triclinic, space group $P\text{-}1$, a = 10.105(2) Å, b = 10.332(2) Å, c = 14.240(3) Å, α = 96.69(3)°, β = 103.93(3)°, γ = 111.72(3)°, *Volume* = 1305.2(5) Å^3, Z = 2, T = 293(2) K, μ = 4.133 mm^{-1}, D_{calc} = 1.642 g/cm^3, F $_{(000)}$ = 640.0, $2\Theta_{max}$ = 4.706 - 63.84, 23525 reflections measured, 6299 unique (R_{int} = 0.0324, R_{sigma} = 0.0280), 6299/0/279 parameters, GooF on F^2 1.077, The final R_1 was 0.0283 (I >2σ (I)) and wR_2 was 0.0760 (all data), Largest diff. peak/hole / e = 0.53 to - 1.26 Å^{-3}.

[Sb(DippForm)I_2] (2.6)

6: $C_{25}H_{35}I_2N_2Sb$ (M = 739.12 g/mol): triclinic, space group *P-1*, a = 10.4137(4) Å, b = 10.5559(4) Å, c = 14.6097(5) Å, α = 95.876(2)°, β = 104.946(2)°, γ = 111.754(2)°, *Volume* = 1405.64(9) Å^3, Z = 2, T = 296(2) K, μ = 3.191 mm^{-1}, D_{calc} = 1.746 g/cm^3, F $_{(000)}$ = 712.0, 2Θ$_{max}$ = 2.958 - 54.996, 35754 reflections measured, 6393 unique (R_{int} = 0.0773, R_{sigma} = 0.0564), 6393/0/279 parameters, GooF on F^2 1.039, The final R_1 was 0.0710 (I >2σ (I)) and wR_2 was 0.2263 (all data), Largest diff. peak/hole / e = 2.98 to - 2.24 Å^{-3}.

[Li_2I(DippForm)(thf)$_3$] (2.7)

7: $C_{37}H_{59}ILi_2N_2O_3$ (M = 720.67 g/mol): monoclinic, space group $P2_1/n$, a = 9.7157(7) Å, b = 18.4703(13) Å, c = 22.9728(15) Å, α = 90°, β = 94.165(4)°, γ = 90°, *Volume* = 4111.6(5) Å^3, Z = 4, T = 296.15 K, μ = 0.810 mm^{-1}, D_{calc} = 1.158 g/cm^3, F $_{(000)}$ = 1496.0, 2Θ$_{max}$ = 2.832 - 60.084, 75506 reflections measured, 12018 unique (R_{int} = 0.1342, R_{sigma} = 0.1301), 12018/0/414 parameters, GooF on F^2 0.910, The final R_1 was 0.0698 (I >2σ (I)) and wR_2 was 0.2284 (all data), Largest diff. peak/hole / e = 0.36 to - 1.40 Å^{-3}.

[Sb(DippForm)(NSiMe$_3$)]$_2$ (2.8)

8: $C_{56}H_{88}N_6Sb_2Si_2$ (M = 1145.05 g/mol): triclinic, space group *P-1*, a = 9.7000(19) Å, b = 11.793(2) Å, c = 14.246(3) Å, α = 74.24(3)°, β = 70.22(3)°, γ = 73.62(3)°, *Volume* = 1443.0(6) Å^3, Z = 2(dimer), T = 100.15 K, μ = 1.017 mm^{-1}, D_{calc} = 1.318 g/cm^3, F $_{(000)}$ = 596.0, 2Θ$_{max}$ = 6.198 - 49.998, 12213 reflections measured, 4429 unique (R_{int} = 0.0234, R_{sigma} = 0.0248), 4429/0/305 parameters, GooF on F^2 1.255, The final R_1 was 0.0950 (I >2σ (I)) and wR_2 was 0.2892 (all data), Largest diff. peak/hole / e = 5.37 to - 2.22 Å^{-3}.

[SiMe$_3$(DippForm)] (2.9)

9: $C_{28}H_{44}N_2Si$ (M = 436.74 g/mol): monoclinic, space group $P2_1/c$, a = 13.873(3) Å, b = 10.859(2) Å, c = 18.874(4) Å, α = 90°, β = 105.06(3)°, γ = 90°, *Volume* = 2745.6(10) Å^3, Z = 1, T = 293(2) K, μ = 0.102 mm^{-1}, D_{calc} = 1.057 g/cm^3, F $_{(000)}$ = 960.0, $2\Theta_{max}$ = 3.04 - 63.946, 29911 reflections measured, 7723 unique (R_{int} = 0.0936, R_{sigma} = 0.0770), 7723/0/291 parameters, GooF on F^2 1.083, The final R_1 was 0.0779 (I >2σ (I)) and wR_2 was 0.2280 (all data), Largest diff. peak/hole / e = 0.59 to -0.85Å^{-3}.

[SbCl$_3$(Me$_2$NC$_2$H$_4$NMe$_2$)] (2.10)

10: $C_6H_{16}Cl_3N_2Sb$ (M = 344.31 g/mol): monoclinic, space group $P2_1/c$, a = 11.140(2) Å, b = 7.1720(14) Å, c = 16.159(3) Å, α = 90°, β = 106.70(3)°, γ = 90°, *Volume* = 1236.6(5) Å^3, Z = 4, T = 173.15 K, μ = 2.838 mm^{-1}, D_{calc} = 1.849 g/cm^3, F $_{(000)}$ = 672.0, $2\Theta_{max}$ = 7.936 - 63.748, 14797 reflections measured, 3118 unique (R_{int} = 0.0465, R_{sigma} = 0.0349), 3118/0/113 parameters, GooF on F^2 1.050, The final R_1 was 0.0388 (I >2σ (I)) and wR_2 was 0.0956 (all data), Largest diff. peak/hole / e = 1.89 to - 0.88 Å^{-3}.

[(DippForm)ClSb(μ-O)SbCl$_2$(Me$_2$NC$_2$H$_4$NMe$_2$)]$_2$.C$_6$D$_6$ (2.11)

11: $C_{34}H_{54}Cl_3N_4OSb_2$ (M = 884.70 g/mol): monoclinic, space group $P2_1/c$, a = 12.741(3) Å, b = 20.780(4) Å, c = 29.811(6) Å, α = 90°, β = 93.53(3)°, γ = 90°, *Volume* = 7878(3) Å3, Z = 8, T = 173.15 K, μ = 1.604 mm^{-1}, *Dcalc* = 1.461 g/cm^3, F (000) = 3432.0, $2\Theta_{max}$ = 2.39 - 50, 96844 reflections measured, 13206 unique (Rint = 0.2557, Rsigma = 0.1178), 13206/0/818 parameters, GooF on F^2 1.021, The final R_1 was 0.0920 (I >2σ (I)) and wR_2 was 0.2837 (all data), Largest diff. peak/hole / e = 3.77 to - 1.31 Å^{-3}.

[Sb(DippForm)Cl(C_6F_5)]$_2$.(THF)$_2$ (2.12)

12: $C_{70}H_{88}Cl_2F_{10}N_4O_2Sb_2$ (M = 1520.90 g/mol): triclinic, space group *P-1*, a = 12.043(2) Å, b = 16.684(3) Å, c = 19.801(4) Å, α = 103.49(3)°, β = 105.17(3)°, γ = 103.72(3)°, Volume = 3540.5(15) Å^3, Z = 2(dimer), T = 293(2) K, D_{calc} = 1.413 g/cm^3, μ = 0.910 mm^{-1}, F $_{(000)}$ = 1538.0, $2\Theta_{max}$ = 2.246 - 55.882°, 58194 reflections collected, 15192 unique (R_{int} = 0.0243, R_{sigma} = 0.0209), 15192/0/817 parameters, GooF on F^2 2.452, The final R_1 was 0.0712 ($I > 2\sigma(I)$) and wR_2 was 0.2834 (all data), Largest diff. peak/hole / e = 3.40 to - 1.80 Å^{-3}.

2.7 *References*

1. M. Gielen, H. Ma, A. Bouhdid, H. Dalil, M. Biesemans and R. Willem, *Met.-Based Drugs*, 1997, **4**, 193-197.
2. C. Ergezinger, F. Weller and K. Dehnicke, *Z. Naturforsch., B: Anorg. Chem. Org. Chem.*, 1988, **43**, 1119–1124.
3. P. J. Bailey, R. O. Gould, C. N. Harmer, S. Pace, A. Steiner and D. S. Wright, *Chem. Commun.*, 1997, 1161-1162.
4. C. L. Raston, B. W. Skelton, V.-A. Tolhurst and A. H. White, *Polyhedron.*, 1998, **17**, 935-942.
5. L. A. Lesikar and A. F. Richards, *J. Organomet. Chem.*, 2006, **691**, 4250-4256.
6. J. Konu, M. S. Balakrishna, T. Chivers and T. W. Swaddle, *Inorg. Chem.*, 2007, **46**, 2627-2636.
7. P. B. Hitchcock, M. F. Lappert, G. Li and M. P. Coles, *Dalton Trans.*, 2009, 7820-7826.
8. B. Lyhs, S. Schulz, U. Westphal, D. Bläser, R. Boese and M. Bolte, *Eur. J. Inorg. Chem.*, 2009, 2247-2253.
9. M. Brym, C. M. Forsyth, C. Jones, P. C. Junk, R. P. Rose, A. Stasch and D. R. Turner, *Dalton Trans.*, 2007, 3282-3288.
10. M. Rhiel, *Angew. Chem. Int. Ed.*, 1994, **33**, 569-570.
11. C. Hering, M. Lehmann, A. Schulz and A. Villinger, *Inorg. Chem.*, 2012, **51**, 8212-8224.
12. A. Schulz, A. Villinger and A. Westenkirchner, *Inorg. Chem.*, 2013, **52**, 11457-11468.
13. M. Yoshifuji, I. Shima, N. Inamoto, K. Hirotsu and T. Higuchi, *J. Am. Chem. Soc.*, 1981, **103**, 4587-4589.
14. C. Jones, *Coord. Chem. Rev.*, 2001, **215**, 151-169.
15. N. Tokitoh, *J. Organomet. Chem.*, 2000, **611**, 217-227.
16. T. Sasamori, E. Mieda, N. Nagahora, K. Sato, D. Shiomi, T. Takui, Y. Hosoi, Y. Furukawa, N. Takagi, S. Nagase and N. Tokitoh, *J. Am. Chem. Soc.*, 2006, **128**, 12582-12588.

17. T. Sasamori, E. Mieda, N. Nagahora, N. Takeda, N. Takagi, S. Nagase and N. Tokitoh, *Chem. Lett.*, 2005, **34**, 166-167.
18. S. P. Green, C. Jones, G. Jin and A. Stasch, *Inorg. Chem.*, 2007, **46**, 8-10.
19. A. Hinz, J. Rothe, A. Schulz and A. Villinger, *Dalton Trans.*, 2016, **45**, 6044-6052.
20. M. Hall and D. B. Sowerby, *J. Organomet. Chem.*, 1988, **347**, 59-70.
21. J.D. Smith, *The Chemistry of Arsenic, Antimony and Bismuth*, Pergamon, 1973, 588-603.
22. A. Otero and P. Royo, *J. Organomet. Chem*., 1978, **154**, 13-19.
23. B. A. Nevett and A. Perry, *Spectrochim. Acta A.*, 1975, **31**, 101-106.
24. P. Raj, A.K. Saxena, K. Singhal, A. Ranjan, *Polyhedron*., 1985, **4**, 251-258.
25. M. Fild, M. Fild, O. Glemser and G. Christoph, *Angew. Chem. Int. Ed*., **3**, 801-801.
26. P. Raj, A. K. Aggarwal and A. K. Saxena, *J. Fluorine Chem.*, 1989, **42**, 163-172.
27. K. Chandrashekar, H. M. Behl, O. P. Sidhu, V. Kumar, C. V. Rao, P. Pushpangadan, R. Kant, S. K. Shukla, K. Singhal and A. K. Saxena, *PCT (Global) Patent*, WO 2006/067800A-1.
28. P. Pyykkö and M. Atsumi, *Chem. Eur. J.*, 2009, **15**, 12770-12779.
29. N. Tokitoh, Y. Arai, T. Sasamori, R. Okazaki, S. Nagase, H. Uekusa and Y. Ohashi, *J. Am. Chem. Soc*., 1998, **120**, 433-434.
30. B. Twamley, C. D. Sofield, M. M. Olmstead and P. P. Power, *J. Am. Chem. Soc.*, 1999, **121**, 3357-3367.
31. M. Sakagami, T. Sasamori, H. Sakai, Y. Furukawa and N. Tokitoh, *Bull. Chem. Soc. Jpn.*, 2013, **86**, 1132-1143.
32. M. Sakagami, T. Sasamori, H. Sakai, Y. Furukawa and N. Tokitoh, *Chem. Asian. J.*, 2013, **8**, 690-693.
33. D. Dange, A. Davey, J. A. B. Abdalla, S. Aldridge and C. Jones, *Chem. Commun.*, 2015, **51**, 7128-7131.
34. Z. Li, S. T. Barry and R. G.Gordon, *J. Am. Chem. Soc*., 2005, **44**, 1728-1735.

35. M. Stender, A. D. Phillips and P. P. Power, *Inorg. Chem.*, 2001, **40**, 5314-5315.
36. S. P. Green, C. Jones, P. C. Junk, K.-A. Lippert and A. Stasch, *Chem. Commun.*, 2006, 3978-3980.
37. A. Stasch, C. M. Forsyth, C. Jones and P. C. Junk, *New J. Chem.*, 2008, **32**, 829-834.
38. S. Nagendran, S. S. Sen, H. W. Roesky, D. Koley, H. Grubmüller, A. Pal and R. Herbst-Irmer, *Organometallics.*, 2008, **27**, 5459-5463.
39. S. Dagorne, R. F. Jordan and V. G. Young, *Organometallics.*, 1999, **18**, 4619-4623.
40. J. Barker and M. Kilner, *Coord. Chem. Rev.*, 1994, **133**, 219-300.
41. W. Clegg, M. R. J. Elsegood, V. Graham, N. C. Norman, N. L. Pickett and K. Tavakkoli, *J. Chem. Soc., Dalton Trans.*, 1994, 1743-1751.
42. A. R. J. Genge, N. J. Hill, W. Levason and G. Reid, *J. Chem. Soc., Dalton Trans.*, 2001, 1007-1012.
43. B. Lyhs, D. Bläser, C. Wölper and S. Schulz, *Chem. Eur. J.*, 2011, **17**, 4914-4920.
44. M. L. Cole, P. C. Junk and L. M. Louis, *J. Chem. Soc., Dalton Trans.*, 2002, 3906-3914.
45. J. Baldamus, C. Berghof, M. L. Cole, D. J. Evans, E. Hey-Hawkins and P. C. Junk, *J. Chem. Soc., Dalton Trans.*, 2002, 2802-2804.
46. R. J. Baker, C. Jones, P. C. Junk and M. Kloth, *Angew. Chem. Int. Ed.*, 2004, **43**, 3852-3855.
47. M. L. Cole, C. Jones, P. C. Junk, M. Kloth and A. Stasch, *Chem. Eur. J.*, 2005, **11**, 4482-4491.
48. M. L. Cole, G. B. Deacon, C. M. Forsyth, K. Konstas and P. C. Junk, *Dalton Trans.*, 2006, 3360-3367.
49. P. C. Junk and M. L. Cole, *Chem. Commun.*, 2007, 1579-1590.
50. R. Fleischer, S. Freitag and D. Stalke, *J. Chem. Soc., Dalton Trans.*, 1998, 193-198.
51. B. M. Gridley, T. J. Blundell, G. J. Moxey, W. Lewis, A. J. Blake and D. L. Kays, *Chem. Commun.*, 2013, **49**, 9752-9754.

52. Y. Tang, L. N. Zakharov, A. L. Rheingold and R. A. Kemp, *Polyhedron.*, 2005, **24**, 1739-1748.
53. M. Lehmann, A. Schulz and A. Villinger, *Eur. J. Inorg. Chem.*, 2010, 5501-5508.
54. J. Schulz, D. Vimont, T. Bordenave, D. James, J. M. Escudier, M. Allard, M. Szlosek-Pinaud and E. Fouquet, *Chem. Eur. J.*, 2011, **17**, 3096-3100.
55. L. Ponikiewski and A. Rothenberger, *Inorg. Chim. Acta.*, 2008, **361**, 43-48.
56. R.-C. Liu, Y.-Q. Ma, L. Yu, J.-S. Li, J.-R. Cui and R.-Q. Wang, *Appl. Organomet. Chem.*, 2003, **17**, 662-668.
57. H. Mahalakshmi, V. K. Jain and E. R. T. Tiekink, *Z. Kristallogr. NCS.*, 2003, **218**, 71-72.
58. G. R. Willey, L. T. Daly, P. R. Meehan and M. G. B. Drew, *J. Chem. Soc., Dalton Trans.*, 1996, 4045-4053.
59. R. M. Roberts, *J. Org. Chem.*, 1949, **14**, 277-284.
60. K. M. Kuhn and R. H. Grubbs, *Org. lett.*, 2008, **10**, 2075-2077.
61. G. B. Deacon, C. M. Forsyth and S. Nickel, *J. Organomet. Chem.*, 2002, **647**, 50-60.
62. G. M. Sheldrick, *Acta Crystallogr., Sect. C: Struct. Chem.*, 2015, **71**, 3-8.
63. G. M. Sheldrick, *SHELXS-97 and SHELXL-97*, 1997.
64. L. J. Barbour, *J. Supramol. Chem.*, 2001, **1**, 189-191.
65. O. V. Dolomanov, L. J. Bourhis, R. J. Gildea, J. A. K. Howard and H. Puschmann, *J. Appl. Crystallogr.*, 2009, **42**, 339-341.

CHAPTER THREE

SYNTHESES AND MOLECULAR STRUCTURES OF HETEROLEPTIC AND HOMOLEPTIC ANTIMONY (III) TETRAFLUOROPHENYLETHYLENEDIAMIDATE COMPLEXES

Outline

This chapter discusses the synthesis of a series of tri-valent antimony N,N′-bis(polyfluorophenyl)ethane-1,2-diaminate complexes. Halo- and nonhalo-polyfluorophenylamido antimony (III) complexes have been successfully gained and fully characterised as monomers in the solid state highlighting a variety of coordination modes. Two antimony (III) tetrafluorophenylethylenediaminate complexes were isolated by metathesis reactions between $SbCl_3$ and Li(*p*-$HC_6F_4N(CH_2)_2NMe_2$), Li(L^{Me}), a common synthetic route to antimony complexes; while the direct reaction between $SbCl_3$ and *p*-$HC_6F_4NH(CH_2)_2NMe_2$, HL^{Me} was alternative pathway for one complex in this chapter. To the best of our knowledge, no examples of antimony compounds supported by a *mono*-anionic N,N-dimethyl-N'-2,3,5,6-tetrafluorophenylethane-1,2-diaminate ligand bound to antimony have been previously reported.

The two types of a pro-ligand used in the metathesis reactions within this chapter were (*p*-$HC_6F_4NH(CH_2)_2NMe_2/Et_2$) ($HL^{Me/Et}$) (Fig. 3.1). The substituted ligands $HL^{Me/Et}$ can be easily synthesised by a slight modification from the published procedure (explained in details in the experimental section of this Chapter).[1] Syntheses of complexes containing these ligands have been reported previously, but with different metals across the periodic table allowing for comparisons in this work.

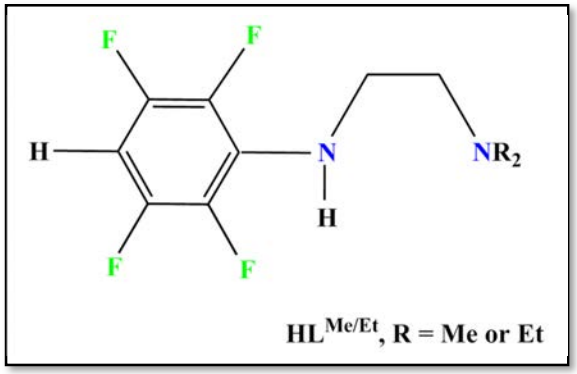

Figure 3.1 Ligand system used in metathesis syntheses ($HL^{Me/Et}$).

3.1 *Introduction*

Tri-valent antimonial compounds have shown to be promising in the therapy of acute promyelocytic leukemia (APL),[2] and could have the potential to be antileishmanial drugs, and this has stimulated many researchers, including us, in this field. The amido–N atoms have the ability to partly saturate the electronic demands of a highly Lewis acidic metal centre, and protect most of the coordination sphere around the metal.[3]

It is believed that the polyfluorophenyl substituents in the chelating organoamide ligands enhance the complexes stability against hydrolysis, which is essential for biological examination.[4,5] Complexes of the type $[Pt\{N(R)CH_2CH_2NY_2\}X(py)]$ (R = polyfluorophenyl (*p*-HC_6F_4 or C_6F_5); Y = Et or Me; X = Cl, Br, I) and $[Pt\{N(R)CH_2\}_2(py)_2]$,[6] which have been prepared previously[1] with *trans* amine ligands and no H atoms on the N donor atoms feature high biological activity against a varied cell lines containing cisplatin resistant variants.[7,8] Moreover, the integration of fluorine atoms is being widely adopted in drug design.[9] This stabilising effect is due to a combination of electronic and steric factors of the ligand. Furthermore, fluorine atoms in the ligand periphery may act as additional donor functions in their bidentate amido complex derivatives. Fluorine-mediated interactions between polyfluorocarbon groups and metal atoms, –CF–M,[10] across the periodic table is a rapidly expanding field due to fundamental interest and also as possible precursors for C–F activation reactions,[11] as –F–M coordination weakens the C–F bond.[12] The carbon-fluorine bond is considered as one of the strongest single bonds in organic chemistry, with typical bond dissociation energies (BDE) of 105.4 kcal/mol.[13] This is due to fluorine being the most electronegative element in the periodic table.

Usually, activation of the C–F bond is more difficult than activation of similar C–H bonds (C-H: normally detected at 98.8 kcal/mol), and affords an important challenge because of its characteristic strength that comes from thermal stability and highest chemical inertness. These properties have attracted studies in this area, as C–F moieties are present already in 30 % of agrochemicals and 20 % of pharmaceuticals.[14] On the other hand, these same properties can also present adverse side effects including the role of chlorofluorocarbons in the ozone layer and the role of hydrofluorocarbons as strong greenhouse gases.[15]

The intensity of C–F bond can be measured by the resultant electrostatic/dipole interactions between the electropositive $C^{\delta+}$ atom and electronegative $F^{\delta-}$ atom, giving the polar-covalent bond a further ionic character. This polarity prevents the fluorine from donating lone pair, and also fluorine overall is a weak coordinator. Furthermore, one of the main difficulties in C-F activation chemistry is the isolation and identification of the final organic product produced from activation. More specifically, it could be more problematical when activation leads to the complete decomposition of the organic molecule.[16]

Although not observed for the antimony tetrafluorophenylaminoaminate complexes, C-F activation of fluorinated aminoamidate ligands has been previously observed for HL^{Me} (HL^{Me} = N,N-dimethyl-N'-2,3,5,6-tetrafluorophenylethane–1,2-diamine) when coordinated to Na and K.[16] In the synthesis of $[Na(L^{Me})]$ and $[K(L^{Me})]$, HL^{Me} was treated with $NaN(SiMe_3)_2$ in THF and $KN(SiMe_3)_2$ in PhMe respectively. Furthermore, the sodium and potassium complexes $[Na(L^{Me})_2Na(tmeda)]$ and $[K_2(L^{Me})_2(tmeda)_2]$,[16] prepared by ligand exchange after treating with the TMEDA display *o*-F-M coordination (Scheme 3.1, *a* and *b*), proposing that tridentate N,N',F coordination may be the main mode for these ligands with electropositive elements.

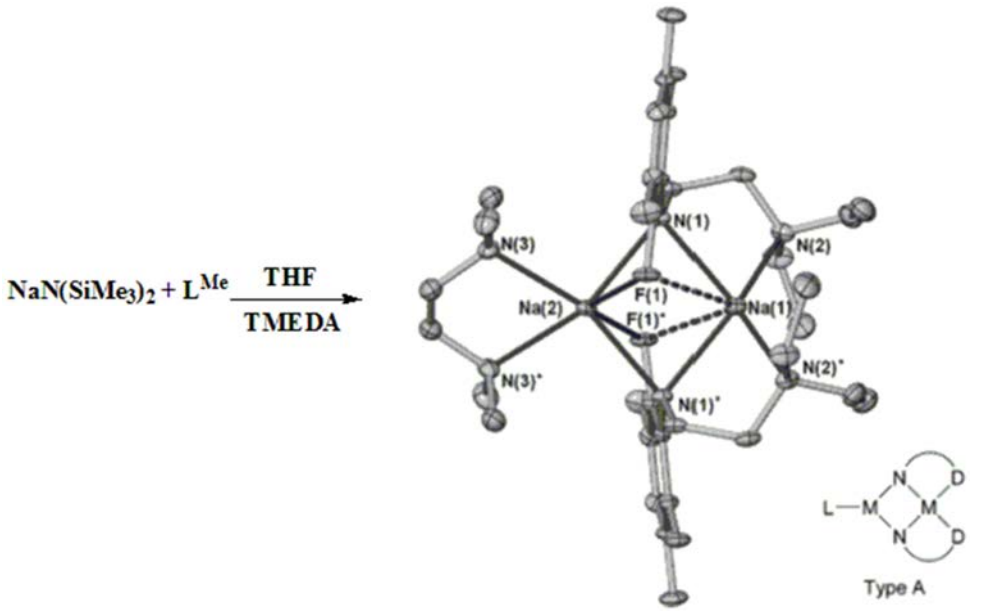

***a*: [Na(L^{Me})$_2$Na(tmeda)]**

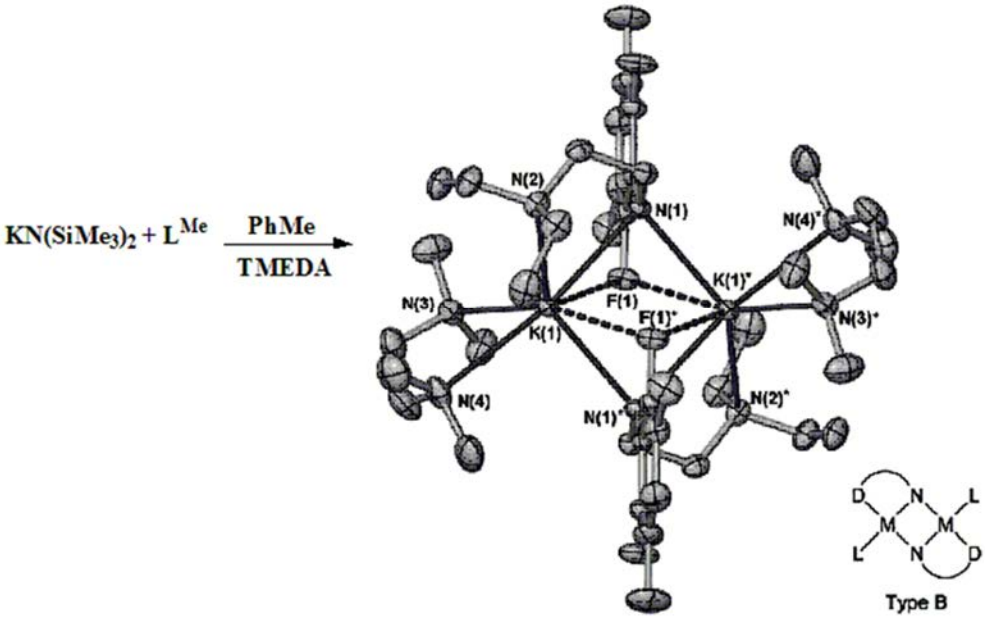

***b*: [K$_2$(L^{Me})$_2$(tmeda)$_2$]**

Scheme 3.1 Synthesis of a: [Na(L^{Me})$_2$Na(tmeda)] and b: [K$_2$(L^{Me})$_2$(tmeda)$_2$] by treatment of HL^{Me} with NaN(SiMe$_3$)$_2$ in THF and KN(SiMe$_3$)$_2$ in PhMe in the presence of TMEDA.[16]

The initial assembled of N,N-dialkyl-N'-2,3,5,6-tetrafluorophenylethane-1,2-di-aminate ligands *in situ* was in a template synthesis of platinum (II) complexes [Pt($L^{Me/Et}$)X(py)] (X= Cl, Br, I) to give probable 'rulebreaker' anticancer drugs.[6,8] The process was a combination between decarboxylation and nucleophilic substitution.[17,18]

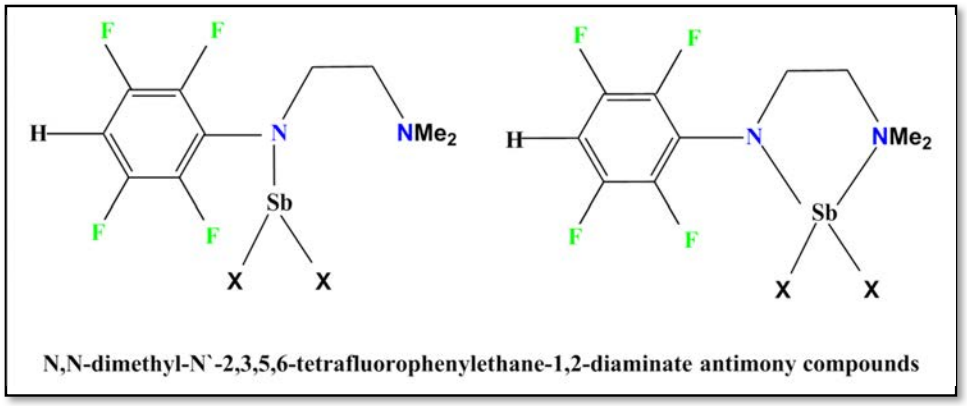

Scheme 3.2 Potential ligand binding mode to Sb.

3.2 *The current study*

This chapter describes the synthesis and characterisation of the first series of halo- and nonhalo-organoantimony (III) complexes of the general type $[SbL^{Me}_{3-n}Cl_n]$ (n = 2, 1, 0) incorporating a bulky amido fluorine ligand tethered with an amino pendant arm, HL^{Me} = *p*-$HC_6F_4NH(CH_2)_2NMe_2$. Although the other type of polyfluorophenylamide ligand: HL^{Et} = *p*-$HC_6F_4NH(CH_2)_2NEt_2$ was involved in the experiments of this chapter, no compounds were easily isolate. Metathesis and direct reactions were carried out in non-coordinating solvents, PhMe and hexane, or in a strong electron donor solvent, THF.

The $HL^{Me/Et}$ pro-ligands attractively features by the existence of many proton environments that can be easily interpreted when conducting ^{1}H-NMR spectra. These ligands are also rather sterically demanding and has F and Me or Et groups to enhance solubility in organic solvents, whereas the N atoms allow a range of structural variation. Furthermore, this type of ligand was chosen to be chelated to Sb either through its two nitrogen or one nitrogen, as well as potentially *o*-F–Sb interactions forming a five-membered chelate ring by a charged amide nitrogen atom together with an amine nitrogen atom chelated with two methyl/ethyl group. Perhaps ephemeral Sb–F interactions can mostly occur in solution by the two *ortho* fluorine atoms, even with some rotation around the *p*-HC_6F_4–N bond. However, the *meta* fluorine atoms existence further away from the antimony atom and characteristically shifted by the *p*-H substituent, as observed in the $^{19}F\{^1H\}$-NMR spectra.

GLOSSARY OF COMPOUNDS AND CODES

The following simplified diagrams are a summary of the complexes discussed throughout this chapter, together with respective codes. These structures show antimony atoms in different colours representing the colours of the compounds observed in the solid state.

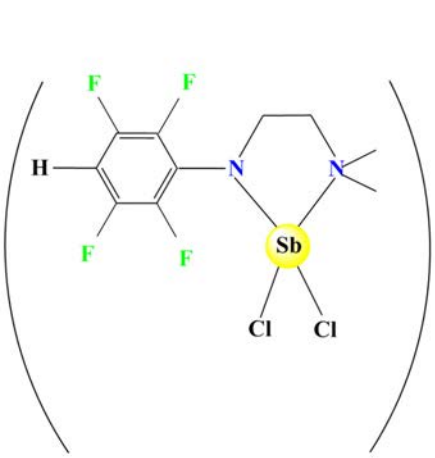

$[Sb(p\text{-}HC_6F_4NC_2H_4NMe_2)Cl_2]$ (3.1)

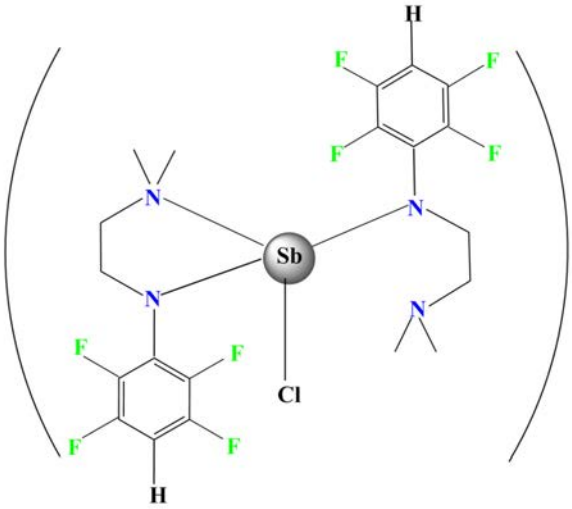

$[Sb(p\text{-}HC_6F_4NC_2H_4NMe_2)_2Cl]$ (3.2)

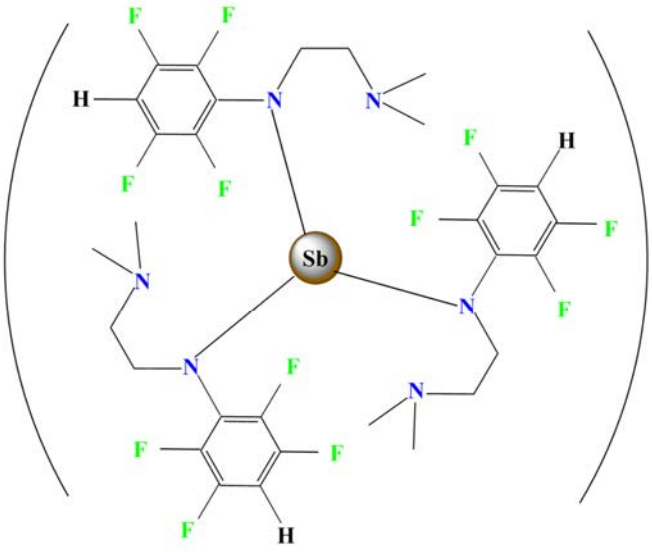

$[Sb(p\text{-}HC_6F_4NC_2H_4NMe_2)_3]$ (3.3)

3.3 *Results and discussion*

3.3.1 Synthesis

Preparation of the amine ligand precursors *p*-$HC_6F_4N(CH_2)_2NR_2$ (R = Me, Et) ($L^{Me/Et}$) became more convenient from nucleophilic substitution based on heating to reflux the appropriate N,N-dialkylethane-1,2-diamine and pentafluorobenzene in EtOH (eqn. 1.3).[1,16] Antimony L^{Me} complexes, [Sb(*p*-$HC_6F_4NC_2H_4NMe_2$)Cl_2] (**3.1**), [Sb(*p*-$HC_6F_4NC_2H_4NMe_2)_2Cl$] (**3.2**) and [Sb(*p*-$HC_6F_4NC_2H_4NMe_2)_3$] (**3.3**), were synthesised by two different methodologies: either direct reaction (DR) between $SbCl_3$ and *p*-$HC_6F_4NH(CH_2)_2NR_2$ (HL^{Me}) (Scheme. 3.3, i), or by means of metathesis between Li(L^{Me}) and $SbCl_3$ (Scheme. 3.3, ii).

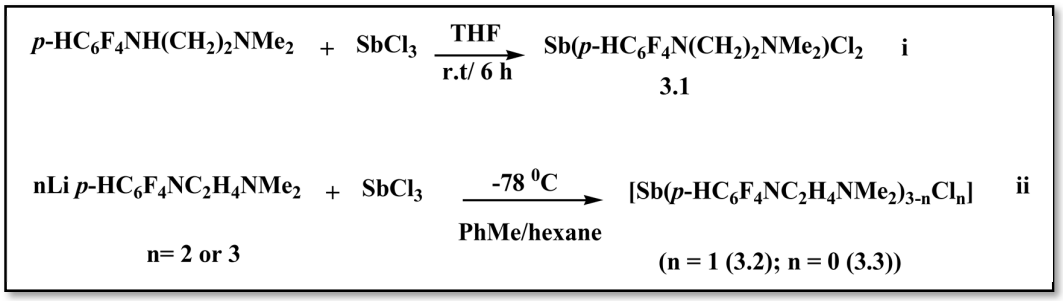

Scheme 3.3 Summary of syntheses of tri-valent antimony L^{Me} complexes by either direct reaction (DR) (Scheme. 3.3, i), or by metathesis (Scheme. 3.3, ii).

Bright yellow crystals of the tri-valent antimony complex [Sb(L^{Me})Cl_2] (**3.1**) was synthesised in reasonable yield by a straightforward synthetic approach to this class of compound. The reaction was between an equivalent molar amount of $SbCl_3$ and HL^{Me} in THF. This antimony complex is thermally stable (M.P = 186-192 ^{0}C) and even on exposure to light, it is robust keeping the same colour both in solution and in the solid state. This complex can also be synthesised in a 1:1 molar ratio by metathesis between Li(L^{Me}) dissolved in hexane and $SbCl_3$ dissolved in PhMe (Scheme 3.4).

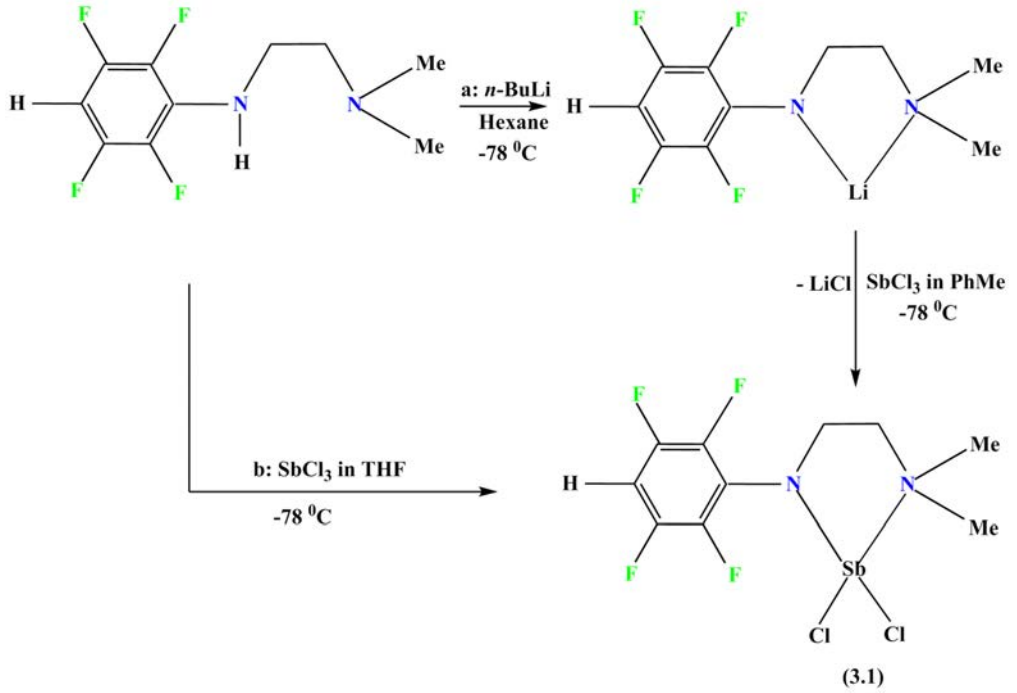

Scheme 3.4 Two routes to synthesise ($Sb(L^{Me})Cl_2$) (**3.1**), a: through the formation of an intermediate compound $Li(L^{Me})$ and b: direct path.

Both synthetic approaches gave the desired complexes in reasonable yield (Direct: 31%; Metathesis: 35%), but one of the key advantages of DR reactions over metathesis is that the synthesis does not require preparation of the air/moisture sensitive $[Li(L^{Me})]_2$ compound, which are often isolated in low yield and impact the purity of the final product. On the other hand, although direct reaction was the faster route to (**3.1**) than the metathesis route, it appears that metathesis is the more effective route for other antimony complexes (e.g. **3.2**, **3.3**). It is possible to monitor reactions by ^{1}H-, ^{7}Li- or $^{19}F\{^{1}H\}$-NMR spectroscopy. $[Li(L^{Me})]_2$ is synthesised via deprotonation of the HL^{Me} by *n*-BuLi in hexane at - 78 ^{0}C (Scheme 3.5). The salt metathesis reaction between $SbCl_3$ in PhMe and $[Li(L^{Me})]_2$ in hexane, readily yielded the analogous metal complexes $[SbL^{Me}{}_{3-n}Cl_n]$ (n = 2, 1, 0) (Scheme 3.5).

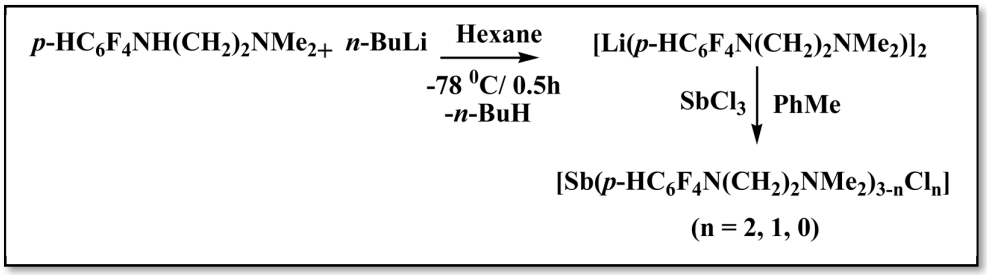

Scheme 3.5 Synthesis of $[Li(L^{Me})]_2$ and subsequently $[SbL^{Me}_{3-n}Cl_n]$ (n = 2, 1, 0).

Following the same technique, the parent amine ligand was first lithiated by *n*-BuLi in hexane at low temperature (- 78 °C) and the observed lithium precursor $Li(L^{Me})$ was *in situ* treated with ⅓ molar equivalent of anhydrous $SbCl_3$ in PhMe and stirred for several days. The reaction result was the trivalent antimony complex, $[Sb(L^{Me})_3]$ (**3.3**) (Scheme 3.6). Because such complexes would have crowded coordination spheres, it is hard to predict their coordination number and whether N,N',F-ligation or even –CF–Sb bonding can potentially occur for some or all ligands. In this complex, the metathesis reaction appeared complete within 2-3 hours, but the precipitate was required approximately two days to settle, and after filtration the solution was immediately left to crystalise. Isolation and characterisation required careful handling as the product was very sensitive to moisture and easily decomposed.

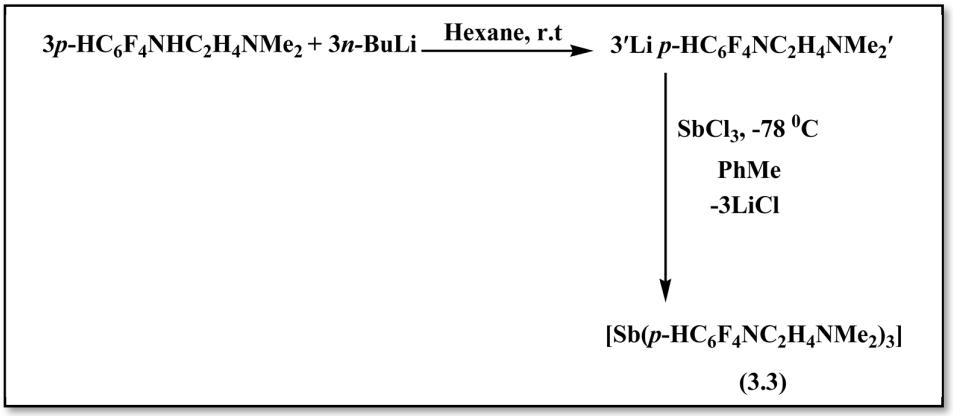

Scheme 3.6: Synthesis of complex (**3.3**).

With the challenge to structurally characterise the more crowded antimony N,N-diethyl- N′-2,3,5,6-tetrafluorophenylethane–1,2-diamine complexes, many attempts were made under varying conditions to examine the possibility of the L^{Et} to be coordinated with antimony (III), namely to synthesise $[SbL^{Et}_{3-n}Cl_n]$ (n = 2,1,0). Although the reactions appeared to be successful with a colour change to deep brown, attempted crystallisation of the trivalent species were met with synthetic difficulties and rapid decomposition. Antimony (III) diethyl substituted complexes have not been synthesised; though, their isolation should be possible, as ytterbium (III) polyfluorophenylamidate complex of the type, $[Yb(L^{Et})_3]$ that has been previously isolated.[19] $[Yb(L^{Et})_3]$ displays remarkable structural variances from reported $[Ln(L^{Et})_3]$ (Ln = La, Ce, Nd) complexes,[20] and highlights an incomplete shift towards N,N′ chelation to the much smaller Yb ion.

3.3.2 Characterisation

Two of the products obtained within this chapter (**3.2**, **3.3**) were isolated from the reaction mixture by filtration from LiCl, followed by fractional crystallisation from PhMe/hexane solution as unsolvated heteroleptic and homoleptic species respectively. Compound (**3.1**) was prepared in THF and for further purification required hexane. All the three complexes experience limited solubility in C_6D_6. Although the polyfluorophenylamide ligands can feature tridentate N,N',F chelation, the spectroscopic data and structural considerations indicate that none of the four F-donors are coordinated to Sb. Where possible, all these isolated compounds (**3.1**, **3.2** and **3.3**) were crystallised and characterised by standard analytical techniques. The main characterisation was authenticated by X-ray crystallography in the solid state using the MX1 beamline at the Australian Synchrotron. Crystal data and refinement details are given in (Table 3.5), and in the experimental section. Further characterisation included IR spectroscopic (Table 3.1), ^{1}H-NMR (Table 3.2), ^{19}F{^{1}H}-NMR spectroscopy (Table 3.3), elemental analyses and melting points determination.

The ^{19}F{^{1}H}-NMR chemical shifts in the N,N-dimethyl-N'-2,3,5,6-tetrafluorophenylethane-1,2-di-aminate antimony complexes are indicative of the coordinative engagement of the ligand; thus, the ^{19}F{^{1}H}-NMR spectra of diamagnetic Sb-L^{Me} complexes at a slightly elevated temperature 60 ^{0}C showed only two almost equal intensity multiple resonances for the *ortho* (δ = −147.26 – 148.20 ppm) reasonably attributable to F2,6; and a signal for the *meta* F atoms (δ = −140.11−140.95 ppm) reasonably attributable to F3,5. The ^{1}H-NMR spectra of diamagnetic Sb L^{Me} complexes at room temperature show an absence of a N-H resonance and simple multiple signals for the C*H*$_2$NMe and C*H*$_2$NAr proton resonances consistent with the single crystal compositions in the solid-state structure. For the ^{1}H-NMR spectra, the very low solubility required use of slightly elevated temperatures to obtain satisfactory NMR spectra. The ^{1}H-NMR spectra were consistent with the proposed composition from X-ray data without PhMe/hexane or THF of crystallisation. NMR scale studies of the decomposition of freshly isolated and pure (**3.1**-**3.3**) (in C_6D_6), showed complete shifts of resonances of the ^{19}F{^{1}H}-NMR signals for these compounds over time.

The reactions containing Li(*p*-$HC_6F_4NC_2H_4NMe_2$), were monitored by $^{19}F\{^1H\}$-NMR spectroscopy, which indicated the formation of Li-containing products, with chemical shifts different from the free ligand over 2 days, none of which could be isolated to be identified by X-ray diffraction. It has been noticed that complex [Sb(*p*-$HC_6F_4NC_2H_4NMe_2)_2Cl$] (**3.2**) has been gained with the highest yield (70 %).

The ^1H-spectrum of [$Sb(L^{Me})Cl_2$] at room temperature shows signals over the range 1.63 to − 6.24 ppm. The $^{19}F\{^1H\}$-NMR spectrum of (**3.1**), two multiple are seen at −140.91 (F3,5) and −147.26 (F2,6) ppm. The $^{19}F\{^1H\}$-NMR spectrum for [$Sb(L^{Me})_2Cl$] is almost similar to that of [$Sb(L^{Me})Cl_2$] and it shows resonances at −140.95 ppm attributable to the (F3,5), which is closely comparable to the resonance −140.8 ppm refers to (F3,5) that reported for [N-(4-bromo-2,3,5,6-tetrafluorophenyl)-N'-(2,3,5,6-tetrafluorophenyl)ethane-1,2-diaminato(2-)] dipyridineplatinum(II)-ether,[21] and another signal at −147.28 ppm, attributable to the (F2,6) atoms.

Although a poorly soluble brown crystalline solid of (**3.3**) was obtained from the filtered reaction mixture, the compound was isolated in 30 % yield as small crystals adequate for X-ray identification, allowing only ^1H- and $^{19}F\{^1H\}$-NMR as further characterisation. The ^1H NMR spectrum revealed that [$Sb(L^{Me})_3$] is the major product of the synthesis process, but also detected the existence of other material recognised from the reaction mixture as minor product, which is an uncoordinated HL^{Me}. The substitution patterns of polyfluorophenylamide groups have been confirmed by comparison of observed and calculated ^1H- and $^{19}F\{^1H\}$-NMR chemical shifts. An attempt to prepare the product in bulk failed.

The IR spectra of the three complexes are similar to those of reported L^{Me} complexes,[20] and they show loss of *ν* (N-H) bands of the reactant *p*-$HC_6F_4NH(CH_2)_2NM_2$ upon complexation, consistent with deprotonation of L^{Me} and coordination to the respective metal (Li and then Sb). Characteristic υ (C-F) absorptions are observed between 927–937 cm^{-1} for the complexes with L^{Me}. Elemental analyses (C,H,N) were consistent with the formation of the compounds (**3.1** and **3.2**) indicating excellent agreement with the single crystal compositions, while (**3.3**) repeatedly gave poor data with extremely low C %, presumably because of the product decomposition during analysis or transport to the analytical centre in London, or the possibility of the formation of metal carbides.

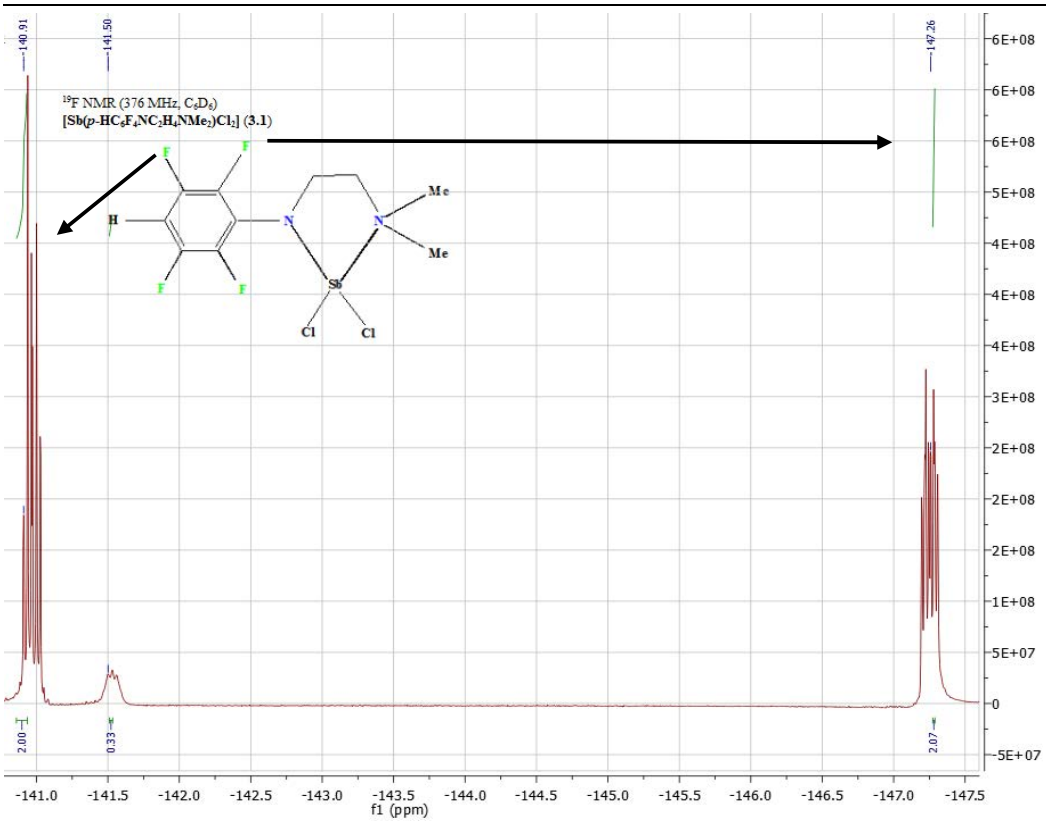

$^{19}F\{^{1}H\}$-NMR (376 MHz, C_6D_6): [Sb(*p*-$HC_6F_4NC_2H_4NMe_2$)Cl_2] (**3.1**)

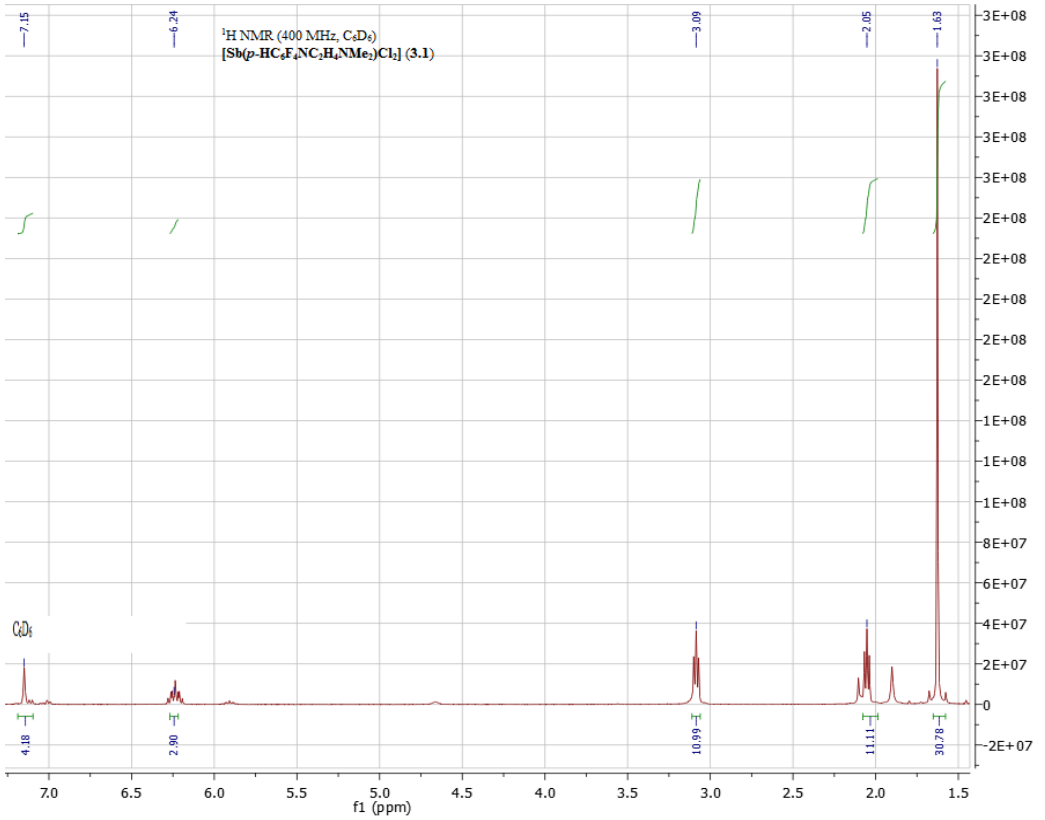

^{1}H-NMR (400 MHz, C_6D_6): [Sb(*p*-$HC_6F_4NC_2H_4NMe_2$)Cl_2] (**3.1**)

Table 3.1 N–C Stretching in IR spectra for antimony (III) tetrafluorophenylaminate complexes 3.1 - 2.3 (υ 4000 - 400 cm^{-1})

Compound		N–C stretching vibration (cm^{-1})
[Sb(*p*-$HC_6F_4NC_2H_4NMe_2$)Cl_2]	(**3.1**)	1651
[Sb(*p*-$HC_6F_4NC_2H_4NMe_2$)$_2$Cl]	(**3.2**)	1647
[Sb(p-$HC_6F_4NC_2H_4NMe_2$)$_3$]	(**3.3**)	1651

Table 3.2 ^{1}H-NMR chemical shift data in ppm for antimony (III) tetrafluorophenylaminate complexes 3.1 - 2.3 in C_6D_6

^{1}H-NMR	**3.1**	**3.2**	**3.3**
Aromatic *H*	6.24-6.28	5.91-5.99	6.14-6.22
N*H*	–	–	–
C*H*$_3$	1.63	1.93	1.95
C*H*$_2$	3.09, 2.05	3.15, 2.14	3.71, 2.06

Table 3.3 ^{19}F{^{1}H}-NMR chemical shift data in ppm for antimony (III) tetrafluorophenylaminate complexes 3.1 - 2.3 in C_6D_6

^{19}F{^{1}H}–NMR	**3.1**	**3.2**	**3.3**
F 3,5	–140.91	–140.95	–140.11
F 2,6	–147.26	–147.28	–148.20

3.3.3 Crystal structure determinations

[Sb(*p*-$HC_6F_4NC_2H_4NMe_2$)Cl_2] (3.1)

The monomeric Sb^{+3} complex [Sb(*p*-$HC_6F_4NC_2H_4NMe_2$)Cl_2] (**3.1**) crystallised in the orthorhombic space group *Pna2₁* (Table 3.5), with one molecule in the asymmetric unit. Bright yellow crystals of (**3.1**) were obtained in moderate yield from the 1:1 direct reaction of HL^{Me} with $SbCl_3$ (Scheme 3.3). Figure 3.2 displays the mononuclear complex (**3.1**) with the antimony centre chelated by N,N'-bis(polyfluorophenyl)ethane-1,2-diaminate and two *cis* chloride ligands, giving the antimony atom centre a coordination number of four. The overall stereochemistry around the antimony centre is best described as heavily distorted tetrahedral. The L^{Me} chelating mode with the Sb atom in (**3.1**) is similar to that observed in [$SbLCl_2$] (L = the multidentate ketoiminato ligand with a bulky substituent on one side = RN(H)C(Me)CHC(Me)=O, R = $C_2H_4NEt_2$), but with square pyramidal geometry.[22] The latter was generated from the *in situ* lithiation of L and subsequent reaction with $SbCl_3$. The N–Sb bond lengths in (**3.1**) are 2.039(3) and 2.372(4) Å, and these values are shorter and longer than the sum of the covalent radii of the corresponding atoms ($\sum r_{cov}$(Sb–N) = 2.11 Å);[23] however, they are comparable to the value observed in the N,N-chelated analogue [C_4H_3N-2-(CH=N-2',6'-*i*$Pr_2C_6H_3$)]$SbCl_2$ [2.0810(15) and 2.3234(17) Å].[24] Deviation from 90° for the N–Sb–N angle is driven by the bite angle (75.70°) of the chelating ligand. The Sb-Cl bond distances found to be 2.405(11) and 2.522(10) Å, which are comparable to the values observed for Sb-Cl in [C_4H_3N-2-(CH=N-2',6'-*i*$Pr_2C_6H_3$)]$SbCl_2$ [2.3691(6) and 2.5616(6) Å].[24] The N–Sb–N angle for [Sb(*p*-$HC_6F_4NC_2H_4NMe_2$)Cl_2] found to be 75.70 (12)°, which is bigger than the N–Sb–N angle of 73.90 (6)° reported for [C_4H_3N-2-(CH=N-2',6'-*i*$Pr_2C_6H_3$)]$SbCl_2$. While, the Cl–Sb–Cl angle for (**3.1**) found to be 87.35 (4)° that is considerably smaller comparing with the Cl–Sb–Cl angle of 92.21 (2)° detected in [C_4H_3N-2-(CH=N-2',6'-*i*$Pr_2C_6H_3$)]$SbCl_2$.[24]

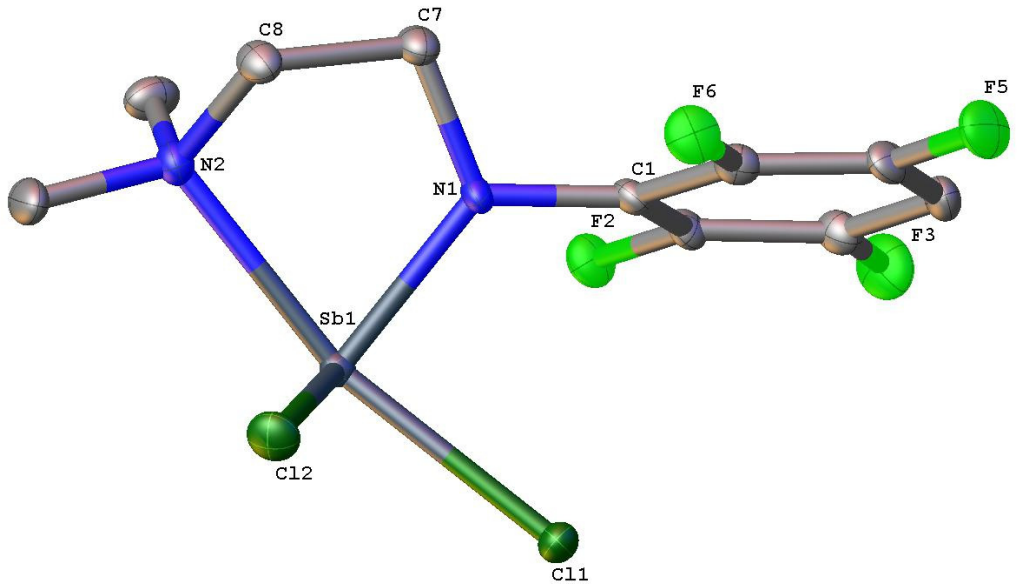

Figure 3.2. Molecular structure of monomeric **[Sb(*p*-$HC_6F_4NC_2H_4NMe_2$)Cl_2] (3.1)** with the atom numbering system; thermal ellipsoids are drawn at the 50 % probability level, and hydrogen atoms have been omitted for clarity. Selected bond lengths (Å) and angles (°): Sb(1)–N(1): 2.039(3), Sb(1)–N(2): 2.372(4), Sb(1)–Cl(2): 2.405(11), Sb(1)–Cl(1): 2.522(10), N(1)–C(1): 1.410(5), N(1)–Sb(1)–N(2): 75.70(12), Cl(2)–Sb(1)–Cl(1): 87.35(4), N(1)–Sb(1)–Cl(1): 88.45(10), N(1)–Sb(1)–Cl(2): 98.65(10), N(2)–Sb(1)–Cl(1): 160.64(8), N(2)–Sb(1)–Cl(2): 84.18(10), C(1)–N(1)–Sb(1): 123.3(2), C(7)–N(1)–Sb(1): 121.1(2), C(10)–N(2)–Sb(1): 115.4(3), C(8)–N(2)–Sb(1): 105.0(2).

[Sb(*p*-$HC_6F_4NC_2H_4NMe_2$)$_2$Cl] (3.2)

The *in situ* lithiation of HL^{Me} and subsequent reaction with $SbCl_3$ in a 2:1 ratio, yields complex [Sb(*p*-$HC_6F_4NC_2H_4NMe_2$)$_2$Cl] (**3.2**) (Scheme 3.5). The monomeric Sb^{+3} complex [Sb(*p*-$HC_6F_4NC_2H_4NMe_2$)Cl_2] (**3.2**) crystallised in the monoclinic space group *P2$_1$/c* (Table 3.5), with the full molecule in the asymmetric unit. Figure 3.3 displays the mononuclear complex (**3.2**). The antimony atom centre is coordinated by two terminal L^{Me} ligands, one adopting typical η^2 (N,N′) coordination through two nitrogen donors of the *p*-$HC_6F_4NC_2H_4NMe_2$ ligand, and the other showing monodentate L^{Me} coordination through one nitrogen donor. The antimony atom also coordinates one terminal chloride ligand, showing Sb-Cl bond length of 2.536(8) Å, giving the antimony atom a coordination number of four (Scheme 3.7). The geometry around the antimony centre can be best described as heavily distorted tetrahedral with a Sb–N distance ranged between 2.049(2) and 2.404(2) Å. As expected, when complex (**3.2**) was analysed by X-ray crystallography, no C-F interactions were observed, owing to coordination saturation by the L^{Me} ligand. Compound (**3.2**) was obtained in almost high (70 %) yield, giving a satisfactory elemental analysis and allowing characterisation (Table 3.1, 3.2 and 3.3).

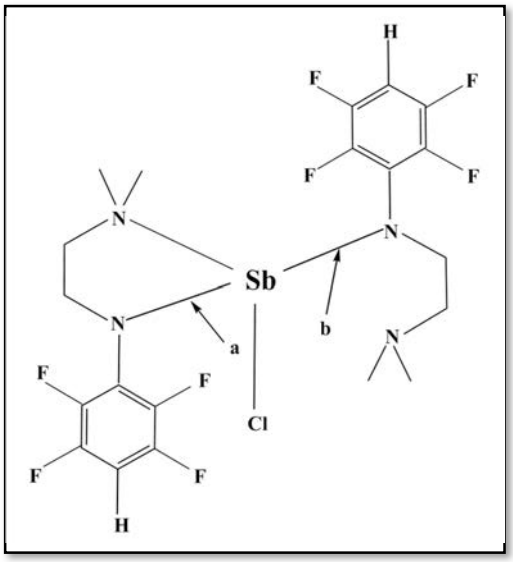

Scheme 3.7 Two coordination modes introduced in [Sb(L^{Me})$_2$Cl], **a**: the chelating mode and **b**: the terminal mode.

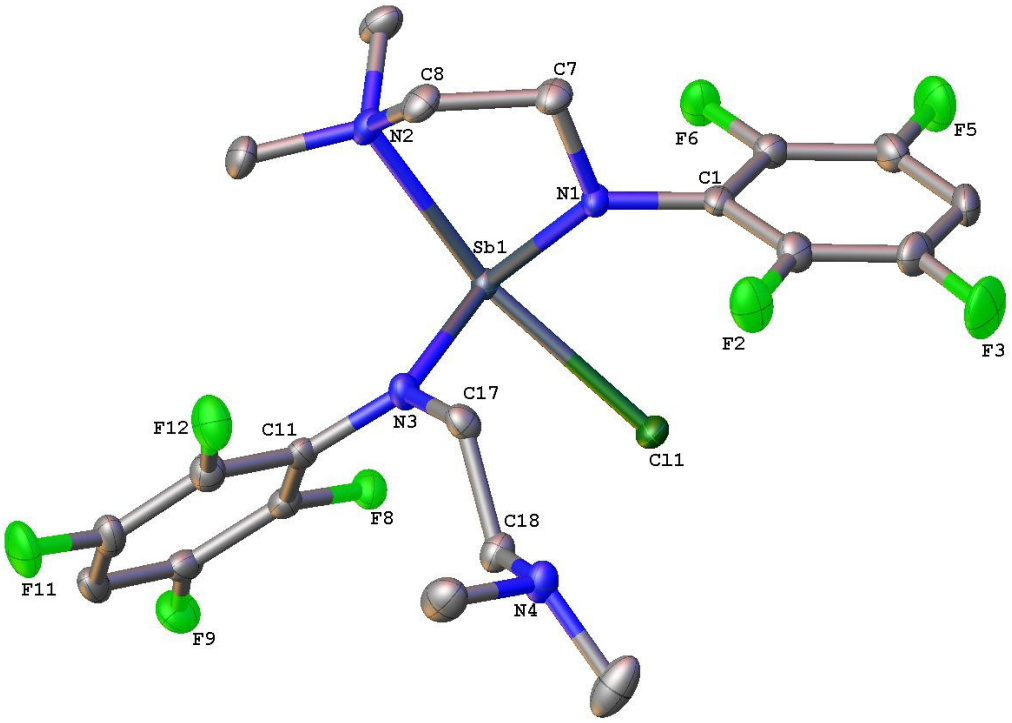

Figure 3.3. Molecular structure of monomeric **[Sb(*p*-$HC_6F_4NC_2H_4NMe_2)_2Cl$] (3.2)** with the atom numbering system; thermal ellipsoids are drawn at the 50 % probability level, and hydrogen atoms have been omitted for clarity. Selected bond lengths (Å) and angles (°): Sb(1)–N(1): 2.049(2), Sb(1)–N(2): 2.404(2), Sb(1)–N(3): 2.059(2), Sb(1)–Cl(1): 2.536(8), N(1)–C(1): 1.406(3), N(3)–C(11): 1.400(3), N(3)–Sb(1)–N(2): 86.29(8), N(1)–Sb(1)–N(2): 75.66(8), N(1)–Sb(1)–N(3): 96.25(8), N(1)–Sb(1)–Cl(1): 85.39(6), N(3)–Sb(1)–Cl(1): 90.74(6), N(2)–Sb(1)–Cl(1): 160.35(5), C(1)–N(1)–Sb(1): 120.42(15), C(7)–N(1)–Sb(1): 120.10(15), C(8)–N(2)–Sb(1): 104.01(14), C(10)–N(2)–Sb(1): 113.03(16), C(11)–N(3)–Sb(1): 120.27(16), C(17)–N(3)–Sb(1): 121.21(15).

[Sb(*p*-$HC_6F_4NC_2H_4NMe_2)_3$] (3.3)

The three coordinate homoleptic complex [$Sb(L^{Me})_3$] crystallised in the orthorhombic space group *Pna2₁* (Table 3.5), with one molecule in the asymmetric unit. The molecular structure of [$Sb(L^{Me})_3$] is shown in (Fig. 3.4).

In complex (**3.3**), three of the amido ligands are monodentate κ^1 (N,N′) with an uncoordinated –$(CH_2)_2NEt_2$ group (2.803, 5.477 and 5.492 Å) (the first value could be regarded as a weak interaction). This signifies an uncommon model of linkage, indicative of weaker coordination of the neutral crowded nitrogen atoms in [$Sb(L^{Me})_3$]. In addition, all tetrafluorophenyl groups are directed away from the metal centre due to the steric crowding. This novel fascinating linkage variation appears to be driven by steric factors. The X-ray crystal structure for (**3.3**) compound shows that in the solid state its geometry exists as mononuclear species with distorted trigonal pyramidal with three tetrafluorophenyl groups bound by N at the base of the pyramid, presumably a lone pair positioned at the apical site. Coordination of the three ligands results in less available coordination space for the three other amino N donors of the ligands (Scheme 3.8), unlike the same type of the ligand in [Eu(*p*-$HC_6F_4N(CH_2)_2NMe_2)_3$] ([$Eu(L^{Me})_3$]),[19] which has *tris*-bidentate binding due to Eu^{+3} being much larger than Sb^{+3}. The Sb (III) centre in (**3.3**) cannot induce C–F activation for the three L^{Me} ligands, probably because of the long distance between the Sb centre and F atoms, (Sb-F2 4.487, Sb-F6 3.164 Å), (Sb-F8 3.091, Sb-F12 4.612 Å), (Sb-F14 4.593, Sb-F18 2.969 Å).

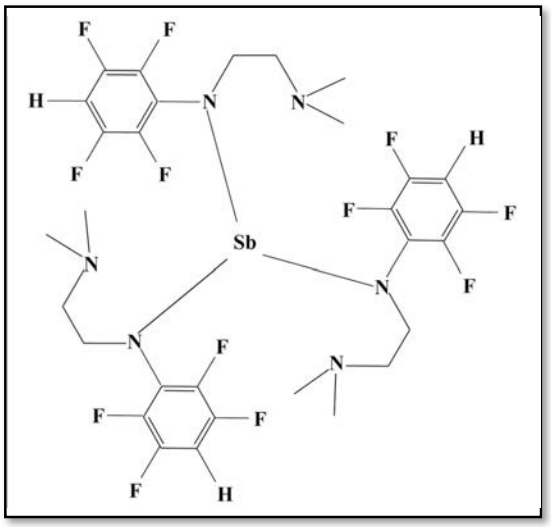

Scheme 3.8 The coordination mode in ($Sb(L^{Me})_3$) complex.

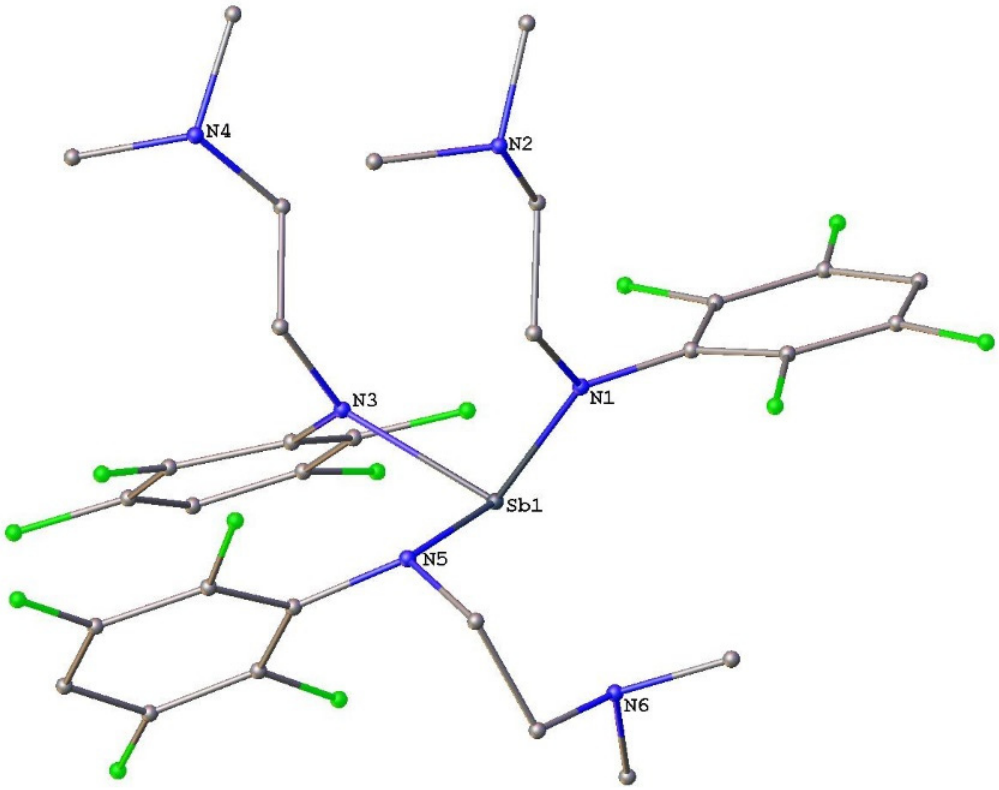

(***a***)

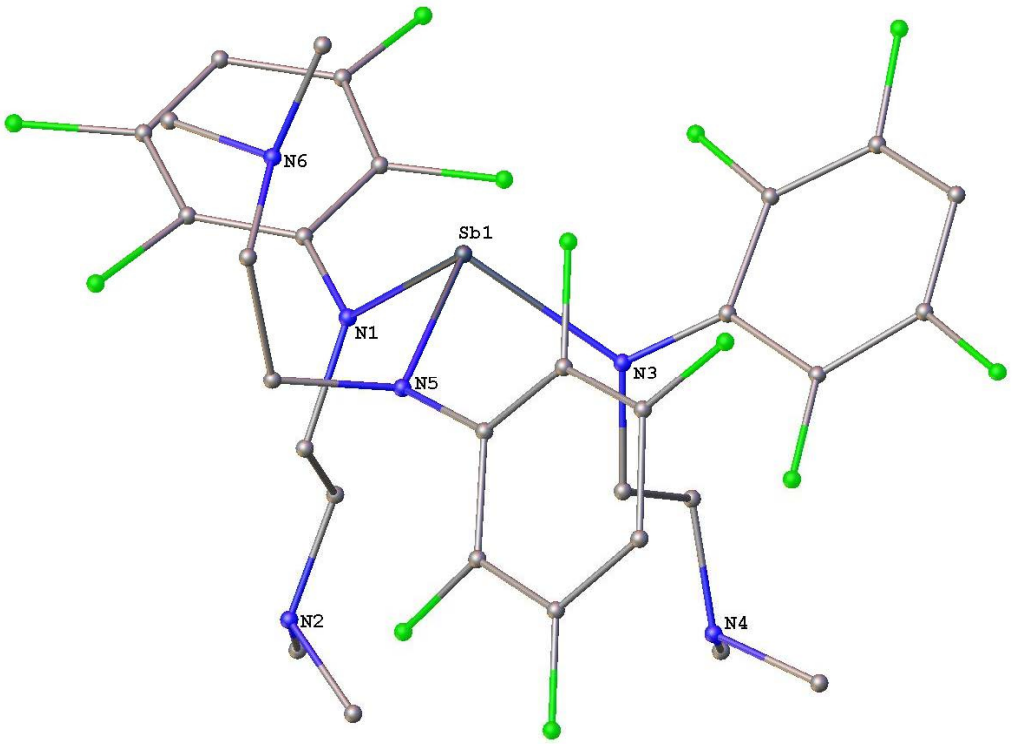

(***b***)

Figure 3.4. Molecular structure of monomeric **[Sb(*p*-$HC_6F_4NC_2H_4NMe_2)_3$] (3.3)** with the atom numbering system; thermal ellipsoids are drawn at the 50 % probability level, and hydrogen atoms have been omitted for clarity; (*a*) Viewed onto the N_3 plane; (*b*) Highlighting the pyramidal nature of the antimony coordination. Selected bond lengths (Å) and angles (°): Sb(1)–N(1): 2.045(12), Sb(1)–N(3): 2.121(16), Sb(1)–N(5): 2.025(15), N(1)–C(1): 1.39(3), N(3)–C(11): 1.34(3), N(5)–C(21): 1.44(3), N(1)–Sb(1)–N(3): 102.9(6), N(5)–Sb(1)–N(3): 86.9(7), N(5)–Sb(1)–N(1): 88.8(7), C(1)–N(1)–Sb(1): 119.0(12), C(7)–N(1)–Sb(1): 125.9(11), C(11)–N(3)–Sb(1) 115.8(13), C(17)–N(3)–Sb(1): 125.2(12), C(21)–N(5)–Sb(1): 117.5(12), C(27)–N(5)–Sb(1): 117.1(14).

The complexes (**3.1**, **3.2** and **3.3**) are notable for the presence of somewhat short Sb–N bond lengths, which are in agreement with the Sb–N bond lengths reported for [$SbLCl_2$] (L = C_4H_2N-2,5-$(CH_2NMe_2)_2$) (Table 3.4).[24] Particularly, Sb(1)–N(1) bond length values for all these complexes are only slightly shorter than the sum of covalent radii of the corresponding atoms ($\sum r_{cov}$ (Sb–N) = 2.11 Å).[23] The average Sb–Cl bond lengths of (**3.1** and **3.2**) found to be 2.48 Å, which is comparable to the average Sb–Cl bond lengths 2.58 Å, reported for [$Sb(C_4H_2N$-2,5-$(CH_2NMe_2)_2)Cl_2$].[24]

	[$Sb(L^{Me})Cl_2$]	**[$Sb(L^{Me})_2Cl$]**	**[$Sb(L^{Me})_3$]**	**[$Sb(C_4H_2N$-2,5-$(CH_2NMe_2)_2)Cl_2$]**
Sb(1)–N(1)	2.039(3)	2.049(2)	2.045(12)	2.033(3)
Sb(1)–N(3)	–	2.059(2)	2.121(16)	2.446(3)
Sb(1)–N(2)	2.372(4)	2.404(2)	2.025(15)	2.462(3)
Sb(1)–Cl(1)	2.405(11)/2.522(10)	2.536(8)	–	2.5573(10)/2.6181(10)

Table 3.4 Selected bond lengths (Å) for [$Sb(L^{Me})Cl_2$], [$Sb(L^{Me})_2Cl$], [$Sb(L^{Me})_3$] and [$Sb(C_4H_2N$-2,5-$(CH_2NMe_2)_2)Cl_2$].[24]

Table 3.5 Crystallographic data for compounds 3.1 - 3.3

Compound	**3.1**	**3.2**	**3.3**
formula	$C_{10}H_{11}Cl_2F_4N_2Sb$	$C_{20}H_{22}ClF_8N_4Sb$	$C_{30}H_{33}F_{12}N_6Sb$
fw	427.87	627.61	827.38
crystal system	orthorhombic	monoclinic	orthorhombic
space group	*Pna2₁*	*P2₁/c*	*Pna2₁*
a, Å	19.127(4)	11.441(2)	9.880(2)
b, Å	9.971(2)	8.8610(18)	39.689(8)
c, Å	7.3740(15)	23.614(5)	8.7610(18)
α, deg	90	90	90
β, deg	90	101.50(3)	90
γ, deg	90	90	90
V, Å^3	1406.3(5)	2345.9(9)	3435.4(12)
Z	4	4	4
T, K	100(2)	100.15	100(2)
no. of rflns collected	14398	28296	28927
no. of indep rflns	2265	4127	5783
R_{int}	0.0618	0.0385	0.0836
Final *R1* values ($I > 2\sigma(I)$)	0.0220	0.0236	0.0902
Final *wR*(F^2) values ($I > 2\sigma(I)$)	0.0521	0.0604	0.2233
Final *R1* values (all data)	0.0220	0.0259	0.0914
Final *wR*(F^2) values (all data)	0.0521	0.0616	0.2235
GooF (on F^2)	1.122	1.055	1.245

3.4 *Conclusion*

In summary, we examined the coordination preferences of the tetrafluorophenylethylenediaminate ligand, along with how preferred metal geometry affects the product outcome. This chapter describes two synthetic methods to Sb (III) polyfluorophenylaminoamidate complexes, namely metathesis or direct reactions. Complex [Sb(*p*-$HC_6F_4NC_2H_4NMe_2$)Cl_2] (**3.1**) was synthesised by direct reaction between N,N-dimethyl-N′-(2,3,5,6-tetrafluorophenyl)ethane-1,2-diaminate (HL^{Me}) (*p*–$HC_6F_4NHC_2H_4NMe_2$) and anhydrous $SbCl_3$ in THF, as well as by metathesis, while the heteroleptic chloride [Sb(*p*-$HC_6F_4NC_2H_4NMe_2)_2Cl$] (**3.2**) and the homoleptic [Sb(*p*-$HC_6F_4NC_2H_4NMe_2)_3$] (**3.3**) were synthesised by treatment of anhydrous $SbCl_3$ in PhMe with [Li(*p*-$HC_6F_4NC_2H_4NMe_2)]_2$ in hexane in 2:1 and 3:1 molar ratio respectively. The yields of the complexes obtained were somewhat similar between the two methods. Both of these synthetic approaches have benefits and shortcomings. The direct route bypasses the need for air-sensitive starting materials; however, monitoring the reaction through the use of ^{1}H- and ^{19}F{^{1}H}-NMR spectroscopy can be done with the metathesis route. Therefore, it can be considered that the synthesis of Sb (III) aminoamidate complexes is more convenient by the metathesis route than the direct route. Attempted production of [$SbL^{Et}_{3-n}Cl_n$] (n = 2, 1, 0) under the conditions studied failed. At this stage, this work is largely incomplete, however a wide range of complexes have been synthesised with both heteroleptic and homoleptic constituents. Such results indicate this area contains rich potential that warrants further investigations. Bidentate (N,N') coordination is predominantly detected with (L^{Me}). However, in the three-coordinate [Sb(L^{Me})$_3$] complex, the three ligands (L^{Me}) are monodentate with η N,N′-binding with a three free –$(CH_2)_2NMe_2$ groups. This novel linkage variation could be attributed to steric factors.

As further comparison, the difficulties associated with the synthesis of a tri-valent antimony L^{Me} complexes are discussed.

The antimony centres in (**3.1**) and (**3.2**) are four-coordinate forming heavily distorted tetrahedral geometry, whereas the stereochemistry of the three-coordinate component (**3.3**) can be described as trigonal pyramidal with three ligands bound at the base. No any evidence of subsequent fluorine bond mediated assembly (C–F activation reactions) shown either in the solid or in the solution state neither at low temperature nor on prolonged heating of the complexes in C_6D_6 at 80 °C, which can be attributed either to the redox unresponsiveness of the Sb (III) state or to the long distance between Sb and F atoms. Molecular structures of all Sb-amide monomeric constructions (**3.1**- **3.3**) were described both in the solid state analysis by mounted single crystals using X–ray crystallography diffraction, and in solution by ^{1}H- and $^{19}F\{^{1}H\}$-NMR spectra. In addition to IR spectroscopy, elemental analysis and melting point. These compounds are now well set for potential reduction to low valent species. Reaction with KC_8 should form isolable low valent Sb complexes and this work could be performed in future work.

3.5 *Experimental*

General Considerations/Air Sensitive Techniques

The lithium compound and antimony complexes described herein are extremely air and/or moisture sensitive, thus all manipulations, including syntheses, were performed under anaerobic and anhydrous conditions requiring use of both conventional standard Schlenk techniques interfaced to a high vacuum (10^{-2} Torr) line, and a glovebox under an inert atmosphere of dry nitrogen. All glassware comprising Schlenk-type flasks were dried at 120 ^{0}C for no less than 12 h before use, then used immediately from the oven to limit exposure to moisture.

Hexane and PhMe were dried and deoxygenated by an LC solvent purification system, whereas tetrahydrofuran was dried/purified and deoxygenated by refluxing over and freshly distilled from sodium wire/benzophenone *ketyl* under nitrogen. After distillation, solvents were stored in vacuum Schlenk flasks and degassed prior to use. The synthesis of the tetrafluorophenylamine ligand, HL^{Me} = N,N-dimethyl-N'-2,3,5,6-tetrafluorophenylethane-1,2-di-amine was according to a slight modification of the published procedure.[18] $Li(L^{Me})$, ($Li[p\text{-}HC_6F_4NC_2H_4NMe_2]$), was prepared in quantitative yield by treating *n*-BuLi with the corresponding polyfluorophenylamine. Anhydrous $SbCl_3$ and other starting materials such as *n*-butyllithium were commercially available from Aldrich and were freshly used as supplied without further purification. Pentafluorobenzene was stored over (4Å) molecular sieves, but was otherwise used as purchased from Aldrich Chemical Company.

All characterisation other than X-ray crystallography was on bulk, vacuum dried (at room temperature) product, either powder or crystals. Multinuclear ^{1}H- and $^{19}F\{^{1}H\}$-NMR spectra of air and moisture sensitive compounds were recorded using J.Young valve inert atmosphere NMR tubes protecting the sample from air on a Bruker AVANCE III HD 400 MHz spectrometer instrument. The chemical shifts are expressed in parts per million (ppm). ^{1}H-NMR resonances were referenced against residual H in C_6D_6 (δ = 7.15 ppm), while $^{19}F\{^{1}H\}$-NMR resonances were referenced against the known resonance of the N,N-dimethyl-N'-2,3,5,6-tetrafluorophenylethane-1,2-di-amine starting materials (δ = –142.3, –161.0 ppm).

Perdeutero-benzene (C_6D_6) (all ≥ 99 atom % D) as solvent for NMR spectroscopy was obtained from Sigma-Aldrich, and was degassed, pre-dried over sodium metal for 24 h and then distilled under an atmosphere of nitrogen before being stored in a resealable greaseless Schlenk flask prior to use.

Infrared spectra were recorded as Nujol mulls between NaCl plates using a Nicolet-Nexus FT-IR spectrophotometer within the range (ύ = 4000-400 cm^{-1}). Samples were sent in sealed glass pipettes under nitrogen for elemental analyses (C, H, N) to the Microanalytical Laboratory service, Science Centre, London Metropolitan University, England, and were performed on the single crystals isolated. Melting points were measured in sealed glass capillaries and are uncalibrated.

Synthesis of ligand (HL^{Me}) followed by deprotonation by *n*-BuLi in hexane

***p*-$HC_6F_4NHC_2H_4NMe_2$ (HL^{Me})**

This synthesis followed a slight modification of the published procedure.[18] Thus, pentafluorobenzene (33.6 g, 22.2 ml, 200 mmol) was added to N,N-dimethylethane-1,2-diamine (17.6 g, 21.85 ml, 200 mmol) and triethylamine (20 g, 27.8 ml, 198 mmol) in dry ethanol (10 ml) and then heated to reflux 70-80 ^{0}C under nitrogen with stirring for 12 h. Evaporating the solution under vacuum, gave an orange gel. The gel was treated with diethyl ether/water and was extracted four times with diethylether. The combined organic extracts were dried over anhydrous $MgSO_4$ and then evaporated under vacuum leaving a high boiling point liquid. Two distillations under vacuum, gave pure **HL^{Me}** (12.0 g, 68 %). B.P. 50 ^{0}C. ^{1}H-NMR (400 MHz, C_6D_6, 25 °C): δ (ppm) = 1.86 (s, 6H, Me_2N), 2.02 (m, 2H, C*H*$_2$NMe), 3.09 (m, 2H, C*H*$_2$NAr), 4.70 (br s, 1H, N*H*), 6.02 (m, 1H, *p*-*H*C_6F_4). ^{19}F{^{1}H}-NMR (376 MHz, C_6D_6, 25 °C): δ (ppm) = −141.78 (m, 2F, *F*3,5), −161.16 (m, 2F, *F*2,6). IR (υ/cm^{-1}, Nujol mull): 3355 (m), 3089 (w), 2979 (m), 2925 (s), 2893 (m), 2860 (m), 2808 (s), 2779 (s), 1655 (s), 1601 (w), 1528 (vs), 1510 (s), 1475 (s), 1459 (s), 1399 (m), 1374 (m), 1342 (m), 1329 (w), 1285 (m), 1260 (m), 1246 (s), 1180 (m), 1166 (vs), 1144 (vs), 1097 (m), 1073 (vs), 1055 (s), 1033 (s), 965 (vs), 921 (s), 875 (w), 785 (m), 719 (m), 662 (w).

[Li_2(*p*-$HC_6F_4NC_2H_4NMe_2$)$_2$] (Li-L^{Me})

To a Schlenk flask charged with a solution of *p*-$HC_6F_4NHC_2H_4NMe_2$ (1.42 g, 6.0 mmol) in hexane (10 ml), was added through a syringe *n*-BuLi solution in cyclohexane (2 M, 3.0 ml, 6.4 mmol) at - 60 ^{0}C under a flow of nitrogen with stirring for ½ h. After the addition, the cooling bath was removed, the reaction mixture was allowed to warm to ambient temperature and the solvent was reduced to *ca.* 5 ml under vacuum. A light yellow crystalline solid precipitated and the slurry was heated gently till the solid redissolved and was left standing overnight. The solution was decanted with a cannula, the residue washed with hexane (2×10 ml) and dried under vacuum for 1 h, and an off white powder (0.95 g, 65 %) was collected. M.P. 124 ^{0}C (decomp).
^{1}H-NMR (400 MHz, C_6D_6, 25 °C): δ (ppm) = 1.50 (s, 6H, Me_2N), 2.08-2.10 (m, 2H, C*H*$_2$NMe), 3.43-3.49 (m, 2H, C*H*$_2$NAr), 6.08-6.11 (m, 1H, *p*-*H*C_6F_4). ^{19}F{^{1}H}-NMR (376 MHz, C_6D_6, 25 °C): δ (ppm) = −143.71 (m, 2F, *F*3,5), −166.38 (m, 2F, *F*2,6). IR (υ/cm^{-1}, Nujol mull): 1635 (s), 1550 (s), 1457 (s), 1379 (m), 1340 (s), 1296 (s), 1242 (m), 1182 (w), 1179 (w), 1139 (m), 1066 (m), 1041 (w), 1005 (m), 914 (s), 859 (m), 779 (w), 750 (w), 731 (m), 710 (w), 689 (w).

Synthesis of trivalent antimony L^{Me} complexes in THF or PhMe/hexane

[Sb(*p*-$HC_6F_4NC_2H_4NMe_2$)Cl_2] (3.1)

a: A solution of HL^{Me} (1.42 g, 6.0 mmol) in THF (20 ml) was added with stirring using a cannula at ‑ 78 ^{0}C to a solution of $SbCl_3$ (1.32 g, 5.8 mmol) in THF (30 ml). An immediate colour change to yellow brown was observed indicating the formation of the desired product. Hydrogen chloride was bubbled through a stirred tetrahydrofuran solution of the reaction mixture indicated the progress of the reaction. Stirring was continued for few days at room temperature; volatiles were removed in vacuo. The yellow brown solution was concentrated to *ca*. 20 ml and set aside for 2 days at -15 ^{0}C, whereupon a bright yellow crystalline compound of unsolvated [Sb(*p*-$HC_6F_4NC_2H_4NMe_2$)Cl_2] (**3.1**) deposited. Crystals for the X-ray crystal structure were obtained by recrystallisation from hexane for further purification. Yield = 0.79 g (31%).

b: In an alternative approach, hexane solution of *n*-BuLi (1.6 M solution in hexanes, 4.0 ml, 6.0 mmol) was added to pre-cooled (-78 ^{0}C) solution of HL^{Me} (1.42 g, 6.0 mmol) in hexane (30 ml) and stirred for 1 h at r.t, generating effectively $[Li(L^{Me})]_2$ as yellow crystals in the solution. Gently heating the crystals and the resulting yellow solution was added to a pre-cooled solution (-78 ^{0}C) of $SbCl_3$ (1.32 g, 6.0 mmol) in PhMe (20 ml). The reaction mixture was stirred for 3 h at r.t. The remaining insoluble solid was required about 2-3 days to be entirely stabilised. Filtration and concentration under reduced pressure of the solution to *ca*.10 ml and storage for two days at − 30 °C afforded the titled compound [Sb(*p*-$HC_6F_4NC_2H_4NMe_2$)Cl_2] (**3.1**) as a bright yellow crystalline solid in good yield (35 %).

3.1: M.P. 186-192 ^{0}C (decomp). ^{1}H-NMR (400 MHz, C_6D_6, 25 °C): δ (ppm) = 1.63 (s, 6H, Me_2N), 2.05-2.14 (m, 2H, C*H*$_2$NMe), 3.09-3.19 (m, 2H, C*H*$_2$NAr), 6.24-6.28 (m, 1H, *p*-*H*C_6F_4); ^{19}F{^{1}H}-NMR (376 MHz, C_6D_6, 25 °C): δ (ppm) = −140.22 (m, 2F, *F*3,5), −147.19 (m, 2F, *F*2,6); Elemental analysis calcd. (%) for $C_{10}H_{11}Cl_2F_4N_2Sb$ (*M* = 427.87 g/mol): C 28.11, H 2.57, N 6.56; found: C 28.11, H 2.76, N 6.67. IR (υ/cm^{-1}, Nujol mull): 1651 (s), 1455 (s), 1376 (s), 1260 (s), 1095 (w), 1018 (m), 937 (s), 798 (s).

[Sb(*p*-$HC_6F_4NC_2H_4NMe_2$)$_2$Cl] (3.2)

A solution of $Li(L^{Me})$ prepared *in situ* from drop-wise addition of *n*-BuLi (2.0 M solution in cyclohexane, 3.0 ml, 6.0 mmol) to a solution of HL^{Me} (1.42 g, 6.0 mmol) in hexane (20 ml) at -78 ^{0}C without stirring. The reaction mixture was allowed to warm to ambient temperature and stirred for 3 h. The hexane solution was then slowly added over 10 minutes by cannula to a stirred suspension of $SbCl_3$ (0.66 g, 3.0 mmol) in PhMe (20 ml) at room temperature. The original yellow-brown reaction progressively turned orange-brown and was allowed to stir overnight. The precipitate was required about 2-3 days to be entirely stabilised. Filtration through a filter cannula and concentration under reduced pressure of the solution to *ca*.10 ml and storage at − 30 °C afforded the titled compound [Sb(*p*-$HC_6F_4NC_2H_4NMe_2$)$_2$Cl] (**3.2**) as brown-yellow crystals. Yield = 1.0 g (70 %).

3.2: M.P. 188-190 ^{0}C (decomp). ^{1}H-NMR (400 MHz, C_6D_6, 25 °C): δ (ppm) = 1.93 (s, 12H, Me_2N), 2.14-2.19 (m, 4H, C*H*$_2$NMe), 3.15-3.17 (m, 4H, C*H*$_2$NAr), 5.91-5.99 (m, 2H, *p*-*H*C_6F_4); ^{19}F{^{1}H}NMR (376 MHz, C_6D_6, 25 °C): δ (ppm) = −140.95 (m, 4F, *F*3,5), −147.28 (m, 4F, *F*2,6); Elemental analysis calcd. (%) for $C_{20}H_{22}ClF_8N_4Sb$ (*M* = 627.61 g/mol): C 38.27, H 3.53, N 8.92; found: C 38.37, H 3.44, N 9.13. IR (υ/cm^{-1}, Nujol mull): 1644 (s), 1610 (w), 1463 (m), 1377 (s), 1275 (s), 1262 (s), 1174 (m), 1081 (m), 1020 (s), 989 (s), 963 (m), 937 (s), 871 (s), 829 (s), 785 (s), 714 (s), 690 (s).

[Sb(*p*-$HC_6F_4NC_2H_4NMe_2)_3$] (3.3)

[Li(*p*-$HC_6F_4NC_2H_4NMe_2$)]$_2$ was synthesised *in situ* by the reaction of *p*-$HC_6F_4NHC_2H_4NMe_2$ (1.42 g, 6.0 mmol) with *n*-BuLi (1.6 M solution in hexanes, 4.0 ml, 6.0 mmol) in hexane (20 ml). Addition of the hexane solution drop-wise through a cannula to a well stirred solution of $SbCl_3$ (0.44 g, 2.0 mmol) in PhMe (10 ml) with cooling to − 78 ^{0}C using a dry ice/acetone bath. The reaction mixture was allowed to warm to ambient temperature and continued stirring for several days. The resultant yellow-brown solution was filtered from LiCl through a filter cannula and the volume was reduced to incipient crystallisation (10 ml). Last step requires highly caution, as the compound can be quickly decomposed on reduction to the point of crystallisation. Storage with slow cooling to − 30 ^{0}C for 48 h of this solution left a brown crystalline solid of [Sb(*p*-$HC_6F_4NC_2H_4NMe_2)_3$] (**3.3**) suitable for X-ray diffraction. Yield = 0.43 g (30 %).

3.3: M.P. 184-186 ^{0}C (decomp). ^{1}H-NMR (400 MHz, C_6D_6, 25 °C): δ (ppm) = 1.95 (s, 18H, Me_2N), 2.06-2.09 (m, 6H, C*H*$_2$NMe), 3.71-3.74 (m, 6H, C*H*$_2$NAr), 6.14-6.22 (m, 3H, *p*-*H*C_6F_4); ^{19}F{^{1}H}-NMR (376 MHz, C_6D_6, 25 °C): δ (ppm) = −140.11 (m, 6F, *F*3,5), −148.20 (m, 6F, *F*2,6). Elemental analysis calcd. (%) for $C_{30}H_{33}F_{12}N_6Sb$ (*M* = 827.38 g/mol): C 43.55, H 4.02, N 10.15; C,H,N couldn't be obtained, as it repeatedly gave poor data with extremely low C %, probably because of product contamination during analysis or transport to the analytical centre in London. IR (υ/cm^{-1}, Nujol mull): 1651 (w), 1600 (m), 1455 (w), 1310 (s), 1262 (w), 1200 (w), 1109 (m), 927 (m), 905 (s), 790 (m), 715 (m), 639 (m), 581 (s).

3.6 *Single crystal X-ray structure determination/analysis and Refinement model description*

Crystals were initially isolated as suitable single crystals and immersed in viscous hydrocarbon oil (Paratone-N) that was used on a glass fibre and mounted on the diffractometer under a stream of liquid nitrogen. X-ray crystallography was used to determine the solid-state structures of the crystalline samples, and was measured providing intensity data on either a Bruker APEX II CCD diffractometer for complex (**3.3**) at 100(2) K using graphite-monochromate MoKα radiation with a single wavelength (λ = 0.71073 Å), or at the Australian Synchrotron diffractometer using the MX1 macromolecular beam lines (**3.1** and **3.2**) at 100(2) K. Structure solutions were performed using SHELXS-97 and SHELXL- 97[25,26] program using Direct Methods via the graphical interface X-Seed[27] and OLEX 2[28] that also were used for generating figures. An absorption correction using MULTISCAN were applied. All CIF files were checked at www.iucr.org. Crystal data and refinement parameters are amassed below.

[Sb(*p*-$HC_6F_4NC_2H_4NMe_2$)Cl_2] (3.1)

1: $C_{10}H_{11}Cl_2F_4N_2Sb$ (M = 427.87 g/mol): orthorhombic, space group $Pna2_1$, a = 19.127(4) Å, b = 9.971(2) Å, c = 7.3740(15) Å, α = 90°, β = 90°, γ = 90°, Volume = 1406.3(5) Å^3, Z = 4, T = 100(2) K, $Dcalc$ = 2.021 g/cm^3, μ = 2.373 mm^{-1}, $F_{(000)}$ = 824.0, $2\Theta_{max}$ = 8.088 - 49.984°, 14398 reflections collected, 2265 unique (R_{int} = 0.0618, R_{sigma} = 0.0412), 2265/1/175 parameters, GooF on F^2 1.122, The final R_1 was 0.0220 (I >2σ (I)) and wR_2 was 0.0521 (all data), Largest diff. peak/hole/e = 0.42 to -0.39 Å^{-3}.

[Sb(*p*-$HC_6F_4NC_2H_4NMe_2$)$_2$Cl] (3.2)

2: $C_{20}H_{22}ClF_8N_4Sb$ (M = 627.61 g/mol): monoclinic, space group $P2_1/c$, a = 11.441(2) Å, b = 8.8610(18) Å, c = 23.614(5) Å, α = 90°, β = 101.50(3)°, γ = 90°, Volume = 2345.9(9) Å^3, Z = 4, T = 100(2) K, $Dcalc$ = 1.777 g/cm^3, μ = 1.370 mm^{-1}, $F_{(000)}$ = 1240.0, $2\Theta_{max}$ = 3.632 - 49.984°, 28296 reflections collected, 4127 unique (R_{int} = 0.0385, R_{sigma} = 0.0209), 4127/0/312 parameters, GooF on F^2 1.055, The final R_1 was 0.0236 (I >2σ (I)) and wR_2 was 0.0617 (all data), Largest diff. peak/hole / e = 0.68 to -0.45 Å^{-3}.

[Sb(*p*-$HC_6F_4NC_2H_4NMe_2)_3$] (3.3)

3: $C_{30}H_{33}F_{12}N_6Sb$ (M = 827.38 g/mol): orthorhombic, space group $Pna2_1$, a = 9.880(2) Å, b = 39.689(8) Å, c = 8.7610(18) Å, α = 90°, β = 90°, γ = 90°, Volume = 3435.4(12) $Å^3$, Z = 4, T = 100(2) K, $Dcalc$ = 1.600 g/cm^3, μ = 0.899 mm^{-1}, $F_{(000)}$ = 1656.0, $2\Theta_{max}$ = 4.122 - 49.998°, 28927 reflections collected, 5783 unique (R_{int} = 0.0836, R_{sigma} = 0.0512), 5783/111/450 parameters, GooF on F^2 1.245, The final R_1 was 0.0902 (I >2σ (I)) and wR_2 was 0.2235 (all data), Largest diff. peak/hole / e = 1.96 to -1.16 $Å^{-3}$.

3.7 *References*

1. D. P. Buxton, G. B. Deacon, A. M. James, S. J. Knowles and T. L. Williams, *Polyhedron.*, 1989, **8**, 2943-2945.
2. S. Wyllie and A. H. Fairlamb, *Biochem. Pharmacol.*, 2006, **71**, 257-267.
3. H. Memmler, K. Walsh, L. H. Gade and J. W. Lauher, *Inorg. Chem.*, 1995, **34**, 4062-4068.
4. M. D. Fryzuk and C. D. Montgomery, *Coord. Chem. Rev.*, 1989, **95**, 1-40.
5. R. L. Cowan and W. C. Trogler, *J. Am. Chem. Soc.*, 1989, **111**, 4750-4761.
6. A. R. Battle, A. M. Bond, A. Chow, D. P. Daniels, G. B. Deacon, T. W. Hambley, P. C. Junk, D. N. Mason and J. Wang, *J. Fluorine Chem.*, 2010, **131**, 1229-1236.
7. L. K. Webster, G. B. Deacon, D. P. Buxton, B. L. Hillcoat, A. M. James, I. A. G. Roos, R. J. Thomson, L. P. G. Wakelin and T. L. Williams, *J. Med. Chem.*, 1992, **35**, 3349-3353.
8. T. Talarico, D. R. Phillips, G. B. Deacon, S. Rainone and L. K. Webster, *Investigational New Drugs.*, 1999, **17**, 1-15.
9. E. J. Cho, T. D. Senecal, T. Kinzel, Y. Zhang, D. A. Watson and S. L. Buchwald, *Science.*, 2010, **328**, 1679-1681.
10. H. Plenio, *Chem. Rev.*, 1997, **97**, 3363-3384.
11. J. D. Crowley and E. L. Gavey, *Dalton Trans.*, 2010, **39**, 4035-4037.
12. H. Takemura, S. Nakashima, N. Kon, M. Yasutake, T. Shinmyozu and T. Inazu, *J. Am. Chem. Soc.*, 2001, **123**, 9293-9298.
13. D. O'Hagan, *Chem. Soc. Rev.*, 2008, **37**, 308-319.
14. K. Müller, C. Faeh and F. Diederich, *Science.*, 2007, **317**, 1881-1886.
15. K. P. Shine and W. T. Sturges, *Science.*, 2007, **315**, 1804-1805.
16. G. B. Deacon, C. M. Forsyth, P. C. Junk and J. Wang, *Chem. Eur. J.*, 2009, **15**, 3082-3092.
17. G. B. Deacon, B. M. Gatehouse and J. Ireland, *Aust. J. Chem.*, 1991, **44**, 1669-1681.
18. D. P. Buxton, G. B. Deacon, B. M. Gatehouse, I. L. Grayson and D. S. Black, *Aust. J. Chem.*, 1988, **41**, 943-956.

19. G. B. Deacon, P. C. Junk, R. P. Kelly and J. Wang, *Dalton trans.*, 2016, **45**, 1422-1435.
20. G. B. Deacon, C. M. Forsyth, P. C. Junk, R. P. Kelly, A. Urbatsch and J. Wang, *Dalton Trans.*, 2012, **41**, 8624-8634.
21. D. P. Buxton and G. B. Deacon, *Polyhedron.*, 1991, **10**, 747-751.
22. L. A. Lesikar, A. F. Gushwa and A. F. Richards, *J. Organomet. Chem.*, 2008, **693**, 3245-3255.
23. P. Pyykkö and M. Atsumi, *Chem. Eur. J.*, 2009, **15**, 12770-12779.
24. I. Vranova, R. Jambor, A. Ruzicka, A. Hoffmann, S. Herres-Pawlis and L. Dostal, *Dalton Trans.*, 2015, **44**, 395-400.
25. G. M. Sheldrick, *Acta Crystallogr., Sect. C: Struct. Chem.*, 2015, **71**, 3-8.
26. G. M. Sheldrick, *SHELXS-97 and SHELXL-97*, 1997.
27. L. J. Barbour, *J. Supramol. Chem.*, 2001, **1**, 189-191.
28. O. V. Dolomanov, L. J. Bourhis, R. J. Gildea, J. A. K. Howard and H. Puschmann, *J. Appl. Crystallogr.*, 2009, **42**, 339-341.

CHAPTER FOUR

SYNTHESES AND STRUCTURAL CHARACTERISATION OF HETEROLEPTIC ALUMINIUM (III) FORMAMIDINATES AND BIMETALLIC ANTIMONY/ALUMINIUM (III) COMPOUNDS

Outline

This chapter describes the synthetic method used to examine different reactions between aluminium (III) halides AlX_3 (X = Cl, Br, I) and deprotonated formamidinate ligands (XylForm) and (DippForm), to increase the range of the haloorgano(formamidinato) aluminium (III) system. In addition, a chlorine/methyl exchange reaction was used for forming bimetallic Al/Sb (III) ionic complexes. The majority of the aluminium (III)-containing compounds have been successfully obtained as monomeric structures in the solid state. The structural nature of the synthesised complexes and reactions pathway are elucidated along with their spectroscopic characterisation.

4.1 *Introduction*

Monodentate nitrogen- or oxygen-based species have been the most common ligands utilised in aluminium chemistry. Extensive attention has been increasing around the coordination chemistry of the four-electron donor, monoanionic ancillary amidinate ligands $[RNC(R')NR]^-$, as it is stated earlier in chapter two of this thesis. This class of ligand features readily substitutable groups associated to the nitrogen atoms and backbone carbon centres, modifying the coordination environment at the metal center.[1,2] Sterically demanding substituents on the carbon and nitrogen atoms thrust the lone pairs of electrons on the nitrogen atoms to the metal centre to form the chelating bonding mode rather the bridging bonding mode. Generally, non-bulky hydrogen and methyl groups attached to the carbon centre tend to form the chelating bonding mode, although in some cases form the bridging or monodentate bonding modes (Figure 4.1).[3] Thus, a range of transition-, lanthanide- and main group-metal amidinate complexes have been synthesised.[4,5]

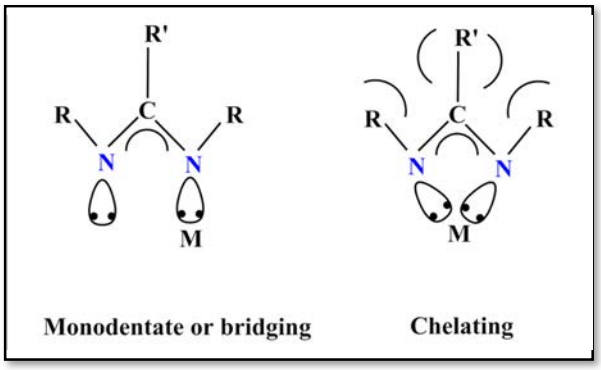

Figure 4.1. Steric effects of ligand substituents.

Over recent years, Group 13 amidinate complexes of metal alkyl and halide fragments haven't been exceptions,[6,7] along with their applications as efficient homogeneous catalysts in olefin polymerisation reactions,[8,9,1,10] and chemical vapour deposition (CVD) precursors.[11] Aluminium amidinate complexes have also served as lone source precursors to materials containing the nitride ion.[12] Considering the emerging importance of amidinato aluminium alkyl and halide complexes to a number of areas, deprotonation of the formamidine by different metal alkyl/amide such as (*n*-BuLi, $LiN(SiMe_3)_2$, $NaN(SiMe_3)_2$, $KN(SiMe_3)_2$) followed by combination with aluminium compounds have been convenient methods to synthesise a variety of hetero aluminium complexes displaying novel structural features.

A recent study was performed on Group 13 metals, Al and Ga, by treatment of formamidines [Form (ArNCHNAr) = EtForm (Ar = 2,6-$Et_2C_6H_3$) or DippForm (Ar = 2,6-$iPr_2C_6H_3$)] with $AlCl_3$ in a 1:3 reaction stoichiometry that led to obtain dialuminium formamidinate complexes [$Me_2Al(\mu$-Form)(μ-Me)$AlMe_2$] in good yields, while protolysis reactions of MMe_3 (M = Al, Ga) with (FormH) in a 1:1 stoichiometry resulted in [M(Form)Me_2] (M = Al, Form = DippForm, EtForm; M = Ga, Form = DippForm) in high yields.[13] Concentration of the thf/*n*-hexane solution of [$Me_2Al(\mu$-DippForm)(μ-Me)$AlMe_2$] to dryness yielded [Al(DippForm)Me_2], which is can also be achieved from reaction of $AlMe_3$ with [Ga(DippForm)Me_2].[13]

In an attempt to investigate the effect of ligand steric bulk on metal-complex formation, nitrogen-bound alkyl groups of varying steric bulk (isopropyl and cyclohexyl) have been treated with phenyllithium yielding lithium amidinates. The latter, when treated with $AlCl(THF)_n$ formed three aluminium (III) amidinate complexes: $[Al\{PhC[N(iPr)]_2\}_3]$, $[Al\{PhC[N(iPr)]_2\}_2Cl]$ and $[Al[PhC(NCy)_2]_2Cl.0.675THF]$.[14] More recently, complexes of the general formula $[Al(Form)_2X]$, [Form = XylForm, EtForm, DippForm] (X = Me, Cl), were produced from the reactions of N,N'-bis(aryl)formamidines/ates with half an equivalent of $AlMe_3/AlCl_3$.[15]

Abeysekera, *et al.* described the synthesis of dialkylaluminium *m*-terphenyl-substituted amidinate complexes, which are robust in the crystalline state and can be simply handled in air for short periods of time without observable decomposition. The syntheses were an aqueous workup reaction of 2,4,6-triphenylphenylbromide, *n*-butyllithium and dialkylcarbodiimides (RN=C=NR, R = cyclohexyl or isopropyl), followed by reaction with an excess of trimethylaluminium in hexane and stirring overnight (Scheme 4.1).[3]

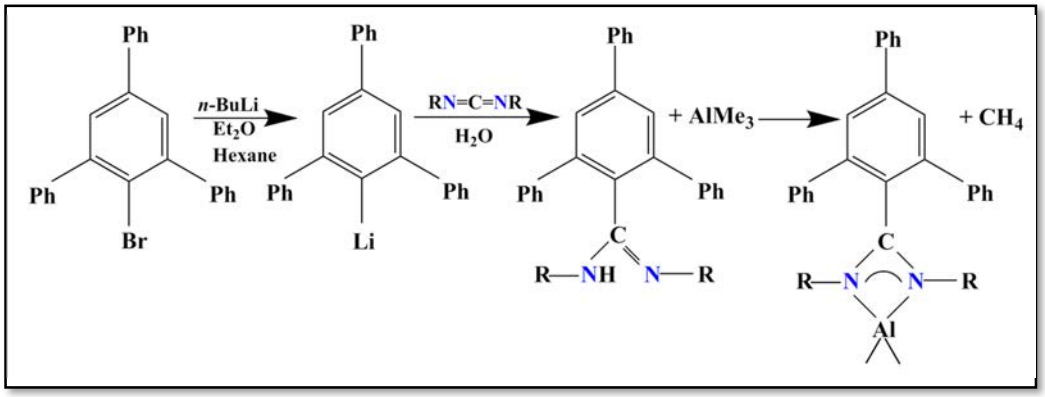

Scheme 4.1 Synthesis of dialkylaluminium *m*-terphenyl-substituted amidinate complexes.

The reaction of the bulky benzamidine N,N'-*bis*(2,6-diisopropylphenyl)-4-toluamidine (HDippAm) with $AlMe_3$ in a 1:1 molar ratio in Et_2O yielded the mononuclear aluminium benzamidinate compound $[Al(DippAm)Me_2]$. This compound displays remarkable thermal and aerobic stability, and was also achieved by salt elimination between dimethylaluminium chloride and $[Li(DippAm)(THF)_2]$.[6] Also, reaction of $[PhC(NSiMe_3)_2]Li(OEt_2)$ with $AlC1_3$ in PhMe afforded the *bis*(N,N'-*bis*(trimethylsilyl)benzamidinato) aluminium chloro compound $[A1\{PhC(NSiMe_3)_2\}_2Cl]$. The latter, when treated with $KBEt_3H$ at room temperature yielded monomeric hydrido derivative $[\{PhC(NSiMe_3)_2\}_2AlH]$.[16]

Treatment of an N-arylanilido-imine ligand $[o\text{-}C_6H_4(NHAr)CH{=}N]_2CH_2CH_2$ (Ar = 2,6-$Me_2C_6H_3$) with $AlMe_3$ in a 1:1 molar ratio affords a monometallic complex $[C_6H_4(NHAr)–CH{=}N)]CH_2CH_2(C_6H_4(NAr)CH{=}NAlMe_2)$. Reaction of this compound with one equivalent of $ZnEt_2$ gave a heterobimetallic complex $[C_6H_4(NAr)–CH{=}NZnEt]CH_2CH_2[C_6H_4(NAr)–CH{=}NAlMe_2]$ (Scheme 4.2). The Al/Zn example reflects the possibility of forming a heterobimetallic complex with an ethylene bridged N-arylanilido-imine ligand. This type of complex is an effective catalyst for ring-opening polymerisation of μ-caprolactone in the presence of benzyl alcohol to produce polymers with narrow polydispersity standards.[17]

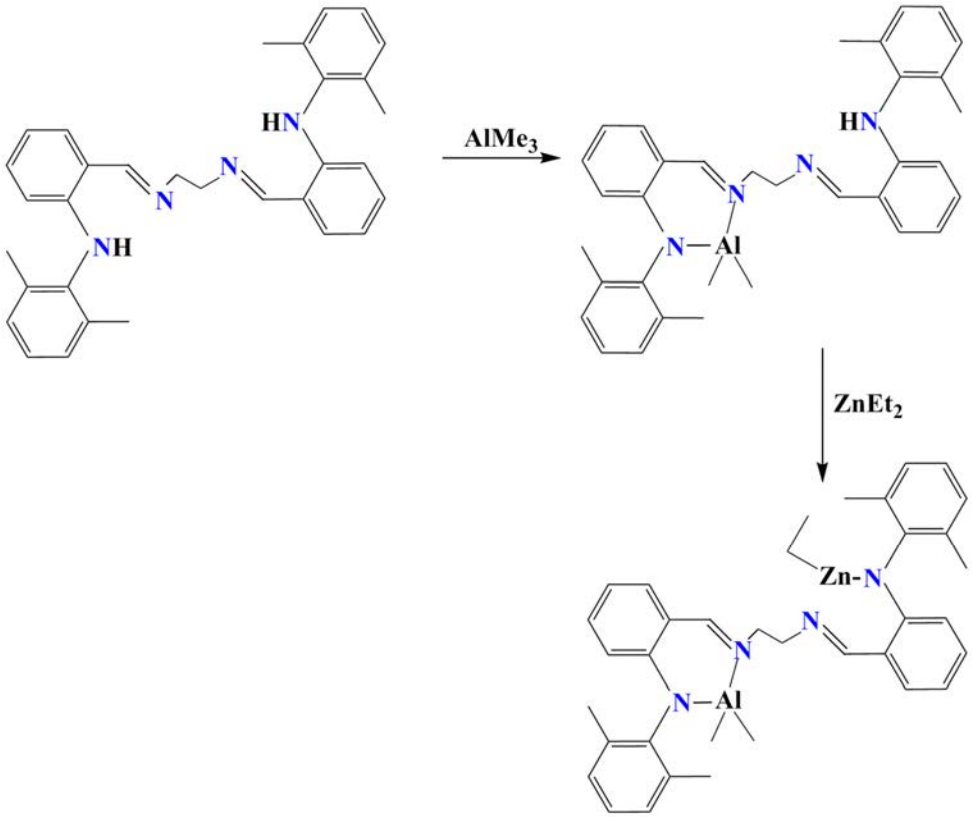

Scheme 4.2 Reaction of ethylene bridged N-arylanilido-imine with $AlMe_3$ and $ZnEt_2$.

Hamidi, *et al.* reported that the structurally interesting bimetallic monomeric six-coordinate formamidinate complexes [Ln(Form)($AlMe_4$)$_2$] (Ln = Y, Form = EtForm (2,6-$Et_2C_6H_3$), MesForm (2,4,6-$Me_3C_6H_2$), DippForm (2,6-*i*$Pr_2C_6H_3$), *t*BuForm (2-*t*BuC_6H_4); Ln = La, Form = DippForm, *t*BuForm) were achieved in high yield by protonolysis reactions between formamidines and Ln($AlMe_4$)$_3$,[18] which could work as pre-catalysts in olefin polymerisation. Also [Y(Form)($AlMe_4$)$_2$] (Form = EtForm, DippForm) were synthesised by treatment of Y(Form)[N($SiHMe_2$)$_2$]$_2$(thf) with $AlMe_3$.

4.2 *The current study*

This chapter describes the synthesis and structural characterisation of eight heteroleptic aluminium (III) formamidinate complexes (Scheme 4.3). Two types of formamidinate ligands were selected, N,N′-bis(2,6-dimethylphenyl) formamidinate (XylForm) and N,N′-*bis*(2,6-diisopropylphenyl)formamidinate (DippForm) as subclasses of amidinate ligands, to study a variation of the possible coordination modes of the formamidinate functional group and compare the synthesised complexes with those reported in the literature. Metathesis reactions were carried out in a donor solvent THF and/or PhMe. Moreover, all complexes were crystallised from THF or PhMe/hexane and their structures have been identified by X-ray crystallography (except for **4.10**), ^{1}H–, ^{13}C–NMR, IR spectroscopy, elemental analyses and melting point.

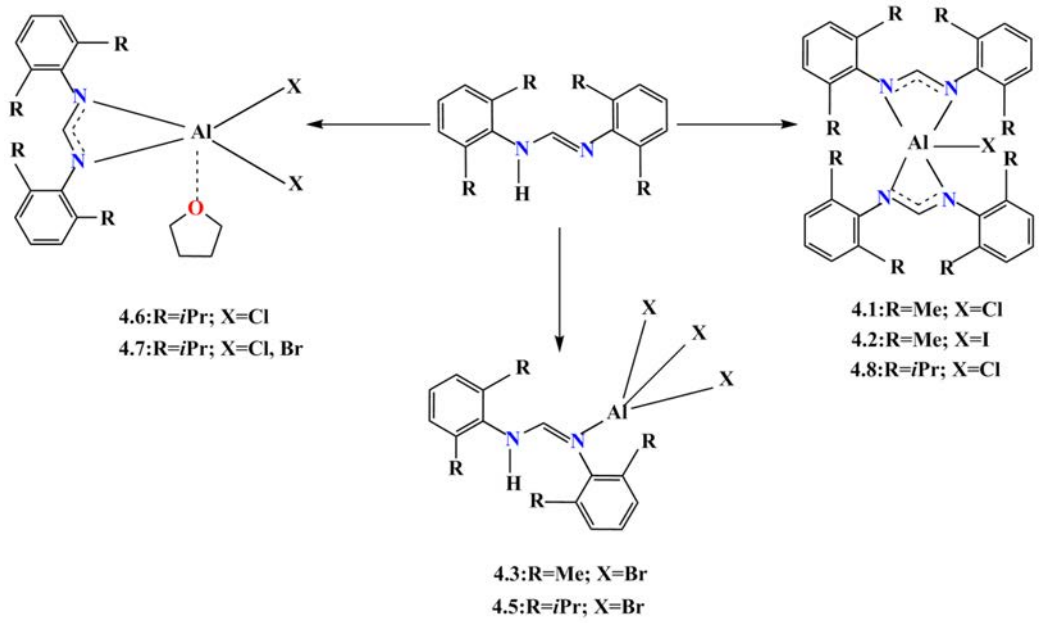

Scheme 4.3. Overall synthetic routes to formamidinato aluminium (III) complexes.

Also included is a *tri*-aluminium formamidinate complex that features both bridging form ligands and a bridging oxygen ion, $[Al_3(XylForm)_2(\mu_3\text{-}O)(OH)Cl_4]_2$.PhMe (**4.4**).

Structural elucidation shows monomeric complexes with a coordinated thf molecule on the Al atom in (**4.6**) and (**4.7**), whereas for (**4.3**) and (**4.5**) species have the formamidine binding in a monodentate mode to the $AlBr_3$ through the lone pair on the non-protonated N-atome. Attempts to achieve homoleptic complexes of the type *tris*-(N,N′-bis(2,6-dimethylphenyl)formamidinato) aluminium (III) [Al(XylForm)$_3$] or *tris*-(N,N′-bis(2,6-diisopropylphenyl)formamidinato) aluminium (III) [Al(DippForm)$_3$] were unsuccessful. Different coordination modes possibly occur, but the two most common ones have been shown in (Figure 4.2).

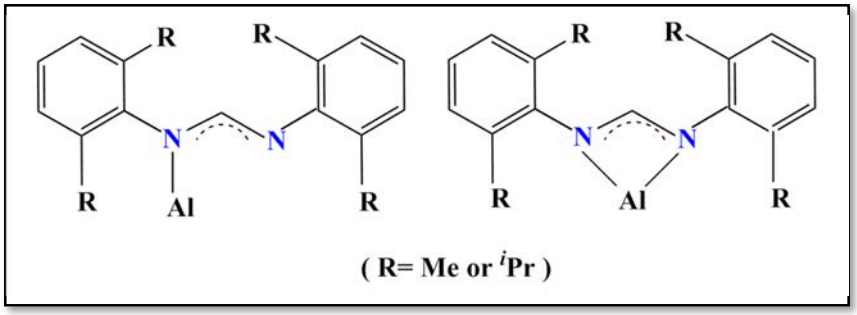

Figure 4.2. Two common coordination modes for substituted formamidinates with aluminium (III).

The proposed goal of forming bimetallic antimony/aluminium (III) complexes by treatment of $AlMe_3$ with $SbCl_3$ in the presence of PhMe gave the tetrachloroaluminate salt bearing a stibinostibonium cation in the form of [Me_3Sb-$SbMe_2$][$AlCl_4$] (**4.9**). The reaction was chlorine/methyl exchange and the complex represents a new route to stibinostibonium cations. A dichloroaluminium salt bearing an anion of [$(Br_4Sb)SbBr_3$]$^-$ in [Br_3Sb-μBr-$SbBr_3$][$AlCl_2(thf)_4$] (**4.10**) was isolated from the reaction of $SbBr_3$ with $AlCl_3$ in THF/PhMe at ambient temperature. The solid state structures for these complexes are described, in which the Sb and Al in (**4.9**) and (**4.10**) performed in relatively rare coordination modes.

GLOSSARY OF COMPOUNDS AND CODES

The following structures are a summary of the notable complexes discussed throughout this chapter, together with respective codes. These structures show aluminium atoms in different colours representing the colours of the compounds observed in the solid state.

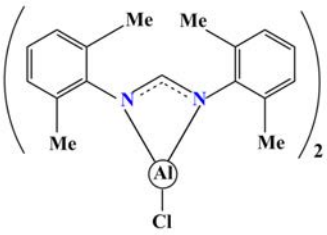

[Al(XylForm)$_2$Cl (4.1)

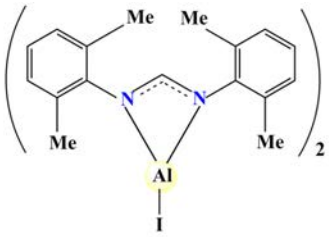

[Al(XylForm)$_2$I].PhMe (4.2)

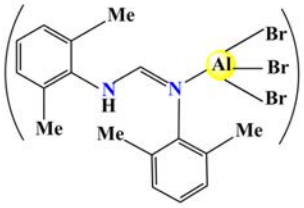

[Al(XylFormH)Br$_3$] (4.3)

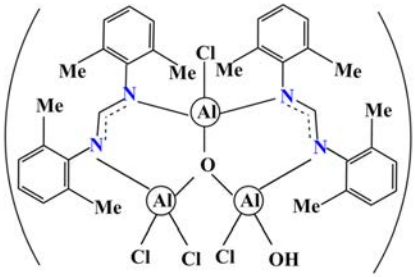

[Al$_3$(XylForm)$_2$(μ_3-O)(OH)Cl$_4$]$_2$.PhMe (4.4)

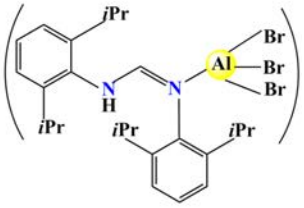

[Al(DippFormH)Br$_3$] (4.5)

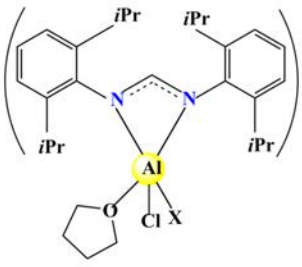

[Al(DippForm)ClX(thf)] (X=Cl (4.6), Br (4.7))

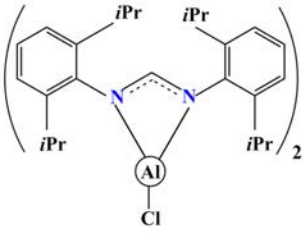

[Al(DippForm)$_2$Cl] (4.8)

4.3 *Results and discussion*

4.3.1 Synthesis by metathesis reactions in THF/PhMe

Following the same method described earlier in chapter two of this thesis to synthesise antimony formamidinato complexes, we turned to another Lewis acid (aluminium compounds) to prepare their formamidinate analogues. Scheme 4.4 and 4.5 show the metathesis reactions used in this study incorporating the two formamidine pro-ligands XylFormH and DippFormH. Syntheses of related complexes with other ligands, have been described previously and can have diverse structural geometry, allowing for comparisons in this work. Initially, to a stirred solution of N,N′-bis(aryl)formamidine in THF or PhMe, ML was added dropwise (M = Li, Na, K; L = *n*-Bu, $N(SiMe_3)_2$) at 0 °C. This was followed by addition of this solution dropwise to a stirred solution of AlX_3 (X = Cl, Br, I) in THF or PhMe at room temperature until an insignificant colour change was observed in the solution (after 10 minutes), indicating the formation of new haloformamidinatoaluminium species. For example, reaction of AlX_3 (X = Cl, I) with two equivalents of a substituted deprotonated N,N-bis(aryl)formamidinate ligand were investigated under varying conditions, and resulted in *bis*-substituted $[Al(Form)_2X]$ complexes: $[Al(XylForm)_2Cl]$ (**4.1**), $[Al(XylForm)_2I]$.PhMe (**4.2**), $[Al(DippForm)_2Cl]$ (**4.8**) (Scheme 4.4 and 4.5). Reaction of $NaN(SiMe_3)_2$ with the formamidine ligands in PhMe, then addition of the reaction mixture to a solution of $AlBr_3$ in PhMe at room temperature in a 1:1 molar ratio produced bromoformamidine aluminium (III) complexes $[Al(FormH)Br_3]$: [FormH = XylFormH (**4.3**), DippFormH (**4.5**)] (Scheme 4.4 and 4.5). $[Al_3(XylForm)_2(\mu_3\text{-}O)(OH)Cl_4]_2$.PhMe (**4.4**) was isolated as unexpected product from attempt to synthesise [Al(XylForm)Cl_2(thf)].PhMe (Scheme 4.4) by reaction of K(XylForm) with $AlCl_3$ in THF/PhMe at room temperature in a 1:1 molar ratio.

Treatment of AlX_3 (X = Cl and/or Br) in the presence of a lithium formamidinate species in a 1:1 molar ratio reactions gave thf solvated haloformamidinate aluminium (III) complexes [Al(DippForm)X_2(thf)]: [X = Cl (**4.6**), Cl and Br (**4.7**)] (Scheme 4.5). In several instances, despite the use of a 3:1 ratio of the formamidinates to AlX_3, only *mono*- and *bis*-substituted complexes were obtained, which reflects the steric bulk of the ligands by the inability for these ligands to bind to the small Al^{+3}.

The *in situ* reaction of $AlMe_3$ with $SbCl_3$ at − 78 ^{0}C in presence of PhMe resulted in low yield colourless crystals of an ionic complex [Me_3Sb-SbMe_2][$AlCl_4$] (**4.9**). In spite of several attempts and different reaction conditions, we were unable to obtain adequate crystals of (**4.9**) from this particular reaction.

Following the route described by Hamidi, *et al.* to synthesise bimetallic complexes but with slight modification,[18] we worked up with antimony and aluminium (eqn. 4.1) to synthesise their analogues, but all attempts to isolate any components involving formamidinato ligands of antimony/aluminium were unsuccessful. Competition between the two Lewis acidic Al^{3+} and Sb^{3+} for N-donor ligands have been attempted. Because of the strong Lewis acid Al^{3+} has a high affinity towards nitrogen donor ligands,[19,20,21] Al^{3+} reflected its highest acidity compared with antimony species, and the results were aluminium (III) N,N′-bis(2,6-dimethyl(or isopropyl)phenyl)formamidinate forms. Surprisingly, no isolated byproduct of formamidinato antimony species such as [Sb(Form)X_2] was noticed from the examined reaction between Al, Sb and formamidine. However, deliberately synthesis of a variety of aluminium formamidinate complexes have been carried out in this study, thereby confirming isolation of pure products. These structures are relatively similar to the previously designated organoaluminium formamidinates.[15]

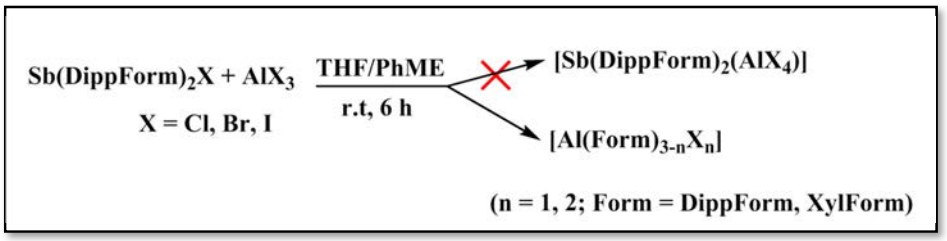

Equation 4.1

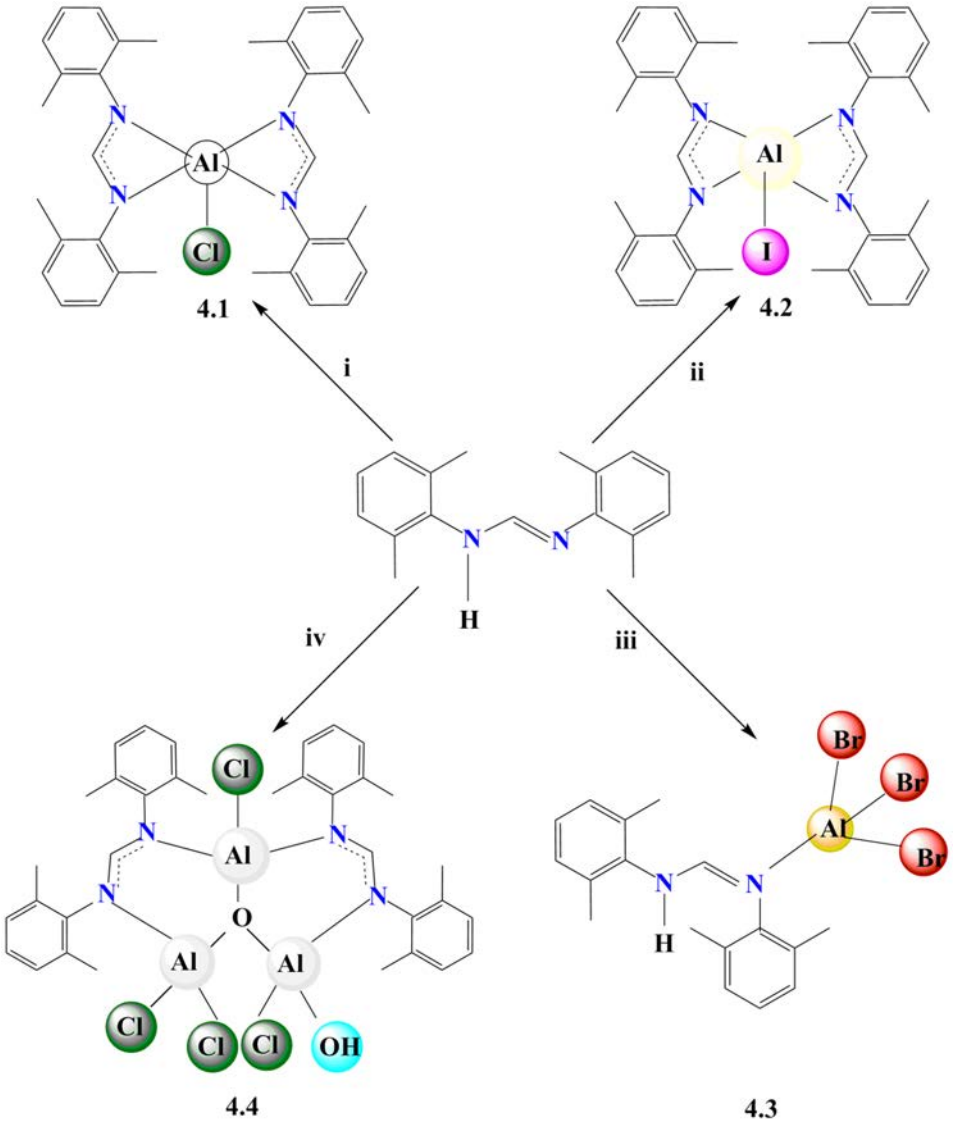

Scheme 4.4. Reagents and Conditions: (i) $AlCl_3$, $LiN(SiMe_3)_2$, r.t, PhMe. (ii) AlI_3, $KN(SiMe_3)_2$, r.t, PhMe. Note: compound (**4.2**) crystallised as a monomer with one PhMe molecule in the crystallographic asymmetric unit. (iii) $AlBr_3$, $NaN(SiMe_3)_2$, r.t, PhMe. (iv) $AlCl_3$, $KN(SiMe_3)_2$, r.t, THF/PhMe.

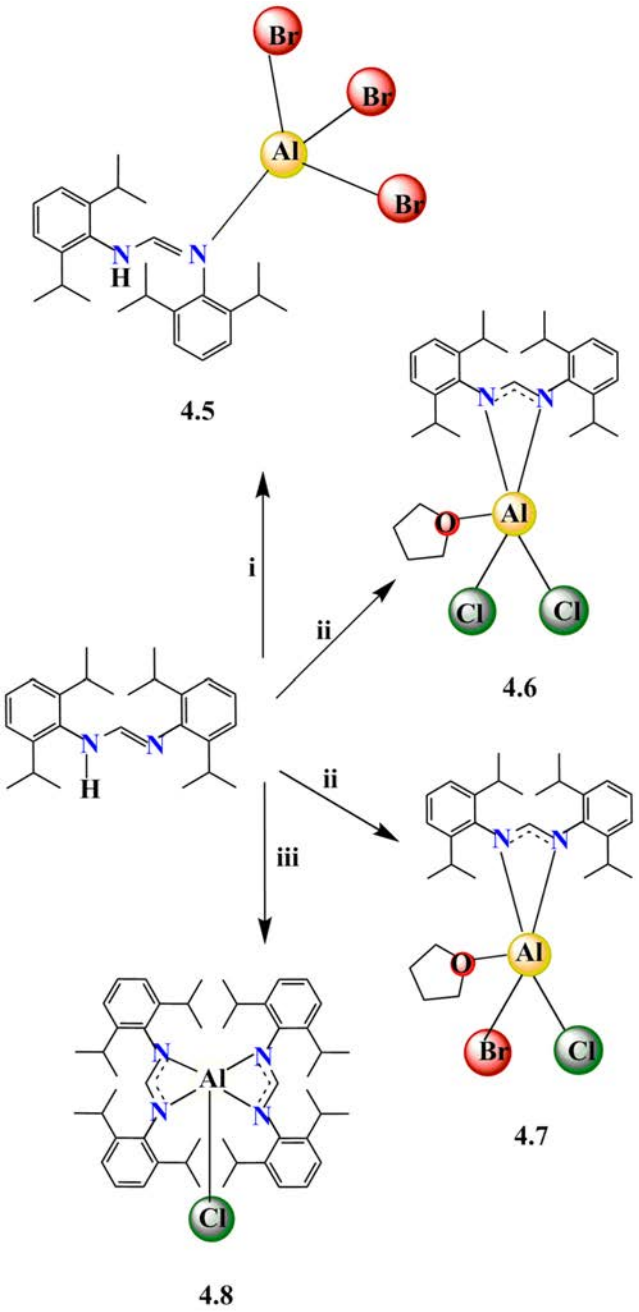

Scheme 4.5. Reagents and Conditions: (i) $AlBr_3$, $NaN(SiMe_3)_2$, r.t, PhMe. (ii) $AlCl_3$ (**4.6**), $AlCl_3$ + $AlBr_3$ (**4.7**), *n*-BuLi, r.t, THF/PhMe. (iii) $AlCl_3$, $LiN(SiMe_3)_2$, r.t, THF/PhMe.

4.3.2 Characterisation

All the aluminium (III) complexes, incorporating XylFormH and DippFormH ligands displayed in Scheme 4.4 and 4.5, were initially isolated as single crystals, and were structurally characterised on the basis of X-ray crystallography using the MX1 beamline at the Australian Synchrotron, and their molecular structures are depicted in (Figures 4.3 – 4.13). Additional characterisations were supported by IR spectroscopic techniques (Table 4.1), ^{1}H- and ^{13}C-NMR spectroscopy (Table 4.2 and 4.3 respectively), and elemental analyses (with the exception of for **4.9** which was obtained only in very poor yield), as well as melting point analysis.

Single crystals for compounds (**4.2**) and (**4.4**) were achieved from solution in PhMe with one uncoordinated PhMe molecule in the asymmetric unit. In contrast, the aluminium centres in (**4.6**) and (**4.7**) are weakly coordinated by a thf molecule, while (**4.1**, **4.3**, **4.5** and **4.8)** were achieved from solution in PhMe as solvent free complexes after storage overnight at – 30 ^{0}C. The formamidinate moieties in (**4.1**, **4.2**, **4.6**, **4.7** and **4.8)** serve as chelating κ^2(N,N') four-electron donor ligands, and the monodentate mode in (**4.3** and **4.5**) is established. A feature of compounds (**4.1** – **4.8**) is that the assemblage of the monomer is favoured rather than a dimer in the solid state, presumably due to the large steric bulk of the ligands inhibiting aggregation. Crystal data, data collection parameters and structure refinement details are summarised in (Tables 4.5, 4.6 and 4.8) and also in the Experimental Section.

Suitable crystals of the stibinostibonium salt of (**4.9**) $C_5H_{15}AlCl_4Sb_2$ were obtained in very low yield (< 8 %), and unequivocally proven by X-ray structure determination. However, the data from the other spectroscopy, ^{1}H-NMR and IR, couldn't be sufficient to allow a detailed discussion and no C, H, N analytical data could be obtained. Crystallisation of this type of complexes, particularly those containing sterically less demanding substituents such as the Me group, is relatively difficult since they normally have low melting points and are very sensitive toward oxygen.[22] Crystals of (**4.9**) are slightly soluble in nonpolar organic solvents. They are colourless, unlike other Sb-Sb bonded compounds, which are normally yellow or red distibines or cyclostibines.

Unfortunately, efforts to accurately refine the anionic $[Br_3Sb\text{-}\mu Br\text{-}SbBr_3]^-$ in (**4.10**) failed, since good quality crystals for X-ray analysis couldn't be obtained. Therefore, X-ray diffraction data for this compound were of lower quality and has only been included as confirmation of connectivity.

Infrared spectroscopic data of (**4.1** – **4.8**) (except $[Al(XylFormH)Br_3]$ (**4.3**) and $[Al(DippFormH)Br_3]$ (**4.5**) as they have formamidine ligands rather than formamidinate ligands) are devoid of an N–H stretch signal usually observed at 3300-3100 cm^{-1}, which is indicative of comprehensive deprotonation of the parent formamidines and complexation with aluminium through the Al-N bond. IR spectra for all the formamidinate complexes showed that the N-H stretch at *ca*. 3300 cm^{-1} reappeared after the formamidinate complexes were exposed to air for two minutes. The N–C stretching for compounds (**4.1** – **4.8**) displayed the characteristic absorption for an aluminium coordinated formamidinate group distinguished at 1637-1651 cm^{-1} (Table 4.1). These results showed successful synthesis of the haloformamidinato aluminium (III) complexes. Crystalline compounds (**4.3** and **4.5**) exhibits a sharp stretch in the IR spectrum at 3322 cm^{-1}, confirming presence of the parent formamidine.[23] An OH stretch for (**4.4**) was confirmed in the infrared spectrum at 3712 cm^{-1}, which is slightly different to that recorded in related complexes.[24,25]

The ^{1}H-NMR spectra studies of the bulk vacuum dried materials show the lack of the signal attributed to the N-H resonance, and distinct resonances consistent with formamidinate ligands, which differs from the parent formamidines. More specifically, the ^{1}H- and ^{13}C-NMR spectra of the complexes pointed out to the expected resonances due to the existence of the organic substituents 2,6 diisopropyl, 2,6 dimethyl and the NC*H*N environment of the formamidinate moiety, which occur almost in the same range as was detected for the corresponding haloformamidinato stibines in the previous chapter of this study. The existence of protonated formamidine in (**4.3**) and (**4.5**) presumably results from inappropriate deprotonation of the formamidine ligands forming Lewis Base/Acid adduct rather than the expected $[Al(Form)Br_2]$ (Form = XylForm, DippForm) complexes.

^{1}H-NMR spectra of (**4.3** and **4.5**) displayed the resonances due to the organic substituents 2,6 dimethyl and 2,6 diisopropyl of the formamidine moiety. However, they show two sets of methyl resonances (C*H*$_3$) at 1.59 and 2.29 ppm in (**4.3**), while for (**4.5**) two sets of methyl resonances CH(C*H*$_3$)$_2$ were found at 1.14 and 1.51 ppm, and two sets of C*H*(CH$_3$)$_2$ at 2.62 and 3.31 ppm, were present all of them in a 1:1 ratio. Also, the presence of the hydrogen atom on N2 represented by a slightly broad doublet peak of N–*H* resonance at δ = 5.69 ppm (**4.3**) and 6.06 ppm (**4.5**) (with *J* value = 12 Hz) for both of the complexes that couple to doublet of NC*H*N at δ = 7.78 ppm (**4.3**) and 8.01 ppm (**4.5**) (with *J* value = 16 Hz) for both of the complexes, which are slightly different from the chemical shifts of 8.98 and 8.67 ppm reported for [Al{MeC(ND*i*pp)$_2$H}I$_3$] and [Ga{HC(ND*i*pp)$_2$H}Cl$_3$] examples, respectively.[26] These data are inclusion proof of a protonated XylFormH/DippFormH and aluminium-XylFormH/aluminium-DippFormH coordination environment in (**4.3** and **4.5**).

The ^{1}H-NMR spectrum of (**4.4**) exhibits three sets of methyl resonances in a 1:2:1 ratio and a well-defined formamidinate NCHN resonance at δ = 7.29 ppm. The terminal hydroxyl group is identified by ^{1}H-NMR with signal at 0.41 ppm that is in the normal range of other reported Al–OH signals.[24,25] Taking into account the relatively good yield of formamidinate complex (**4.4**), (65 %), we assumed that the presence of oxygen arises from ring-opining of the THF molecule, or more probably moisture introduced from accidental exposure to moisture. This highlight to the extreme sensitivity of these compounds to moisture. Such sensitivity caused even difficulties in handling.

Frustration to achieve acceptable C, H, N microanalytical data for complex (**4.4**) could be resulted from the occurrence of oxygen (O^{2-} and OH^{-}) arising from adventitious H_2O. It is worth mentioning that many aluminium compounds used in this chapter react violently towards the air and moisture,[27,28,29,30,31,18] thus attempts to achieve satisfactory carbon, hydrogen and nitrogen microanalytical data for some complexes (**4.1**, **4.2, 4.5** and **4.10**) (except **4.9** obtained in low yield < 8 %), were unsuccessful. However, the other products (**4.3**, **4.6**, **4.7** and **4.8**) were isolated as pure crystalline species. Yields ranged from low such as (**4.7**) (0.14 g, 40 %) to moderate such as (**4.8**) (0.51 g, 70 %).

Table 4.1 N–C Stretching in IR spectra for aluminium formamidinate complexes 4.1 - 4.8 (υ 4000 - 400 cm^{-1})

Compound		N–C stretching vibration (cm^{-1})
$[Al(XylForm)_2Cl]$	(**4.1**)	1651
$[Al(XylForm)_2I].PhMe$	(**4.2**)	1644
$[Al(XylFormH)Br_3]$	(**4.3**)	1642
$[Al_3(XylForm)_2(\mu_3\text{-}O)(OH)Cl_4]_2.PhMe$	(**4.4**)	1637
$[Al(DippFormH)Br_3]$	(**4.5**)	1646
$[Al(DippForm)Cl_2(thf)]$	(**4.6**)	1639
$[Al(DippForm)ClBr(thf)]$	(**4.7**)	1640
$[Al(DippForm)_2Cl]$	(**4.8**)	1641

Table 4.2 ^{1}H-NMR chemical shift data in ppm for aluminium formamidinate complexes 4.1 - 4.8 in C_6D_6

^{1}H-NMR	4.1	4.2	4.3	4.4	4.5	4.6	4.7	4.8
NC*H*N	7.36	7.97	7.78	7.29	8.01	7.50	7.53	7.85
Aromatic *H*	6.91-7.10	6.75-6.88	6.68-6.90	6.76-7.04	7.02-7.09	6.99-7.10	7.01-7.11	6.98-7.10
C*H*$(CH_3)_2$	–	–	–	–	3.31	3.77	3.80	3.51
O*H*	–	–	–	0.41	–	–	–	–
N*H*	–	–	5.69	–	6.06	–	–	–
OCH_2, thf	–	–	–	–	–	3.56	3.54	–
CH_2, thf	–	–	–	–	–	1.03	1.02	–
Ar*H*, PhMe	–	7.18	–	7.25	–	–	–	–
CH_3, PhMe	–	2.16	–	2.24	–	–	–	–
CH_3/CH(CH_3)$_2$	2.34	2.32	2.29	2.47	1.51	1.25	1.26	1.48

Table 4.3 ^{13}C-NMR chemical shift data in ppm for aluminium formamidinate complexes 4.1 - 4.8 in C_6D_6

^{13}C-NMR	4.1	4.2	4.3	4.4	4.5	4.6	4.7	4.8
N*C*N	173.0	159.3	159.9	152.4	160.11	151.44	151.01	160.4
Aromatic *C*	125.2-143.2	127.8-141.5	127.8-148.2	126.8-142.8	124.4-144.6	123.4-144.4	123.7-144.6	124.5-144.8
*C*H(CH$_3$)$_2$	–	–	–	–	28.77	28.05	28.26	28.66
O*C*H$_2$, thf	–	–	–	–	–	70.46	70.27	–
*C*H$_2$, thf	–	–	–	–	–	24.12	24.58	–
Ar*C*, PhMe	–	134.5	–	131.20	–	–	–	–
*C*H$_3$, PhMe	–	20.16	–	21.43	–	–	–	–
*C*H$_3$/CH(*C*H$_3$)$_2$	19.64	18.41	19.19	19.93	23.74	24.55	24.89	23.66

4.3.3 Crystal structure determinations

[Al(XylForm)$_2$X] (X = Cl (4.1) and I (4.2).PhMe)

The trivalent aluminum complexes **[**Al(XylForm)$_2$X] (X = Cl (**4.1**) and I (**4.2**).PhMe) were synthesised (Scheme 4.4). The monomeric complex (**4.1**) crystallised in the monoclinic space group *P2$_1$/c*, while complex (**4.2**) crystallised in the triclinic space group *P-1* (Table 4.5), with one molecule within the asymmetric unit. The coordination environment for the Al atom in (**4.2**), except the existence of additional PhMe solvent molecule, is similar to that observed in trivalent (**4.1**), where the iodide replaces the chloride ligand. The structural parameters observed for (**4.2**) were very similar to that of (**4.1**), although crystallising in different space groups. The Al^{+3} metal centre in both complexes is five-coordinate, bound by two deprotonated κ^2(N,N') XylForm ligands through the nitrogen donor atoms, and one terminal halide ligand (Cl (**4.1**) and I (**4.2**). X-ray crystallographic analysis for the two complexes (**4.1** and **4.2**) showed that the coordination geometries about Al^{+3} are distorted from trigonal bipyramid and square pyramid due to the very narrow bite of the formamidinate ligand (Figures 4.3 and 4.4).

As expected, compound (**4.1**) exhibits Al–N bond lengths 1.919(4) Å shorter comparing with those in the axial positions 2.033(4) Å. These distances are similar to 1.925(12) and 2.096(12) Å detected for N_{eq}–Al, N_{ax}–Al, respectively, in the related complexes [Al{MeC(N*i*Pr)$_2$}$_2$Me],[32] 1.914(2) and 2.041(2) Å [Al{MeC(N*i*Pr)$_2$}$_2$Cl],[33] 1.9324(12) and 2.1005(13) Å [Al(XylForm)$_2$Me],[15] in addition to 1.928(3) and 2.093(3) Å reported in [Al{HC(ND*i*pp)$_2$}$_2$Me].[34] The bond angles in (**4.1**): N(3)–Al(1)–Cl(1) 103.21(14), N(1)–Al(1)–Cl(1) 102.24(13) and N(3)–Al(1)–N(1) 154.54(19) ° confirm the formation of distorted square pyramid rather distorted trigonal bipyramid geometry.

Likewise the related aluminium structures [{MeC(N*i*Pr)$_2$}$_2$AlCl],[33] [{MeC(N*i*Pr)$_2$}$_2$AlMe],[32] [{PhC(NSiMe$_3$)$_2$}$_2$AlH],[16] and [{HC(ND*i*pp)$_2$}$_2$AlH],[35] the N(1)–Al(1)–N(4) bond angle of 100.65(17) °in (**4.1**), displays a high distortion from the expected 180 ° that may due to the rather acute bite angles of 67.52(16) ° and 67.27(16) ° for N(1)–Al(1)–N(2) and N(3)–Al(1)–N(4), respectively. Same observation was found in (**4.2**). It is worthy to mention that although there are size and electronic differences between CH, CPh and CMe of the C backbone, the structural differences between (**4.1**) and [Al{PhC(N(*i*Pr))$_2$}$_2$Cl], [Al{MeC(N(*i*Pr))$_2$}$_2$Cl] are insignificant, with bond lengths that mostly agree within 0.02 Å.

The C–N bond lengths of NCN in (**4.1**) suggest delocalisation of the anionic charge across the backbone (N1/N2–C9: 1.313(6) and 1.336(6) Å, N3/N4–C26: 1.310(6) and 1.333(6) Å; DippFormH: 1.311(17) and 1.310(16) Å).[1,5] In addition, the NCN angle of 112.1(4) ° and Al–N bond lengths of Al1–N1/N2: 2.033(4) and 1.919(4), Al1–N3/N4: 2.040(4) and 1.925(4) Å, (Figure 4.3), are reasonably typical for bulky formamidinate coordinated to aluminium (analogous angles and bond lengths for [Al(DippForm)$_2$Me]; NCN 111.7(3)/113.1(3) °, Al1–N1/N2: 1.928(3) and 2.093(3), Al1–N3/N4: 1.923(3) and 2.113(3) Å).[34] Same findings can be seen with structure (**4.2**) (Figure 4.4). In comparison between bond lengths of N-C(N) with N-C(C$_6$H$_3$-2,6-Me$_2$) in complex (**4.1**), the N-C(N) bond lengths are in the range of 1.310 (6) – 1.336 (6) Å and the N-C(C$_6$H$_3$-2,6-Me$_2$) bond lengths are in the range 1.414 (6) – 1.425 (6) Å (Scheme 4.6).

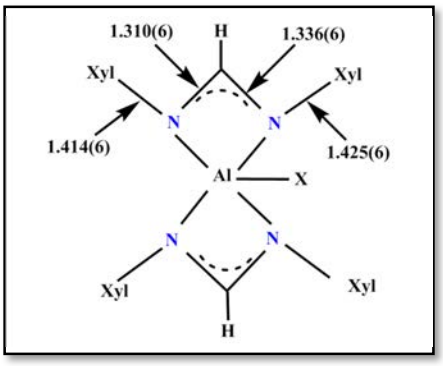

Scheme 4.6. Comparison between N-C(N) and N-C(C$_6$H$_3$-2,6-Me$_2$) distances in (**4.1**).

The Al–Cl bond length of (**4.1**) found to be 2.119 (2) Å which is slightly shorter than the Al–Cl bond length (2.141 (15) Å) reported for [Al(EtForm)$_2$Cl][15] and significantly shorter than the Al–Cl bond lengths (2.16 – 2.20 Å) for those of the seven reported [Al(Form)$_2$Cl] complexes (Form = chelating amidinate), noting an increase in bulk (2,6-dimethylphenyl vs. 2,6-diethylphenyl) and at the N-substituents (2,6-dimethylphenyl vs. N-isopropyl or N-cyclohexyl).[11,36,37,14] While, Al–Cl bond length in (**4.1**) is in close agreement with those reported in the heteroleptic aluminium amidinate [Al{MeC(N(*i*Pr))$_2$}Cl$_2$] (2.1057(10) and 2.1078(11) Å).[38]

In (**4.2**), the Al–I bond length of 2.5456 (9) Å is in the normal range;[4, 33,36,26] however, the Al–I connection is slightly longer than those of [Al(Priso)I$_2$] (2.50, 2.51 Å)[39] and [Al(CGiso)I$_2$] (2.50 Å),[15] even though two sites of the Al centre are occupied by the bulky formamidinate ligands (2 vs. 1). The bond lengths and angles in (**4.2**) are relatively similar to those in [Al(CGiso)I$_2$] [Cgiso = N,N′-bis(2,6-disopropylphenyl)-N′′-dicyclohexylguanidinate].[15] In general, the bond lengths in (**4.2**) are within 0.02 Å of those reported in [Al(Priso)I$_2$],[39] and the angles in (**4.2**) are similarly close. The N–C(N) bond lengths are 1.311 (3) – 1.343 (3) and 1.304 (3) – 1.341 (3) Å, with the N–C(C$_6$H$_3$-2,6-Me$_2$) bond lengths are 1.418 (3), 1.434 (3), 1.414 (3) and 1.436 (3) Å respectively.

	4.1	**4.2**	**[Al{HC(NDipp)$_2$}$_2$Me]**	**[Al{Me$_2$NC(NiPr)$_2$}$_2$Cl]**
Al-N1	2.033(4)	1.925(2)	1.928(3)	1.927(1)
Al-N2	1.919(4)	2.031(19)	2.093(3)	1.979(1)
Al-N3	2.040(4)	1.924(2)	1.923(3)	1.993(1)
Al-N4	1.925(4)	2.038(19)	2.113(3)	1.929(1)

Table 4.4 Selected Al-N bond lengths (Å) for complexes: [Al(XylForm)$_2$Cl] (**4.1**), [Al(XylForm)$_2$I] (**4.2**) and [Al{HC(NDipp)$_2$}$_2$Me][34] and [Al{Me2NC(NiPr)2}2Cl].[39]

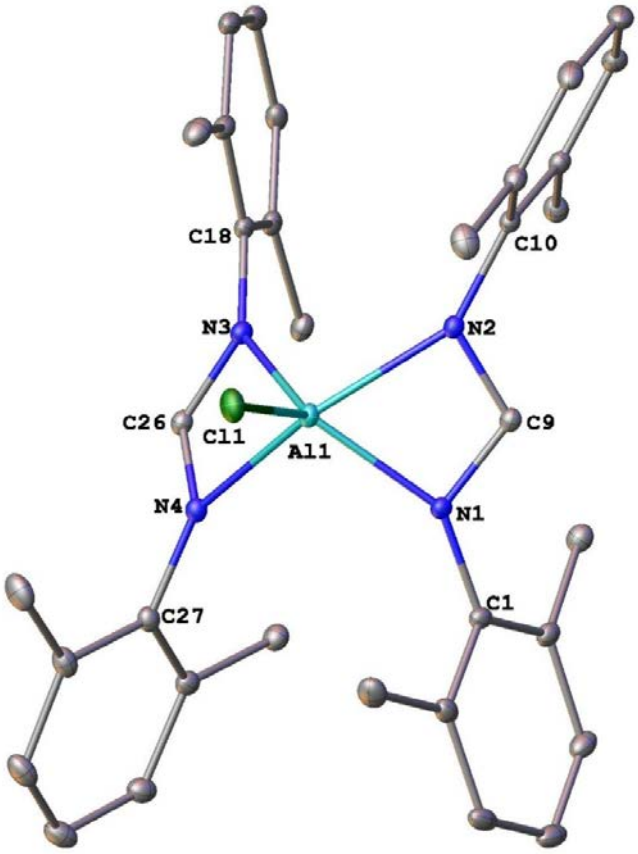

Figure 4.3. Molecular structure of monomeric **[Al(XylForm)$_2$Cl] (4.1)** with the atom numbering system; thermal ellipsoids are drawn at the 50 % probability level, hydrogen atoms have been omitted for clarity. Selected bond lengths (Å) and angles (°): Al(1)–N(1): 2.033(4), Al(1)–N(2): 1.919(4), Al(1)–N(3): 2.040(4), Al(1)–N(4): 1.925(4), Al(1)–Cl(1): 2.119(2), N(2)–C(10): 1.414(6), N(2)–C(9): 1.336(6), N(1)–C(1): 1.425(6), N(1)–C(9): 1.313(6), N(3)–C(18): 1.422(6), N(3)–C(26): 1.310(6), N(4)–C(27): 1.425(6), N(4)–C(26): 1.333(6), N(2)–Al(1)–N(1): 67.52(16), N(4)–Al(1)–N(3): 67.27(16), N(2)–Al(1)–N(3): 99.04(17), N(4)–Al(1)–N(1): 100.65(17), N(4)–Al(1)–N(2): 122.07(19), N(1)–Al(1)–N(3): 154.54(19), N(2)–Al(1)–Cl(1): 118.86(15), N(4)–Al(1)–Cl(1): 119.07(15), Cl(1)–Al(1)–N(1): 102.24(13), Cl(1)–Al(1)–N(3): 103.21(14), N(1)–C(9)–N(2): 112.1(4), N(3)–C(26)–N(4): 112.6(4), C(10)–N(2)–Al(1): 143.9(3), C(1)–N(1)–Al(1): 149.9(3), C(18)–N(3)–Al(1): 148.6(3), C(27)–N(4)–Al(1): 143.3(3), C(9)–N(2)–Al(1): 92.3(3), C(9)–N(1)–Al(1): 88.0(3), C(26)–N(3)–Al(1): 87.9(3), C(26)–N(4)–Al(1): 92.2(3), C(1)–N(1)–C(9): 123.30(10), C(9)–N(2)–C(10): 121.87(10), C(18)–N(3)–C(26): 123.91(11), C(26)–N(4)–C(27): 122.76(11).

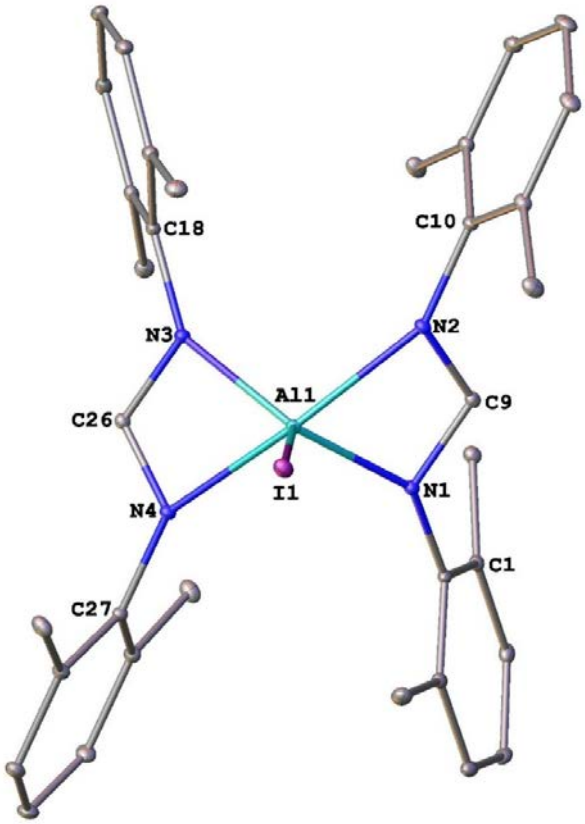

Figure 4.4. Molecular structure of monomeric **[Al(XylForm)$_2$I].PhMe (4.2)** with the atom numbering system; thermal ellipsoids are drawn at the 50 % probability level, hydrogen atoms have been omitted for clarity. Selected bond lengths (Å) and angles (°): Al(1)–N(1): 1.925(2), Al(1)–N(2): 2.0317(19), Al(1)–N(3): 1.924(2), Al(1)–N(4): 2.0382(19), Al(1)–I(1): 2.5456(9), N(2)–C(10): 1.434(3), N(2)–C(9): 1.311(3), N(1)–C(1): 1.418(3), N(1)–C(9): 1.343(3), N(3)–C(18): 1.414(3), N(3)–C(26): 1.341(3), N(4)–C(27): 1.436(3), N(4)–C(26): 1.304(3), N(2)–Al(1)–N(1): 67.48(8), N(4)–Al(1)–N(3): 67.33(8), N(2)–Al(1)–N(3): 100.88(9), N(4)–Al(1)–N(1): 100.47(8), N(1)–Al(1)–N(3): 125.40(9), N(4)–Al(1)–N(2): 154.95(8), N(2)–Al(1)–I(1): 102.07(6), N(4)–Al(1)–I(1): 102.98(6), I(1)–Al(1)–N(1): 117.61(7), I(1)–Al(1)–N(3): 116.98(7), N(1)–C(9)–N(2): 111.95(19), N(3)–C(26)–N(4): 112.45(19), C(10)–N(2)–Al(1): 149.99(16), C(1)–N(1)–Al(1): 144.39(15), C(18)–N(3)–Al(1): 144.26(14), C(27)–N(4)–Al(1): 149.86(16), C(9)–N(2)–Al(1): 88.44(13), C(9)–N(1)–Al(1): 92.11(14), C(26)–N(3)–Al(1): 92.05(14), C(26)–N(4)–Al(1): 88.16(13), C(1)–N(1)–C(9): 123.34(10), C(9)–N(2)–C(10): 121.22(19), C(18)–N(3)–C(26): 123.59(11), C(26)–N(4)–C(27): 121.81(11).

[Al(XylFormH)Br$_3$] (4.3)

The reaction of Na(XylForm) with $AlBr_3$ in PhMe at room temperature was performed with the goal of isolating [Al(XylForm)Br_2], however, **[Al(XylFormH)Br_3]** was isolated instead in moderate yield (56 %) (Scheme 4.4). Complex (**4.3**) crystallised from PhMe in the monoclinic space group *P2$_1$/n* (Table 4.5), with one molecule within the asymmetric unit. In (**4.3**) the aluminum atom, Al1, is coordinated with a dative nitrogen from the formamidine ligand (through κ^1(N1) XylForm), and three terminal bromine atoms. Complex (**4.3**) showed a distorted tetrahedral geometry about the four-coordinate trivalent aluminium (Figure 4.5).

In the molecular structure of (**4.3**), the Al1–N1 bond length was found to be 1.904 (2) Å in the normal range.[33] Complex (**4.3**) is geometrically remarkable as the monodentate coordination mode of aluminium in formamidinate/formamidine chemistry fairly rare.[26] Assessment of the N1– C9 and N2– C9 bond lengths: 1.315(3) and 1.326(3) Å, respectively, suggests delocalisation of the double bond.

It is believed that the crystal structure of the metal complex crystallises better as the E isomer with respect to the N1–C9 bond if the hydrogen was attached to the NCN backbone, rather than a more bulky alkyl group such as the methyl group. For instance, the formamidinate gallium complex, [Ga{HC(NDipp)$_2$H}Cl_3],[26] and [Al{HC(NDipp)$_2$H}$MeCl_2$] and [Al{HC(NDipp)$_2$H}$Cl_{1.4}I_{1.6}$],[34] crystallise as the E isomer, while the acetamidinate aluminium [Al{MeC(NDipp)$_2$H}I_3][26] and molybdenum [Mo{MeC(NDipp)$_2$H}$(CO)_5$][40] complexes crystallise in the Z form.[41] However, product (**4.3**) is very unusual having a hydrogen attached to the NCN backbone and displaying Z form. As expected, the Al–N distance 1.904(2) Å is shorter than those Al–N distances in the higher coordination number complexes (**4.1** and **4.2**) with range between 1.919 (4) – 2.084 (13) Å even though the ligand is uncharged in (**4.3**).

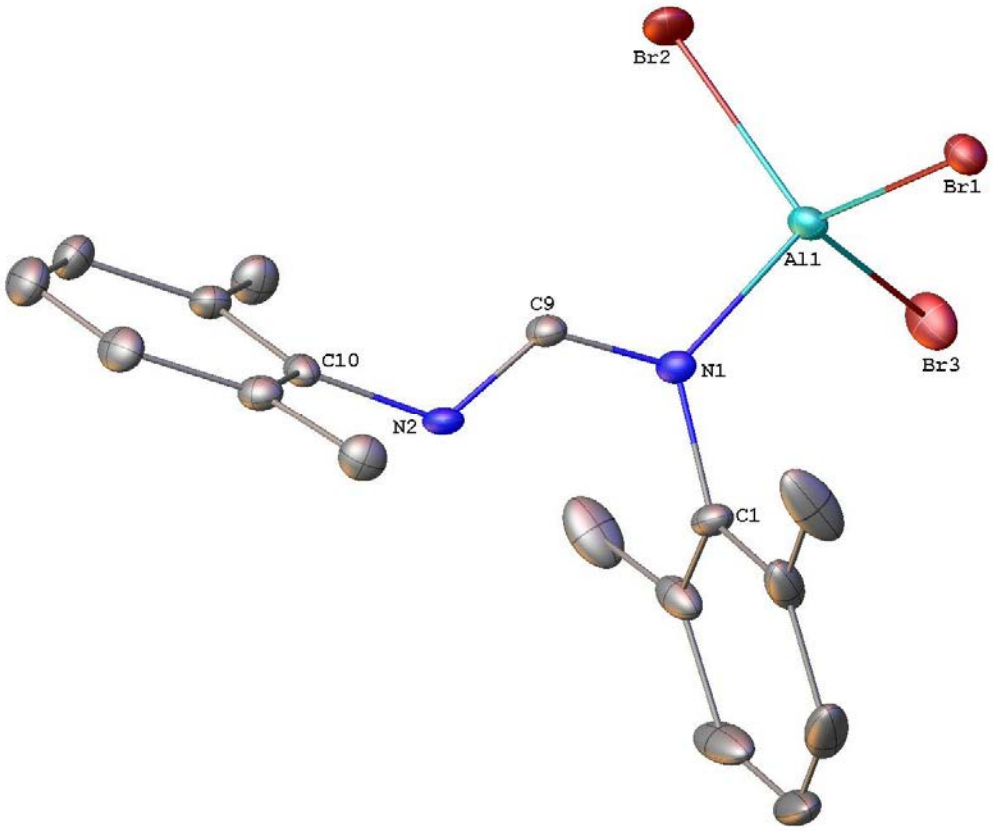

Figure 4.5. Molecular structure of monomeric **[Al(XylFormH)Br$_3$] (4.3)** with the atom numbering system; thermal ellipsoids are drawn at the 50 % probability level, hydrogen atoms have been omitted for clarity. Selected bond lengths (Å) and angles (°): Al(1)–N(1): 1.904(2), N(1)–C(1): 1.455(3), N(1)–C(9): 1.315(3), N(2)–C(9): 1.326(3), N(2)–C(10): 1.441(3), Br(1)–Al(1): 2.3038(10), Br(2)–Al(1): 2.2916(10), Br(3)–Al(1): 2.2687(9), C(1)–N(1)–Al(1): 120.90(18), C(9)–N(1)–Al(1): 121.03(18), C(9)–N(1)–C(1): 117.9(2), C(9)–N(2)–C(10): 121.8(2), N(2)–C(9)–N(1): 126.3(2), Br(2)–Al(1)–Br(1): 107.99(4), Br(3)–Al(1)–Br(1): 110.64(4), Br(3)–Al(1)–Br(2): 114.24(4), N(1)–Al(1)–Br(1): 110.32(8), N(1)–Al(1)–Br(2): 105.84(8), N(1)–Al(1)–Br(3): 107.70(7).

Table 4.5 Crystallographic data for compounds 4.1 – 4.3

Compound	**4.1**	**4.2**	**4.3**
formula	$C_{34}H_{38}AlClN_4$	$C_{41}H_{46}AlIN_4$	$C_{17}H_{20}AlBr_3N_2$
fw	565.11	748.70	519.06
crystal system	monoclinic	triclinic	monoclinic
space group	$P2_1/c$	$P\text{-}1$	$P2_1/n$
a, Å	8.0280(16)	8.2260(16)	7.7260(15)
b, Å	8.5240(17)	15.064(3)	14.013(3)
c, Å	44.624(9)	15.169(3)	18.307(4)
α, deg	90	93.96(3)	90
β, deg	92.20(3)	96.63(3)	93.93(3)
γ, deg	90	96.34(3)	90
V, Å^3	3051.4(11)	1849.3(7)	1977.3(7)
Z	4	2	4
T, K	100(2)	100(2)	100(2)
no. of rflns collected	35848	22141	15215
no. of indep rflns	5120	5936	3240
R_{int}	0.0477	0.0338	0.0572
Final $R1$ values ($I > 2\sigma(I)$)	0.0588	0.0273	0.0348
Final $wR(F^2)$ values ($I > 2\sigma(I)$)	0.1535	0.0735	0.0960
Final $R1$ values (all data)	0.0656	0.0293	0.0358
Final $wR(F^2)$ values (all data)	0.1568	0.0748	0.0970
$GooF$ (on F^2)	1.198	1.064	1.071

$[Al_3(XylForm)_2(\mu_3\text{-}O)(OH)Cl_4]_2$.PhMe (4.4)

In an attempt to examine the chemistry of the system, we looked to synthesise [Al(XylForm)Cl_2(thf)].PhMe. The *in situ* reaction of K(XylForm) in THF with $AlCl_3$ in PhMe was performed in a 1:1 molar ratio (Scheme 4.4), however, colourless crystals of the unexpected **$[Al_3(XylForm)_2(\mu_3\text{-}O)(OH)Cl_4]_2$.PhMe** were isolated from PhMe. The fact that the compound has O^{2-} and OH^- present indicates the high air and moisture sensitivity of these compounds. Complex (**4.4**) crystallised in triclinic space group *P-1* (Table 4.6). Two crystallographically unique molecules, with similar fundamental coordination geometries are present in the asymmetric unit. The difference between the two molecules which is most pronounced in the opposite positions of the formamidinate rings (Fig. 4.6). The X-ray crystallographic study for complex (**4.4**) showed that each of the two molecules has two deprotonated ligands supporting three aluminium centres through a μ-[κ^1-N: κ^1-N] mode, forming a bridged formamidinate structure (Fig. 4.7). A terminal chlorides and a terminal OH^- group are present on each aluminium centre. It is assumed that the occurrence of oxygen (O^{2-} and OH^-) arises from adventitious H_2O highlighting the reactivity of (**4.4**).[42,43,44,45]

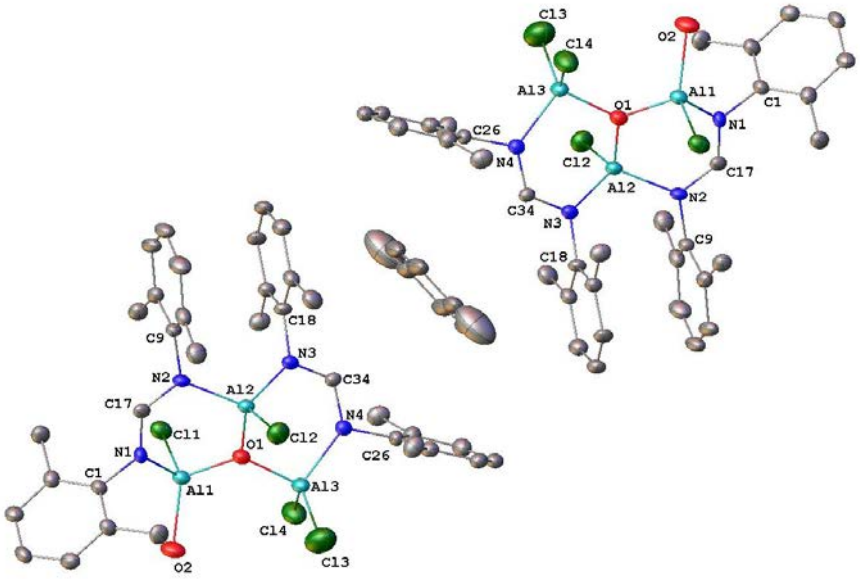

Figure 4.6. A view of (**4.4**), showing the two crystallographically unique molecules and the atom-numbering scheme.

Three aluminium atoms are present in complex (**4.4**). The aluminium atom, Al1, is bonded by one nitrogen donor atom, N1, one chloride atom, one OH group, and is connected to a μ_3 oxygen atom O1 that links the three aluminium centres. The second aluminium centre, Al2, is bridged by two nitrogen atoms from the two XylForm ligands, N2 and N3 displaying κ^1(N,N') bridged mode, as well as bonded to one chloride atom and connected to the μ_3 oxygen atom O1. The third aluminium centre, Al3, is bonded by one nitrogen donor atom, N4, two chloride atoms, and connected to the μ_3 oxygen atom O1. Overall, the coordination sites around the μ_3 oxygen atom centre O^{2-} are occupied by the three aluminium atoms. Models of a three-coordinate oxygen centre with bonds to three aluminium atoms are exceptional but not unprecedented.[46,47,48] The best description for this structure is two merged six membered rings, that share Al2 and O1. Each Al centre has slightly distorted tetrahedral geometry.

The cationic charge of + 9 about the three Al^{3+} ions is balanced by a – 1 charge observed for each NCN ligand, (– 2), and a – 1 charge for each terminal chloride ion, (– 4), a –1 charge for terminal hydroxyl group, (–1), as well as a charge on the central bridged oxygen ion, (– 2). The Al (III) centre in each of the monomeric [Al(XylForm)$_2$Cl] (**4.1**) and [Al(XylForm)$_2$I].PhMe (**4.2**) is bound by the four nitrogen atoms of the chelating ligands, displaying κ^2(N,N') chelating mode, while in the trinuclear (**4.4**) each Al centre is bridged by one of the nitrogen atoms of the ligand.

The Al—N bond lengths are in the range between 1.891(5) – 1.935(5) Å, and together with NCN angles are similar to those reported in neutral chelated formamidinate complexes.[32,33] Of these, the Al2—N2 and Al2—N3 bond lengths are slightly shorter than the others, which is may not be chemically significant. As observed in complex (**4.4**) the bond lengths of the ligand: N3/N4–C26 and N1/N2–C9 are 1.317(6)/1.462(6) and 1.329(6)/1.455(6) Å, respectively. These distances are intermediate between that of single and double bond distances. Single and double bond distances are reported previously in Chapter two of this thesis, indicating the π delocalisation within the NCN unit. The Al—N metric parameters are very comparable to those of the heteroleptic Al (III) amidinate complex reported by Lesikar and Richards.[34] The bond lengths and bond angles equivalent to within ± 0.07 Å and ± 2 °, respectively.

Complex $[Al_3(XylForm)_2(\mu_3\text{-}O)(OH)Cl_4]_2.PhMe$ exhibits Al1/Al2/Al3–O1 distances of 1.795(4), 1.769(4) and 1.809(4) Å, respectively, which correspond closely to the $[\{DippNCHDipp\}_2Al_3\mu_3O(OH)_2(Cl/OH)ClMe]$ complex with distances of 1.782(4), 1.772(4) and 1.792(4) Å respectively.[34] The Al–O bond lengths in both complexes are significantly shorter than the ionic radii of Al–O bond lengths (l.90 Å),[49] but slightly shorter than the Al–O bond length of 1.827(3) Å reported for $[Me_2AlO(CH_2)_2OMe]_2$. However, the three Al–O–Al bond angles in (**4.4**) at the values 125.7(2), 119.9(2) and 114.3(2) ° are larger than the Al–O–Al bond angle of 103° identified in $[Me_2AlO(CH_2)_2OMe]_2$.[50,51]

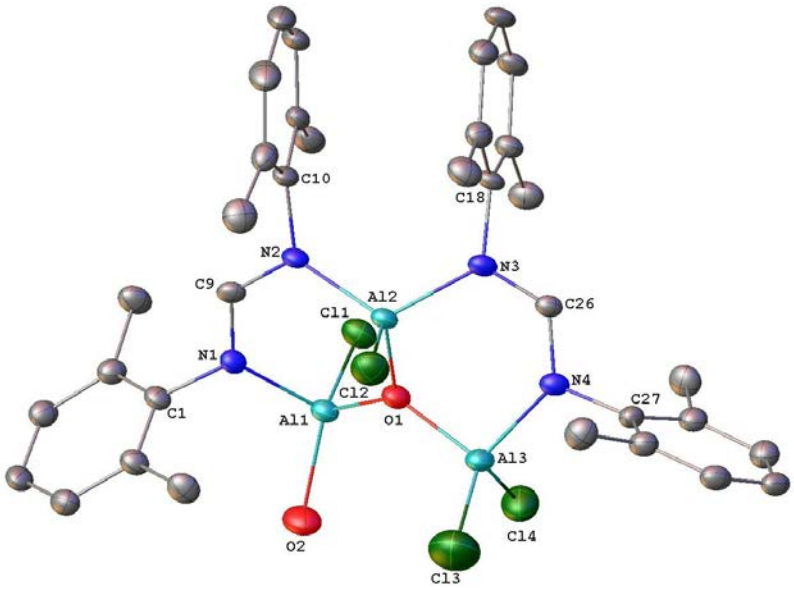

Figure 4.7. Molecular structure of trinuclear **$[Al_3(XylForm)_2(\mu_3\text{-}O)(OH)Cl_4]_2$.PhMe (4.4)** with the atom numbering system; thermal ellipsoids are drawn at the 50 % probability level, hydrogen atoms have been omitted for clarity. Selected bond lengths (Å) and angles (°): Al(1)–N(1): 1.935(5), Al(2)–N(2): 1.891(5), Al(2)–N(3): 1.892(4), Al(3)–N(4): 1.931(4), Al(1)–Cl(1): 2.164(2), Al(1)–O(1): 1.795(4), Al(1)–O(2): 1.974(4), Al(2)–Cl(2): 2.080(2), Al(2)–O(1): 1.769(4), Al(3)–Cl(4): 2.126(3), Al(3)–Cl(3): 2.031(3), Al(3)–O(1): 1.809(4), N(2)–C(10): 1.340(6), N(1)–C(1): 1.448(6), N(1)–C(9): 1.329(6), N(2)–C(9): 1.455(6), N(3)–C(18): 1.454(6), N(3)–C(26): 1.317(6), N(4)–C(27): 1.330(6), N(4)–C(26): 1.462(6), N(2)–Al(2)–N(3): 115.42(18), N(2)–Al(1)–N(3): 102.1(7), N(2)–Al(2)–Cl(2): 111.48(16), N(3)–Al(2)–Cl(2): 110.35(16), N(4)–Al(3)–Cl(4): 109.83(16), N(4)–Al(3)–Cl(3): 114.52(17), O(1)–Al(1)–Cl(1): 106.54(14), O(2)–Al(1)–Cl(1): 114.50(17), O(1)–Al(2)–Cl(2): 107.46(14), O(1)–Al(3)–Cl(4): 107.05(16), O(1)–Al(3)–Cl(3): 113.34(16), O(1)–Al(1)–N(1): 100.26(19), O(1)–Al(2)–N(2): 108.84(19), O(1)–Al(2)–N(3): 102.64(19), O(1)–Al(3)–N(4): 100.64(18), O(1)–Al(1)–O(2): 117.2(2), N(1)–Al(1)–Cl(1): 105.46(15), N(1)–Al(1)–O(2): 111.38(19), Cl(3)–Al(3)–Cl(4): 110.82(12), Al(1)–O(1)–Al(3): 125.7(2), Al(2)–O(1)–Al(1): 119.9(2), Al(2)–O(1)–Al(3): 114.3(2), C(9)–N(1)–Al(1): 126.7(3), C(1)–N(1)–Al(1): 116.3(3), C(10)–N(2)–Al(2): 120.8(3), C(9)–N(2)–Al(2): 122.0(3), C(26)–N(4)–Al(3): 115.0(3), C(27)–N(4)–Al(3): 129.9(4), C(18)–N(3)–Al(2): 123.8(3), C(18)–N(3)–Al(2): 119.9(3). Atoms generated by symmetry: [1]1-X,1-Y,-Z.

[Al(DippFormH)Br$_3$] (4.5)

Examination of the reaction of $AlBr_3$ with one equivalent of Na(DippForm) in PhMe at room temperature generated the resultant tribromoaluminium formamidine complex **[Al(DippFormH)Br$_3$]**, which was isolated in good yield (61 %). The monomeric (**4.5**) crystallised in the monoclinic space group *P2$_1$/c* (Table 4.6), with one molecule within the asymmetric unit. Structural determination revealed an aluminum atom, Al1, is four coordinated with a dative nitrogen from the formamidine ligand (through κ^1(N1) XylForm), and three terminal bromine atoms, showing an overall distorted tetrahedral geometry.

The molecular structure of compound (**4.5**) is depicted in (Figure 4.8), showing Al1–N1 bond length of 1.885(3) Å in the normal range.[33] The coordination environment for the aluminium bromide formamidine compound (**4.5**) is isostructural with that observed in trivalent (**4.3**), where the bulky DippFormH ligand replaces the XylFormH ligand. A feature of compounds (**4.3** and **4.5**) is that the formation of the monomer is favoured rather than a dimer and this presumably arises due to the steric bulk of the ligands limiting bridging halides. Attempts to repeat the synthesis of [Al(Form)Br$_2$] (Form = XylForm, DippForm) met with repeated failure. The X-ray analysis showed the formation of the formamidine ligand (XylFormH (**4.3**) or DippFormH (**4.5**)) binding in a monodentate mode to the $AlBr_3$ through the lone pair on the non-protonated N-atom and protonated at the other nitrogen atom.

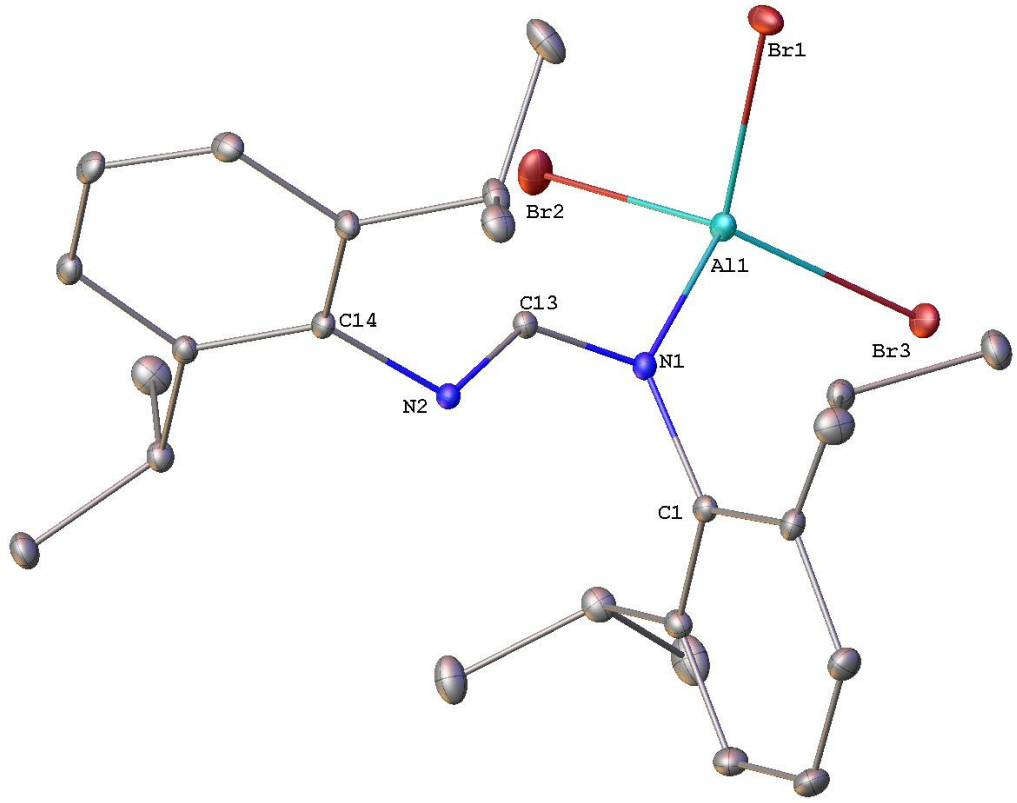

Figure 4.8. Molecular structure of monomeric **[Al(DippFormH)Br$_3$] (4.5)** with the atom numbering system; thermal ellipsoids are drawn at the 50 % probability level, hydrogen atoms have been omitted for clarity. Selected bond lengths (Å) and angles (°): Al(1)–N(1): 1.885(3), N(1)–C(1): 1.446(4), N(1)–C(13): 1.309(4), N(2)–C(13): 1.311(4), N(2)–C(14): 1.444(4), Br(1)–Al(1): 2.2774(12), Br(2)–Al(1): 2.2783(13), Br(3)–Al(1): 2.2502(11), C(1)–N(1)–Al(1): 126.5(2), C(13)–N(1)–Al(1): 115.0(2), C(13)–N(1)–C(1): 118.5(3), C(13)–N(2)–C(14): 118.7(3), N(2)–C(13)–N(1): 128.8(3), Br(2)–Al(1)–Br(1): 106.27(5), Br(3)–Al(1)–Br(1): 114.02(4), Br(3)–Al(1)–Br(2): 115.35(5), N(1)–Al(1)–Br(1): 106.58(9), N(1)–Al(1)–Br(2): 104.70(9), N(1)–Al(1)–Br(3): 109.19(9).

[Al(DippForm)X_2(thf)] (X = Cl (4.6), Cl, Br (4.7))

In order to compare the coordination preferences and products obtained from aluminium halide reactions with the deprotonated DippformH ligand, two reactions with AlX_3 (X = Cl, Br) were performed. The monomeric complexes of (**4.6** and **4.7**) were found to crystallise in the triclinic space group *P-1* (Table 4.6). The five-coordinate aluminium centre in each of the complexes (**4.6** and **4.7**) is ligated by two nitrogen atoms from the formamidinato ligand, and the other three sites are occupied by a two halide atoms (2Cl (**4.6**) and ClBr (**4.7**)) and a tetrahydrofuran solvent molecule. The coordination geometry of Al^{+3} in (**4.6** and **4.7**) assume distorted from trigonal bipyramid and square pyramid due to the very narrow bite of the DippForm ligand (Scheme 4.5). The coordination environment for the Al atom in (**4.7**) is similar to that observed in trivalent (**4.6**), where the bromide ligand replaced one of the chloride ligands. The formamidinate moieties in (**4.6** and **4.7**) serve as (η^2) N,N'-chelating four–electron donor ligands and they are almost similar to the structures observed for the corresponding [$GaMe_2$(PhNCPhNPh)],[12] [E{RC(NR')$_2$}Cl_2] [E = Sb, R = *t*Bu, R' = *i*Pr, Cy, 2,6-*i*$Pr_2C_6H_3$ (DippForm); R= *n*Bu, R' = *i*Pr; E = Bi, R = *t*Bu, R' = *i*Pr , DippForm][52] and [Sb(Form)X_2] [X = F, N_3; Form = *t*BuC(N*i*Pr)$_2$ or *t*BuC(N{2,6-*i*$Pr_2C_6H_3$})$_2$].[53] In addition, in the solid state of these two complexes showed comparable structures to the bismuth formamidinate complexes of the type [Bi(Form)X_2(Et_2O)] (X = Cl, Br), except the latter have formed solvent-coordinated (Et_2O).[54] Al1–N1 and Al1–N2 distances in (**4.6** and **4.7**) were found to be 1.928(3)/2.104(3) and 1.925(5)/2.118(5) Å that are in the usual range.[32,33,34,4] The formation of a four-membered Al-N-C-N ring system confirmed the distorted delocalisation of the π-electrons in the formamidinate backbone, which is supported by the very slightly dissimilar bond lengths between N1–C13 1.329(4)/N2–C13 1.300(4) Å (**4.6**) and N1–C13 1.314(7)/N2–C13 1.299(7) Å (**4.7**). The N1–Al–N2 bond angle of 66.1(2) ° in complex (**4.7**) is slightly bigger than that in complex (**4.6**) 65.8(11) °, and both of them are normal for metal formamidinate complexes. Also, the most prominent structural consistency between (**4.6**) and (**4.7**) is shown by the exocyclic X(1)–Al–X(2) bond angles (X = Cl and/or Br), 115.14(9) ° in complex (**4.6**) which is identical with that in complex (**4.7**) 115.15(11) ° (Fig. 4.9 and 4.10).

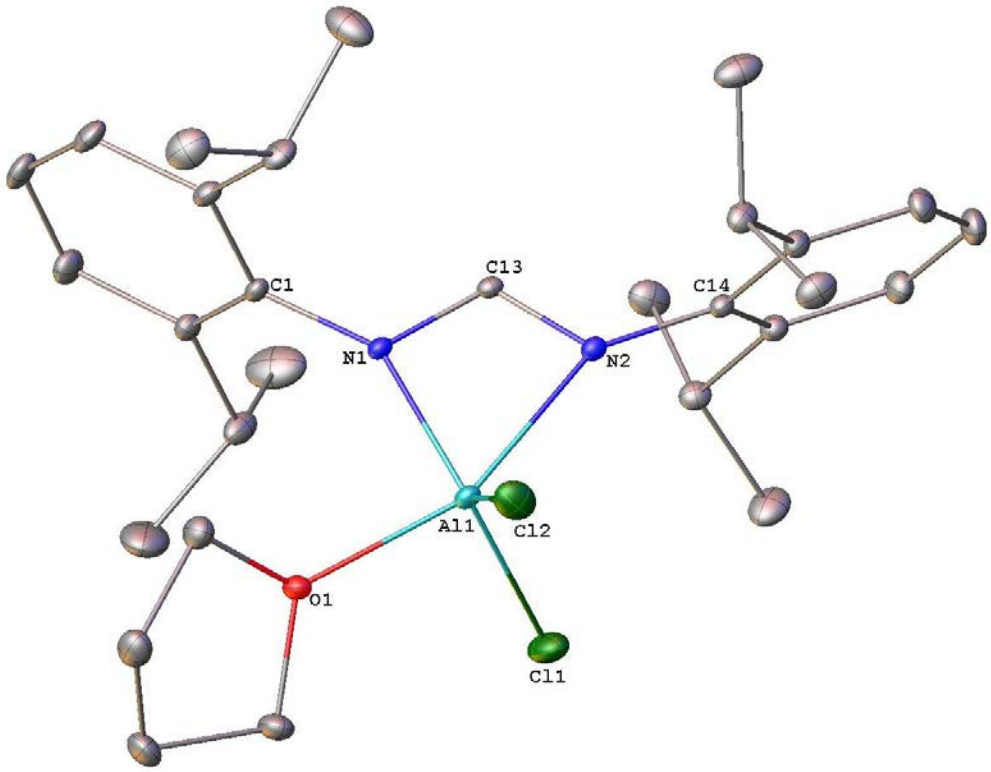

Figure 4.9. Molecular structure of monomeric **[Al(DippForm)Cl_2(thf)] (4.6)** with the atom numbering system; thermal ellipsoids are drawn at the 50 % probability level, hydrogen atoms have been omitted for clarity. Selected bond lengths (Å) and angles (°): Al(1)–N(1): 1.928(3), Al(1)–N(2): 2.104(3), N(1)–C(1): 1.429(4), N(1)–C(13): 1.329(4), N(2)–C(14): 1.421(4), N(2)–C(13): 1.300(4), Cl(1)–Al(1): 2.0851(18), Cl(2)–Al(1): 2.1094(18), Al(1)–O(1): 2.000(3), C(1)–N(1)–Al(1): 145.6(2), C(13)–N(1)–Al(1): 93.91(19), C(13)–N(2)–Al(1): 87.0(2), C(13)–N(1)–C(1): 120.4(3), C(13)–N(2)–C(14): 122.4(3), C(14)–N(2)–Al(1): 149.6(2), N(2)–C(13)–N(1): 113.2(3), Cl(1)–Al(1)–Cl(2): 115.14(9), O(1)–Al(1)–Cl(1): 94.43(10), O(1)–Al(1)–Cl(2): 93.57(10), O(1)–Al(1)–N(2): 156.29(12), N(1)–Al(1)–Cl(1): 123.98(11), N(2)–Al(1)–Cl(1): 97.00(9), N(1)–Al(1)–Cl(2): 120.16(11), N(2)–Al(1)–Cl(2): 100.20(10), N(1)–Al(1)–O(1): 90.60(12), N(1)–Al(1)–N(2): 65.80(11).

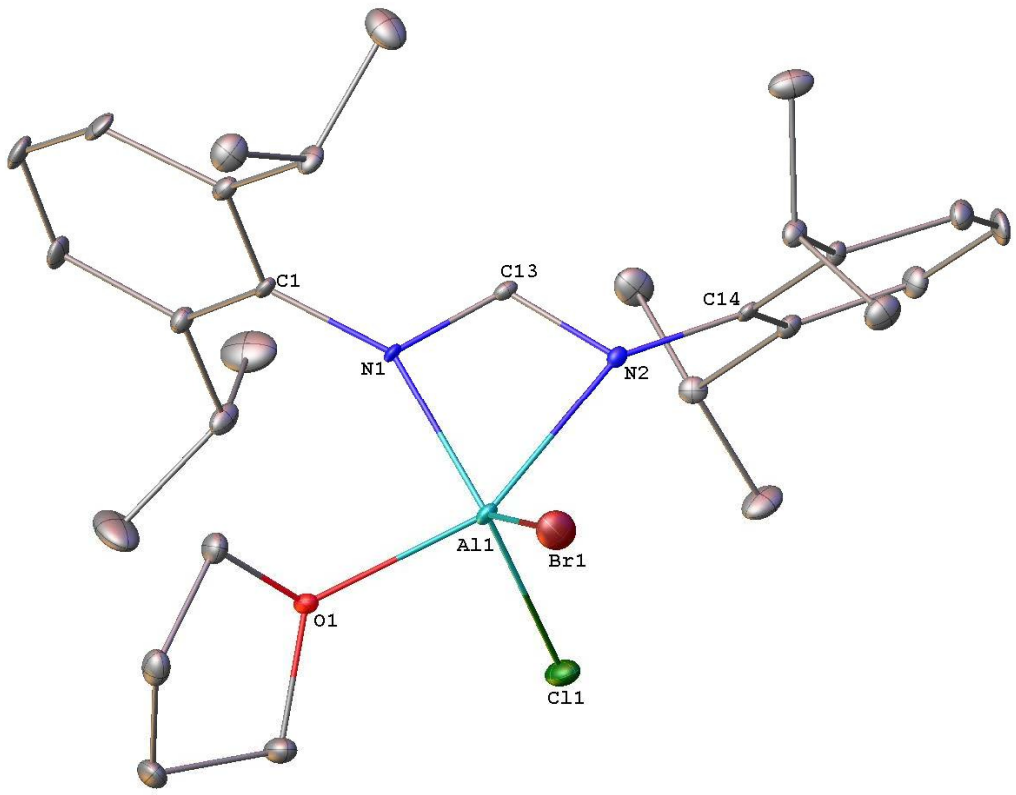

Figure 4.10. Molecular structure of monomeric **[Al(DippForm)ClBr(thf)] (4.7)** with the atom numbering system; thermal ellipsoids are drawn at the 50 % probability level, hydrogen atoms have been omitted for clarity. Selected bond lengths (Å) and angles (°): Al(1)–N(1): 1.925(5), Al(1)–N(2): 2.118(5), N(1)–C(1): 1.412(7), N(1)–C(13): 1.314(7), N(2)–C(14): 1.424(8), N(2)–C(13): 1.299(7), Br(1)–Al(1): 2.284(2), Cl(1)–Al(1): 2.177(3), Al(1)–O(1): 2.017(5), C(1)–N(1)–Al(1): 146.4(4), C(13)–N(1)–Al(1): 93.2(4), C(13)–N(2)–Al(1): 85.2(4), C(13)–N(1)–C(1): 120.4(5), C(13)–N(2)–C(14): 123.4(5), C(14)–N(2)–Al(1): 150.1(4), N(2)–C(13)–N(1): 115.5(6), Cl(1)–Al(1)–Br(1): 15.15(11), O(1)–Al(1)–Br(1): 92.94(15), O(1)–Al(1)–Cl(1): 95.88(16), O(1)–Al(1)–N(2): 155.7(2), N(1)–Al(1)–Br(1): 118.57(16), N(2)–Al(1)–Br(1): 99.63(15), N(1)–Al(1)–Cl(1): 125.58(18), N(2)–Al(1)–Cl(1): 97.45(16), N(1)–Al(1)–O(1): 89.6(2), N(1)–Al(1)–N(2): 66.1(2), C(26)–O(1)–Al(1): 120.7(4), C(29)–O(1)–Al(1): 123.9(4).

Table 4.6 Crystallographic data for compounds 4.4 - 4.7

Compound	**4.4**	**4.5**	**4.6**	**4.7**
formula	$C_{75}H_{86}Al_6Cl_8N_8O_4$	$C_{25}H_{36}AlBr_3N_2$	$C_{29}H_{43}AlCl_2N_2O$	$C_{29}H_{43}AlBrClN_2O$
fw	1609.00	631.27	533.53	577.99
crystal system	triclinic	monoclinic	triclinic	triclinic
space group	*P-1*	*P2₁/c*	*P-1*	*P-1*
a, Å	10.906(2)	10.278(2)	10.3175(4)	10.222(2)
b, Å	12.427(3)	19.974(4)	10.7120(4)	10.720(2)
c, Å	16.934(3)	14.178(3)	14.7854(5)	14.529(3)
α, deg	87.83(3)	90	91.983(2)	91.85(3)
β, deg	72.56(3)	108.59(3)	98.268(2)	98.80(3)
γ, deg	67.89(3)	90	103.631(2)	104.04(3)
V, Å^3	2021.2(9)	2758.7(11)	1567.57(10)	1522.3(6)
Z	2	4	2	2
T, K	100(2)	100(2)	296(2)	173(2)
no. of rflns collected	17460	27489	15311	18551
no. of indep rflns	6653	4822	5297	4871
R_{int}	0.0926	0.0384	0.0408	0.0297
Final *R1* values ($I > 2\sigma(I)$)	0.0846	0.0385	0.0821	0.0674
Final *wR*(F^2) values ($I > 2\sigma(I)$)	0.2249	0.0993	0.2646	0.1998
Final *R1* values (all data)	0.1312	0.0415	0.0990	0.0686
Final *wR*(F^2) values (all data)	0.2590	0.1015	0.2880	0.2007
GooF (on F^2)	1.040	1.081	1.052	1.111

[Al(DippForm)$_2$Cl] (4.8)

The heteroleptic chloride-bis(N,N'-diisopropylphenylformamidinato) aluminium (III) complex **[Al(DippForm)$_2$Cl]** crystallised in the monoclinic space group *P2$_1$/n*, as a solvent-free complex (Table 4.8), with one molecule within the asymmetric unit. Complex (**4.8**) has been synthesised in reasonable yield (70 %). This compound was previously reported in the literature with weak data and very poor quality and the structure was reported ″for connectivity only″.[15] Therefore, we intended to resynthesise it and collect much improved data and this is presented here.

The two formamidinate moieties in (**4.8**) serve as chelating η^2(N,N') four-electron nitrogen donor ligands, similarly to those was previously observed for [Bi(DippForm)$_2$Bu^n] complex.[54] X-ray crystallographic analysis for (**4.8**) displayed that the coordination geometry about Al^{+3} distorted from trigonal bipyramid and square pyramid due to the very narrow bite of the DippForm ligand (Figures 4.11). The two formamidinate ligands are symmetrically bound to Al with the four N atoms forming a fairly accurate trapezium with the Al atom in the centre of the structure (N(2)–Al–N(3) 104.22(5)◦ and N(1)–Al–N(4) 103.87(5)◦).

The structure of the chloride complex (**4.8**) is analogous to those of Al(XylForm)$_2$Cl (**4.1**) and [Al(XylForm)$_2$I].PhMe (**4.2**) above, but shows a different ligand arrangement. The variance in the Al–N bond lengths (0.146, 0.124 Å) are different from those of the Al(XylForm)$_2$Cl (**4.1**) (0.114, 0.115 Å) and [Al(XylForm)$_2$I].PhMe (**4.2**) (0.106, 0.114 Å) complexes above. The Al–Cl bond is perpendicular to the AlN4 plane and the bond length at the value of (2.1531(10) Å) is typical for Al chloride bond,[11,14,15,36,37] but is longer than those found in (**4.1**) with the value of 2.119 (2) Å. The ^{i}Pr groups are occupied above and below the plane.

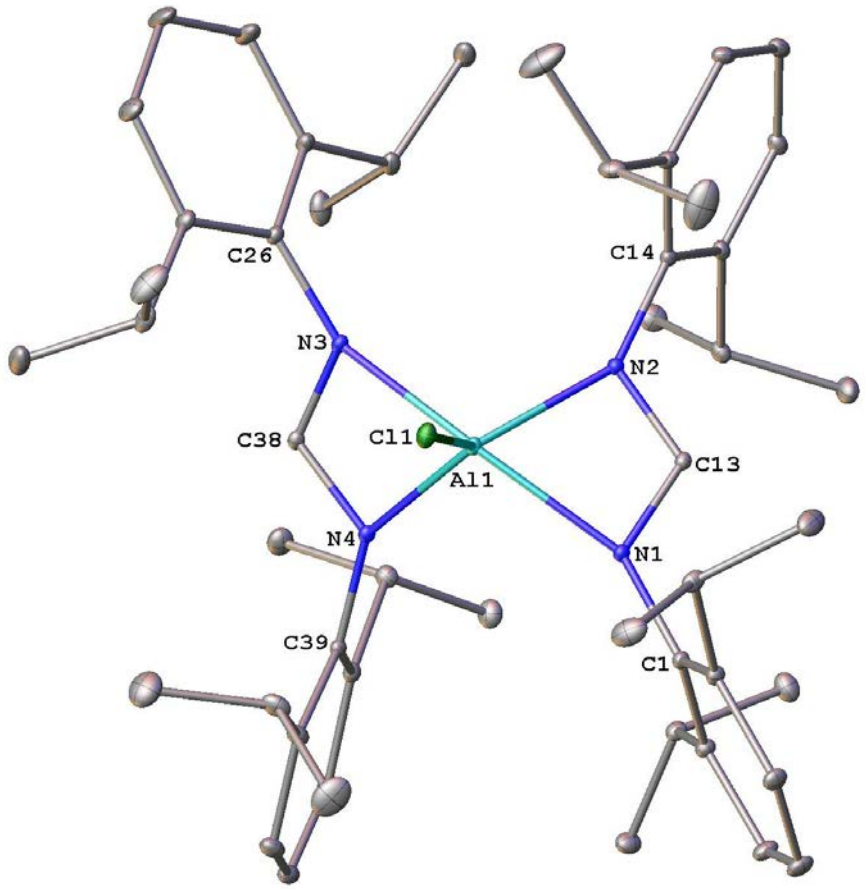

Figure 4.11. Molecular structure of monomeric **[Al(DippForm)$_2$Cl] (4.8)** with the atom numbering system; thermal ellipsoids are drawn at the 50 % probability level, hydrogen atoms have been omitted for clarity. Selected bond lengths (Å) and angles (°): Al(1)–N(1): 2.0610(13), Al(1)–N(2): 1.9158(13), Al(1)–N(3): 2.0423(13), Al(1)–N(4): 1.9185(13), Al(1)–Cl(1): 2.1531(10), N(2)–C(14): 1.4324(18), N(2)–C(13): 1.3397(18), N(1)–C(1): 1.4398(18), N(1)–C(13): 1.3108(19), N(3)–C(26): 1.4281(18), N(3)–C(38): 1.3068(19), N(4)–C(38): 1.3359(18), N(4)–C(39): 1.4234(19), N(2)–Al(1)–N(1): 67.48(5), N(2)–Al(1)–N(3): 104.22(5), N(2)–Al(1)–Cl(1): 117.19(4), N(1)–Al(1)–N(3): 161.82(5), N(4)–Al(1)–N(2): 126.87(6), N(4)–Al(1)–N(1): 103.87(5), N(4)–Al(1)–N(3): 67.36(5), N(4)–Al(1)–Cl(1): 115.94(4), N(1)–C(13)–N(2): 113.14(13), Cl(1)–Al(1)–N(1): 100.02(4), Cl(1)–Al(1)–N(3): 98.16(4), C(13)–N(2)–Al(1): 92.35(9), C(14)–N(2)–Al(1): 146.78(10), C(1)–N(1)–Al(1): 152.11(10), C(13)–N(1)–Al(1): 86.92(9), N(3)–C(38)–N(4): 112.61(13), C(38)–N(3)–Al(1): 87.59(9), C(26)–N(3)–Al(1): 147.21(11), C(39)–N(4)–Al(1): 144.99(10), C(38)–N(4)–Al(1): 92.11(9).

The N(1)–Al(1)–N(2) 67.48(5) and N(3)–Al(1)–N(4) 67.36(5)° are larger than the typical bond angle in the metal amidinate complexes (60°). The N(1)–C(13)–N(2) 113.14(13) and N(3)–C(38)–N(4) 112.59(13)° angles of (**4.8**) are almost identical and the sum of bond angles at C(13) 359.9, C(38) 360.0, N(1) 359.3, N(2) 359.8, N(3) 357.8 and N(4) 359.6°, pointing to sp^2-hybridised carbon and nitrogen atoms. On the other hand, the delocalisation of the π-electrons in the formamidinate backbone is slightly distorted as indicated by the difference of bond lengths C(13)–N(1)/(2) 1.310 (19)/1.339 (18) and C(38)–N(3)/(4) 1.306 (19)/1.335 (18) Å. Analogous findings were previously detected in formamidinate complexes of the type $[Al(L)_2Cl]$ complexes [L = chelating formamidinate].[11,14, 36, 37]

Table (4.7) displays all the selected bond lengths for each of the obtained trivalent aluminium compounds. These Al-N bond lengths are virtually asymmetric. The shortest Sb-N bond length for the trivalent species observed in the four-coordinate $[Al(DippFormH)Br_3]$ (**4.5**) (1.885 Å), while the longest Sb-N bond length was observed for the five-coordinate [Al(DippForm)ClBr(thf)] (**4.7**) (2.118 Å).

	4.1	**4.2**	**4.3**	**4.4**	**4.5**	**2.6**	**2.7**	**2.8**
Al-N1	2.033(4)	1.925(2)	1.904(2)	1.935(5)	1.885(3)	1.928(3)	1.925(5)	2.061(13)
Al -N2	1.919(4)	2.031(19)	-	1.891(5)	-	2.104(3)	2.118(5)	1.915(13)
Al -N3	2.040(4)	1.924(2)	-	1.892(4)	-	-	-	2.042(13)
Al -N4	1.925(4)	2.038(19)	-	1.931(4)	-	-	-	1.918(13)

Table 4.7 Selected bond lengths (Å) for complexes: $[Al(XylForm)_2Cl]$ **(4.1)**, $[Al(XylForm)_2I].PhMe$ **(4.2)**, $[Al(XylFormH)Br_3]$ (**4.3**), $[Al_3(XylForm)_2(\mu_3\text{-}O)(OH)Cl_4]_2.PhMe$ (**4.4**), $[Al(DippFormH)Br_3]$ (**4.5**), $[Al(DippForm)Cl_2(thf)]$ (**4.6**), [Al(DippForm)ClBr(thf)] (**4.7**) and $[Al(DippForm)_2Cl]$ (**4.8**).

$[Me_3Sb\text{-}SbMe_2][AlCl_4]$ (4.9)

$[Me_3Sb\text{-}SbMe_2][AlCl_4]$ crystallised in the monoclinic space group $P2_1/c$ (Table 4.8), with one molecule in the asymmetric unit. The cation of complex (**4.9**) can be considered a trimethylstibine adduct of the dimethylstibenium ion, involving a slightly distorted trigonal pyramidal Me_3Sb unit bound to a bent Me_2Sb unit through an antimony-antimony bond. The tetrachloroaluminium anion adopts tetrahedral geometry (Fig. 4.12).

The Sb–Sb bond distance observed in the antimony backbone of the cation of (**4.9**) is short (2.823(4) Å), showing a typical single bond since it is virtually equidistant with the calculated Sb–Sb single bond covalent radii (Σr_{cov}(Sb–Sb) = 2.80 Å),[55] but is shorter than the sum of the van der Waals radii (Sb: 4.12 Å).[56] Also, the Sb–Sb bond length lies in good agreement with those identified in $[PhSb_2]^{-3}$ [2.8198(7)],[57] $[Me_2Sb–SbMe_2–SbMe_2][Me_2SbBr_2]$ [2.8203(4)],[58] $[Me_3Sb\text{-}SbMe_2]_2[(MeSbBr_3)_2]$ [2.8205(12)][59] and $[Me_3Sb\text{-}SbMe_2]_2[GaCl_4]$ [2.8273(3) Å],[60] but is a little shorter compared to those stated in tetramethyldistibane $[Me_2Sb\text{-}SbMe_2]^{+2}$ [2.862(2)][61], tetraphenyldistibane $[Ph_4Sb_2]^{+2}$ [2.867(1)],[62] ($Me_3Sb–Sb(Me)I_2$) [2.859(1)][63] and ($Me_3Sb–SbI_3$.thf) [2.843(1) Å].[64] The Sb–C single bonds of the tetracoordinated (stibonium) and the tricoordinated Sb atoms (stibino centers) are in the predictable range (2.112(5) – 2.154(5) Å, (Σr_{cov} (Sb–C) = 2.15 Å).[55] The average bond angles in (**4.9**) of C–Sb–C are 101.9(3) ° and C–Sb–Sb 105.9(17) °, which are slightly larger than those reported for $[Me_3Sb\text{-}SbMe_2][GaCl_4]$.[60] Comparable findings can be observed for transition metal complexes of tetramethyldistibine such as $[(OC)_5Cr]_2[Sb_2Me_4]$.[65]

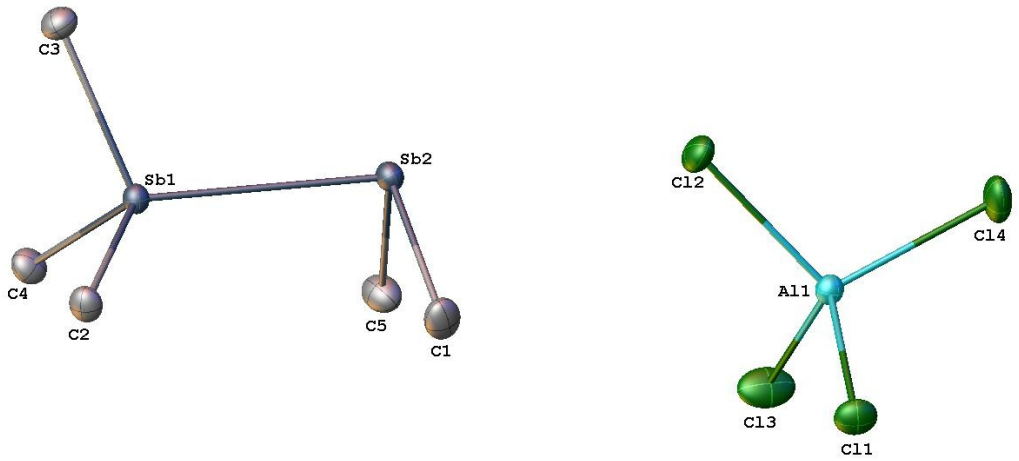

Figure 4.12. Molecular structure of ionic **[Me_2Sb-SbMe_3][$AlCl_4$] (4.9)** with the atom numbering system; thermal ellipsoids are drawn at the 50 % probability level, hydrogen atoms have been omitted for clarity. Selected bond lengths (Å) and angles (°): Al(1)–Cl(1): 2.1280(18), Al(1)–Cl(2): 2.1244(17), Al(1)–Cl(3): 2.118(2), Al(1)–Cl(4): 2.1219(19), Sb(1)–Sb(2): 2.8238(4), Sb(2)–C(5): 2.149(5), Sb(1)–C(2): 2.119(4), Sb(1)–C(3): 2.115(5), Sb(1)–C(4): 2.112(5), Sb(2)–C(1): 2.154(5), C(2)–Sb(1)–Sb(2): 116.99(13), C(5)–Sb(2)–C(1): 96.1(3), C(3)–Sb(1)–Sb(2): 110.03(15), Cl(2)–Al(1)–Cl(1): 110.29(8), C(3)–Sb(1)–C(2): 104.0(2), Cl(3)–Al(1)–Cl(1): 108.40(8), C(4)–Sb(1)–Sb(2): 114.78(15), Cl(3)–Al(1)–Cl(2): 109.77(10), C(4)–Sb(1)–C(2): 106.3(2), Cl(3)–Al(1)–Cl(4): 109.99(10), C(4)–Sb(1)–C(3): 103.4(2), Cl(4)–Al(1)–Cl(1): 110.14(9), C(1)–Sb(2)–Sb(1): 94.09(16), Cl(4)–Al(1)–Cl(2): 108.24(8), C(5)–Sb(2)–Sb(1): 93.82(17).

[Br_3Sb-μBr-$SbBr_3$][$AlCl_2(thf)_4$] (4.10)

In an attempt to form bimetallics involving DippFormH, $AlCl_3$ and $SbBr_3$, the three were mixed in THF/PhMe and produced complex (**4.10**) in moderate yield, as very shiny cubic crystals. Crystals of complex (**4.10**) crystallised in the triclinic space group *P-1* (Table 4.8). The formation of these crystals was accompanied by dark red/purple plates, which only diffracted very poorly. These crystals were obtained on multiple occasions, but we were unable to achieve a good X-ray data set, so were not explored any further.

Unfortunately, good quality crystals for X-ray analysis of (**4.10**) could not be obtained. As a result, X-ray diffraction data for this compound were of lower quality and has only been included as confirmation of connectivity. The molecular structure of the crystalline compound (**4.10**) is shown in (Fig. 4.13). The coordination environment of (**4.10**) consists of an anionic hexabromodiantimonate (III), with Sb1 and Sb2 are tetrahedrally share the Br4 bridge [Br_3Sb-μBr-$SbBr_3$] $^-$. While the cation involves four thf solvation coordinated dichloroaluminium. The Sb–Br bond lengths are in the range of 2.532(4) – 2.960(4), in which the bromine bridges of Sb(1)–Br(4) 2.901(4) and Sb(2)–Br(4) 2.960(4) are almost identical. However, Clegg, *et al.* reported that the same type of bromine bridges were established with bond lengths 2.8280(12) and 3.5954(12) for which the difference is 0.767 Å in [$Sb_3Br_3(dmpe)_3$].[66] Same Sb-Br linkages, but is anionic cyclic tetramers observed for crystal structures of empirical formula [$C_3H_5N_2]_6[Bi_4Cl_{18}$],[67] and the two polymorphic of pyrazolium bromoantimonates (III), [$C_3N_2H_5]_6Sb_4Br_{18}\cdot 2H_2O$: α modification– tetragonal form and β modification– triclinic form.[68]

The average Sb–$Br_{(terminal\ bromine)}$ bond lengths of [Br_3Sb-μBr-$SbBr_3$][$AlCl_2(thf)_4$] was found to be 2.70 Å, which is approximately in agreement with the average Sb–$Br_{(terminal\ bromine)}$ 2.78 Å reported for bis(diisobutylammonium) octabromodiantimonate (III), [(*i*-$C_4H_9)_2NH_2]_2Sb_2Br_8$,[69] but the average of Sb–$Br_{(bridge\ bromine)}$ bond lengths of [Br_3Sb-μBr-$SbBr_3$][$AlCl_2(thf)_4$] was found to be 2.93 Å that is significantly shorter than the average of Sb–$Br_{(bridge\ bromine)}$ 3.14 Å bond length of [(*i*-$C_4H_9)_2NH_2]_2Sb_2Br_8$.[69]

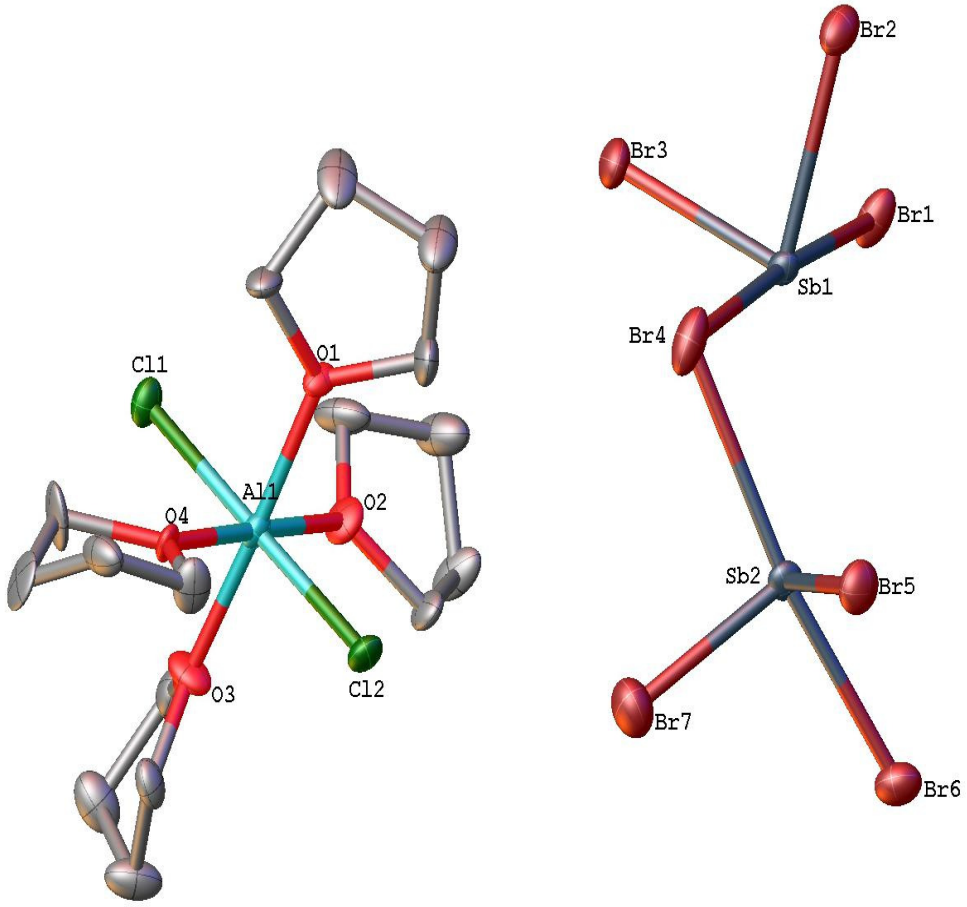

Figure. 4.13. Molecular structure of ionic **[Br_3Sb-μBr-$SbBr_3$][$AlCl_2(thf)_4$] (4.10)** with the atom numbering system; thermal ellipsoids are drawn at the 50 % probability level, hydrogen atoms have been omitted for clarity. Selected bond lengths (Å) and angles (°): Sb(1)–Br(1) 2.582(4), Sb(1)–Br(2) 2.748(4), Sb(1)–Br(3) 2.532(4), Sb(1)–Br(4) 2.901(4), Sb(2)–Br(4) 2.960(4), Sb(2)–Br(5) 2.691(4), Sb(2)–Br(6) 2.911(4), Sb(2)–Br(7) 2.791(4), Al(1)–Cl(1) 2.237(4), Al(1)–Cl(2) 2.280(4), Al(1)–O(1) 1.976(4), Al(1)–O(2) 1.940(4), Al(1)–O(3) 1.954(4), Al(1)–O(4) 1.904(4).

Table 4.8 Crystallographic data for compounds 4.8 - 4.10

Compound	**4.8**	**4.9**	**4.10**
formula	$C_{50}H_{70}AlClN_4$	$C_5H_{15}AlCl_4Sb_2$	$C_{16}H_{32}AlCl_2Br_7O_4Sb_2$
fw	789.53	487.45	1189.09
crystal system	monoclinic	monoclinic	triclinic
space group	*P2₁/n*	*P2₁/c*	*P-1*
a, Å	14.509(3)	9.1410(9)	23.604(5)
b, Å	16.288(3)	10.0801(10)	33.287(7)
c, Å	21.112(4)	17.3566(17)	23.911(5)
α, deg	90	90	89.97(3)
β, deg	109.86(3)	96.993(4)	105.23(3)
γ, deg	90	90	89.97(3)
V, Å^3	4692.6(18)	1587.4(3)	18127.2
Z	4	4	2
T, K	100(2)	296(2)	100
no. of rflns collected	56762	18644	173092
no. of indep rflns	8217	3644	67470
R_{int}	0.0369	0.0519	0.0539
Final *R1* values ($I > 2\sigma(I)$)	0.0491	0.0334	0.2527
Final *wR*(F^2) values ($I > 2\sigma(I)$)	0.1226	0.0886	0.5710
Final *R1* values (all data)	0.0527	0.0428	0.3604
Final *wR*(F^2) values (all data)	0.1249	0.0950	0.6352
GooF (on F^2)	1.118	1.033	1.735

Note. X-ray diffraction data of (**4.10**) has been included as confirmation of connectivity only.

4.4 *Conclusions*

In conclusion, this chapter describes utilising two formamidinate ligands of large, but varying steric bulk, electronic properties and functionality (XylForm and DippForm) that led to isolation of eight new aluminium (III) formamidinate complexes. The reactions were metathesis routes between stoichiometric amounts of metal alkyl/amide such as (*n*-BuLi, $LiN(SiMe_3)_2$, $NaN(SiMe_3)_2$, $KN(SiMe_3)_2$) and the two formamidinate ligands in THF and/or PhMe, followed by combination with AlX_3 (X = Cl, Br, I), and resulted in the complexes $[Al(XylForm)_2Cl]$ (**4.1**), $[Al(XylForm)_2I].PhMe$ (**4.2**), $[Al(XylFormH)Br_3]$ (**4.3**), $[Al(DippFormH)Br_3]$ (**4.5**) and $[Al(DippForm)_2Cl]$ (**4.8**). Using the bulkier formamidinate ligand (DippForm) allowed the isolation of the thf solvate dichlorido- or chloridobromido-(N,N'-diisopropylformamidinato) aluminium (III), $[Al(DippForm)Cl_2(thf)]$ (**4.6**) and $[Al(DippForm)ClBr(thf)]$ (**4.7**) respectively. The common feature of these complexes is formation of monomers. The heteroleptic aluminium complex $[Al_3(XylForm)_2(\mu_3\text{-}O)(OH)Cl_4]_2.PhMe$ (**4.4**) was isolated as a monomer and represents a compound containing three aluminium atoms bridged by an oxygen atom. The synthesised complexes have been fully characterised by X-ray crystallography in the solid state, and characterised by ^1H- and ^{13}C-NMR, IR spectroscopic techniques, elemental analysis as well as melting points. Dichloroaluminium and tetrachloroaluminate salts bearing different stibinostibonium cations and anions such as $[Me_3Sb\text{-}SbMe_2]^+$ and $[(Br_4Sb)SbBr_3]^-$ were isolated from $SbCl_3$, $SbBr_3/AlMe_3$, $AlCl_3$ mixtures, depending on the reaction conditions. The cation of $[Me_3Sb\text{-}SbMe_2][AlCl_4]$ has a tetrahedral Me_3Sb bound to a bent $SbMe_2$ unit with a short (2.82 Å) Sb-Sb bond, and the anion adopts the geometry of tetrahedral, consequently this form represents a type of heterobimetallic complex containing antimony and aluminium. Overall, this work has enriched the knowledge regarding formamidinato aluminium (III) complexes and much more information has been obtained concerning their structures and bonding modes. Many of these compounds could be used as a useful precursors in the search for low valent aluminium compounds, after treating the haloaluminium complexes with strong reducing agents such as KC_8.

4.5 *Experimental*

General Considerations/Air Sensitive Techniques

All aluminium complexes described herein are extremely air and/or moisture sensitive, decomposing immediately with dramatic colour changes (colourless to brown) upon exposure to air. Therefore, all manipulations, including syntheses, were performed under oxygen- and moisture-free conditions requiring Schlenk-type glassware (flask), using both conventional standard Schlenk techniques interfaced to a high vacuum (10^{-2} Torr) on a double manifold vacuum line, and under an inert atmosphere of high purity dry nitrogen in a glovebox. All glassware were oven-dried at 120 ^{0}C for no less than of 12 h before use, then used immediately from the oven to avoid exposure to moisture.

Solvents were purified/dried and deoxygenated by an LC solvent purification system (hexane and PhMe), and by refluxing over and fresh distilled from sodium wire/benzophenone *ketyl* under nitrogen (tetrahydrofuran). After distillation solvents were stored in vacuum Schlenk flasks and degassed prior to use. The synthesis of the two sterically bulky formamidine proligands: XylFormH = N,N′-bis(2,6-dimethylphenyl)formamidine and DippFormH = N,N′-bis(2,6-diisopropylphenyl)formamidine, was according to a published procedure.[70,71] Anhydrous $AlMe_3$, $AlCl_3$, $AlBr_3$, AlI_3 and other starting materials such as lithium-/sodium-/potassium-bis(trimethylsilyl)amide and *n*-butyllithium, were purchased from Sigma Aldrich Chemical Co and used as received without further purification.

^{1}H- and ^{13}C-NMR spectra of air and moisture sensitive compounds were recorded by J.Young valve inert atmosphere NMR tubes protecting the sample from air at 25 ^{0}C on a Bruker AVANCE III HD 400 MHz spectrometer instrument. The chemical shifts are expressed in parts per million (ppm). ^{1}H-NMR resonances were referenced against residual H in C_6D_6 (δ = 7.15), whereas ^{13}C-NMR resonances were referenced to the deuterated C_6D_6 solvent (δ = 128.39). *Perdeutero*-benzene C_6D_6 (all ≥ 99 atom % D) was obtained from Sigma-Aldrich, pre-dried over sodium metal for 24 h, then distilled under an atmosphere of nitrogen before being stored in resealable greaseless Schlenk flasks and freeze-thaw degassed prior to use.

Infrared spectra were obtained from samples in Nujol mulls between NaCl plates, with a Nicolet-Nexus FTIR spectrophotometer within the range (ύ = 4000-400 cm^{-1}). Elemental analyses (C, H, N) were performed on single crystals by sending samples in sealed glass pipettes under nitrogen to the Microanalytical Laboratory Service, Science Centre, London Metropolitan University, England. Melting points were determined in sealed glass capillaries under nitrogen and are uncalibrated.

Synthesis of trivalent aluminium formamidinato (XylForm and DippForm) complexes by metalation reactions in THF or PhMe/hexane

[Al(XylForm)$_2$Cl] (4.1)

$LiN(SiMe_3)_2$ (1 M solution in THF, 2.0 ml, 2.0 mmol) was added dropwise to XylFormH (0.50 g, 2.0 mmol) in PhMe (20 ml), forming the solution of Li(XylForm). This solution was added dropwise through a cannula to a solution of $AlCl_3$ (0.13 g, 1.0 mmol) in PhMe (10 ml) at room temperature with stirring. The reaction mixture was stirred for 18 h to yield a yellow solution with a white precipitate of LiCl. Filtration and concentration to the point of incipient crystallisation, followed by cooling to − 30 ^{0}C overnight afforded a colorless crystalline sample of (**4.1**) suitable for X-ray diffraction structure determination. Yield = 0.20 g (40 %).

4.1: M.P. 172-174 ^{0}C (dec). ^{1}H-NMR (400 MHz, C_6D_6, 25 ^{0}C): δ (ppm) = 2.34 (s, 24H, C*H*$_3$), 6.91 (m, 4H, *p*-Ar*H*), 7.03 (m, 8H, *m*-Ar*H*), 8.95 (s, 2H, NC*(H)*N); ^{13}C-NMR (101 MHz, C_6D_6, 25 ^{0}C): δ (ppm) = 19.02 (*C*H$_3$), 125.26 (*p*-*C*), 133.86 (*m*-*C*), 136.75 (*o*-*C)*, 141.66 (N-*C*), 173.37 (N*C*N); Elemental analysis calcd. (%) for $C_{34}H_{38}AlClN_4$ (*M* = 565.18 g/mol): C 72.25, H 6.77, N 9.91; found: C 50.49, H 6.66, N 6.23 (significantly low C and N percentage). IR (υ/cm^{-1}, Nujol mull): 2727 (s), 2451 (m), 2352 (s), 2022 (m), 1933 (m), 1908 (s),1841 (s), 1772 (s), 1735 (w), 1651 (s), 1588 (s), 1557 (s), 1455 (s), 1377 (s), 1304 (m), 1260 (s), 1201 (s), 1150 (m), 1096 (m), 1024 (m), 972 (m), 888 (s), 803 (m), 771 (m), 758 (s), 722 (s), 662 (m), 620 (w).

[Al(XylForm)$_2$I].PhMe (4.2)

A solution of K(XylForm), prepared from XylFormH (0.50 g, 2.0 mmol) in PhMe (20 ml) and KN(SiMe$_3$)$_2$ (0.5 M solution in PhMe, 4 ml, 2.0 mmol) at room temperature, was added dropwise through a cannula to a solution of AlI$_3$ (0.41 g, 1.0 mmol) in PhMe (10 ml) at room temperature with stirring. The reaction mixture was continued stirring for 18 h to yield a yellow solution with a white precipitate of KI. Filtration, concentration and slow cooling to − 30 ^{0}C overnight of this solution deposited light yellow crystals of (**4.2**). Yield = 0.31 g (62 %).

4.2: M.P. 140-144 ^{0}C (dec). ^{1}H-NMR (400 MHz, C$_6$D$_6$, 25 ^{0}C): δ (ppm) = 2.15 (s, 3H, C*H*$_3$-PhMe), 2.32 (s, 24H, C*H*$_3$), 6.54 (m, 4H, *p*-Ar*H*), 6.75 (m, 8H, *m*-Ar*H*), 6.88 (m, 5H, Ar*H*-PhMe), 7.97 (s, 2H, NC(*H*)N); ^{13}C-NMR (101 MHz, C$_6$D$_6$, 25 ^{0}C): δ (ppm) = 18.41 (C*H*$_3$), 20.16 (*C*H$_3$, PhMe), 129.24 (*p*-*C*), 130.15 (*m*-*C*), 133.47 (*o*-*C)*, 134.53 (Ar*C*, PhMe), 136.22 (N-*C*), 159.36 (N*C*N); Elemental analysis calcd. (%) for C$_{41}$H$_{46}$AlIN$_4$ (*M* = 748.72 g/mol): C 65.78, H 6.19, N 7.48. Calcd (%) for C$_{34}$H$_{38}$AlIN$_4$ (656.58 g/mol after loss of PhMe solvation): C 62.19, H 5.83, N 8.53; found: C 34.22, H 5.04, N 4.81 (significantly low C and N percentage). IR (υ/cm^{-1}, Nujol mull): 2924 (s), 2411 (m), 2360 (s), 2335 (s), 2172 (w), 2023 (w), 1963 (s), 1871 (vs), 1785 (s), 1644 (s), 1462 (vs), 1376 (vs), 1257 (w), 1146 (w), 1022 (w), 917 (m), 892 (m), 835 (m), 720 (s), 625 (w).

[Al(XylFormH)Br$_3$] (4.3)

A solution of Na(XylForm), prepared from XylFormH (0.25 g, 1.0 mmol) in PhMe (20 ml) and NaN(SiMe$_3$)$_2$ (0.6 M solution in PhMe, 0.6 ml, 1.0 mmol), was added dropwise to a solution of AlBr$_3$ (0.27 g, 1.0 mmol) in PhMe (10 ml) at room temperature with stirring. The reaction mixture was continued stirring for 12 h to yield a yellow solution with a white precipitate of NaBr. Filtration, concentration and slow cooling to − 30 ^{0}C overnight of this solution leaving slightly unexpected white crystals of (**4.3**). Yield = 0.14 g (56 %).

4.3: M.P. 168-170 ^{0}C (dec). ^{1}H-NMR (400 MHz, C_6D_6, 25 ^{0}C): δ (ppm) = 2.29 (s, 12H, *C*H$_3$), 5.69 (d, *J* = 12 Hz, 1H, N*H*), 6.68 (br m, 2H, *p*-Ar*H*), 6.90 (br m, 4H, *m*-Ar*H*), 7.78 (d, *J* = 16 Hz, 1H, NC(*H*)N); ^{13}C-NMR (101 MHz, C_6D_6, 25 ^{0}C): δ (ppm) = 19.19 (*C*H$_3$), 129.29 (*p*-*C*), 130.18 (*m*-*C*), 133.33(*o*-*C*), 134.41 (N-*C*), 159.35 (N*C*N); Elemental analysis calcd. (%) for $C_{17}H_{19}AlBr_3N_2$ (*M* = 518.03 g/mol): C 39.41, H 3.69, N 5.40; found: C 39.28, H 5.01, N 5.42. IR (υ/cm^{-1}, Nujol mull): 3186 (w), 2727 (m), 2408 (w), 2347 (m), 2281 (w), 2201 (w), 2033 (m), 1956 (m), 1880 (m), 1778 (s), 1677 (w), 1642 (m), 1588 (m), 1454 (s), 1376 (s), 1305 (w), 1192 (s), 1090 (s), 946 (s), 892 (m), 828 (s),768 (s), 722 (s), 628 (w).

[Al$_3$(XylForm)$_2$(μ_3-O)(OH)Cl$_4$]$_2$.PhMe (4.4)

A solution of K(XylForm), prepared from XylFormH (0.75 g, 3.0 mmol) and KN(SiMe$_3$)$_2$ (0.5 M solution in PhMe, 6 ml, 3.0 mmol) in THF (30 ml), was added dropwise through a cannula to a solution of AlCl$_3$ (0.39 g, 3.0 mmol) in PhMe (30 ml) at room temperature with stirring. The reaction mixture was stirred for 18 h to yield a yellow solution with a white precipitate of KCl. Volatiles were removed under reduced pressure, and the residue dried to the point of dryness and extracted into PhMe (20 ml) to ensure the complete composition of KCl. Filtration, concentration and slow cooling to − 30 ^{0}C overnight deposited light white crystals of (**4.4**). Yield = 0.49 g (65 %).
4.4: M.P. 196-198 ^{0}C (dec). ^{1}H-NMR (400 MHz, C_6D_6, 25 ^{0}C): δ (ppm) = 0.41 (s, Al–O*H*), 2.24 (br m, 3H, C*H*$_3$-PhMe), 2.47 (br m, 24H, C*H*$_3$), 6.76 (m, 4H, *p*-ArH), 7.04 (m, 8H, *m*-Ar*H*), 7.25 (m, 5H, Ar*H*-PhMe), 8.19 (s, 2H, NC(*H*)N); ^{13}C-NMR (101 MHz, C_6D_6, 25 ^{0}C): δ (ppm) = 19.93 (*C*H$_3$), 21.43 (*C*H$_3$, PhMe), 129.23 (*p*-*C*), 133.54 (*m*-*C*), 134.39 (*o*-*C*), 137.10 (Ar*C*, PhMe), 139.81 (N-*C*), 172.49 (N*C*N) (partially obscured by resonances probably from the C_6D_6 impurities). Elemental analysis calcd. (%) for $C_{75}H_{86}Al_6Cl_8N_8O_4$ (*M* = 1609.0 g/mol): C 55.98, H 5.38, N 6.96. Calcd (%) for $C_{68}H_{78}Al_6Cl_8N_8O_4$ (1516.96 g/mol after loss of PhMe solvation): C 53.84, H 5.18, N 7.38; found: C 34.22, H 5.04, N 4.81 (significantly low C and N percentage).

IR (υ/cm^{-1}, Nujol mull): 2830 (w), 2730 (s), 2665 (w), 2468 (w), 2418 (vs), 2337 (s), 2280 (m), 2114 (m), 2055 (s), 2038 (s),1936 (s), 1875 (vs), 1857 (s),1781 (s), 1637 (s), 1596 (s), 1537 (m), 1439 (w), 1366 (w), 1257 (s), 1205 (s), 1169 (s), 1093 (s), 1020 (s), 987 (vs), 936 (s), 917 (vs), 891 (s), 846 (s),782 (w), 720 (m), 602 (s), 584 (s), 557 (s), 424 (w).

[Al(DippFormH)Br$_3$] (4.5)

A solution of Na(DippForm), prepared from DippFormH (1.08 g, 3.0 mmol) and NaN(SiMe$_3$)$_2$ (0.6 M solution in PhMe, 1.8 ml, 3.0 mmol) in PhMe (20 ml), was added dropwise through a cannula to a solution of AlBr$_3$ (0.81 g, 3.0 mmol) in PhMe (10 ml) at room temperature with stirring. The reaction mixture was continued stirring for 2 h to yield a yellow solution with a white precipitate of NaBr. Filtration, concentration under vacuum to the point of crystallisation *ca*.5 ml, and slow cooling to − 30 ^{0}C over 12 h gave pink-white crystals of (**4.5**). The single crystals were dried under vacuum after separated from the mother solution via syringe. Yield = 0.65 g (61 %).
4.5: M.P. 168-170 ^{0}C. ^{1}H-NMR (400 MHz, C$_6$D$_6$, 25 ^{0}C): δ (ppm) = 1.51 (d, J = 6.6 Hz, 24H, CH(C*H*$_3$)$_2$), 3.31 (sept, 4H, C*H*(CH$_3$)$_2$), 6.06 (d, J = 12 Hz, 1H, N*H*), 7.02 (br m, 2H, *p*-Ar*H*), 7.09 (br m, 4H, *m*-Ar*H*), 8.01 (d, J = 16 Hz, 1H, NC(*H*)N); ^{13}C-NMR (101 MHz, C$_6$D$_6$, 25 ^{0}C): δ (ppm) = 24.33 (*C*H$_3$-*i*Pr), 28.77 (*C*H-*i*Pr), 124.46 (*p*-*C*), 125.83 (*m*-*C*), 132.44 (*o*-*C*), 146.6 (N-*C*), 160.57 (N*C*N); Elemental analysis calcd. (%) for C$_{25}$H$_{36}$AlBr$_3$N$_2$ (M = 631.25 g/mol): C 47.56, H 5.74, N 4.43; found: C 43.10, H 7.25, N 4.17 (low in C and high in H percentage). IR (υ/cm^{-1}, Nujol mull): 2727 (m), 2665 (w), 2360 (s), 2340 (w), 1733 (s), 1646 (s), 1623 (s), 1506 (s), 1418 (s), 1339 (w), 1152 (m), 1095 (w), 934 (m), 835 (m), 776 (s), 721 (vs), 668 (vs).

[Al(DippForm)Cl_2(thf)] (4.6)

A solution of Li(DippForm), was prepared from DippFormH (0.36 g, 1.0 mmol) and *n*-BuLi (1.6 M solution in hexanes, 0.6 ml, 1.0 mmol) in THF (20 ml) at room temperature. After 2 h stirring, the solution was added dropwise through a cannula to a stirred solution of $AlCl_3$ (0.13 g, 1.0 mmol) in THF (10 ml) at 0 ^{0}C. The reaction mixture was continued stirring for 16 h. After 1 day the reaction mixture was dried under vacuum to the point of dryness and extracted into PhMe (20 ml), forming a precipitate of LiCl. Filtration and concentration to the point of incipient crystallisation, followed by cooling − 30 ^{0}C overnight afforded a white crystalline sample of (**4.6**) suitable for X-ray diffraction. Yield = 0.15 g (42 %).

4.6: M.P. 160-162 ^{0}C; ^{1}H-NMR (400 MHz, C_6D_6, 25 ^{0}C): δ (ppm) = 1.03 (br m, 4H, C*H*$_2$-thf), 1.25 (d, *J* = 6.9 Hz, 24H, CH(C*H*$_3$)$_2$), 3.56 (br m, 4H, OC*H*$_2$-thf), 3.77 (sept, 4H, C*H*(CH$_3$)$_2$), 6.99 (br m, 2H, *p*-Ar*H*), 7.10 (br m 4H, *m*-Ar*H*), 7.50 (s, 1H, NC(*H*)N); ^{13}C-NMR (101 MHz, C_6D_6, 25 ^{0}C): δ (ppm) = 24.12 (*C*H$_2$-thf), 24.55 (*C*H$_3$-*i*Pr), 28.05 (*C*H-*i*Pr), 70.46 (O*C*H$_2$-thf), 123.48 (*p*-*C*), 125.93 (*m*-*C*), 139.69 (*o*-*C*), 145.45 (N-*C*), 166.36 (N*C*N); Elemental analysis calcd. (%) for $C_{29}H_{44}AlCl_2N_2O$ (*M* = 534.56 g/mol): C 65.15, H 8.29, N 5.24. Calcd for $C_{27}H_{40}AlCl_2N_2O$ (506.50 g/mol after lost ½ of thf solvation) C 64.02, H 7.96, N 5.53. Found: C 64.55, H 7.90, N 5.36. IR (υ/cm^{-1}, Nujol mull): 2928 (w), 2721 (s), 2636 (m), 2504 (s), 2415 (s), 2379 (s), 2294 (s), 2223 (w), 2040 (s), 1993 (s), 1870 (s), 1799 (s), 1639 (s), 1555 (m), 1459 (m), 1383 (m), 1259 (w), 1104 (s), 1057 (w), 924 (m), 802 (s), 757 (s), 668 (w), 592 (s), 566 (s).

[Al(DippForm)ClBr(thf)] (4.7)

A solution of Li(DippForm), prepared from DippFormH (0.36 g, 1.0 mmol) and *n*-BuLi (1.6 M solution in hexanes, 0.6 ml, 1.0 mmol) in THF (20 ml), was added dropwise through a cannula to a solution of $AlBr_3$ (0.135 g, 0.5 mmol) and $AlCl_3$ (0.065 g, 0.5 mmol) in THF (10 ml) at room temperature with stirring. The colourless reaction mixture was continued stirring for 16 h at ambient temperature. The solvent was evaporated under vacuum to the point of dryness and PhMe (20 ml) added. The mixture was then filtered to remove LiCl. The solvent was then concentrated under reduced pressure, then slowly cooled to –30 ^{0}C, whereupon colourless crystals of (**4.7**) were deposited. Yield = 0.14 g (40 %).

4.7: M.P. 158-160 ^{0}C (dec). ^{1}H-NMR (400 MHz, C_6D_6, 25 ^{0}C): δ (ppm) = 1.02 (br m, 4H, C*H*$_2$-thf), 1.26 (d, *J* = 6.8 Hz, 24H, CH(C*H*$_3$)$_2$), 3.54 (br m, 4H, OC*H*$_2$-thf), 3.80 (sept, 4H, C*H*(CH$_3$)$_2$), 7.01 (br m, 2H, *p*-Ar*H*), 7.11 (br m 4H, *m*-Ar*H*), 7.53 (s, 1H, NC(*H*)N); ^{13}C-NMR (101 MHz, C_6D_6, 25 ^{0}C): δ (ppm) = 24.58 (*C*H$_2$-thf), 24.89 (*C*H$_3$-*i*Pr), 28.26 (*C*H-*i*Pr), 70.27 (O*C*H$_2$-thf), 123.73 (*p*-*C*), 125.97 (*m*-*C*), 139.83 (*o*-*C*), 144.64 (N-*C*), 165.47 (N*C*N); Elemental analysis calcd. (%) for $C_{29}H_{44}AlBrClN_2O$ (*M* = 579.01 g/mol): C 60.15, H 7.65, N 4.83. Calcd for $C_{27}H_{40}AlBrClN_2O$ (550.95 g/mol after lost ½ of thf solvation) C 58.86, H 7.31, N 5.08. Found: C 58.44, H 7.02, N 4.71. IR (υ/cm^{-1}, Nujol mull): 2721 (s), 2662 (s), 2611 (m), 2504 (s), 2414 (s), 2357 (s), 2293 (s), 2245 (s), 2221 (m), 2169 (s), 2035 (vs), 1993 (vs), 1934 (s), 1867 (vs), 1799 (vs), 1658 (s), 1640 (s), 1436 (w), 1289 (w), 1105 (s), 921 (m), 803 (s), 770 (s), 665 (w), 556 (s), 406 (w).

[Al(DippForm)$_2$Cl] (4.8)

Li(DippForm) was prepared from DippFormH (0.72 g, 2.0 mmol) and LiN(SiMe$_3$)$_2$ (1 M solution in thf, 2.0 ml, 2.0 mmol) in THF (20 ml) at room temperature. This solution was added dropwise via a cannula to a solution of AlCl$_3$ (0.13 g, 1.0 mmol) in THF (10 ml) at room temperature with stirring. The reaction mixture was subsequently continued stirring over the course of 24 h, and after that dried in vacuum and extracted into PhMe (25 ml). Filtration, concentration to approximately (10 ml) and storage at – 30 ^{0}C for 48 h yielded light off white blocks of (**4.8**) on the glass wall of the flask. Yield = 0.51 g (70 %).

4.8: M.P. 208-210 ^{0}C (dec). ^{1}H-NMR (400 MHz, C$_6$D$_6$, 25 ^{0}C): δ (ppm) = 1.48 (d, J = 6.7 Hz, 48H, CH(C*H*$_3$)$_2$), 3.51 (sept, 8H, C*H*(CH$_3$)$_2$), 6.98 (m, 4H, *p*-Ar*H*), 7.10 (m, 8H, *m*-Ar*H*), 7.85 (s, 2H, NC(*H*)N); ^{13}C-NMR (101 MHz, C$_6$D$_6$, 25 ^{0}C): δ (ppm) = 23.66 (*C*H$_3$-*i*Pr), 28.66 (*C*H-*i*Pr), 24.5 (*p*-*C*), 125.7 (*m*-*C*), 139.3 (*o*-*C*), 144,8 (N-*C*), 160.40 (N*C*N); Elemental analysis calcd. (%) for C$_{50}$H$_{70}$AlClN$_4$ (*M* = 789.56 g/mol): C 76.06, H 8.93, N 7.09; found: C 75.35, H 8.76, N 6.66. IR (υ/cm^{-1}, Nujol mull): 2923 (w), 2757 (s), 2593 (m), 2464 (w), 2361 (w), 2024 (m), 1959 (s), 1887 (s), 1813 (s), 1641 (m), 1586 (s), 1381 (w), 1058 (w), 980 (w), 756 (s), 580 (w).

[Me$_2$Sb-SbMe$_3$][AlCl$_4$] (4.9)

To a solution of SbCl$_3$ (0.66 g, 3.0 mmol) in PhMe (10 ml) was added a solution of AlMe$_3$ (2 M in PhMe, 1.5 ml, 3.0 mmol) dropwise by syringe under a nitrogen stream without stirring at − 78 ^{0}C. The resulting colourless reaction mixture was allowed to warm to ambient temperature and stirred very slowly for half an hour. Upon concentration to *ca*. 5 ml an oily dark layer deposited with a clear white supernatant on top. The supernatant was removed followed by extraction of the black oily residue with hexane (5 ml). The hexane extract was then concentrated to (3 ml) and allowed to rest at ambient temperatures for 1 day; after which a few colourless crystals of (**4.9**) formed. Yield = 0.08 g (8 %).

4.9: M.P. 120–123 ^{0}C (smooth decomposition starts at 211 ^{0}C). ^{1}H-NMR (400 MHz, C_6D_6, 25 ^{0}C): δ (ppm) = 1.15 (s, Sb(CH_3)$_3$), 1.02 (s, Sb(CH_3)$_2$). No ^{13}C-NMR could be obtained due to the poor yield. Elemental analysis calcd. (%) for $C_5H_{15}AlCl_4Sb_2$ (M = 847.47 g/mol): C 7.08, H 17.84 (very low yield). IR (υ/cm^{-1}, Nujol mull): 2959 (m), 2923 (s), 2853 (s), 2725 (m), 2668 (w), 2349 (s), 1630 (w), 1461 (s), 1376 (s), 1304 (w), 1262 (s), 1163 (w), 1094 (m), 1020 (m), 899 (w), 805 (s), 726 (s), 716 (s), 676 (m), 400 (w).

[Br_3Sb-μBr-$SbBr_3$][$AlCl_2(thf)_4$] (4.10)

To a solution of $SbBr_3$ (0.36 g, 1.0 mmol) in PhMe (10 ml), was added dropwise through a cannula a mixture of DippFormH (0.36 g, 1.0 mmol) and $AlCl_3$ (0.13 g, 1.0 mmol) in THF (10 ml) at room temperature with stirring, as an attempt to exam the possibility of forming a bimetallic formamidinate complex. The reaction mixture was continued stirring for 12 h. The residue was extracted with hexane (20 ml). Filtration and solvent evaporation then slow cooling to – 30 ^{0}C of this solution, produced very shiny cubic crystals of (**4.10**). Yield = 0.17 g (48 %).

4.10: M.P. 184-186 ^{0}C (dec). ^{1}H-NMR (400 MHz, C_6D_6, 25 ^{0}C): δ (ppm) = 1.32 (s, 16H, CH_2-thf), 3.43 (s, 16H, OCH_2-thf); ^{13}C-NMR (101 MHz, C_6D_6, 25 ^{0}C): δ (ppm) = 25.66 (*C*H_2-thf), 67.81 (O*C*H_2-thf); Elemental analysis calcd. (%) for $C_{16}H_{32}AlCl_2Br_7O_4Sb_2$ (M = 1189.09 g/mol): C 16.16, H 2.71. Calcd for $C_2H_4AlCl_2Br_7Sb_2$ (928.75 g/mol after lost 3½ of thf solvation) C 2.58, H 4.34. Found: C 3.77, H 1.92 (slightly high in C and low in H percentage). IR (υ/cm^{-1}, Nujol mull): 2360 (s), 2340 (s), 1772 (s), 1646 (s), 1569 (s), 1507 (s), 1418 (s), 1395 (s), 1257 (m), 1092 (w), 806 (w), 668 (m).

4.6 *Single crystal X-ray structure determination/analysis and Refinement model description*

Crystals were initially isolated as suitable single crystals immersed in viscous hydrocarbon oil (Paratone-N) and mounted on a glass fibre that was placed on the diffractometer under a stream of liquid nitrogen. Crystalline samples were measured providing intensity data on either a Bruker APEX II CCD diffractometer for complexes (**4.1**, **4.8**, **4.10**), or at the Australian Synchrotron diffractometer using the MX1 or MX2 macromolecular beam lines for complexes (**4.2**, **4.3**, **4.4**, **4.5**, **4.6**, **4.7**, **4.9**) at 173 or 293 K using graphite monochromated Mo-Kα X-ray radiation with a single wavelength (λ = 0.71073 Å). Structure solutions and refinements package were performed using SHELXS-97 and SHELXL- 97,[72,73] program using Direct Methods via the graphical interface X-Seed,[74] and OLEX2,[75] both of which were also used for figures' generating. Absorption improvements using MULTISCAN were applied. All CIF files were checked at www.iucr.org. A summary of crystallographic data and collection parameters can be found for each compound below.

[Al(XylForm)$_2$Cl] (4.1)

1: $C_{34}H_{38}AlClN_4$ (M = 565.11 g/mol): monoclinic, space group $P2_1/c$, a = 8.0280(16) Å, b = 8.5240(17) Å, c = 44.624(9) Å, α = 90°, β = 92.20(3)°, γ = 90°, *Volume* = 3051.4(11) Å^3, Z = 4, T = 100(2) K, μ = 0.184 mm^{-1}, D_{calc} = 1.230 g/cm^3, F $_{(000)}$ = 1200.0, $2\Theta_{max}$ = 1.826 - 49.998, 35848 reflections measured, 5120 unique (R_{int} = 0.0477, R_{sigma} = 0.0244), 5120/0/370 parameters, GooF on F^2 1.198, The final R_1 was 0.0588 (I >2σ (I)) and wR_2 was 0.1568 (all data), Largest diff. peak/hole/e = 0.54 to - 0.51 Å^{-3}.

[Al(XylForm)$_2$I].PhMe (4.2)

2: $C_{41}H_{46}AlIN_4$ (M = 748.70 g/mol): triclinic, space group *P-1*, a = 8.2260(16) Å, b = 15.064(3) Å, c = 15.169(3) Å, α = 93.96(3)°, β 96.63(3)°, γ = 96.34(3)°, *Volume* = 1849.3(7) Å^3, Z = 2, T = 100(2) K, μ = 0.923 mm^{-1}, D_{calc} = 1.345 g/cm^3, F $_{(000)}$ = 772.0, $2\Theta_{max}$ = 2.712 - 49.998, 22141 reflections measured, 5936 unique (R_{int} = 0.0338, R_{sigma} = 0.0292), 5936/0/434 parameters, GooF on F^2 1.064, The final R_1 was 0.0273 (I >2σ (I)) and wR_2 was 0.0748 (all data), Largest diff. peak/hole/e = 0.45 to - 0.69 Å^{-3}.

[Al(XylFormH)Br$_3$] (4.3)

3: $C_{17}H_{20}AlBr_3N_2$ (M = 519.06 g/mol): monoclinic, space group $P2_1/n$, a = 7.7260(15) Å, b = 14.013(3) Å, c = 18.307(4) Å, α = 90°, β 93.93(3)°, γ = 90°, *Volume* = 1977.3(7) Å^3, Z = 4, T = 100(2) K, μ = 6.165 mm^{-1}, D_{calc} = 1.744 g/cm^3, F $_{(000)}$ = 1016.0, $2\Theta_{max}$ = 3.664 - 49.998, 15215 reflections measured, 3240 unique (R_{int} = 0.0572, R_{sigma} = 0.0439), 3240/0/212 parameters, GooF on F^2 1.071, The final R_1 was 0.0348 (I >2σ (I)) and wR_2 was 0.0970 (all data), Largest diff. peak/hole/e = 0.52 to -0.98 Å^{-3}.

[Al$_3$(XylForm)$_2$(μ_3-O)(OH)Cl$_4$]$_2$.PhMe (4.4)

4: $C_{75}H_{86}Al_6Cl_8N_8O_4$ (M = 1609.0 g/mol): triclinic, space group $P\text{-}1$, a = 10.906(2) Å, b = 12.427(3) Å, c = 16.934(3) Å, α = 87.83(3)°, β = 72.56(3)°, γ = 67.89(3)°, *Volume* = 2021.2(9) Å^3, Z = 2, T = 100(2) K, μ = 0.396 mm^{-1}, D_{calc} = 1.322 g/cm^3, F $_{(000)}$ = 838.0, $2\Theta_{max}$ = 2.53 - 50, 17460 reflections measured, 6653 unique (R_{int} = 0.0926, R_{sigma} = 0.1001), 6653/6/463 parameters, GooF on F^2 1.040, The final R_1 was 0.0846 (I >2σ (I)) and wR_2 was 0.2590 (all data), Largest diff. peak/hole/e = 0.53 to - 1.41 Å^{-3}.

[Al(DippFormH)Br$_3$] (4.5)

5: $C_{25}H_{36}AlBr_3N_2$ (M = 631.27 g/mol): monoclinic, space group $P2_1/c$, a = 10.278(2) Å, b = 19.974(4) Å, c = 14.178(3) Å, α = 90°, β = 108.59(3) °, γ = 90°, *Volume* = 2758.7(11) Å^3, Z = 4, T = 100(2) K, μ = 4.434 mm^{-1}, D_{calc} = 1.520 g/cm^3, F $_{(000)}$ = 1272.0, $2\Theta_{max}$ = 3.652 - 49.998, 27489 reflections measured, 4822 unique (R_{int} = 0.0384, R_{sigma} = 0.0252), 4822/0/289 parameters, GooF on F^2 1.081, The final R_1 was 0.0385 (I >2σ (I)) and wR_2 was 0.1015 (all data), Largest diff. peak/hole/e = 1.71 to -1.29 Å^{-3}.

[Al(DippForm)Cl_2(thf)] (4.6)

6: $C_{29}H_{43}AlCl_2N_2O$ (M = 533.53 g/mol): triclinic, space group *P-1*, a = 10.3175(4) Å, b = 10.7120(4) Å, c = 14.7854(5) Å, α = 91.983(2)°, β = 98.268(2)°, γ = 103.631(2)°, *Volume* = 1567.57(10) $Å^3$, Z = 2, T = 296(2) K, μ = 0.257 mm^{-1}, D_{calc} = 1.130 g/cm^3, $F_{(000)}$ = 572.0, $2\Theta_{max}$ = 2.79 - 49.996, 15311 reflections measured, 5297 unique (R_{int} = 0.0408, R_{sigma} = 0.0350), 5297/0/324 parameters, GooF on F^2 1.052, The final R_1 was 0.0821 (I >2σ (I)) and wR_2 was 0.2880 (all data), Largest diff. peak/hole/e = 0.42 and - 0.94 $Å^{-3}$.

[Al(DippForm)ClBr(thf)] (4.7)

7: $C_{29}H_{43}AlBrClN_2O$ (M = 577.99 g/mol): triclinic, space group *P-1*, a = 10.222(2) Å, b = 10.720(2) Å, c = 14.529(3) Å, α = 91.85(3)°, β = 98.80(3)°, γ = 104.04(3)°, *Volume* = 1522.3(6) $Å^3$, Z = 2, T = 173(2) K, μ = 1.490 mm^{-1}, D_{calc} = 1.261 g/cm^3, $F_{(000)}$ = 608.0, $2\Theta_{max}$ = 4.166 - 50, 18551 reflections measured, 4871 unique (R_{int} = 0.0297, R_{sigma} = 0.0256), 4871/0/318 parameters, GooF on F^2 1.111, The final R_1 was 0.0674 (I >2σ (I)) and wR_2 was 0.2007 (all data), Largest diff. peak/hole/e = 1.27 to -1.64 $Å^{-3}$.

[Al(DippForm)$_2$Cl] (4.8)

8: $C_{50}H_{70}AlClN_4$ (M = 789.53 g/mol): monoclinic, space group $P2_1/n$, a = 14.509(3) Å, b = 16.288(3) Å, c = 21.112(4) Å, α = 90°, β = 109.86(3)°, γ = 90°, *Volume* = 4692.6(18) $Å^3$, Z = 4, T = 100(2) K, μ = 0.137 mm^{-1}, D_{calc} = 1.118 g/cm^3, $F_{(000)}$ = 1712.0, $2\Theta_{max}$ = 2.992 - 49.994, 56762 reflections measured, 8217 unique (R_{int} = 0.0369, R_{sigma} = 0.0199), 8217/0/521 parameters, GooF on F^2 1.118, The final R_1 was 0.0491 (I >2σ (I)) and wR_2 was 0.1249 (all data), Largest diff. peak/hole/e = 0.72 to -0.57 $Å^{-3}$.

[Me_2Sb-$SbMe_3$][$AlCl_4$] (4.9)

9: $C_5H_{15}AlCl_4Sb_2$ (M = 487.45 g/mol): monoclinic, space group $P2_1/c$, a = 9.1410(9) Å, b = 10.0801(10) Å, c = 17.3566(17) Å, α = 90°, β = 96.993(4)°, γ = 90°, *Volume* = 1587.4(3) Å^3, Z = 4, T = 296(2) K, μ = 4.094 mm^{-1}, D_{calc} = 2.040 g/cm^3, F $_{(000)}$ = 912.0, $2\Theta_{max}$ = 4.49 to 54.998, 18644 reflections measured, 3644 unique (R_{int} = 0.0519, R_{sigma} = 0.0393), 3644/0/114 parameters, GooF on F^2 1.033, The final R_1 was 0.0334 (I >2σ (I)) and wR_2 was 0.0950 (all data), Largest diff. peak/hole/e = 1.03 to -0.86 Å^{-3}.

[Br_3Sb-μBr-$SbBr_3$][$AlCl_2(thf)_4$] (4.10)

Note. X-ray diffraction data has been included as confirmation of connectivity only.

10: $C_{16}H_{32}AlCl_2Br_7O_4Sb_2$ (M = 1189.09 g/mol): triclinic, space group $P\text{-}1$, a = 23.604(5) Å, b = 33.287(7) Å, c = 23.911(5) Å, α = 89.97(3)°, β = 105.23(3)°, γ = 89.97(3)°, *Volume* = 18127(7) Å^3, Z = 2, T = N/A K, μ = 9.214 mm^{-1}, D_{calc} = 2.2220 g/cm^3, F $_{(000)}$ = 10966.8, $2\Theta_{max}$ = 1.76 to 52.74, 173092 reflections measured, 67470 unique (R_{int} = 0.0539, R_{sigma} = 0.0649), 67470/0/3286 parameters, GooF on F^2 1.735, The final R_1 was 0.2527 (I >2σ (I)) and wR_2 was 0.6352 (all data), Largest diff. peak/hole/e = 61.76 to - 13.50Å^{-3}.

4.7 *References*

1. S. Dagorne, R. F. Jordan and V. G. Young, *Organometallics.*, 1999, **18**, 4619-4623.
2. A. Hilger, J.-P. Gisselbrecht, R. R. Tykwinski, C. Boudon, M. Schreiber, R. E. Martin, H. P. Lüthi, M. Gross and F. Diederich, *J. Am. Chem. Soc.*, 1997, **119**, 2069-2078.
3. D. Abeysekera, K. N. Robertson, T. S. Cameron and J. A. C. Clyburne, *Organometallics.*, 2001, **20**, 5532-5536.
4. F. T. Edelmann, *Coord. Chem. Rev.*, 1994, **137**, 403-481.
5. J. Barker and M. Kilner, *Coord. Chem. Rev.*, 1994, **133**, 219-300.
6. R. T. Boere, M. L. Cole and P. C. Junk, *New J. Chem.*, 2005, **29**, 128-134.
7. J. A. R. Schmidt and J. Arnold, *Organometallics.*, 2002, **21**, 2306-2313.
8. S. Dagorne, I. A. Guzei, M. P. Coles and R. F. Jordan, *J. Am. Chem.Soc.*, 2000, **122**, 274-289.
9. G. Talarico and P. H. M. Budzelaar, *Organometallics.*, 2000, **19**, 5691-5695.
10. M. P. Coles, D. C. Swenson and R. F. Jordan, *Organometallics.*, 1998, **17**, 4042-4048.
11. M. P. Coles, D. C. Swenson and R. F. Jordan, *Organometallics.*, 1997, **16**, 5183-5194.
12. J. Barker, N. C. Blacker, P. R. Phillips, N. W. Alcock, W. Errington and M. G. H. Wallbridge, *J. Chem. Soc., Dalton Trans.*, 1996, 431-437.
13. S. Hamidi, H. M. Dietrich, D. Werner, L. N. Jende, C. Maichle-Mössmer, K. W. Törnroos, G. B. Deacon, P. C. Junk and R. Anwander, *Eur. J. Inorg. Chem.*, **2013**, 2460-2466.
14. D. H. Mayo, Y. Peng, P. Zavalij, K. H. Bowen and B. W. Eichhorn, *Acta Crystallogr. Sect. C: Cryst. Struct. Commun.*, 2013, **69**, 1120-1123.
15. M. L. Cole and P. C. Junk, *Z. Anorg. Allg. Chem.*, 2015, **641**, 2233-2244.
16. R. Duchateau, A. Meetsma and J. H. Teuben, *Chem. Commun.*, 1996, 223-224.
17. A.-H. Gao, W. Yao, Y. Mu, W. Gao, M.-T. Sun and Q. Su, *Polyhedron.*, 2009, **28**, 2605-2610.

18. S. Hamidi, L. N. Jende, H. M. Dietrich, C. Maichle-Mössmer, K. W. Törnroos, G. B. Deacon, P. C. Junk and R. Anwander, *Organometallics.*, 2013, **32**, 1209-1223.
19. M. Zimmermann, F. Estler, E. Herdtweck, K. W. Törnroos and R. Anwander, *Organometallics.*, 2007, **26**, 6029-6041.
20. Q. Knijnenburg, J. M. M. Smits and P. H. M. Budzelaar, *Organometallics.*, 2006, **25**, 1036-1046.
21. M. Bruce, V. C. Gibson, C. Redshaw, G. A. Solan, A. J. P. White and D. J. Williams, *Chem. Commun.*, 1998, 2523-2524.
22. A. Kuczkowski, A. Kuczkowski, S. Heimann, A. Weber and S. Schulz, *Organometallics.*, 2011, **30**, 4730-4735.
23. P. C. Junk and M. L. Cole, *Chem. Commun.*, 2007, 1579-1590.
24. G. Bai, S. Singh, H. W. Roesky, M. Noltemeyer and H.-G. Schmidt, *J. Am. Chem. Soc.*, 2005, **127**, 3449-3455.
25. H. Zhu, J. Chai, C. He, G. Bai, H. W. Roesky, V. Jancik, H.-G. Schmidt and M. Noltemeyer, *Organometallics.*, 2005, **24**, 380-384.
26. C. Jones, P. C. Junk, M. Kloth, K. M. Proctor and A. Stasch, *Polyhedron.*, 2006, **25**, 1592-1600.
27. E. Le Roux, F. Nief, F. Jaroschik, K. W. Tornroos and R. Anwander, *Dalton Trans.*, 2007, 4866-4870.
28. M. Zimmermann, W. Törnroos Karl and R. Anwander, *Angew. Chem. Int. Ed.*, 2008, **47**, 775-778.
29. M. Zimmermann, W. Törnroos Karl , H. Sitzmann and R. Anwander, *Chem. Eur. J.*, 2008, **14**, 7266-7277.
30. D. Robert, P. Spaniol Thomas and J. Okuda, *Eur. J. Inorg. Chem.*, 2008, 2801-2809.
31. M. Zimmermann, J. Volbeda, K. W. Törnroos and R. Anwander, *C. R. Chim.*, 2010, **13**, 651-660.
32. C. N. Rowley, G. A. DiLabio and S. T. Barry, *Inorg. Chem.*, 2005, **44**, 1983-1991.
33. R. J. Keaton, L. A. Koterwas, J. C. Fettinger and L. R. Sita, *J. Am. Chem. Soc.*, 2002, **124**, 5932-5933.

34. L. A. Lesikar and A. F. Richards, *Polyhedron.*, 2010, **29**, 1411-1422.
35. M. L. Cole, C. Jones, P. C. Junk, M. Kloth and A. Stasch, *Chem. Eur. J.*, 2005, **11**, 4482-4491.
36. A. L. Brazeau, G. A. DiLabio, K. A. Kreisel, W. Monillas, G. P. A. Yap and S. T. Barry, *Dalton Trans.*, 2007, 3297-3304.
37. A. P. Kenney, G. P. A. Yap, D. S. Richeson and S. T. Barry, *Inorg. Chem.*, 2005, **44**, 2926-2933.
38. M. P. Coles, D. C. Swenson, R. F. Jordan and V. G. Young, *Organometallics.*, 1997, **16**, 5183-5194.
39. S. J. Bonyhady, D. Collis, G. Frenking, N. Holzmann, C. Jones and A. Stasch, *Nat. Chem.*, 2010, **2**, 865-869.
40. R. T. Boere, V. Klassen and G. Wolmershauser, *J. Chem. Soc., Dalton Trans.*, 1998, 4147-4154.
41. M. L. H. Green and P. L. I. Nagy, *Adv. Organomet. Chem.*, eds. F. G. A. Stone and R. West, Academic Press, 1965, **2**, 325-363.
42. Z. Jiang, L. V. Interrante, D. Kwon, F. S. Tham and R. Kullnig, *Inorg. Chem.*, 1992, **31**, 4815-4822.
43. Z. Jiang and L. V. Interrante, *Chem. Mater.*, 1990, **2**, 439-446.
44. F. C. Sauls and L. V. Interrante, *Coord. Chem. Rev.*, 1993, **128**, 193-207.
45. K. M. Waggoner and P. P. Power, *J. Am. Chem. Soc.*, 1991, **113**, 3385-3393.
46. M. M. Olmstead, W. J. Grigsby, D. R. Chacon, T. Hascall and P. P. Power, *Inorg. Chim. Acta.*, 1996, **251**, 273-284.
47. G. Anantharaman, V. Chandrasekhar, M. G. Walawalkar, H. W. Roesky, D. Vidovic, J. Magull and M. Noltemeyer, *Dalton Trans.*, 2004, 1271-1275.
48. S. Jana, R. Fröhlich and W. Mitzel Norbert, *Chem. Eur. J.*, 2005, **12**, 592-599.
49. R. D. Shannon, *Acta Crystallogr., Sect. B: Struct. Crystallogr. Cryst. Chem.*, 1969, **25**, 925-946.
50. G. Wilke and H. Müller, *Justus Liebigs Ann. Chem.*, 1960, **629**, 222-240.
51. R. Benn, A. Rufińska, H. Lehmkuhl, E. Janssen and C. Krüger, *Angew. Chem. Int. Ed.*, 1983, **22**, 779-780.

52. B. Lyhs, S. Schulz, U. Westphal, D. Bläser, R. Boese and M. Bolte, *Eur. J. Inorg. Chem.*, 2009, 2247-2253.
53. B. Lyhs, D. Bläser, C. Wölper and S. Schulz, *Chem. Eur. J.*, 2011, **17**, 4914-4920.
54. M. Brym, C. M. Forsyth, C. Jones, P. C. Junk, R. P. Rose, A. Stasch and D. R. Turner, *Dalton Trans.*, 2007, 3282-3288.
55. P. Pyykkö and M. Atsumi, *Chem. Eur. J.*, 2009, **15**, 12770-12779.
56. M. Mantina, A. C. Chamberlin, R. Valero, C. J. Cramer and D. G. Truhlar, *J. Phys. Chem.*, 2009, **113**, 5806-5812.
57. K. Wiesler and N. Korber, *Polyhedron.*, 2005, **24**, 1565-1568.
58. J. Breunig Hans, M. Denker and E. Lork, *Angew. Chem. Int. Ed.*, 1996, **35**, 1005-1006.
59. H. Althaus, H. J. Breunig and E. Lork, *Chem. Commun.*, 1999, 1971-1972.
60. C. Hering, M. Lehmann, A. Schulz and A. Villinger, *Inorg. Chem.*, 2012, **51**, 8212-8224.
61. A. J. Ashe, E. G. Ludwig, J. Oleksyszyn and J. C. Huffman, *Organometallics.*, 1984, **3**, 337-338.
62. G. Becker, H. Freudenblum and C. Witthauer, *Z. Anorg. Allg. Chem.*, 1982, **492**, 37-51.
63. H. J. Breunig, M. Denker and K. H. Ebert, *J. Chem. Soc., Chem. Commun.*, 1994, 875-876.
64. H. J. Breunig, M. Denker, R. E. Schulz and E. Lork, *Z. Anorg. Allg. Chem.*, 1999, **624**, 81-84.
65. H. J. Breunig, I. Ghesner, M. E. Ghesner and E. Lork, *J. Organomet. Chem.*, 2003, **677**, 15-20.
66. W. Clegg, M. R. J. Elsegood, V. Graham, N. C. Norman, N. L. Pickett and K. Tavakkoli, *J. Chem. Soc., Dalton Trans.*, 1994, 1743-1751.
67. A. Piecha, R. Jakubas, A. Pietraszko and J. Baran, *J. Mol. Struct.*, 2007, **844-845**, 132-139.
68. A. Piecha, A. Białońska, R. Jakubas and W. Medycki, *Solid State Sci.*, 2008, **10**, 1469-1479.

69. M. Wojciechowska, P. Szklarz, A. Bialonska, J. Baran, R. Janicki, W. Medycki, P. Durlak, A. Piecha-Bisiorek and R. Jakubas, *CrystEngComm*, 2016, **18**, 6184-6194.
70. R. M. Roberts, *J. Org. Chem.*, 1949, **14**, 277-284.
71. K. M. Kuhn and R. H. Grubbs., *Org. lett.*, 2008, **10**, 2075-2078.
72. G. M. Sheldrick, *Acta Crystallogr. Sect. C: Cryst. Struct. Chem.*, 2015, **71**, 3-8.
73. G. M. Sheldrick, *SHELXS-97 and SHELXL-97*, 1997.
74. L. J. Barbour, *J. Supramol. Chem.*, 2001, **1**, 189-191.
75. O. V. Dolomanov, L. J. Bourhis, R. J. Gildea, J. A. K. Howard and H. Puschmann, *J. Appl. Crystallogr.*, 2009, **42**, 339-341.

APPENDICES

A0.1: General Experimental Information. The complexes described in the appendices own highly air- and moisture-sensitive nature, an inert atmosphere of dry nitrogen had to be maintained throughout the reaction and subsequent characterisation steps, requiring a glovebox and Schlenk techniques. All solvents were per-dried over sodium metal, and then further dried by distillation over sodium wire/benzophenone. Anhydrous $SbCl_3$ and $AlCl_3$ along with other starting materials such as $LiN(SiMe_3)_2$ and phenol ligand (2,6-di–*tert*-butyl-4-Me) were procured from Sigma-Aldrich and were used as supplied without further purification although in the case of the phenol, it was essential for this to be dried. Microanalytical Laboratory service, Science Centre, London Metropolitan University, England, performed the elemental analyses (C,H,N). Listed infrared data using a Nicolet-Nexus FTIR spectrometer, are of a Nujol mull for the region ($\acute{\upsilon}$ = 4000 - 400 cm^{-1}). ^1H- and ^{13}C-NMR spectra were recorded on a Bruker AVANCE III HD 400 MHz spectrometer. ^1H-NMR resonances were referenced against residual H in C_6D_6 (δ = 7.15), whereas ^{13}C-NMR resonances were referenced to the deuterated C_6D_6 solvent (δ = 128.39). X-ray structure determinations were performed on either a Bruker APEX II CCD diffractometer or at the Australian Synchrotron diffractometer using the MX1 macromolecular beam lines. Further details regarding general considerations were described in Chapter two (experiment section 2.5), Chapter three (experiment section 3.5) and Chapter four (experiment section 4.5).

APPENDIX 1

The Synthesis and X-ray Structure Determination of [Sb(OC$_6$H$_2$-2,6-*t*Bu$_2$-4-Me)$_3$]

A1.1: Introduction. The homoleptic mononuclear phenolates of antimony are extremely rare, being limited to just [Sb(OC$_6$H$_3$-2,6-Me$_2$)$_3$],[1] and [Sb{OC$_6$H$_3$-2,6-(C$_6$H$_5$)$_2$}$_3$],[2] representing the phenols with sterically demanding 2,6-substituents. This study presents only the third example of homoleptic, mononuclear antimony (III) phenolate to be structurally characterised as [Sb(OAr)$_3$] (OAr = OC$_6$H$_2$-2,6-*t*Bu$_2$-4-Me).

A1.2: Synthesis of [Sb(OC$_6$H$_2$-2,6-*t*Bu$_2$-4-Me)$_3$] by metathesis in THF/PhMe and Characterisation by ^{1}H-, ^{13}C-NMR, IR spectroscopy, C,H,N analysis and melting point. A solution of HOAr (0.66 g, 3.0 mmol) in THF (20 ml) was treated successively with LiN(SiMe$_3$)$_2$ (1 M solution in THF, 3.0 ml, 3.0 mmol). The solution of Li(OAr) was added dropwise to a Schlenk flask charged with a cooled (– 78 ^{0}C) solution of SbCl$_3$ (0.22 g, 1.0 mmol) in THF (10 ml) with stirring (Scheme A1.1). Colour changed to yellow brown and the solution was then stirred further for 24 h at room temperature. After this time, the resulting solution was evaporated under vacuum to dryness and then PhMe added. The solution was filtered and the filtrate was concentrated to *ca*.10 ml and stand at – 15 ^{0}C for 2 days, during which time a moisture-sensitive small shiny white-yellow crystals formed and were characterised by X-ray crystallography. Yield = 0.46 g (69 %).

M.P. 175-177 ^{0}C (dec); ^{1}H-NMR (400 MHz, C$_6$D$_6$, 25 ^{0}C): δ (ppm) = 1.48 (m, 54H, C(C*H*$_3$)$_3$), 2.20 (s, 9H, C*H*$_3$-*p*Me), 7.08 (m, 6H, *m*-Ar*H*); ^{13}C-NMR (101 MHz, C$_6$D$_6$, 25 ^{0}C): δ (ppm) = 21.23 (*C*H$_3$-*p*Me), 33.96 (C(*C*H$_3$)$_3$), 36.25 (*C*(CH$_3$)$_3$), 127.74 (*p*-*C*), 128.03 (*m*-*C*), 141.47 (*o*-*C*), 155.71 (O-*C*); Elemental analysis calcd. (%) for C$_{45}$H$_{69}$O$_3$Sb (*M* = 779.80 g/mol): C 69.31, H 8.91; found: C 68.84, H 9.05. IR (υ/cm^{-1}, Nujol mull): 1747 (s), 1564 (s), 1448 (w), 1313 (w), 1254 (m), 1105 (s), 1026(s), 926 (s), 880 (s), 860 (s), 726 (s), 644 (s), 613 (s), 553 (m).

APPENDIX 1

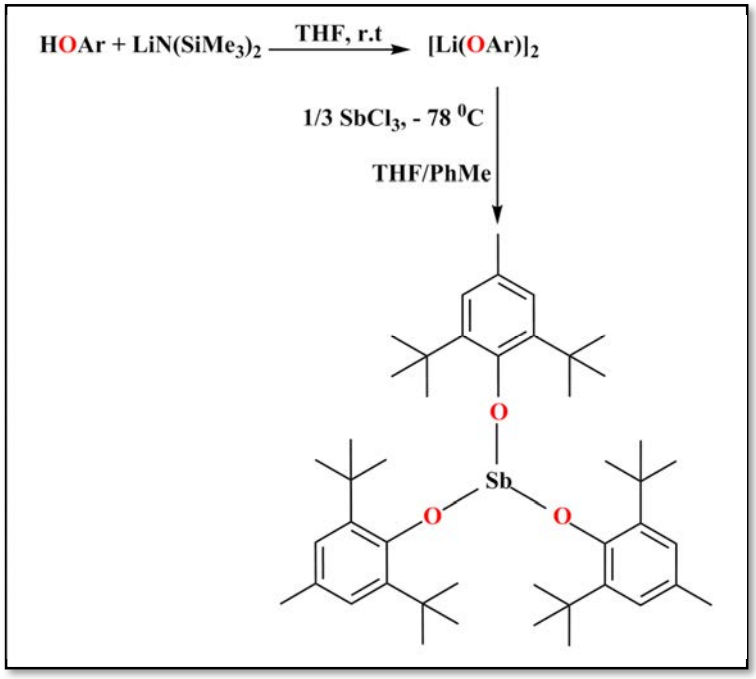

Scheme A1.1: The proposed synthesis of [Sb(OC_6H_2-2,6-*t*Bu_2-4-Me)$_3$].

A1.3: X-ray single crystal structure determination of [Sb(OC_6H_2-2,6-*t*Bu_2-4-Me)$_3$]. Complex **[Sb(OC_6H_2-2,6-*t*Bu_2-4-Me)$_3$]** crystallised in the triclinic space group *P-1* (A1.4), with one monomer within the asymmetric unit. The antimony atom is surrounded by three phenolate oxygens. The arene rings form a propeller-like arrangement around the antimony. The molecular structure of **[Sb(OC_6H_2-2,6-*t*Bu_2-4-Me)$_3$]** shows a mononuclear Sb^{+3} complex which is isostructural with the literature complexes [Sb(OC_6H_3-2,6-Me_2)$_3$],[1] and [Sb{OC_6H_3-2,6-(C_6H_5)$_2$}$_3$].[2] [Σ O–Sb–O = 283.7(6) °] and the O-Sb-O angles are close to 90 ^{0} giving a stereochemistry for Sb^{+3} in **[Sb(OC_6H_2-2,6-*t*Bu_2-4-Me)$_3$]** best described as heavily distorted three-coordinate trigonal pyramidal with a stereochemically active lone pair residing in a fourth coordination site (Figure A1.1). The O-Sb-O angles in **[Sb(OC_6H_2-2,6-*t*Bu_2-4-Me)$_3$]** are comparable with those of [Sb(OC_6H_3-2,6-Me_2)$_3$],[1] whereas these angles are bigger than those observed in [Sb{OC_6H_3-2,6-(C_6H_5)$_2$}$_3$],[2] that are described as acute from orthogonality. Furthermore, it was found that an average Sb-O bond length in **[Sb(OC_6H_2-2,6-*t*Bu_2-4-Me)$_3$]**: 1.969(15) Å, range: 1.973 (15) - 1.961 (15) Å and Sb–O–C angle 119.4(14) °, range: 117.31(14) - 120.54(13) °, which are very similar in overall comparing with those in [Sb(OC_6H_3-2,6-Me_2)$_3$],[1] and [Sb{OC_6H_3-2,6-(C_6H_5)$_2$}$_3$].[2]

APPENDIX 1

Generally, the three structures are slightly different due to the ligand environments. For example, in [Sb{OC_6H_3-2,6-$(C_6H_5)_2$}$_3$],[2] the three phenyl rings formed a cone-shaped cavity covering the lone pair, dissimilar to the isostructural complexes **[Sb(OC_6H_2-2,6-*t*Bu_2-4-Me)$_3$]** and [Sb(OC_6H_3-2,6-Me_2)$_3$].[1]

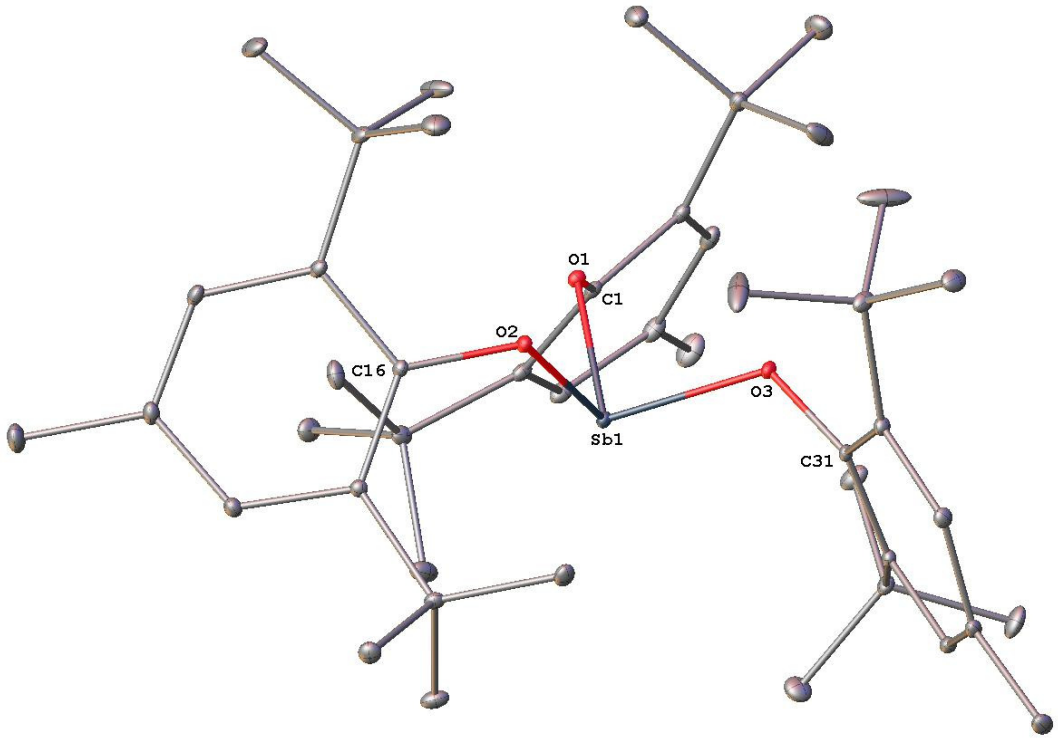

(a)

APPENDIX 1

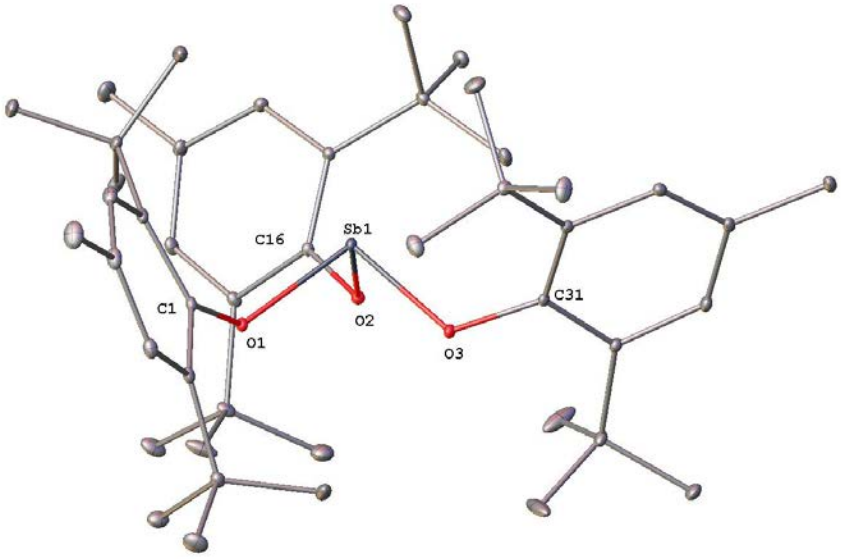

(b)

Figure A1.1 Molecular structure of monomeric **[Sb(OC$_6$H$_2$-2,6-*t*Bu$_2$-4-Me)$_3$]** with the atom numbering system; thermal ellipsoids are drawn at the 50 % probability level, and hydrogen atoms have been omitted for clarity; (*a*) Viewed onto the O_3 plane; (*b*) Highlighting the pyramidal nature of the antimony coordination. Selected bond lengths (Å) and angles (°): Sb(1)–O(1): 1.9739(15), Sb(1)–O(2): 1.9753(15), Sb(1)–O(3): 1.9616(15), C(1)–O(1): 1.394(3), C(16)–O(2): 1.393(3), C(31)–O(3): 1.398(3), O(1)–Sb(1)–O(2): 94.65(6), O(2)–Sb(1)–O(3): 93.74(6), O(3)–Sb(1)–O(1): 95.36(7), C(1)–O(1)–Sb(1): 120.54(13), C(16)–O(2)–Sb(1): 117.31(14), C(31)–O(3)–Sb(1): 120.37(14).

A1.4: Crystal Refinement Data. $C_{45}H_{69}O_3Sb$ (M = 779.80 g/mol): triclinic, space group *P-1*, a = 9.8926(5) Å, b = 11.5120(6) Å, c = 20.1505(10) Å, α = 80.523(2)°, β = 89.109(2)°, γ = 77.142(2)°, Volume = 2206.2(2) Å^3, Z = 2, T = 296(2) K, $Dcalc$ = 1.174 g/cm^3, μ = 0.660 mm-1, $F_{(000)}$ = 828.0, $2\Theta_{max}$ = 2.05 - 54.994°, 41366 reflections collected, 10070 unique (R_{int} = 0.0409, R_{sigma} = 0.0326), 10070/0/464 parameters, GooF on F^2 1.065, The final R_1 was 0.0320 ($I > 2\sigma(I)$) and wR_2 was 0.0928 (all data), Largest diff. peak/hole/e = 0.57 to-0.42 Å^{-3}.

A1.5: References

1. G. A. Horley, M. F. Mahon, K. C. Molloy, M. M. Venter, P. W. Haycock and C. P. Myers, *Inorg. Chem.*, 2002, **41**, 1652-1657.
2. M. Brym, C. Jones and P. C. Junk, *Main Group Chem.*, 2006, **5**, 13-19.

APPENDIX 2

The Synthesis and X-ray Structure Determination of [Al(OC$_6$H$_2$-2,6-*t*Bu$_2$-4-Me)(OH)Cl(thf)]

A2.1: Introduction. An unexpected product [Al(OC$_6$H$_2$-2,6-*t*Bu$_2$-4-Me)(OH)Cl(thf)] was isolated from an attempt to synthesise [Al(OC$_6$H$_2$-2,6-*t*Bu$_2$-4-Me)$_2$Cl], in order to examine the capability of metathesis method, and also the ability of the symmetrical substituted phenol ligand HOC$_6$H$_2$-2,6-*t*Bu$_2$-4-Me to promote a variety of structural types depending on the choice of the metal. This finding strengthen the already impressive reputation of the metathesis reaction and it introduces a simple example of halogenated heteroleptic species in this study.

A2.2: Synthesis of [Al(OC$_6$H$_2$-2,6-*t*Bu$_2$-4-Me)(OH)Cl(thf)] by metathesis in THF and Characterisation by ^{1}H-, ^{13}C-NMR, IR spectroscopy, C,H,N analysis and melting point. A solution of Li(OC$_6$H$_2$-2,6-*t*Bu$_2$-4-Me) was prepared *in situ* from dried HOAr (0.22 g, 1.0 mmol) and LiN(SiMe$_3$)$_2$ (1 M solution in THF, 1.0 ml, 1.0 mmol) in THF (20 ml). The solution of Li(OAr) was added dropwise to a Schlenk flask charged with a solution of AlCl$_3$ (0.13 g, 1.0 mmol) in THF (10 ml), with stirring at room temperature, which resulted in an immediate colour change to bright yellow (Scheme A2.1). The reaction mixture was stirred further for 36 h. The mixture was allowed to stand overnight and the white precipitate was filtered off. The volume of the yellow solution was reduced to about *ca*. 5 ml under vacuum and stored at – 30 ^{0}C for two days during which time small off white crystals formed. The crystals were suitable for X-ray crystallography determination. Yield = 0.12 g (54.5 %).

M.P. 144-146 ^{0}C. ^{1}H-NMR (400 MHz, C$_6$D$_6$, 25 ^{0}C): δ (ppm) = 1.49 (m, 18H, C(C*H*$_3$)$_3$), 2.01 (br s, 4H, C*H*$_2$-thf), 2.23 (s, 3H, C*H*$_3$-*p*Me), 3.49 (br s, 4H, OC*H*$_2$-thf), 4.68 (s, 1H, Al-O*H*), 7.05 (m, 2H, *m*-Ar*H*); ^{13}C-NMR (101 MHz, C$_6$D$_6$, 25 ^{0}C): δ (ppm) = 21.39 (*C*H$_3$-*p*Me), 25.07 (*C*H$_2$-thf), 30.58 (C(*C*H$_3$)$_3$), 34.32 (*C*(CH$_3$)$_3$), 70.61 (O*C*H$_2$-thf), 126.02 (*p*-*C*), 127.64 (*m*-*C*), 136.13 (*o*-*C*), 152.04 (O-*C*). Elemental analysis calcd. (%) for C$_{19}$H$_{32}$AlClO$_3$ (*M* = 370.81 g/mol): C 61.37, H 8.94. Calcd (%) for C$_{15}$H$_{24}$AlClO$_2$ (298.78 g/mol after loss the lonely THF solvation): C 60.30, H 8.10; found: C 56.51, H 7.98, showing low in carbon percentage. IR (υ/cm^{-1}, Nujol mull): 2730 (vs), 2710 (m), 2586 (m), 2524 (m), 2465 (s), 2413 (m), 2378 (s), 2282 (s), 2221 (s), 2146 (s), 2060 (s), 1939 (s), 1902 (s), 1862 (s), 1793 (s), 1756 (s), 1657 (s), 1568 (m), 1459 (w), 1252 (w), 1128 (m), 1039 (m), 989 (m), 773 (s), 622 (m).

APPENDIX 2

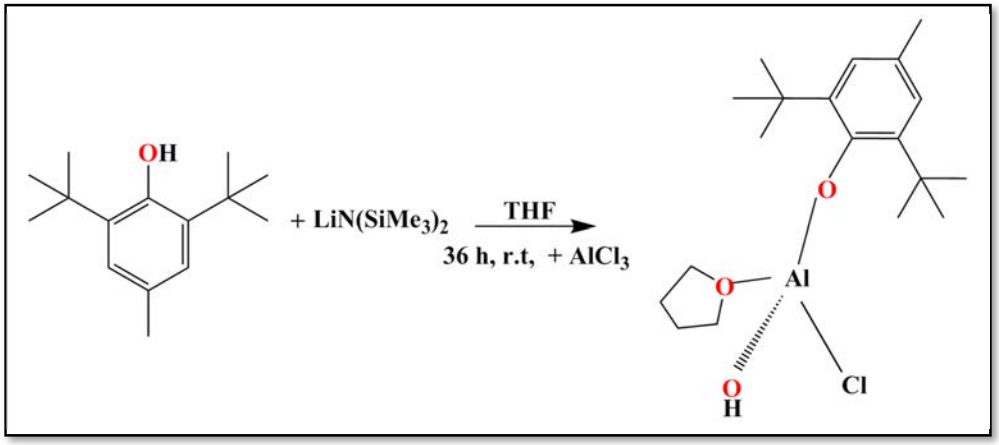

Scheme A2.1: The proposed synthesis of [Al(OC_6H_2-2,6-*t*Bu_2-4-Me)(OH)Cl(thf)].

A2.3: X-ray single crystal structure determination of [Al(OC_6H_2-2,6-*t*Bu_2-4-Me)(OH)Cl(thf)]. The Al^{+3} complex **[Al(OC_6H_2-2,6-*t*Bu_2-4-Me)(OH)Cl(thf)]** crystallised in the monoclinic space group *P2₁/n* (A2.4), with one molecular within the asymmetric unit. As it can be seen from the crystal structure depicted in (Figure A2.1), complex **[Al(OC_6H_2-2,6-*t*Bu_2-4-Me)(OH)Cl(thf)]** is monomeric, in which the central aluminum atom is tetra-coordinate by one phenolate oxygen, OH group, chloride anion and weakly coordinated thf molecule, assuming a distorted tetrahedral arrangement. There are very few instances of monomeric chloroaluminum aryloxides reported in the literature.[1] Compound **[Al(OC_6H_2-2,6-*t*Bu_2-4-Me)(OH)Cl(thf)]** is slightly comparable to those structures of [Al(OC_6H_2-2,6-*t*Bu_2-*p*-Me)Cl_2(Et_2O)],[2] and [Al(OC_6H_2-2,6-*t*Bu_2-*p*-Me)Cl_2(nmp)],[3] the two differences being the existence of an unanticipated (OH) group instead of one of the chloride anion and the solvent associated. The Al–Cl bond length 2.101(2) Å is in the typical range described for terminal Al–Cl bonds.[1,2] The Al–Cl 2.101(2) Å and Al–O 1.695(3) Å bond lengths are shorter by approximately 0.011(1) Å and 0.13(1) Å, respectively, compared to those in [Al(OC_6H_2-2,6-*t*Bu_2-*p*-Me)Cl_2(Et_2O)],[2] and [Al(OC_6H_2-2,6-*t*Bu_2-*p*-Me)Cl_2(nmp)].[3]

APPENDIX 2

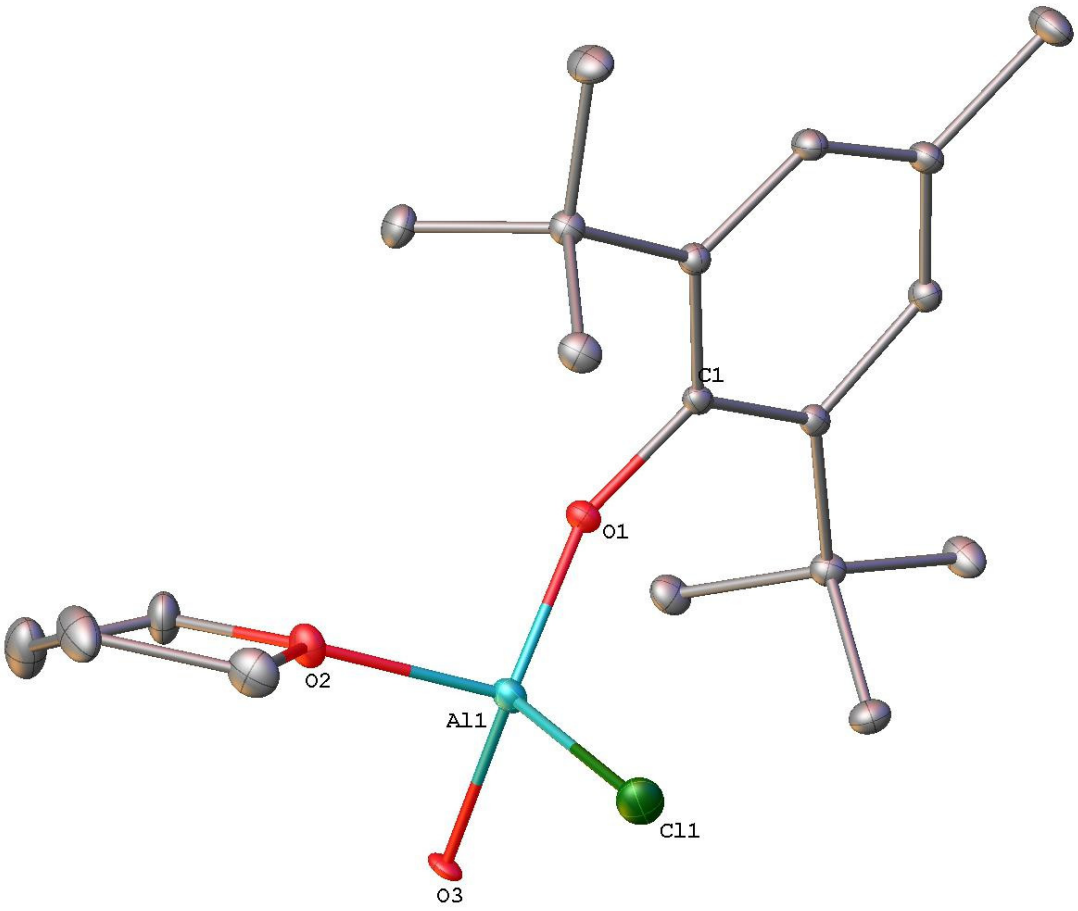

Figure A2.1 Molecular structure of monomeric **[Al(OC$_6$H$_2$-2,6-*t*Bu$_2$-4-Me)(OH)Cl(thf)]** with the atom numbering system; thermal ellipsoids are drawn at the 50 % probability level, and hydrogen atoms have been omitted for clarity. Selected bond lengths (Å) and angles (°): Al(1)–O(1): 1.695(3), Al(1)–O(2): 1.885(3), Al(1)–O(3): 2.050(3), Cl(1)–Al(1): 2.101(2), O(2)–C(1): 1.376(4), C(1)–O(2)–Al(1): 156.4(3), O(2)–Al(1)–Cl(1): 114.24(12), O(2)–Al(1)–O(1): 104.54(14), O(2)–Al(1)–O(3); 120.21(13), O(1)–Al(1)–Cl(1): 105.08(13), O(1)–Al(1)–O(3): 100.46(13), O(3)–Al(1)–Cl(1): 109.99(11), C(16)–O(1)–Al(1): 121.4(3), C(19)–O(1)–Al(1): 127.7(3).

APPENDIX 2

A2.4: Crystal Refinement Data. $C_{19}H_{32}AlClO_3$ (M = 370.81 g/mol): monoclinic, space group $P2_1/n$, a = 10.4416(9) Å, b = 18.9928(17) Å, c = 10.9866(9) Å, α = 90°, β = 97.676(4)°, γ = 90°, *Volume* = 2159.3(3) Å^3, Z = 4, T = 296(2) K, μ = 0.230 mm^{-1}, D_{calc} = 1.138 g/cm^3, $F_{(000)}$ = 796.0, $2\Theta_{max}$ = 4.29 to 49.996, 18376 reflections measured, 3566 unique (R_{int} = 0.0809, R_{sigma} = 0.0819), 3566/0/225 parameters, GooF on F^2 1.046, The final R_1 was 0.0735 ($I > 2\sigma(I)$) and wR_2 was 0.2734 (all data), Largest diff. peak/hole/e = 0.76 to - 0.51 Å^{-3}.

A2.5: References

1. S. Schulz, H. W. Roesky, M. Noltemeyer and H.-G. Schmidt, *J. Chem. Soc., Dalton Trans.*, 1995, 177-180.
2. M. D. Healy, J. W. Ziller and A. R. Barron, *Organometallics.*, 1992, **11**, 3041-3049.
3. M. Veith, H. Ullah Wazir, T. Kirs and V. Huch, *Z. Anorg. Allg. Chem.*, 2011, **637**, 923-929.